Structure, Function and FliM Interaction Studies of $CheY_6$ in *Rhodobacter sphaeroides*

Matthew William Smith

Linacre College
University of Oxford
Trinity Term 2015

A thesis submitted for the degree of

Doctor of Philosophy

Abstract

Structure, Function and FliM Interaction Studies of $CheY_6$ in *Rhodobacter sphaeroides*

Matthew William Smith

Linacre College, University of Oxford
Submitted for the degree of Doctor of Philosophy, Trinity Term 2015

Bacteria control their swimming direction by signalling from chemoreceptors via a small protein, CheY, to the rotary flagellar motor. *Rhodobacter sphaeroides* has a complex chemosensory network with two pathways, including three different CheYs controlling a stop-start motor. Deletions of these *che*Ys result in a non-chemotactic phenotype. $CheY_6$ is essential for chemotaxis, whereas $CheY_3$ and $CheY_4$ have some functional redundancies. Although $CheY_6$ alone can stop the motor, the presence of either $CheY_3$ or $CheY_4$ is required for a chemotactic phenotype. To date, little is known about how these three CheY proteins interact with the flagellar motor, or the switch mechanism used between the inactive and active states.

Structural studies of $CheY_6$ using NMR experiments, highlighted a flexible loop region (residues S109-K118) that is not present in $CheY_3$, $CheY_4$ or CheYs in other bacterial species. This elongated loop region was deleted ($CheY_6$-ΔLoop), and *in vivo* studies were used to investigate its function. $CheY_6$-ΔLoop is folded, retains the ability to be phosphorylated by $CheA_3$, localises at the cytoplasmic chemoreceptor cluster, but appears unable to stop the flagellar motor. Circular dichroism and NMR data suggest that $CheY_6$-ΔLoop is a folded protein that shows similar peak shifts to wild type $CheY_6$ upon activation. In wild type $CheY_6$, residues in this loop show chemical shift changes upon addition of the phosphoryl mimic BeF_3^-, suggesting that the loop is involved in the activation mechanism.

The switch mechanism of $CheY_6$ was probed using multidimensional NMR studies. The active state was mimicked using BeF_3^-. Wild type $CheY_6$ was shown to undergo structural changes upon addition of BeF_3^-. In particular, the $\beta4$-$\alpha4$-loop and residues located near the phosphorylatable D56 show large changes in chemical shift. Superposition of this loop region revealed possible steric clashes with the N-terminus of FliM. S83 shows evidence of involvement in the switch mechanism. Residual dipolar coupling experiments suggest that the published crystal of $CheY_6$ in complex with $CheA_3$, is more like the inactive conformation in solution. CheY has been shown to interact with the motor switch protein FliM in other bacterial species. $CheY_6$-FliM interactions were probed using a combination of *in vitro* and *in vivo* studies. Bacterial two hybrid assays and NMR studies suggest that $CheY_6$ cannot interact with monomeric FliM. Single molecule total internal reflection microscopy revealed $CheY_6$ does interact with the motor *in vivo*.

The data in combination suggests a model in which $CheY_6$-P only interacts with FliM when it is part of the switch ring, and structural changes involved in stopping the motor depend on the large conformational changes in the $\beta4$-$\alpha4$-loop.

Declaration

The work in this thesis was undertaken in the Department of Biochemistry at the University of Oxford. Work was completed between October 2011 and October 2015 under the supervision of Prof. C. Redfield and Prof. J. P. Armitage. All the work in this thesis is my own unless stated and has not been submitted for a degree at this or any other university.

Acknowledgments

Special thanks go to Prof. Christina Redfield and Prof. Judith Armitage for direction, advice and support throughout my DPhil. Thank you for the patience and freedom to pursue and experience a wide range of experimental techniques.

Thank you to Dr. Nick Delalez and Dr. Lorena Varela-Alvarez for the introduction to, and teaching of laboratory techniques. Thanks goes to Diana Di Paolo for the collaborative work visualising electroporated protein.

I would like to thank my friends, family and all of the people I met during my time at Oxford. You all made it a fantastic experience. Every member of the Armitage Lab has been great to work and play with.

Finally, thank you to the BBSRC for providing financial support throughout my research.

Contents

List of Figures

List of Tables

Abbreviations

3D	Three dimensional
AcP	Acetyl phosphate
ATP	Adenosine triphosphate
Bp	Base pair
BSA	Bovine serum albumin
CA	Catalytic and ATPase domain
CFP	Cyan fluorescent protein
CCW	Counter-clockwise
CW	Clockwise
DIC	Differential interference contrast
DNA	Deoxyribonucleic acid
dNTP	deoxynucleoside-5’-triphosphate
FRET	Fluorescence resonance energy transfer
GFP	Green fluorescent protein
HAP	His-Asp-phosphorelay
HetNOE	Heteronuclear NOE
HK	Histidine kinase
Hpt	Histidine phosphotransferase
HSQC	Heteronuclear single quantum coherence

IPTG	Isopropyl β-D-thiogalactoside
Kan	Kanamycin
kb	kilo base
kDa	Kilo dalton
MCP	Methyl accepting protein
Nal	Nalidixic acid
NMR	Nuclear magnetic resonance
NOE	Nuclear overhauser effect
$OD600_{nm}$	Optical density at 600 nm
$OD700_{nm}$	Optical density at 700 nm
P	Phosphoryl group
PBD	Peptidoglycan binding domain
PMF	Proton motive force
RR	Response regulator
TCS	Two component system
Tlp	Transducer like protein
$t_{1/2}$	Half-time
WT	Wild type
YFP	Yellow fluorescent protein

Chapter 1

Introduction

1.1 Bacterial Motility and Taxis

The ability to adapt and respond to environmental stimuli is often crucial to a species' survival. Bacteria in the laboratory are frequently grown in rich media, supplying them with perfect growth conditions. However, this is not the case in their natural environments. Resource availability can vary enormously in the wild, so bacteria must be able to adapt to rapidly changing surroundings to maintain optimum growth. To ensure survival, bacteria employ multiple adaptation methods such as changes in gene expression and thus phenotype.

A good example of a rapid response to fluctuating conditions is taxis. This is the process by which bacteria move towards more favourable conditions and away from unfavourable conditions. Bacterial species demonstrate taxis towards a very diverse range of stimuli. Examples include taxis towards metabolites (chemotaxis) (Adler 1976), temperature (thermotaxis) (Gluch *et al.* 1995), oxygen (aerotaxis) (Romagnoli,

Packer, and Armitage 2002), magnetic fields (magnetotaxis) (Lefèvre and Bazylinski 2013), the internal energetic state of the cell (energy taxis) (Alexandre 2010) and light (phototaxis) (Sackett *et al.* 1997).

Bacteria have evolved a wide and diverse range of methods for motility and taxis (review (Jarrell and McBride 2008)). For instance, different mechanisms are used for swimming through liquid media compared to moving on solid surfaces (Figure 1.1). *Myxococcus xanthus* employs two different mechanisms (S- and A-motility) for surface motility. S-motility, also referred to as twitching motility, involves the extension and retraction of a Type IV pilus (Bulyha *et al*. 2009). A-motility, a type of gliding motility, involves focal adhesion complexes attaching to the surface and propelling the cell body forward (Mignot *et al*. 2007). *Flavobacterium johnsoniae* uses a rapid gliding technique over solid surfaces. This is mediated by surface attachment and flow of proteins located in the outer membrane. The overall result is directed movement of the cell body (Nakane *et al*. 2013). Co-ordinated rotation of a semi-rigid helical filament (flagellum) can also facilitate movement across a solid surface (review (Kaiser 2007)).

Flagella driven motility is used by bacteria to swim through aqueous environments (Berg and Anderson 1973). The architecture, positioning and number of flagella vary quite significantly between bacterial species. A variety of different approaches to flagella motility and swimming patterns are discussed in Section 1.2.

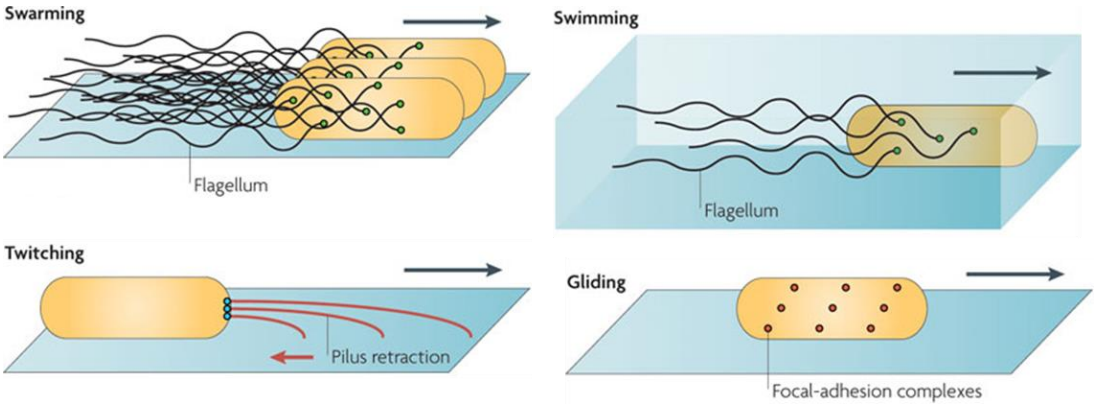

Figure 1.1 – Types of motility utilised by different bacterial species. Swarming is driven by multiple helical flagella, across a solid surface. Swimming is employed by individual bacteria in liquid, and is also driven by rotating flagella. Twitching is movement across a surface, powered by the extension and retraction of pili. These attach to the surface and retract, pulling the cell body towards the site of attachment. Gliding does not use flagella or pili. Instead it involves focal adhesion of complexes to move across a solid surface (taken from (Kearns 2010)).

Motile and tactic cells gain an advantage over non-motile and non-tactic cells, not only in the search for resources, but also to interact with individuals of the same species, other bacterial species, and surfaces in biofilm formation. The majority of bacteria not only move, but also switch to a sedentary lifestyle, or biofilm. Motility can be important in biofilm formation, as it brings bacteria to surfaces. Biofilms are surface growth within an extra cellular polysaccharide matrix, and have been identified in the majority of species including *Rhodobacter sphaeroides* (Wilkinson *et al*. 2011), *Vibrio cholerae* (Moorthy and Watnick 2005) and *Agrobacterium tumefaciens* (Merritt, Danhorn, and Fuqua 2007).

Many symbiotic relationships are dependent on chemotaxis and motility. Non-motile mutants of *Vibrio fisheri* are unable to colonise the light organ of the squid *Euprymna scolopes* (Graf, Dunlap, and Ruby 1994). *Azospirillum brasilense* (a nitrogen fixing bacterium) uses both chemotaxis and motility to colonise wheat roots (Vande Broek, Lambrecht, and Vanderleyden 1998). Many bacterial species rely on favourable interactions with other organisms during their life cycles. Chemotaxis and motility often play an important role in the initiation of these interactions. *Helicobacter pylori* (which infects the stomach, and may produce ulcers) exhibits reduced infection and pathogenicity when the chemotaxis signalling pathway is disrupted, as it cannot reach the protective mucus layer (Rolig *et al*. 2012).

Motility and taxis, although they convey competitive advantages, are energetically expensive activities because they both require synthesis of large protein complexes. For instance, *Salmonella enterica serovar typhimurium* when grown in rich media, becomes non-flagellate (hence non-motile) within 10 days due to spontaneous mutations (Macnab 1992). The non-flagellated cells benefit from an increased growth rate of ~2% over WT cells that have been grown in rich media for one day.

The diverse use and large energy cost of producing flagella and taxis machinery highlights their importance to bacterial species in natural environments. Investigation and understanding of these processes could aid drug development and discovery. For example, taxis and motility are essential for *H. pylori* to colonise the

gastric mucosa (Foynes *et al*. 2000). Biofilm formation is associated with ~80% of human infections, and thought to require both taxis and motility for development (Römling and Balsalobre 2012).

1.2 Flagella-Driven Motility

Flagella-driven motility is achieved by rotating a helical flagellum (or flagella) powered by an ion gradient across the cytoplasmic membrane (Berg 2003). The architecture, positioning and number of flagella are diverse amongst bacterial species. Examples of bacteria possessing a single flagellum (monotrichous) include *R. sphaeroides* (Porter, Armitage, and Wadhams 2008) and *Caulobacter crescentus* (Anderson, Smith, and Hoover 2010). Although both have one flagellum, they position it differently. *R. sphaeroides* has a randomly positioned single flagellum whereas *C. crescentus* locates its flagellum at a specific cell pole, highlighting differences between monotrichous bacteria.

Examples of bacteria that possess multiple flagella (peritrichous) are *Escherichia coli* and *S. typhimurium*. Both produce between ~4-8 flagella that protrude from the cell body. During swimming, these flagella bundle together behind one of the cell poles (Armitage 1992). *Proteus mirabilis* is able to produce hundreds of flagella which are utilised in swarming motility to move across solid surfaces (Pearson *et al*. 2010). *V. fisheri* produces multiple flagella but positions them specifically at one cell pole (Wolfe *et al*. 2004), these bacteria are termed lophotrichous. Some species, such as *Rhodospirillum rubrum*, produce bipolar flagellated cells (Lee and Fitzsimons 1976).

Not all bacterial species use external flagella. Spirochaetes, such as *Treponema pallidum*, possess flagella that are contained within the periplasm and do not protrude outside the cell (Charon *et al*. 1992). Cellular motion is generated by rotation of the flagella, resulting in rotation of the flexible spiral shaped cell body. This motion drives the cell through viscous environments.

Some bacteria encode more than one set of flagella genes. *Vibrio parahaemolyticus* expresses multiple lateral flagella when moving across surfaces but expresses just a single polar flagellum (from a different regulon) when swimming (Kim and McCarter 2000).

The flagellar motor of *E. coli* is able to rotate both clockwise (CW) and counter-clockwise (CCW). The switch between the two rotational states results in a change of the swimming direction. Directed movement cannot be generated by flagella alone and hence, other processes must be employed for bacteria to show tactic behaviour. Motion of a swimming tactic cell can be divided into two stages: a 'run' and a 'tumble'. A run consists of a period of time where the cell body is driven forward by rotation of flagella. A tumble consists of a period of time where forward motion ceases and the cell re-orientates itself randomly. When the bacterium has no control over the frequency of tumbling events, there is no net directionality. This is known as a 'random walk' (Figure 1.2A). Directional movement is accomplished using a 'biased random walk' (Figure 1.2B). This consists of an increased frequency of tumbles in response to worsening conditions, and a decreased frequency of

tumbles in response to improving conditions. The overall result is net movement towards more favourable conditions. The biased random walk is necessary for temporal sensing (not spatial sensing), as bacteria are too small to sense a gradient along the cell body. Living at low Reynolds number allows the use of a rotary filament, as bacteria have no inertia (Purcell 1976).

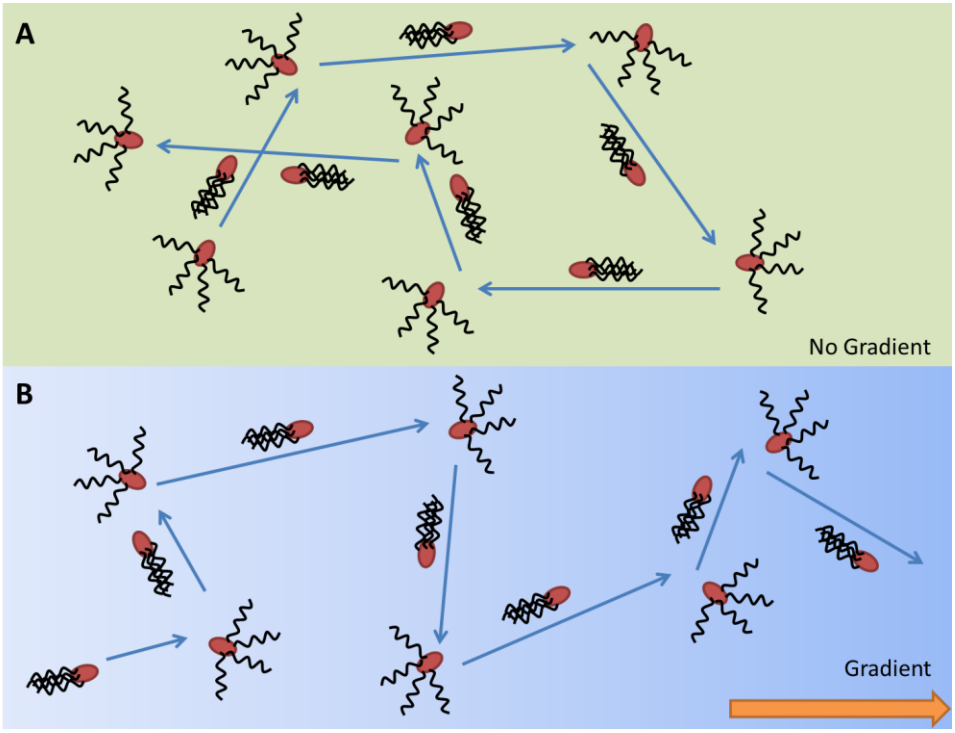

Figure 1.2 – Flagella-driven directional movement of bacteria. **A)** In the absence of a chemical gradient, there is no net directional movement and the bacterium moves using a random walk. **B)** In the presence of a chemical gradient (light (unfavourable) to dark (favourable) blue), net directional movement is observed up the gradient.

All flagellate species have a common general mechanism for flagellar driven motility, with variations in morphology, signalling and flagella architecture. The most studied and current paradigm for flagella-driven motility and chemotaxis is the *E. coli* model. CCW rotation of the flagellar motors result in smooth swimming (a 'run') by bundling

of the rotating flagella behind the cell body, pushing the cell forward. CW rotation results in a 'tumble' by one or more flagella uncoupling from the bundle and 'kicking out', causing a change in direction (Berg and Brown 1972). There are variations on the mechanism for directional switching. Examples of different 'tumbles' include that of *Chromatium minus* which causes a reversal in swimming direction (Mitchell *et al*. 1991). *R. sphaeroides* uses a brake mechanism where the flagellum stops rotation and the cell is reoriented by Brownian motion (Delalez *et al*. 2010).

1.3 The Flagellar Motor

The flagellar motor is one of the largest and most complex macromolecular machines found in nature (Figure 1.3). It can reach speeds in excess of 300 Hz (Chen and Berg 2000). For successful motor assembly, at least 13 genes encoding structural components are required and at least a further 25 genes encoding components that control expression and assembly (Macnab 2003). Flagellar motors in Gram negative bacteria span both inner and outer lipid membranes, the peptidoglycan layer and the periplasm, a distance of ~50 nm.

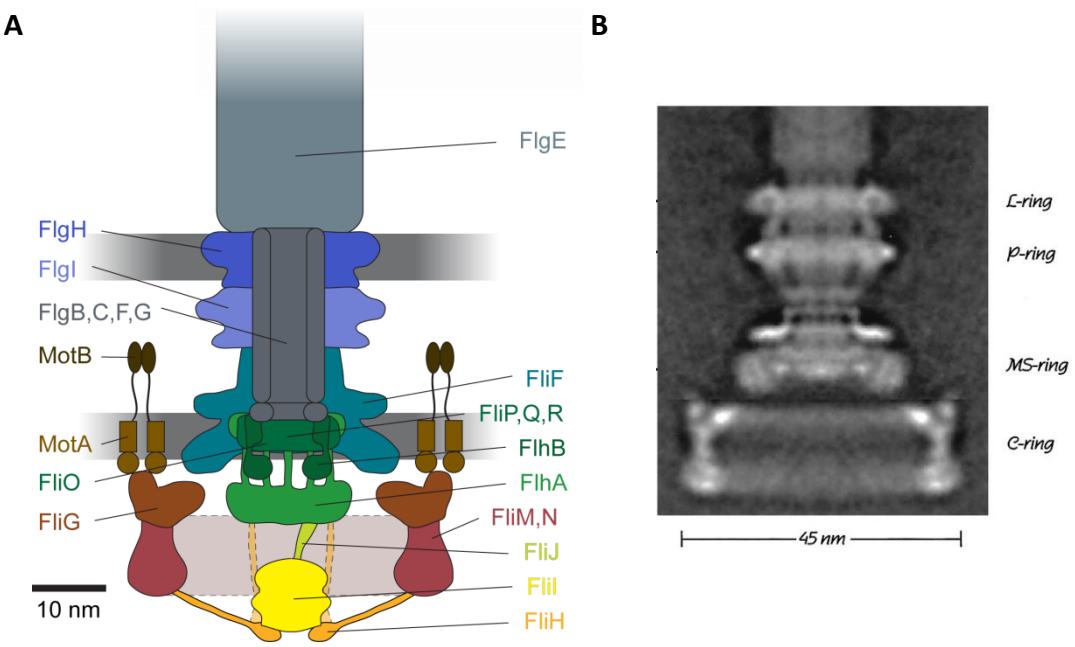

Figure 1.3 – The structure of the *E. coli* flagellar motor. **A)** 3D model (adapted from (Diepold and Armitage 2015)) showing the MS-ring, C-ring and stator units. **B)** Electron micrograph of the basal body reconstructed from ~100 rotationally averaged images (taken from (Berg 2003)). Individual sections of the flagellar motor are labelled. The filament (FliC) is not shown.

The quaternary structure of the flagellar motor is fairly well conserved throughout all bacterial species (Chen *et al*. 2011). The core structural components made up of the filament, the hook and the basal body are consistent throughout bacterial species. However, there can be subtle differences in other components (Figure 1.4).

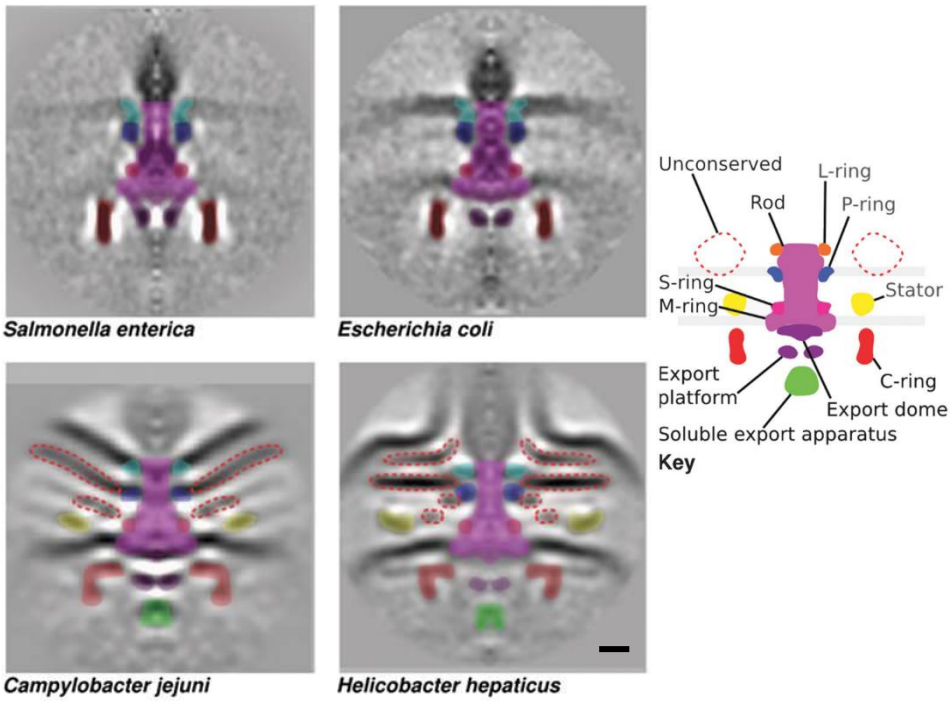

Figure 1.4 – Electron cryotomographs of **A)** *S. typhimurium* **B)** *E. coli* **C)** *Campylobacter jejuni* and **D)** *Helicobacter hepaticus* flagella. Solid colours indicate conserved motor components and dotted regions indicate variable components (taken from (Chen *et al*. 2011)). The key indicates each section of the flagellar motors. Scale bar, 10 nm.

1.3.1 The Filament

The primary role of the filament is to drive cellular motion by rotation, essentially acting like a propeller. Divergence in structure has been highlighted across bacterial species (Galkin *et al*. 2008). The filament in *E. coli* is made from FliC, a 51.3 kDa protein that is transported unfolded by the export apparatus through the central cavity, where it polymerises at the distal end of the growing flagellum. 11 protofilaments coil around a hollow central cavity (~30 Å) and span the entire length of the filament. The filament can reach a length of 15 μm (consisting of ~20k

proteins) and has a diameter of ~220 Å (Berry and Armitage 1999). The C and N-terminal regions involved in polymerisation are located in the core of the filament, with the variable antigenic regions located on the outside (Mimori-Kiyosue, Vonderviszt, and Namba 1997). The protofilaments of *S. typhimurium* exist in two states, right (R) handed and left (L) handed. The R state is ~1.6% shorter than the L state, which gives rise to the helical structure of the filament (Figure 1.5) (Galkin *et al*. 2008).

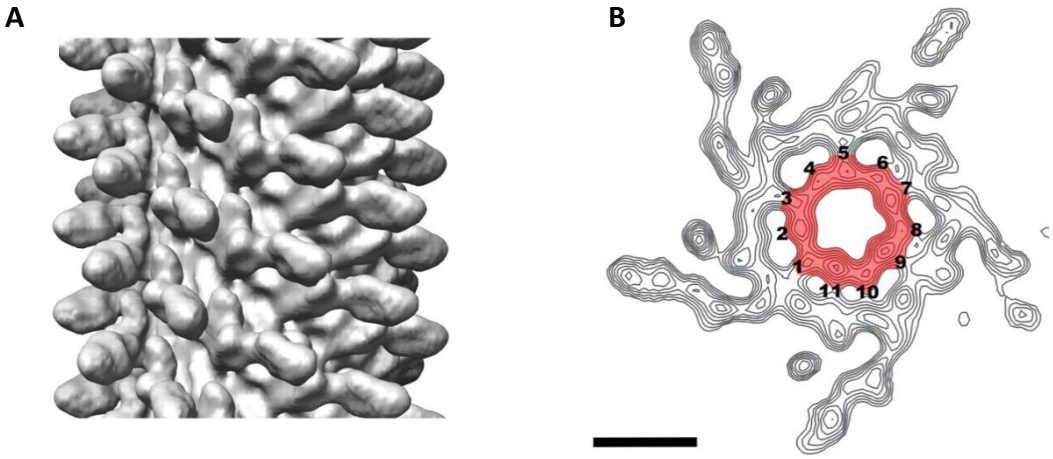

Figure 1.5 – Atomic model reconstructions (cryo-EM) of a 3D flagellar filament from *S. typhimurium*. **A** shows a typical filament. **B** shows a cross section of **A**. The scale bar for **B** indicates 50 Å (adapted from (Galkin *et al*. 2008)).

1.3.2 The Hook

The flagellar hook, composed of FlgE, connects the basal body to the filament. In *E. coli*, this 42 kDa protein is exported in its unfolded state, through the basal body and incorporated into the hook by FliD. Hook length is tightly controlled by

regulatory proteins FliK and FlhB (Minamino *et al*. 2004). For instance, the hook of *S. typhimurium* is always 55 nm in length (Hirano *et al*. 1994). Despite this tight regulation, hook size and structure are diverse among bacterial species (Egelman 2009). FlgK and FlgL are Hook Accessory Proteins (HAPs) that act as adaptor proteins between the hook and filament. The hook behaves as a joint between the basal body and the filament and in peritrichous bacteria (such as *S. typhimurium*), it is curved and flexible (Samatey *et al*. 2004) (Figure 1.6A). In *R. sphaeroides* (a monotrichous bacterium), the hook is straight and currently thought to have a more rigid structure (West and Dreyfus 1997) (Poggio *et al*. 2007) (Figure 1.6B). As *R. sphaeroides* is monotrichous, the single flagellum does not need to accommodate other flagella in a bundle and hence, may not need a more flexible hook.

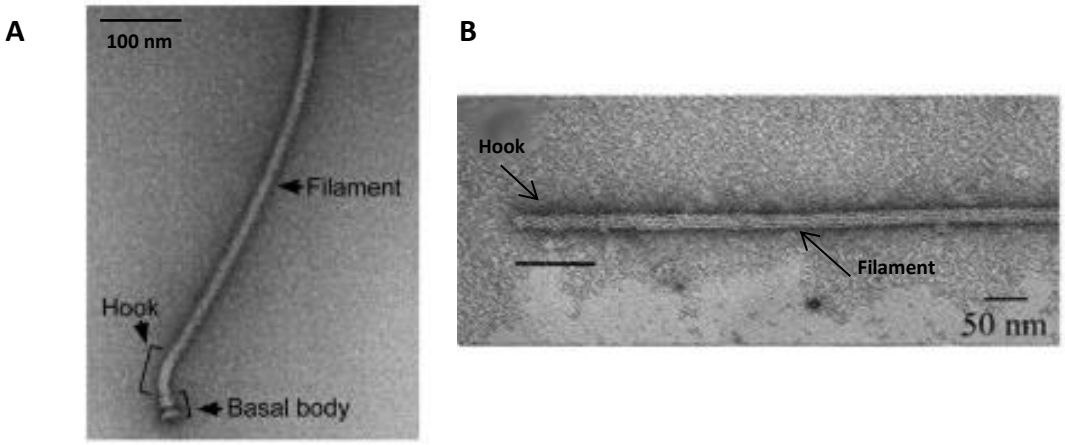

Figure 1.6 – Electron microscopy image of the hook and filament of **A)** *S. typhimurium* (taken from (Minamino, Imada, and Namba 2008)) and **B)** *R. sphaeroides* (taken from (Poggio *et al*. 2007)).

1.3.3 The Basal Body

Studies using cryo-electron microscopy and tomography have elucidated the structure of the basal body (also known as the rotor) (Chen *et al*. 2011). It is

composed of a central rod and the C-, MS-, P- and L-rings. The basal body acts as a drive shaft. Torque is generated at the C-ring and transmitted through the cell membranes and wall to the hook and filament. The rod, composed of five proteins (FlgB, FlgC, FlgF, FlgG and FliE), rotates with the C- and MS-rings. The P- and L-rings, made of FlgI and FlgH respectively, enable motor rotation between the cell membranes and wall (essentially acting as a cylindrical lining or bushing). Bacterial species (such as *V. alginolyticus*) that use a Na^+ ion gradient as a driving force contain an extra ring, the T-ring (Terashima *et al*. 2006). Made up of two proteins (MotX and MotY), the T-ring sits below the LP-ring and assists stator localisation. The MS-ring, consisting of protein FliF, acts as a transmission between the C-ring and the rod and is located in and above the cytoplasmic membrane. Both biochemical analysis and electron microscopy (Suzuki, Yonekura, and Namba 2004) suggest the copy number of FliF in the MS-ring is 26.

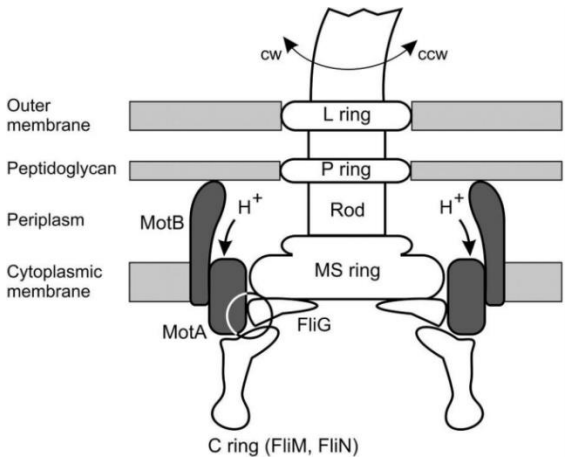

Figure 1.7 – Structure of the basal body. The core components are highlighted, which include the rod, C-ring, MS-ring, P-ring and L-ring. The C-ring diameter is ~45 nm (taken from (Schmitt 2003)).

1.3.4 Stators

Flagellar rotation is accomplished using the torque generating rotor-stator interaction. The stator harnesses the energy of the proton motive force (PMF) across the membrane and converts it into conformational changes. Stator units are stable complexes comprised of two membrane proteins, MotA and MotB. Bacterial species that utilise Na^+ driven motors, such as *V. alginolyticus*, use homologous proteins PomA and PomB (Sato and Homma 2000). MotA is a 4-transmembrane α-helix protein with a cytoplasmic domain between α-helices two and three. MotB contains a single transmembrane α-helix and a long linker to the peptidoglycan-binding domain (PBD). This PBD is thought to anchor the stator complex in place (Braun *et al*. 2004). Each stator unit is a hexamer containing four MotA and two MotB proteins ($MotA_4MotB_2$), which create two ion channels through the membrane (Kojima and Blair 2004). An aspartate residue (Asp33 in $MotB_{EC}$, Asp24 in $PomB_{VA}$) has been shown to be essential for ion transduction (Morimoto and Minamino 2014). To date, there are no high resolution structures of the stator complex. Extensive analyses using cysteine cross-linking and site-directed mutagenesis have provided insight into the mechanism and structure of the complex (Braun *et al*. 2004) (Kim *et al*. 2008) (Figure 1.8). Torque transmission from the stator to the rotor, comprises of a structural change of the stator unit induced by the binding of the ion to the Asp residue, which is then passed on to the C-ring (switch complex) through changes in the charged interaction with FliG (Blair 2003). The switching mechanism uses the interactions between the stator units, FliG and the C-ring. Conformational changes

in the C-ring (upon CheY binding (discussed in Section 1.6)) disrupt the FliG-Stator interface, and cause a change in rotation.

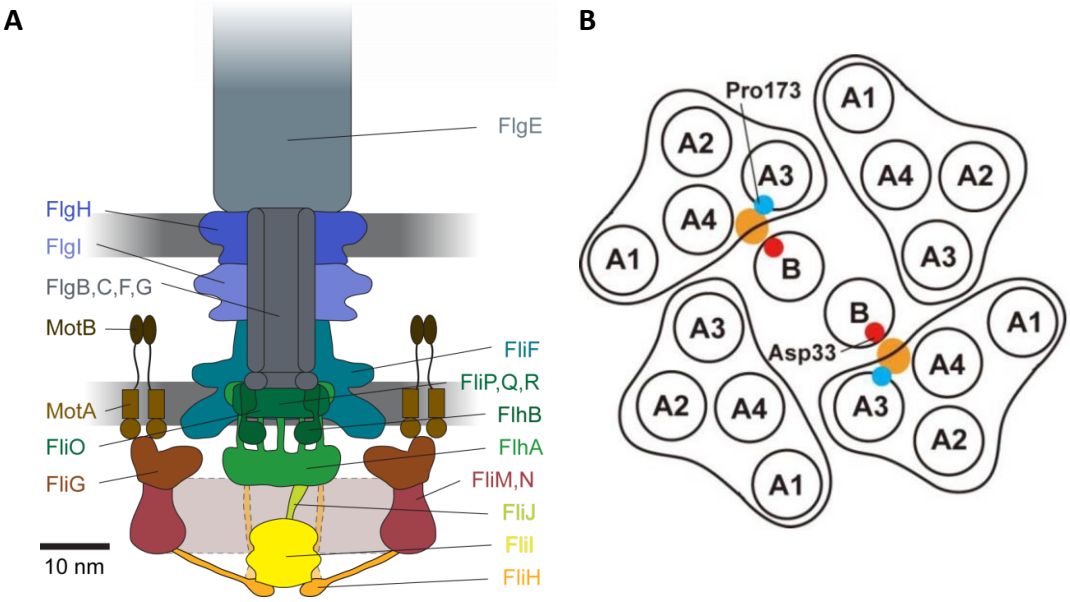

Figure 1.8 – **A)** Architecture of the flagellar motor. The stator (brown) positions are indicated. (adapted from (Diepold and Armitage 2015)). **B)** Arrangement of the Stator Complex $MotA_4MotB_2$. Helices are represented as circles. The image is taken from the periplasmic side of the membrane. Orange circles indicate the proton channels (taken from ((Morimoto and Minamino 2014)). A1-A4 are transmembrane helices found in MotA.

1.3.5 The Switch Complex

The switch complex (also known as the C-ring), is located at the base of the basal body and is composed of three cytoplasmic proteins: FliG, FliM and FliN (Figure 1.9). The complex is involved in motor switching events and, as discussed earlier, stator-FliG interactions generate torque. The switch complex in *E. coli* exchanges with pools of free proteins, whilst functionally active (Delalez, Berry, and Armitage 2014).

FliG

FliG provides an interface between the FliM-FliN complex, the MS-ring and the stators. Fusions of FliF-FliG resulted in folded protein that localised successfully into a working flagellar motor (Francis *et al*. 1992). It was therefore proposed that FliG had a 1:1 relationship with FliF, suggesting 26-fold symmetry in the FliG ring. This however, does not fit with information known about FliM. Monomeric FliM is known to interact with stable FliN tetramers (over 100 copies per rotor) and thought to have 34-fold symmetry (Paul and Blair 2006). There is still confusion over the FliG:FliM ratio but a crystal structure of FliG from *Aquifex aeolicus* suggested evidence for a 1:1 ratio. A model C-ring has been produced suggesting 34 FliG monomers (Lee *et al*. 2010).

FliM

FliM has been shown to interact (affinity blotting) with FliG, FliN and CheY-P (Toker and Macnab 1997). It forms a ring with ~34 monomers underneath the FliG ring. There is evidence that the copy number of FliM is variable, and exchange occurs with a pool a free protein in the cytoplasm (Delalez *et al*. 2014). The crystal structure of FliM from *T. maritima* has been solved and showed structure homology between FliM and the CheY-P phosphatases CheC and CheX (Park *et al*. 2006). FliM has not been shown to have any catalytic activity. CheY-P binding events are believed to trigger a conformational change in FliM, which spreads around the ring (conformational spread model) (Duke, Le Novère, and Bray 2001) (Bai *et al*. 2010). This change in ring conformation causes a switch in motor rotation.

FliN

The crystal structure of FliN from *T. maritima* has been solved. It showed that FliN forms a doughnut-shaped homotetramer (Brown *et al*. 2005). Each tetramer associates with a FliM monomer to form a stable complex with stoichiometry $FliM_1FliN_4$ (Paul and Blair 2006). FliN has been shown to interact (pull-down assay) with CheY-P (Sarkar, Paul, and Blair 2010), but the role of FliN has not been fully elucidated. It is essential for flagellar switching and assembly.

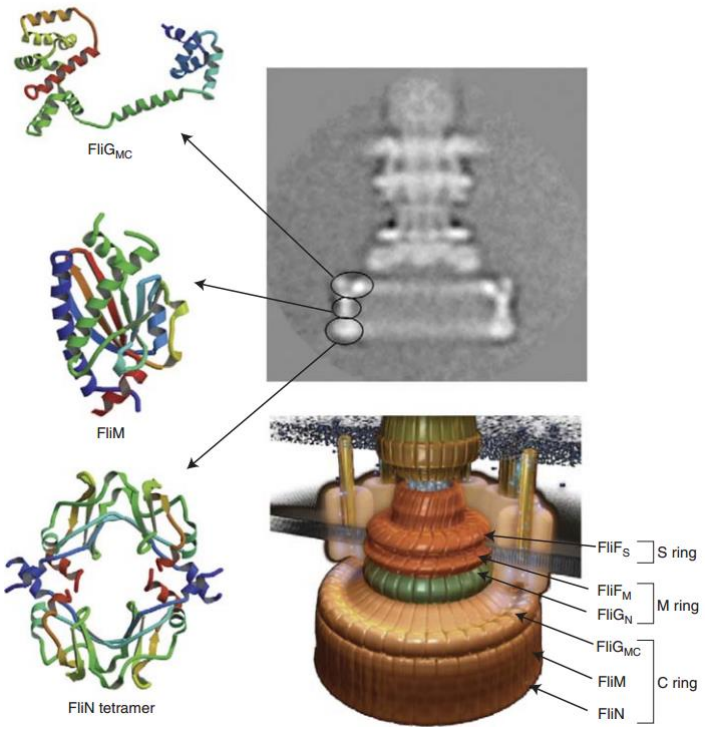

Figure 1.9 – (**Left**) Crystal structures of $FliG_{MC}$, FliM and FliN tetramer from *T. maritima*. (**Upper right**) Cryo-EM image of the hook-basal-body complex. (**Lower right**) Model of the C-ring and basal body (taken from (Minamino *et al*. 2008)). Subscript M and C indicate the middle and C-terminal domains respectively of the associated proteins. $FliF_S$ indicates the S-ring domain of FliF.

Motor Switching

The motor switching mechanism is not completely understood. CheY-P induced conformational changes in the FliM ring are currently thought to be responsible for switching. The *E. coli* motor has been shown to be ultrasensitive to CheY-P concentration (Hill coefficient of ~10) (Cluzel, Surette, and Leibler 2000). Rapid motor switching has been observed in *S. typhimurium*, with motor rotation changing from 100 Hz CCW to 100 Hz CW in less than 1 ms (Kudo, Magariyama, and Aizawa 1990). Conformational changes in a single FliM monomer are likely to be transferred throughout the FliM ring to trigger a switch. Therefore, any switching model must account for cooperativity between FliM units. A number of mechanisms have been proposed, such as the 'conformational spread' model (Duke *et al*. 2001). A CheY-FliM binding event causes a conformational change in the FliM monomer. This effectively behaves as a 'nucleus' to bias neighbouring FliM units to switch. This new conformation can either spread through the whole ring, or revert, returning to the original ring conformation. Incomplete switching events in *E. coli* have provided evidence for such a model (Bai *et al*. 2010). Another suggested mechanism involves fluctuations in the FliM content of the switch complex. During CCW rotation, FliM binding to the C-ring has been shown to strengthen (ring content increases), and motor exchange decreases. This increases the number of CheY-P binding sites and therefore increases motor sensitivity, i.e. motor adaptation (Lele *et al*. 2012). The increase in FliM binding is consistent with the observation of turnover within the FliM ring.

1.4 Two Component Systems

Bacterial chemotaxis operates through a specialised two component system (TCS). These are signalling mechanisms employed by bacteria and a small number of eukaryotic organisms. A classic TCS is composed of a histidine kinase (HK) which senses a specific signal, and a response regulator (RR) (phosphorylated by the HK) that provides a specific output (Nixon, Ronson, and Ausubel 1986) (Laub and Goulian 2007) (Figure 1.10). Genomic analysis of bacteria has illustrated the range of importance of TCSs: *Mycoplasma genitalium* (Mizuno 1998) has no TCS proteins, *M. xanthus* has 272 (Shi *et al*. 2008) whereas *E. coli* has 60 (Mizuno 1997) .

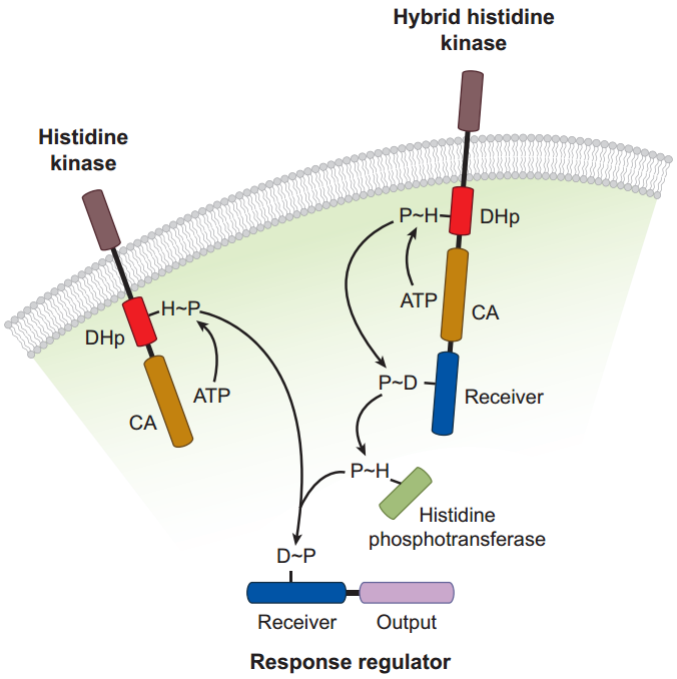

Figure 1.10 – Schematic representation of a standard and hybrid two component system. The catalytic and ATPase (CA) domain of the histidine kinase binds ATP, and catalyses autophosphorylation of the histidine phosphotransferase (DHp) domain. Transfer of the phosphoryl group (P) then occurs to a conserved Asp residue within the response regulator. Phosphorylation of the RR leads to the desired output. In a hybrid system, a phosphotransferase is required to transfer the phosphoryl group to the RR (taken from (Laub and Goulian 2007)).

A typical TCS is comprised of three basic chemical reactions: autophosphorylation, phosphotransfer and dephosphorylation. The first reaction involves the γ-phosphoryl group of ATP being transferred to a conserved histidine residue found in the HK. The phosphoryl group is then transferred to a conserved aspartic acid residue found in the RR. The final dephosphorylation step consists of a hydrolysis reaction between the aspartic acid residue and water. Dephosphorylation can be catalysed by specific phosphatases, such as CheZ in *E. coli* (Zhao *et al*. 2002).

1.4.1 Histidine Kinases

A typical HK structure consists of a diverse sensing domain coupled to a conserved histidine kinase domain. Adaptation of HKs for use in other specific pathways is common in bacterial species due to the modular nature of these proteins. Two distinct classes of HKs have been defined: orthodox and hybrid. Orthodox HKs consist of a sensing domain and a catalytic domain. Hybrid HKs contain other domains, such as a phosphorylation domain. *E. coli* contains 30 different HKs, five of which are hybrid kinases (Mizuno 1997). The organisation and function of HKs can vary (Figure 1.11).

HKs typically function as periplasmic membrane receptors. EnvZ, a sensor kinase, contains two transmembrane α-helices that anchor it to the membrane. Not all HKs are anchored to the membrane. The chemotaxis kinase CheA and the nitrogen regulatory kinase NtrC are both soluble and found in the cytoplasm (Stock *et al*. 1988) (Macfarlane and Merrick 1985). All HKs contain a common catalytic core that

consists of a catalytic and ATPase (CA) domain, and a dimerization and histidine phosphotransferase (DHp) domain (Stock 1999). NMR and crystallographic structures of the catalytic core have been solved: examples include the EnvZ kinase NMR solution structure (Tanaka *et al*. 1998) (Tomomori *et al*. 1999) and the X-ray crystallography structure of the atypical CheA kinase (Bilwes *et al*. 1999) (Figure 1.12).

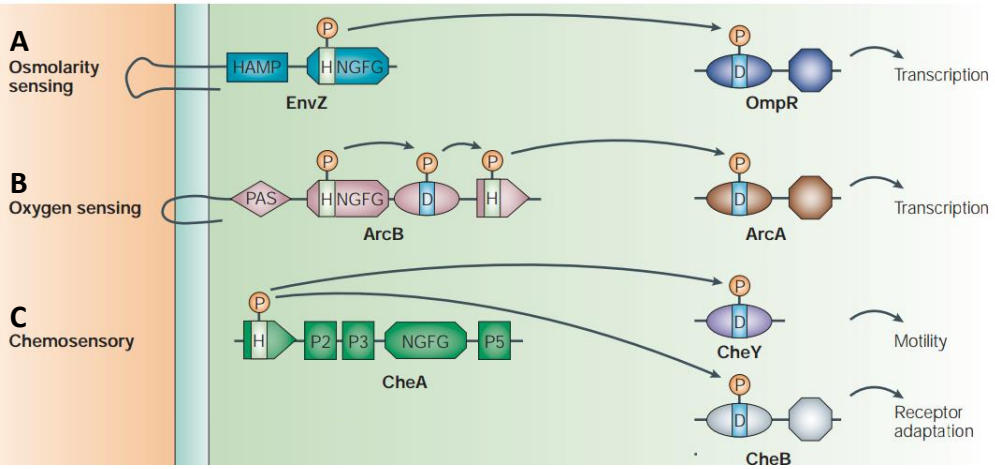

Figure 1.11 – Domain organisation of selected two component systems. **A)** EnvZ/OmpR HAP system of *E. coli* that regulates transcription of outermembrane porins OmpF and OmpC. EnvZ responds to changes in osmolarity and controls the activity of OmpR. **B)** ArcB/ArcA HAP system of *E. coli* senses redox state changes in components of the respiratory electron-transport chain using a PAS (PER, ARNT, SIM) domain. **C)** Chemosensory system of *E. coli* that controls motility. CheA, a soluble HK, consists of five domains (P1-P5) per monomer and senses chemical changes through transmembrane chemoreceptors. Conserved phosphorylatable His residues (light green rectangles), conserved phosphorylatable Asp residues (light blue rectangles) and phosphoryl groups (orange circles) are all highlighted. NGFG indicates the kinase domain. The HAMP domain (histidine kinases, adenylyl cyclases, methyl-binding proteins and phosphatase domains) is a linker domain. For simplicity, HKs are shown as monomers despite their dimeric nature (adapted from (Wadhams and Armitage 2004)).

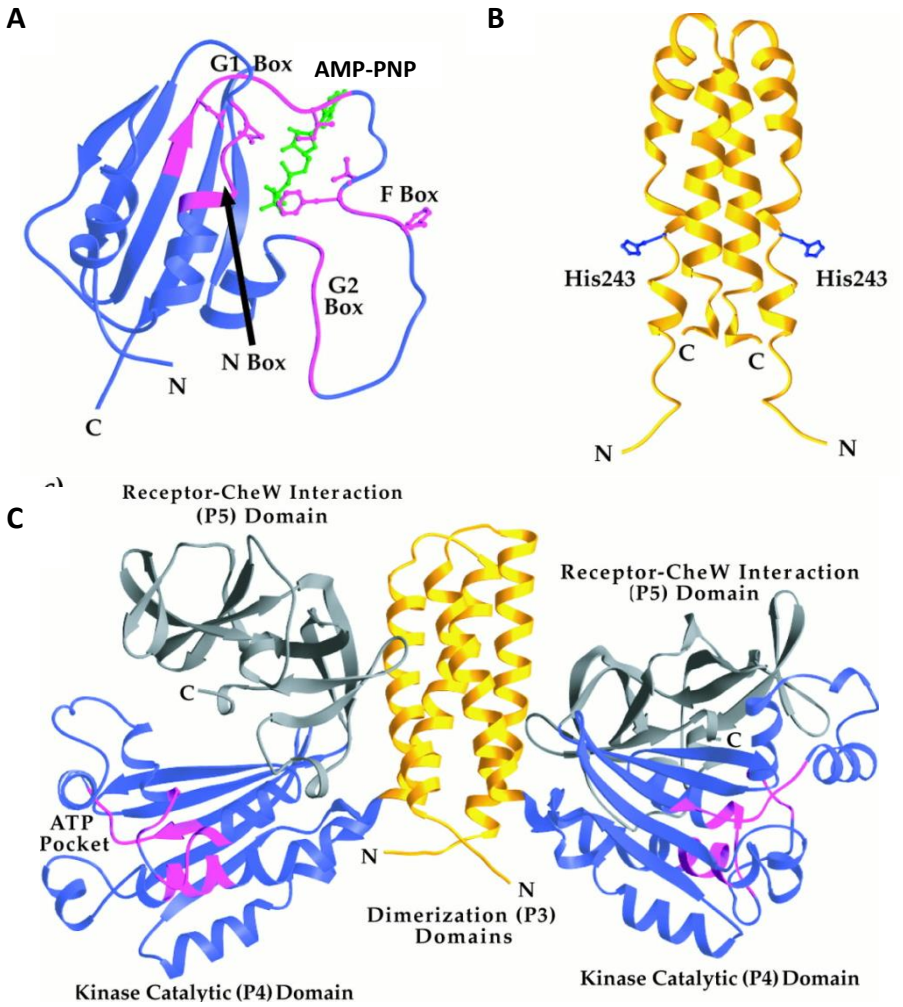

Figure 1.12 – The histidine kinase core. NMR solution structures of the **A)** catalytic domain and **B)** dimerization domain of EnvZ from *E. coli*. **C)** The crystal structure of the CheA dimer (C-terminal half) from *T. maritima*. EnvZ and CheA show high conservation of the kinase core (taken from (Stock, Robinson, and Goudreau 2000)). N, F, G1 and G2 boxes define the nucleotide binding cleft. Adenosine 5'- β, γ-imidotriphosphate (AMP-PNP) is a non-hydrolysable analogue of ATP, which inhibits ATP-dependent reactions.

1.4.2 Response Regulators

Upon activation by a HK, the response regulator/s (kinase dependent) provides the specific output of the TCS. RRs usually consist of two domains; the phosphoryl-

accepting regulatory domain and the variable effector domain (Figure 1.11). The transfer of a phosphoryl group occurs from the conserved His residue of the HK-P (His-P), to a conserved Asp residue in a different domain of the same HK. Of the 32 RRs found in *E. coli*, 25 were found to be DNA-binding effectors. This is the most common output for RRs (Mizuno 1997). The cAMP phosphodiesterase RegA (cAMP signalling) (Thomason *et al*. 1999) and the methylesterase CheB (chemotaxis pathway) (Simms, Keane, and Stock 1985) are examples of RRs that do not bind DNA. CheY binds directly to FliM in the flagellar motor switch complex (Welch *et al*. 1993). The typical regulatory domain of a RR contains a core of five parallel β-strands surrounded by five α-helices (Stock *et al*. 1989) (Figure 1.13).

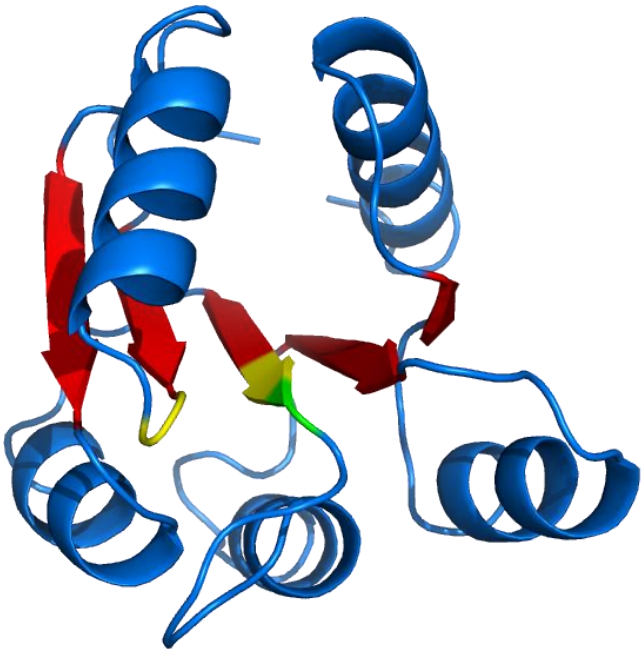

Figure 1.13 – The CheY response regulator from *E. coli*. A typical regulatory domain is seen containing five α-helices (blue) and five β-strands (red). The phosphorylatable D56 residue (green) and the conserved acidic pocket (D12, D13 and S55 (yellow)) are highlighted (Structural co-ordinates obtained from PDB:3CHN).

The conserved phosphorylatable aspartate residue is located between β3 and α3 on an exposed loop (Sanders, Gillece-Castro, *et al*. 1989). This Asp residue sits in an 'acidic pocket' with two other acidic residues (both Asp in CheY), a conserved Ser and a conserved Thr. A magnesium ion is coordinated within this acidic pocket. The magnesium ion is vital for phosphotransfer and dephosphorylation (Lukat, Stock, and Stock 1990). The central cores of RRs are well conserved across bacterial species. Divergences in structure become apparent in the surrounding α-helices and surface loops (Feher *et al*. 1997) (Djordjevic *et al*. 1998).

With such a diverse range of RRs and effector domains, a common activation mechanism is unlikely. However, some evidence suggests that the shift between the active and inactive states of RR regulatory domains affect the variable effector domains in a similar manner. For instance, the variable effector domains of NtrC and PhoB induce dimerization upon phosphorylation (Fiedler and Weiss 1995). The short half-life of phosphorylated RRs (RR-P) has hindered the elucidation of structural information on the active and inactive conformations of RRs. Hence, determining the mechanisms involved in activation has been difficult. Some NMR studies have been able to detect large shifts in conformation upon Mg^{2+} binding or activation (Kojetin *et al*. 2005), but crystal structures have largely disagreed. For instance, X-ray crystallography indicated that conformational changes upon Mg^{2+} binding were the same as upon phosphorylation, however, NMR studies disagreed with these findings (Jiang *et al*. 1997) (Lowry *et al*. 1994) (Bellsolell *et al*. 1994).

1.5 Bacterial Chemotaxis

1.5.1 *E. coli* Chemotaxis

Chemotactic behaviour is dependent on the capacity to control tumbling frequencies in response to chemical stimuli. A link must therefore be established between environmental conditions (input) and the flagellar motor (output). A modified TCS (as discussed above) is utilised to form this link. The most studied and best understood chemotaxis pathway is that of *E. coli* (Wadhams and Armitage 2004). It contains a HK (CheA) and two RRs (CheB and CheY). CheA is an atypical HK as it does not detect chemical stimuli directly. Instead, CheA interacts with transmembrane chemoreceptors termed methyl-accepting chemotaxis proteins (MCP). The CheA-MCP interaction is coupled by the adaptor protein CheW and CheA interacts directly with the response regulators CheB and CheY (Wadhams and Armitage 2004) (Figure 1.14).

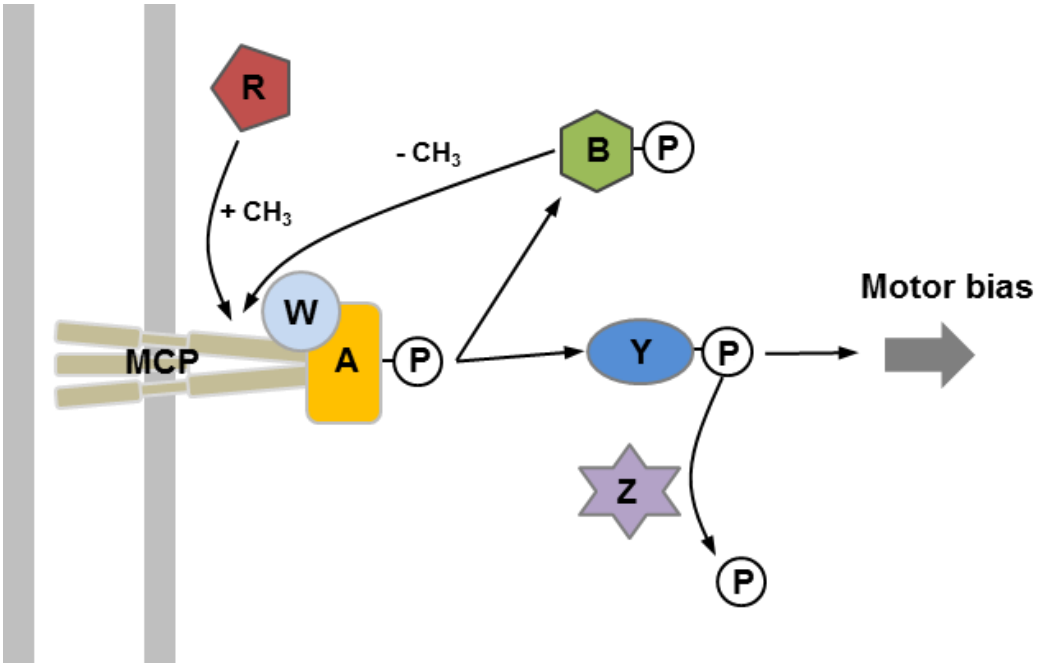

Figure 1.14 – The chemosensory network of *E. coli* - Transmembrane MCPs sense changes in chemoeffector concentrations. These MCPs transduce a signal, through CheW, to CheA. Upon ligand binding of specific repellents to the MCPs, CheA is autophosphorylated. Phosphotransfer then occurs from phosphorylated CheA (CheA-P) to either of its response regulators CheB or CheY. The methylesterase CheB-P mediates adaptation in conjunction with the methyltransferase CheR. CheY-P binds to the motor switch complex and promotes a change in direction of rotation (counter clockwise to clockwise) causing the cell to tumble. The specific phosphatase CheZ dephosphorylates CheY-P which allows signal termination.

Chemoreceptors

Direct spatial sensing of chemical gradients is not possible on micrometre scale environments, as a bacterial cell body is too small. Bacteria instead use temporal sensing, by comparing previous conditions to present conditions. MCP clusters are used as a primitive form of memory, where adaptation occurs to continual stimuli (Vladimirov and Sourjik 2009). Spanning the plasma membrane, the MCPs sensing

domain is located in the periplasmic space. Hence, MCPs detect chemical stimuli within the periplasm. This information is transduced across the membrane and into the cytoplasm. MCPs exist as homodimers, and further assemble as trimers of dimers. Thousands of trimers of dimers form a hexagonal array with chemotaxis proteins CheA and CheW at the cell poles (Figure 1.15). This conformation is specifically required for CheA control, and not transmembrane signalling or ligand binding (Boldog *et al*. 2006). *E. coli* contains four MCPs and one redox receptor that sense a diverse range of chemical stimuli. These include sugars, amino acids, dipeptides and redox potential (Taylor 2007). Some MCPs have multiple mechanisms for detecting chemical stimuli. For instance, the Tar MCP senses maltose through interactions with maltose-binding-protein, and senses aspartate through direct binding (Mowbray and Koshland 1987). Upon ligand binding, a transmembrane α-helix shifts and rotates (piston like displacement) to transduce a signal across the membrane (Chervitz and Falke 1996). This alters the interactions between CheA, CheW and the distal tip of the MCPs, which changes the rate of autophosphorylation of CheA (Hazelbauer and Lai 2010).

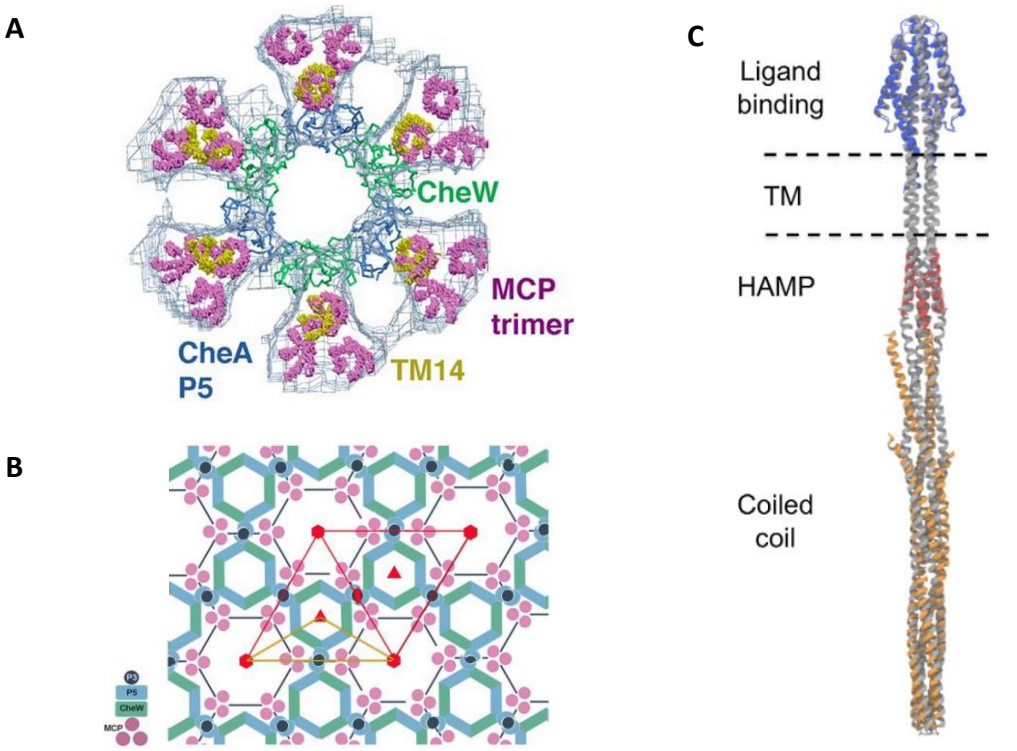

Figure 1.15 – **A)** The quaternary structure of the chemotaxis proteins CheA.P5 (blue), CheW (green) and MCP trimers (pink) from *T. maritima*. **B)** The arrangement of the components produces a large hexagonal array, with a CheA:CheW:MCP subunit stoichiometry of 1:1:6 (adapted from (Briegel *et al*. 2012)). **C**) Side view of a MCP dimer (taken from (Hall, Armitage, and Sansom 2012))

CheA

CheA activity controls the concentration of phosphorylated CheY (CheY-P) within the cell. CheA has five domains (P1-P5). The P1 domain contains the phosphorylatable histidine residue and catalyses the transfer of the phosphoryl group to the RRs. The P2 domain binds the competing RRs CheY and CheB, the P3 domain is involved in homodimerization and the P4 domain (kinase domain) phosphorylates P1. The regulatory domain P5 binds the chemoreceptors and CheW, and controls kinase activity in response to chemoreceptor signalling. Increasing the

autophosphorylation of CheA increases the concentration of CheY-P and hence, an increase in cell tumbling is observed. Decreasing the autophosphorylation rate of CheA has the opposite effect. As CheY-P concentration decreases, fewer tumbling events occur and extended runs are observed.

CheW

CheW interacts with the regulatory domain (P5) of CheA and the signalling domain of the chemoreceptors. CheW is essential for linking the activity of CheA to the signalling state of the chemoreceptors. Polar cluster formation is dependent on CheW (Maddock and Shapiro 1993). Deletion of *che*W in *E. coli* produces a smooth swimming strain as CheA can no longer be activated (Sanders, Mendez, and Koshland 1989).

CheY

CheY-P is able to bind to the switch complex of the flagellar motor. With sufficient CheY-P concentration, a tumbling event is triggered by a switch in rotation of the motor (Welch *et al*. 1993). CheY is discussed in more detail in Section 1.6.

CheB and CheR

Bacterial species require a mechanism by which they can compare present conditions to recently experienced conditions. CheB is another response regulator phosphorylated by CheA. CheB contains a methylesterase domain and acts alongside

CheR (a methyl-transferase) to form the adaptation system. This adaptation system allows bacterial species to sense and respond to relative environmental changes.

CheB (methylesterase) and CheR (methyltransferase) both interact with specific glutamate and glutamine residues found in MCPs. The methylation state of these glutamate residues modulates the sensitivity of the MCP to stimuli (Hazelbauer and Engstrom 1981). CheR is constitutively active. Upon phosphorylation by CheA, CheB activity increases 100-fold (Anand, Goudreau, and Stock 1998). Binding of attractant to the MCPs results in a decrease in CheA activity, therefore reducing the CheB-P concentration. This causes an increase in methylated MCPs, decreasing their affinity for ligand. Decreased ligand binding leads to increased CheA activity and therefore an increase in CheB-P. The increased CheB-P returns the MCPs to their pre-stimulus state (Hazelbauer, Falke, and Parkinson 2008).

CheZ

CheZ is a phosphatase, that dephosphorylates CheY-P (Zhao *et al*. 2002). It reduces the half-life of CheY-P from ~20 s to ~200 ms (Lukat and Stock 1993) (Wadhams and Armitage 2004). This fast rate of CheY-P dephosphorylation allows bacteria to respond quickly to environmental changes whilst moving. Deletion mutants lacking CheZ are found to tumble excessively; the reduced rate of signal termination results in continuous signalling from longer-lived CheY-P.

Due to its relative simplicity and ease of output measurement (CCW or CW rotation), the chemotaxis pathway of *E. coli* became the paradigm of the chemotaxis system. Genomic analysis of motile bacterial species revealed more than 50% contained multiple homologues of the core chemotaxis proteins (CheA, CheB, CheR, CheW and CheY) (Hamer *et al*. 2010). Therefore, *E. coli* based models may be insufficient to describe more complicated chemotactic signalling in other species.

1.5.2 *Rhodobacter sphaeroides* Chemotaxis

R. sphaeroides has two chromosomes (CI and CII) that contain multiple sets of homologous chemotaxis genes, which are encoded in three operons (*che*Op_1, *che*Op_2 and *che*Op_3) and several loci (*che*BRA and *che*Y_4-*mcp*G) (Hamblin *et al*. 1997) (Figure 1.16). *che*Op_1 and *che*BRA are not expressed or required for chemotaxis under laboratory conditions (Porter *et al*. 2008). Known chemotaxis proteins include: 13 MCPs, six CheY homologues, four CheW homologues, four CheA homologues, three CheR homologues and two CheB homologues. *R. sphaeroides* does not have a CheZ homologue.

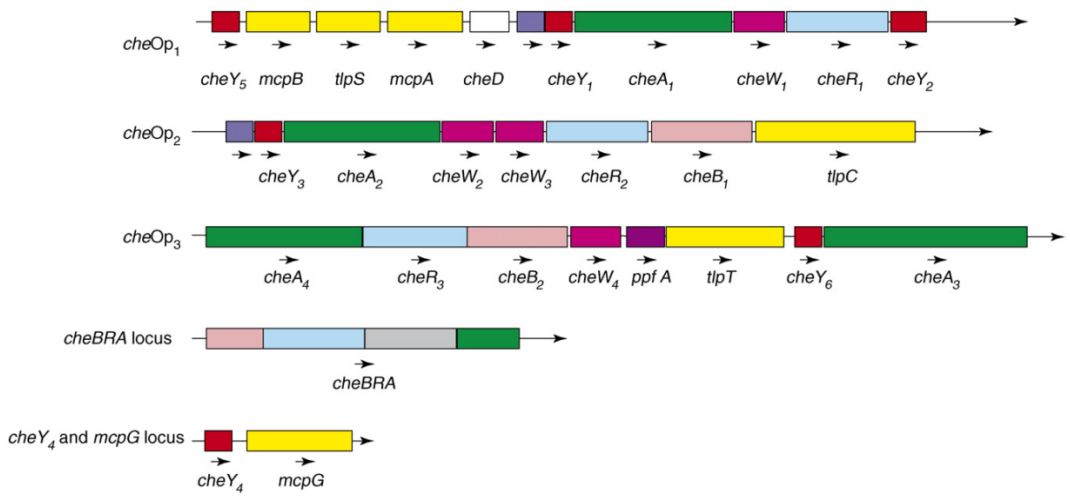

Figure 1.16 – The chemotaxis operons and loci of *R. sphaeroides*. *che*Op1, *che*Op2, *che*Op3 and *che*BRA are encoded on chromosome I. The *che*Y_4-*mcp*G locus is encoded on chromosome II (taken from (Porter *et al*. 2008)).

The *R. sphaeroides* genome also encodes two different sets of flagellar motor genes (*fla*1 and *fla*2) (Poggio *et al*. 2007). Only *fla*1 (single sub-polar flagellum) is expressed under laboratory conditions. However, *fla*2 expressing cells were isolated using a Δ*fla*1 mutant (Poggio *et al*. 2007). Further analysis revealed that *fla*2 expression produces a tuft of polar flagella controlled by *che*Op_1 (Del Campo *et al*. 2007).

Early studies of *R. sphaeroides* investigated the function and purpose of having multiple copies of *che* genes, and looked to compare their function to the *E. coli* model. *che*Op_2 and *che*Op_3 signalling behave in a similar way to the *E. coli* system, but with some key differences. Fluorescent protein fusions and immuno-gold electron microscopy showed two regions of localisation within *R. sphaeroides* (Wadhams *et al*. 2003). *che*Op_2 chemotaxis proteins (excluding TlpC) localise at the cell pole with transmembrane chemoreceptors (MCPs) (Wadhams, Martin, and

Armitage 2000). *che*Op$_3$ chemotaxis proteins localise approximately at mid cell to form the cytoplasmic cluster (Figure 1.17). Chemoreceptors found at the cytoplasmic cluster lack a transmembrane domain and are termed transducer like proteins (Tlps). TlpC and TlpT have been shown to localise to the cytoplasmic cluster (Wadhams *et al*. 2003) (Wadhams *et al*. 2002).

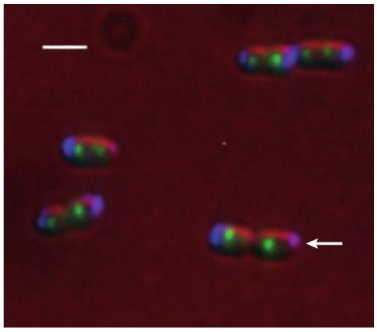

Figure 1.17 – The transmembrane (CheW$_3$ – blue) and cytoplasmic (CheW$_4$ - green) chemotaxis clusters of *R. sphaeroides*. The scale represents 2 μm (taken from (Porter, Wadhams, and Armitage 2011)).

Both chemosensory clusters are necessary for *R. sphaeroides* to be fully chemotactic. The polar cluster is thought to sense changes in the external environment, whereas the cytoplasmic cluster is thought to sense the metabolic state of the cell (Figure 1.18). Deletion of any component of either cluster leads to loss of chemotaxis. Although swapping localisation domains of the CheA kinases leads to switching of their localisation, chemotaxis is abolished which suggests a high level of specificity to its particular cluster (Scott *et al*. 2010).

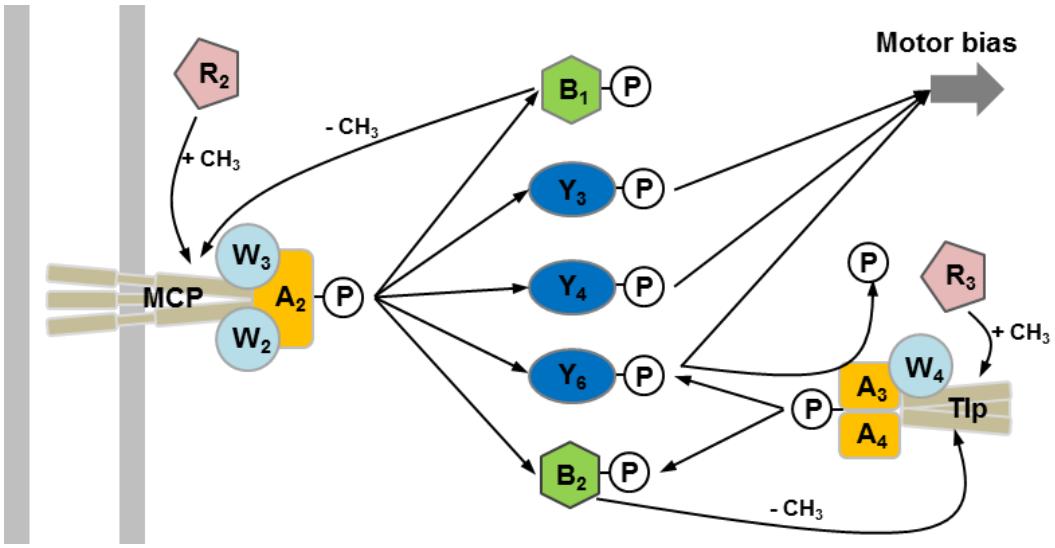

Figure 1.18 – The chemosensory network of *R. sphaeroides* – Two distinct signalling clusters of chemoreceptors are observed, the transmembrane cluster (MCPs) which senses the periplasmic concentration of attractants and the cytoplasmic cluster (Tlps) which senses the metabolic state of the cell. Specific CheA and CheW homologues localise to each cluster. Numerous response regulators are phosphorylated by both $CheA_2$ and $CheA_3$. Some RRs such as $CheY_3$ are kinase specific; others like $CheY_6$ can be phosphorylated by kinases found in both clusters. $CheY_6$-P is required to stop rotation of the motor and either $CheY_3$-P or $CheY_4$-P is required to maintain a chemotactic phenotype.

The polar cluster in *R. sphaeroides* is similar in composition to that of the *E. coli* polar cluster. A hexagonal array was found for the MCPs quaternary structure in *R. sphaeroides* (Briegel *et al*. 2014). It is therefore thought that signal transduction occurs in a similar manner. This cluster contains a single CheA ($CheA_2$) and two CheW ($CheW_2$ and $CheW_3$) homologues. The purpose of two CheW proteins is still unclear. *In vitro* studies have shown $CheA_2$ is able to transfer phosphoryl to RRs $CheB_1$, $CheB_2$, $CheY_3$, $CheY_4$ and $CheY_6$. *In vivo* studies have provided evidence that

$CheB_2$ and $CheY_6$ are mainly associated with the cytoplasmic cluster, indicating their predominant interactions. Localisation experiments have provided evidence that $CheY_6$ localises to the cytoplasmic cluster, and $CheY_3$ and $CheY_4$ localise to the polar cluster (Porter *et al*. 2006). The cytoplasmic cluster of *R. sphaeroides* is considerably different to both its own polar cluster and the polar cluster of *E. coli*. Two CheA homologues are located there, $CheA_3$ and $CheA_4$. A typical CheA histidine kinase is comprised of five domains (P1-P5). Both $CheA_3$ and $CheA_4$ are atypical kinases, with $CheA_3$ made of only P1 and P5 domains and $CheA_4$ the P3, P4 and P5 domains. Neither CheA can trans-autophosphorylate as a homodimer, so a different mechanism is used. The kinase domain (P4) of $CheA_4$ phosphorylates the P1 domain of $CheA_3$. Phosphotransfer then occurs from $CheA_3$ to either (and only) $CheB_2$ or $CheY_6$ (Porter *et al*. 2008) (Figure 1.18).

R. sphaeroides does not have a CheZ homologue. The long linker region (794 amino acids, instead of P2, P3 and P4) between P1 and P5 of $CheA_3$ has been shown to act as a $CheY_6$-P phosphatase (Porter *et al*. 2008). Not much is known about the structure of the long linker region. Pondr (Predictor of naturally disordered regions) software (Li *et al*. 1999) indicates that the long linker region contains ordered and disordered regions. This phosphatase activity is necessary to achieve rapid signal termination and for chemotactic ability.

CheB and CheR proteins are thought to be responsible for adaptation of the chemoreceptors encoded in the same operon. For example, $CheR_2$ is responsible for

polar cluster adaptation. Cross-talk between clusters has been suggested as $CheA_4$ is able to transfer a phosphoryl group to $CheA_2$ and $CheA_3$ (Porter and Armitage 2004). However, this seems unlikely as $CheA_4$ does not localise to the transmembrane cluster.

Six CheY homologues have been found in *R. sphaeroides*, three of which are expressed under laboratory conditions ($CheY_3$, $CheY_4$ and $CheY_6$). $CheY_3$ and $CheY_4$ only interact with the polar cluster whereas $CheY_6$ mainly interacts with the cytoplasmic cluster (Porter *et al*. 2006). $CheY_6$ was shown to be essential for chemotaxis, whereas $CheY_3$ and $CheY_4$ have some functional redundancies. Only $CheY_6$ is able to trigger a tumbling event. Although $CheY_6$ can stop the motor alone, *R. sphaeroides* requires the presence of either $CheY_3$ or $CheY_4$ to retain its chemotactic ability (Porter *et al*. 2006). This would suggest different roles of each CheY in signal transduction and upon binding to the switch complex.

1.6 The CheY Response Regulator

E. coli CheY is a 14 kDa response regulator that interacts with CheA, FliM and CheZ. CheB and CheY compete for binding to the P2 domain (CheY/CheB binding domain) of CheA (Li *et al*. 1995). Phosphotransfer occurs from the histidine residue (H48) in the P1 domain of CheA to the aspartic acid (D57) residue of CheY (Sanders, Gillece-Castro, *et al*. 1989) (Borkovich and Simon 1989). CheY undergoes a conformational change upon phosphorylation, increasing its binding affinity (from 680 μM to 27 μM, 20-fold stronger) to the FliM component of the switch complex in the flagellar motor

(Bren and Eisenbach 1998). In *E. coli*, sufficient FliM-CheY-P binding triggers a tumbling event by switching flagellar motor rotation from CCW to CW (Welch *et al*. 1993). In *R. sphaeroides*, rotation of the flagellar motor is stalled by $CheY_6$-P (Porter *et al*. 2008). The autophosphatase activity of $CheY_{EC}$-P displays first order kinetics ($t_{1/2}$ = ~20s). In *E. coli*, CheZ enhances this activity by a factor of 100 (Lukat and Stock 1993).

The structure of unphosphorylated $CheY_{EC}$ has been determined several times by X-ray crystallography (Figure 1.19) (the first structure by (Volz and Matsumura 1991)). It consists of five α-helices and five β-strands in the classic RR fold, where the α-helices surround the β-strands. The conserved site of phosphorylation, D57, forms a Mg^{2+}-binding acid pocket with D12 and D13. A salt bridge is formed between the highly conserved K109 and the carboxylic acid group of D57. Upon phosphorylation, the sidechain of Y106 switches from surface exposed to buried (Zhu *et al*. 1996) (Zhu *et al*. 1997). An unphosphorylated mutant of CheY (D13KY106W - phosphorylation state mimic) is able to bind FliM to the same extent as CheY-P (Scharf *et al*. 1998). This evidence suggests that the increased affinity CheY-P has for FliM is not a product of phosphorylation, but instead a conformational shift induced by phosphorylation. In agreement with this, the site of phosphorylation (D57) is distant from the FliM binding site (α4).

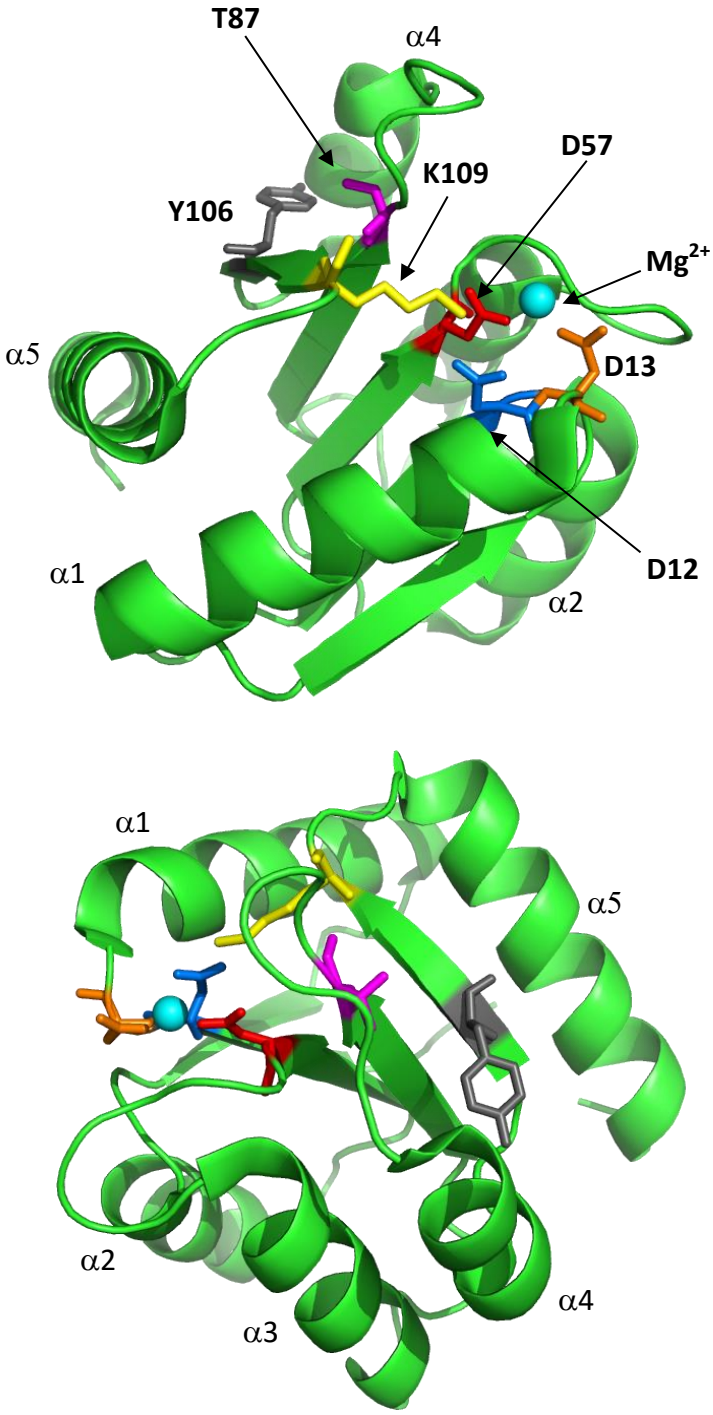

Figure 1.19 – The structure of unphosphorylated *E. coli* CheY with a coordinated magnesium ion (cyan), in two different orientations. Important residues have been highlighted: D12 (blue), D13 (orange), D57 (red), Y106 (grey), K109 (yellow) and T87 (magenta). (Structural co-ordinates obtained from PDB:1CHN).

1.6.1 The Classic Y-T Switch Mechanism

In the CheY response regulator family, positions 87 and 106 are highly conserved as a threonine/serine residue and an aromatic residue, respectively. In CheY, Y106 can either be solvent exposed (outside) or buried (inside) (Zhu *et al*. 1997). The conformation of T87 has been postulated to influence the side-chain conformation of Y106 (Ganguli *et al*. 1995). In the structure of CheY-T87I, the mutation forces the side-chain of Y106 to be solvent exposed in both the apo and the phosphorylated states. *In vivo* studies showed a non-chemotactic phenotype (smooth swimming) and *in vitro* work found it could still be phosphorylated. Combining these results suggest this mutant cannot undergo activation by phosphorylation due to steric hindrance (Ganguli *et al*. 1995). In a mutant containing CheY-Y106W, cells tumble more frequently than in wild type. It is thought the W106 side-chain is always buried, and therefore mimics the active state. The double mutant CheY-T87I/Y106W confers the same phenotype as T87I, probably due to I87 forcing the W106 side-chain to be solvent exposed. The structural and behavioural studies indicate that the side-chain orientation of Y106 is involved in activation upon phosphorylation (Jiang *et al*. 1997). Crystal structures of T87I and Y106W $CheY_{EC}$ mutants have been produced and their conformations examined (Figure 1.20). The simplest model would state the 'in' position corresponds to the active form and the 'out' position corresponds to the inactive form.

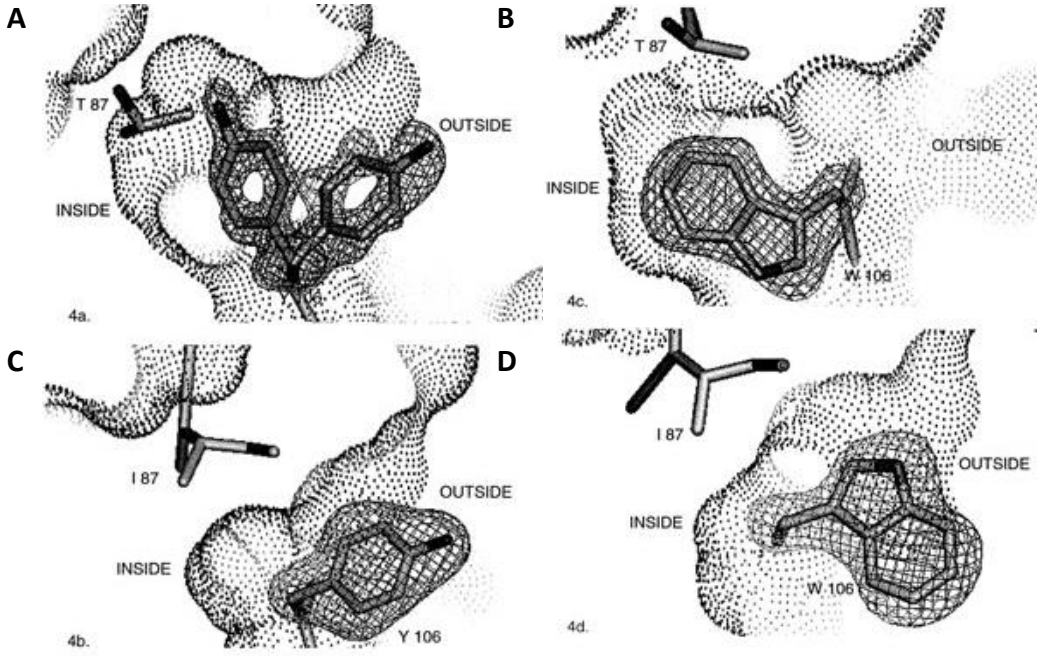

Figure 1.20 – Zoomed in region of mutant CheY proteins showing the different orientations of T87 and Y106. **A)** Wild type CheY. **B)** CheY-Y106W. **C)** CheY-T87I. **D)** CheY-T87I/Y106W (taken from (Zhu *et al*. 1997)).

1.6.2 Active-Inactive State Dynamics

Growing evidence suggests that response regulator conformational states exist as a dynamic equilibrium between inactive (unphosphorylated) and active (phosphorylated) forms. Perturbations like phosphorylation or specific mutations then force the equilibrium towards the active conformation. This is known as the equilibrium shift model (Figure 1.21). In this model, both active and inactive states exist without any external perturbations. In contrast, the induced fit model (Figure 1.21) predicts phosphorylation and conformational switching are concomitant. The induced fit model suggests that the active conformation cannot be formed until phosphorylation occurs. Nuclear magnetic resonance (NMR) studies of the response

regulators NtrC and Spo0F have demonstrated dynamic structural changes (on the ms to μs time scale) consistent with coordinated conformational fluctuations (Feher and Cavanagh 1999) (Volkman *et al*. 2001). The authors suggested the fluctuations were a result of conformational switching between active and inactive states.

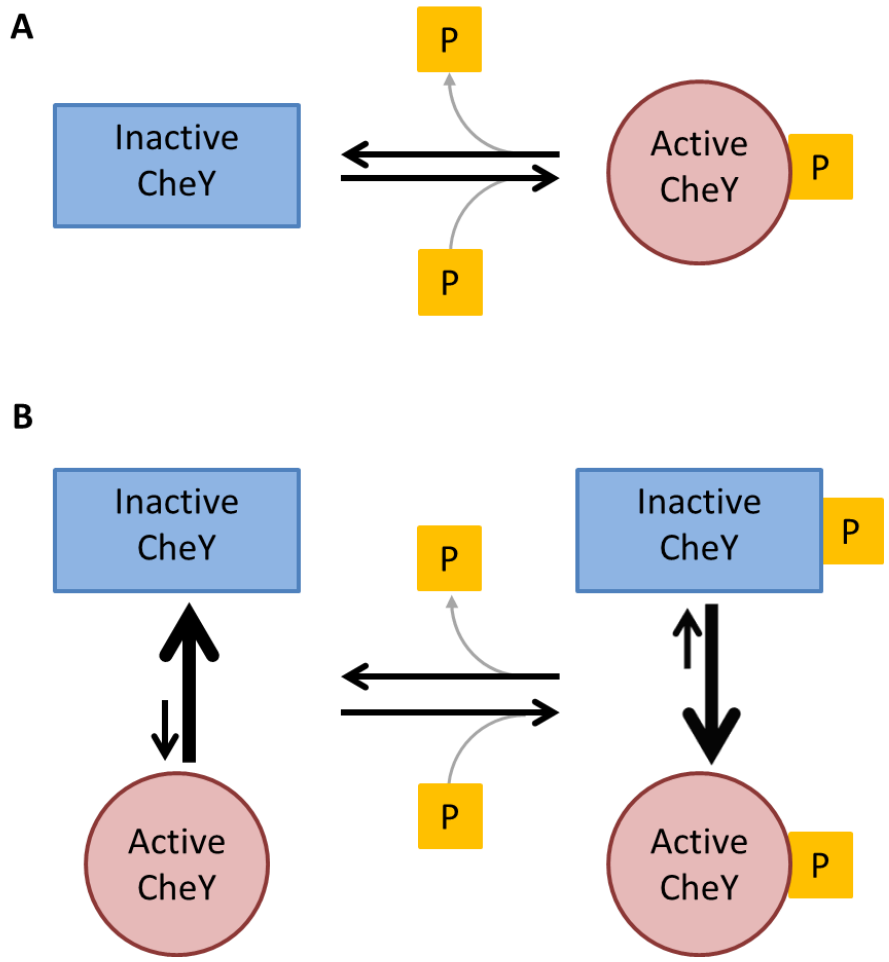

Figure 1.21 – Two different activation models of CheY. **A)** The induced fit model. Phosphorylation switches CheY from an inactive to an active conformation. **B)** The equilibrium shift model. Phosphorylation stabilises the active conformation and forces the equilibrium towards this conformation.

The N-terminal region of *E. coli* FliM ($FliM_{16}$, 1-16) has been identified as the main site of CheY interaction. The equilibrium shift model would predict the unphosphorylated Mg^{2+}-CheY bound to $FliM_{16}$ (N-terminus) to have the same structure as CheY-P. Evidence has shown this to be partially true. The network of conserved residues demonstrated active-like conformations in agreement with the equilibrium shift model. However, more remote regions from the binding site such as $\alpha1$ and the $\beta5$-$\alpha5$ loop showed poor agreement (Figure 1.22). Phosphorylation therefore seems to be a prerequisite for a complete conformational shift from inactive to active (Dyer and Dahlquist 2006).

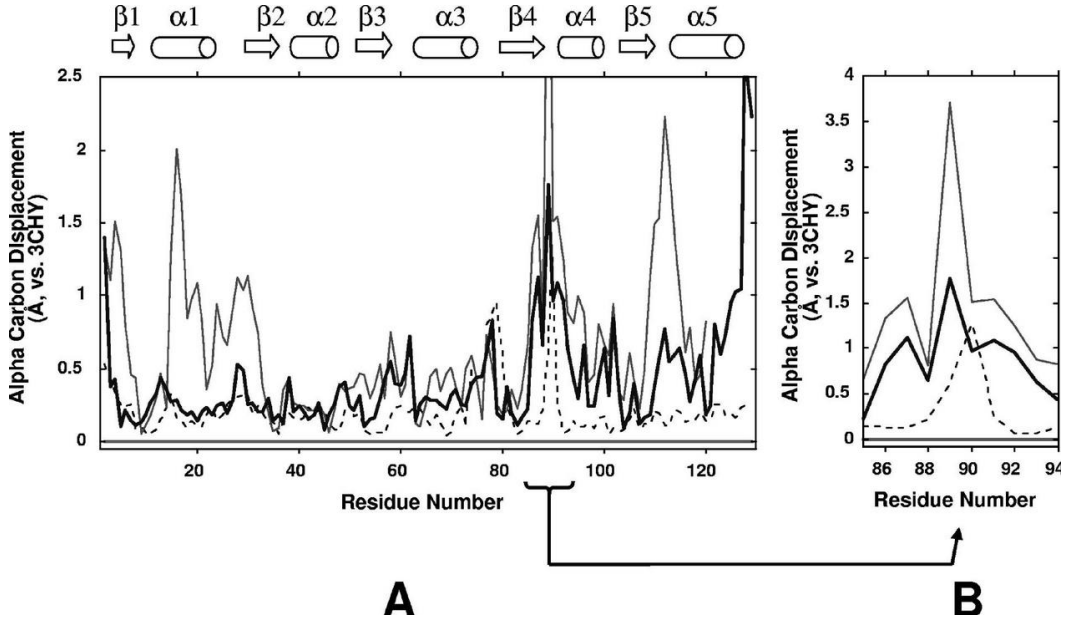

Figure 1.22 – Displacement of C_α atoms in CheY-$FliM_{16}$ (heavy line, PDB 2B1J), CheY-BeF_3^- (light upper line, PDB 1F4V) and meta-active apo-CheY substructure (dashed line, PDB 1JBE) following a least-squares overlay with inactive CheY (3CHY). **A)** Shows displacement of all residues. **B)** Zoomed in section of $\beta4$-$\alpha4$ loop (taken from (Dyer and Dahlquist 2006)).

1.6.3 CheY Interactions with CheA

The interactions between *E. coli* CheA and CheY have been investigated using techniques such as NMR and X-ray crystallography. Nuclear Overhauser effect spectroscopy (NOESY) experiments were used to probe the CheA-CheY interaction (Mo *et al*. 2012). In total, 26 intermolecular NOEs were observed between CheY and CheA.P1 (Figure 1.23). The major interaction interface was between the α1 region (N-terminus, residues 16, 18-20, 23, 24) of CheY and the α1 region (N-terminus, residues 3, 5, 8 and 11-16) of CheA. $^{1}H,^{15}N$-HSQC perturbations using a spin label were in excellent agreement with the NOE data (Mo *et al*. 2012).

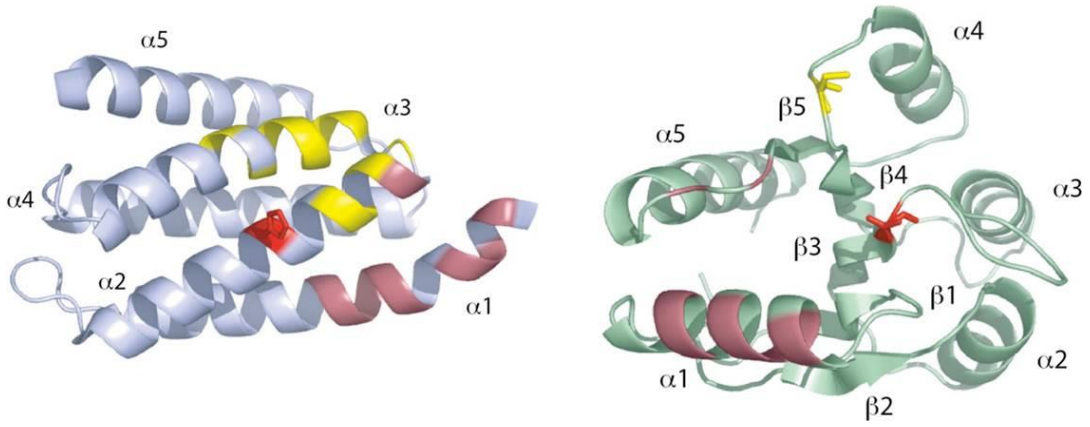

Figure 1.23 – CheA-CheY (left and right respectively) interactions using NMR. Residues giving intermolecular NOEs are highlighted in dark red. The phosphorylatable histidine and aspartic acid residues are shown in bright red. Paramagnetic broadening of P1 amide resonances by the E89C spin labelled variant are indicated in yellow (taken from (Mo *et al*. 2012)).

The chemosensory network of *E. coli* has been characterised extensively (Baker, Wolanin, and Stock 2006). Other bacterial species contain more complex chemosensory networks. *R. sphaeroides* contains four CheA homologues and eight

RR proteins. The CheAs display differing phosphotransfer specificity (Porter *et al*. 2006) (Martin *et al*. 2001). As discussed earlier, the histidine kinases found at the cytoplasmic cluster ($CheA_3$ and $CheA_4$) are atypical. $CheA_3$-P is a specific phosphodonor for $CheY_1$, $CheY_6$ and $CheB_2$. The $CheY_6$-$CheA_3$P1 crystal structure has been solved and gives insight into the binding activity (Bell *et al*. 2010) (Figure 1.24).

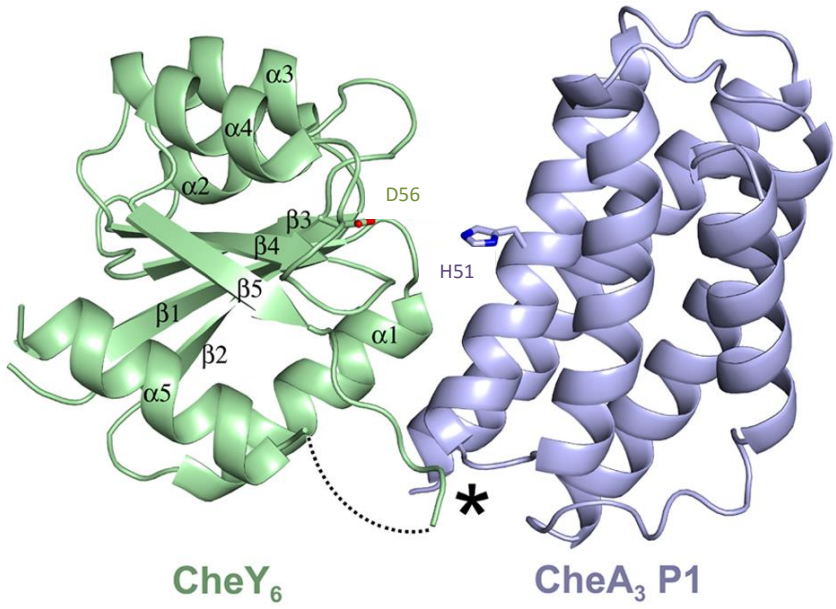

Figure 1.24 – Crystal structure of the $CheA_3$P1.$CheY_6$ complex. The H51 phosphodonor of $CheA_3$ (green) and the D56 phosphoacceptor of $CheY_6$ (blue) are highlighted. Residues 113-118 showed no electron density so are represented with a dotted line (taken from (Bell *et al*. 2010)) (PDB:3KYJ).

The interaction interface between $CheY_6$ and $CheA_3$P1 is dominated by hydrophobic interactions with one hydrogen bond and no salt bridges. A weak interaction is indicated as the buried surface area is small (530 $Å^2$). With the transient nature of the interaction, a weak interaction is to be expected. The major site of interaction is located at the N-terminal end of α1 on $CheY_6$ and αA/αB on $CheA_3$P1 and accounts for ~70% of the total buried surface area. The helices αA (I11, L14 and Y15) and αB

(N56, V59 and L60) of $CheA_3$ form a hydrophobic pocket, in which the methionine finger (M13) protruding from α1 of $CheY_6$ fits neatly. This accounts for 60% of the binding interface. A sequence alignment of the RRs showed that only $CheY_6$ and $CheB_2$ have this Met residue. $CheA_3$-P is unable to phosphorylate the other RRs $CheY_2$, $CheY_3$, $CheY_4$, $CheY_5$ and $CheB_1$ (Porter and Armitage 2004) (Porter and Armitage 2002). Attempts have been made to give $CheY_3$ and $CheY_4$ specificity for $CheA_3$. Mutation of $CheY_3$ and $CheY_4$ (P12AS13M) allowed successful phosphotransfer from $CheA_3$P1-P (P12 was mutated due to concerns of cis-trans isomerisation) (Bell *et al*. 2010). This demonstrated that substituting two residues is sufficient to alter the phosphotransfer specificity of some RRs.

1.6.4 CheY interactions with FliM

In vivo fluorescence resonance energy transfer (FRET) experiments have been used to investigate the interaction of CheY-P with FliM (Figure 1.25). Chemoeffectors were used to generate a chemotactic response. Addition of chemoattractant triggers an exponential decay of CheY bound to FliM with a rate constant of 2 s^{-1}. Removal of the chemoattractant increased the FliM occupancy with a rate constant of 20 s^{-1} (Sourjik and Berg 2002).

A number of FliM (both N-terminal peptide and full length) bound CheY (CheY-BeF_3^-) crystal structures have been solved, including that of *E. coli* and *T. maritima* (Ahn *et al*. 2013). Comparison of these two structures revealed similar interfaces of interaction (Figure 1.26).

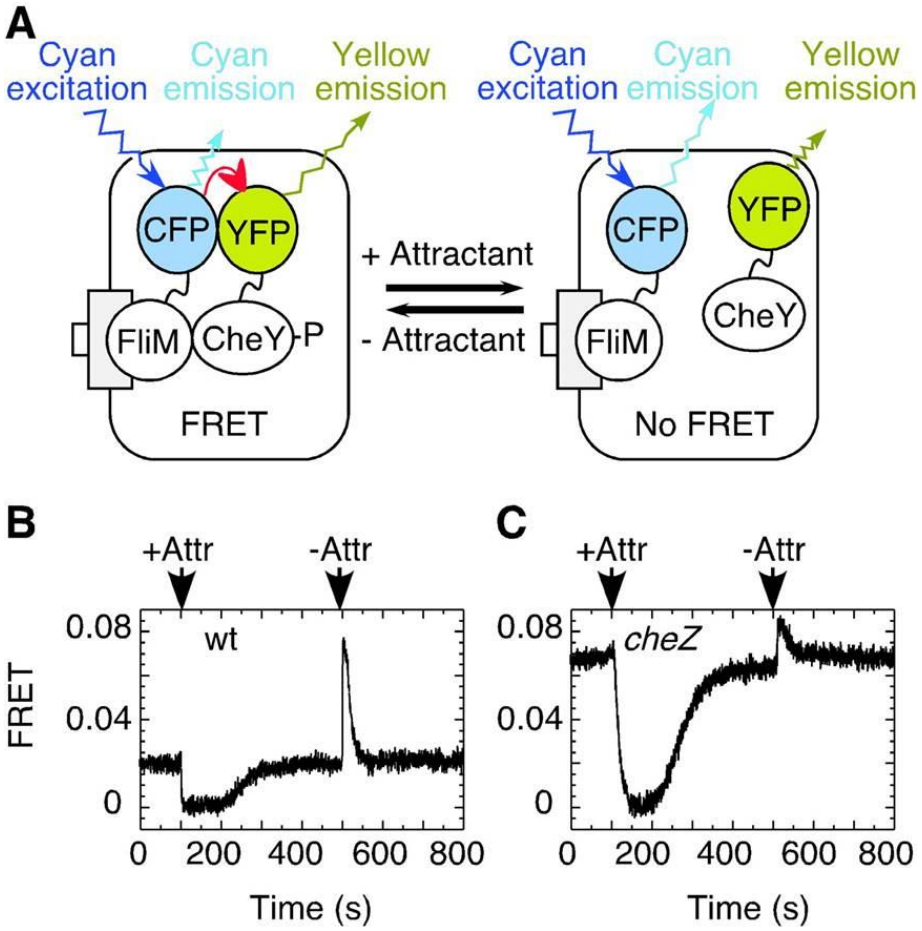

Figure 1.25 – Fluorescence resonance energy transfer (FRET) of the interaction of CheY with FliM. **A)** Schematic outlining the principles of FRET. Addition and removal of attractant 30 µM α-methylaspartate) to **B)** wild type cells and **C)** Δ*che*Z cells. Δ*che*Z cells show a higher level of FRET due to a higher steady-state level of CheY-P. The subsequent increased half-life upon addition of attractant leads to a slower response (taken from (Sourjik and Berg 2002)).

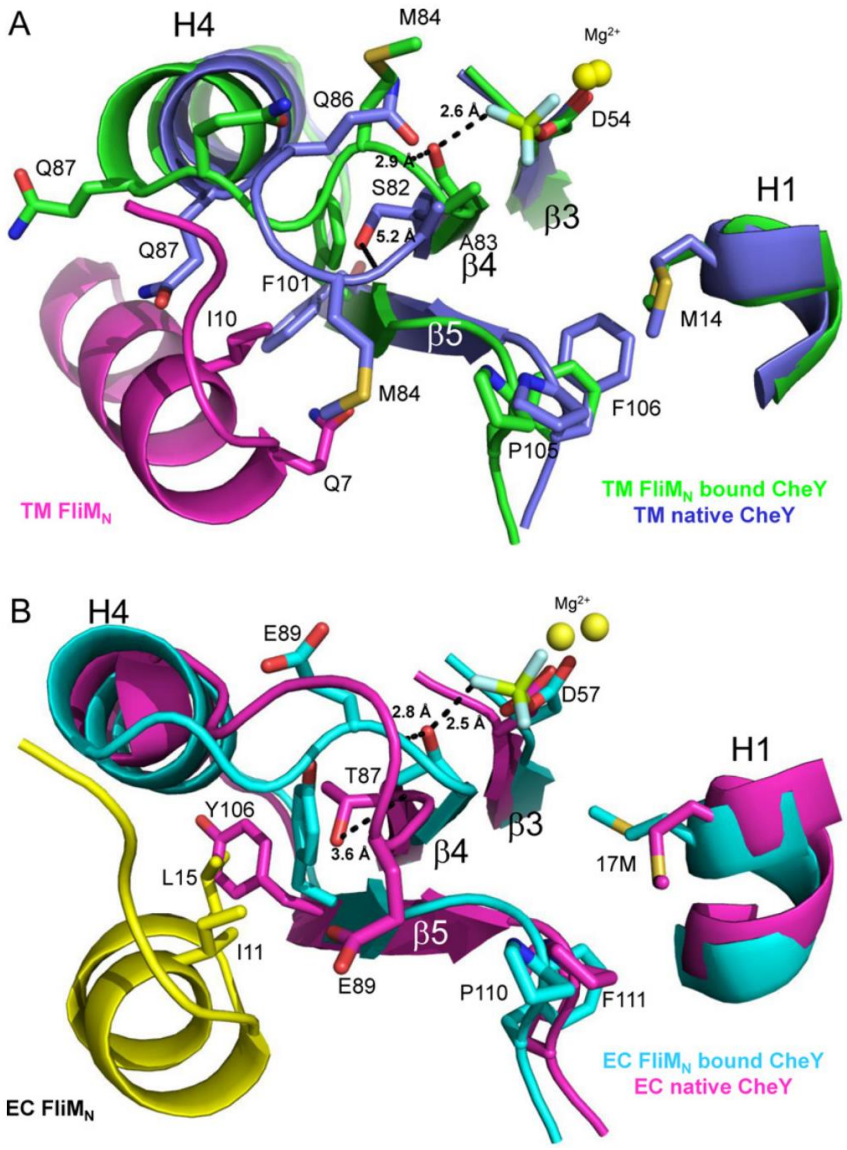

Figure 1.26 – Crystal structures of **A)** CheY (bound – green, unbound - blue) and $FliM_N$ (residues 1-20) (magenta) from *T. maritima* (PDB:4IGA, PDB:4TMY) and **B)** CheY (bound – cyan, unbound - magenta) and $FliM_N$ (residues 1-20) (yellow) from *E. coli* (PDB:1CHN and 1F4V). The native conformation of CheY has been superimposed for comparison in both **A** and **B** to highlight steric clashes (taken from (Ahn *et al*. 2013)). BeF_3^- was used to mimic the phosphorylated (active) state of CheY.

The α4-β5 region in both *E. coli* and *T. maritima* CheY and $FliM_N$ form the interaction interface. The crystal structures also give evidence for the Y-T coupling mechanism.

In the unphosphorylated $CheY_{EC}$ structure, the Y106 side-chain would sterically clash with L15 from FliM. Once in the FliM bound conformation with BeF_3^-, T87 moves towards β3 and the Y106 side-chain becomes buried, removing the steric clash. A similar mechanism is seen in the *T. maritima* structures. In the unbound *T. maritima* CheY structure, the F101 side-chain would sterically clash with I11 from FliM. Once in the bound (BeF_3^-) conformation, S82 moves towards β3 and the F101 side-chain is buried, removing the steric clash.

The reduced ability of unphosphorylated CheY, relative to CheY-P, to form stabilising contacts with FliM provides a molecular basis for its reduced affinity. The equilibrium shift model relies on the assumption that CheY can only access two conformations and that phosphorylation forces the equilibrium towards the active state. Conformational subpopulations are challenging or even impossible to detect. The crystal structures (Figure 1.26) possibly identify a simple structural origin for selectivity involving side-chain interactions (Ahn *et al*. 2013).

NMR experiments have also been used to determine the interaction interface between FliM and CheY, with the aim to develop a model for motor switching. $^1H,^{15}N$-HSQC perturbations in the CheY-BeF_3^- spectrum, indicated binding to $FliM_M$, which is adjacent to the FliM-FliM interface (Dyer *et al*. 2009). It was also found that FliG binds to this FliM region with mutual exclusivity to activated CheY (Dyer *et al*. 2009). It was proposed that activated CheY displaces the $FliG_C$ domain from FliM,

disrupting the MotA-FliG$_C$ interaction. The disruption of the MotA-FliG$_C$ interface then causes a switch of the direction of rotation (Figure 1.27).

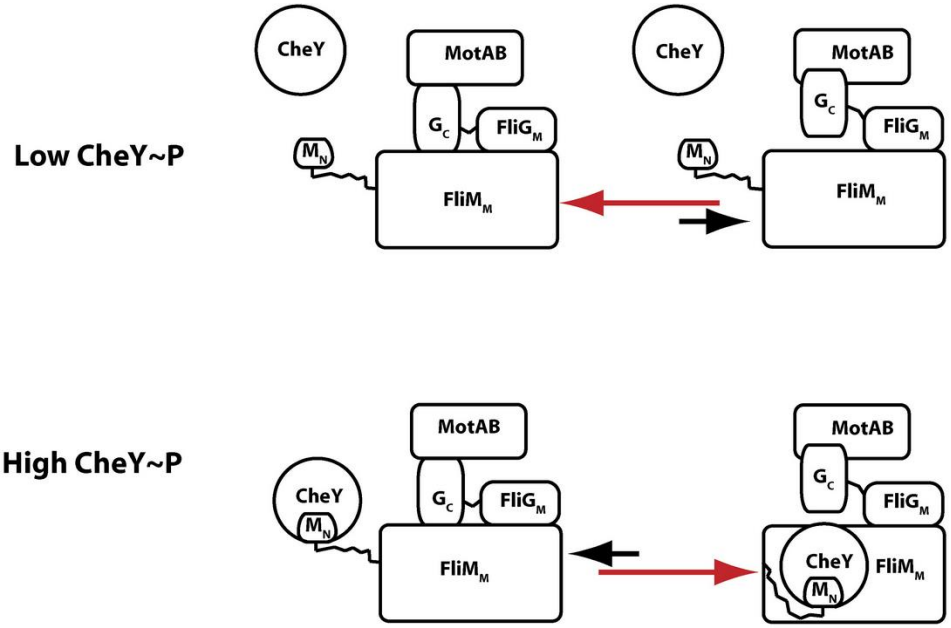

Figure 1.27 – The proposed molecular mechanism for motor switching in *E. coli*, mediated by CheY. At low concentrations of CheY-P, motor interaction is low. As CheY-P concentration increases, CheY-P sequentially interacts with FliM$_N$ and FliM$_M$. The CheY-FliM$_M$ interaction displaces the FliG$_C$-FliM$_M$ binding site, and leads to a disruption in the MotA-FliG$_C$ interface. This disruption causes a switch in rotation (taken from (Dyer *et al*. 2009)).

Not much is known about the interaction interface of the CheYs and FliM of *R. sphaeroides*. A study has suggested that all CheYs of *R. sphaeroides* are able to bind to FliM (Ferré *et al*. 2004) (Figure 1.28). CheY proteins were immobilised on sepharose beads and incubated with FliM, with and without acetyl phosphate (AcP).

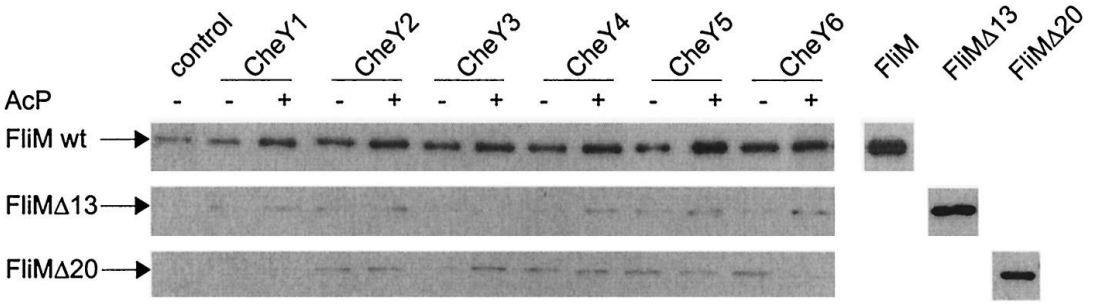

Figure 1.28 – CheY and CheY-P binding to FliM of *R. sphaeroides*. All CheY proteins were assayed in the presence and absence of acetyl phosphate. Anti-FliM antibody was used to detect the presence of FliM. Non-specific binding is seen in the control experiment that contained no CheY protein (taken from (Ferré *et al*. 2004)). Acetyl phosphate is used to phosphorylate the CheYs *in vitro*.

All CheY proteins are able to bind to FliM, both in the absence and presence of AcP. This is consistent with the conformational nature of the CheYs, i.e. that an equilibrium exists between active and inactive states, without phosphorylation. However, this work has not been reproducible and no other studies to date have been able to provide evidence of FliM-CheY interactions in *R. sphaeroides*.

1.6.5 The CheYs of *R. sphaeroides*

$CheY_6$, the motor stopping CheY of *R. sphaeroides*, displays the typical topology ($\alpha5/\beta5$) of the superfamily of CheY response regulators (Volz and Matsumura 1991). A great degree of structural conservation (rmsd of 1.4Å over 115 C_α atoms, to *E. coli* CheY) is observed, but with a low sequence identity of 26%. The metal binding residues Asp9, Asp10 and Asp56 are also very similar to the Mg^{2+} binding site in *E. coli* CheY (Stock *et al*. 1993). $CheY_6$ contains an elongated loop region between $\beta5$

and α5, comprised of 13 residues (107-119). Other CheYs contain a small loop region, for example, the loop in *E. coli* CheY is comprised of three residues (109-111). This elongated loop region in $CheY_6$ showed no electron density in the crystal structure, suggesting it is flexible (Bell *et al*. 2010). $CheY_6$ was shown to be essential for chemotaxis, whereas $CheY_3$ and $CheY_4$ have some functional redundancies (Porter *et al*. 2006). Only $CheY_6$ is able to trigger a stop in rotation of the motor. Although $CheY_6$ alone can stop the motor, *R. sphaeroides* requires the presence of either $CheY_3$ or $CheY_4$ to retain its chemotactic ability (Porter *et al*. 2006). $CheY_6$ does not have the conserved aromatic residue required for the classic Y-T coupling mechanism. This could indicate a novel conformational switch upon activation.

1.7 Aims of Project

- Investigate solution structure and dynamics of $CheY_6$:
    - Collect multidimensional NMR spectra of $CheY_6$ at pH 5.5 and 7.2, with and without BeF_3^-.
    - Assign and analyse NMR spectra to identify structural changes associated with activation by phosphorylation (mimicked by BeF_3^-).
    - Characterise backbone dynamics of inactive and active $CheY_6$ using the $\{^1H\}$-^{15}N heteronuclear NOE.

- Using NMR parameters such as chemical shifts, residual dipolar couplings, hydrogen-deuterium exchange and ^{1}H-^{1}H NOEs, characterise the structure of active and inactive $CheY_6$ in solution.

- Investigate $CheY_6$-FliM interactions using a number of different techniques:
  - 2-Hybrid assays to observe $CheY_6$-FliM interactions *in vivo*.
  - NMR studies of $CheY_6$-FliM interactions to investigate key residues upon binding.
  - Single molecule microscopy of chemically tagged $CheY_6$ and fluorescently tagged fusions of FliM in *R. sphaeroides*.

- Investigate the function of the elongated loop region (109-118) in $CheY_6$ by:
  - Deletion of the elongated loop region.
  - Assess chemotactic ability with the use of swim plates.
  - Evaluate motor response using tethered cell assays.
  - Epifluorescence microscopy to determine localisation of mutant proteins.
  - Phosphotransfer assays to assess phosphotransfer of mutant proteins.
  - Collect, assign and analyse NMR data of $CheY_6$-Δloop to investigate structural changes upon activation.

Chapter 2

Materials and Methods

2.1 Strains and Plasmids

2.1.1 Bacterial Strains

Strain	Species	Genotype/Description	Source
XL-1 Blue	*E. coli*	General cloning strain – Plasmid creation and modification. Tetracycline resistance.	Stratagene
BL21 (DE3) pLysS	*E. coli*	Protein expression strain. Chloramphenicol resistance.	Promega
S17-1 λ-pir	*E. coli*	Plasmid mobilising strain – Introduced plasmids into *R. sphaeroides* strains. Streptomycin resistance.	(Penfold and Pemberton 1992)
DMH1α	*E. coli*	Bacterial 2-hybrid strain – 200 bp deletion in *cya* gene. *cya* gene encodes adenylate cyclase.	(Karimova, Dautin, and Ladant 2005)
WS8N	*R. sphaeroides*	Wild type strain containing spontaneous nalidixic acid resistance.	(Sockett and Armitage 1991)
JPA1336	*R. sphaeroides*	Δ*cheY*$_6$ – Derivative of WS8N.	S. L. Porter
JPA467	*R. sphaeroides*	*Δσ28* – Derivative of WS8N	E. Byles unpublished
JPA1216	*R. sphaeroides*	*cheY*$_6$*-(D56A)* – Derivative of WS8N	(Porter *et al*. 2006)
JPA1422	*R. sphaeroides*	*cfp-cheA*$_3$ – Derivative of WS8N	G. H. Wadhams

Table 2.1 – Strains

2.1.2 Plasmids

Plasmid	Description	Source
pQE80	4.8 kb, IPTG inducible plasmid. Contains an N-terminal His$_6$-tag. Ampicillin Resistance.	Qiagen
pQE80-*cheY*$_6$	*cheY*$_6$ cloned into pQE80.	This Study
pQE80-*cheY*$_6$*-(A134C)*	*cheY*$_6$ cloned into pQE80.	This Study
pQE80-*cheY*$_6$*-Δloop*	*cheY*$_6$*-Δloop* cloned into pQE80.	This Study
pQE80-*cheA*$_3$	*cheA*$_3$ cloned into pQE80.	This Study
pQE80-*cheA*$_4$	*cheA*$_4$ cloned into pQE80.	This Study
pQE80-*cheY*$_3$*-loop*	*cheY*$_3$*-loop* cloned into pQE80.	This Study

pQE80-*cheY$_3$-loop-(F107K)*	*cheY$_3$-loop-(F107K)* cloned into pQE80.	This Study
pQE80-*cheY$_3$-(F107K)*	*cheY$_3$-(F107K)* cloned into pQE80.	This Study
pIND4	8.4 kb, IPTG inducible plasmid. Kanamycin resistance.	(Ind *et al*. 2009)
pIND4-*yfp-cheY$_6$*	*yfp-cheY$_6$* cloned into pIND4.	This Study
pIND4-*yfp-cheY$_6$-Δloop*	*yfp-cheY$_6$-Δloop* cloned into pIND4.	This Study
pUT18	3.0 kb, IPTG inducible plasmid. C-Terminal tag. Ampicillin resistance.	(Karimova, Ullmann, and Ladant 2001)
pUT18C	3.0 kb, IPTG inducible plasmid. N-Terminal tag. Ampicillin resistance.	(Karimova *et al*. 2001)
pKNT25	3.4 kb, IPTG inducible plasmid. C-Terminal tag. Kanamycin resistance.	(Karimova *et al*. 2005)
pKT25	3.4 kb, IPTG inducible plasmid. N-Terminal tag. Kanamycin resistance.	(Karimova *et al*. 2001)
pKT25-zip	Sequence coding for leucine zipper region of GCN4 yeast protein (N-Terminal). Kanamycin resistance. IPTG inducible. Used as a positive control.	(Karimova *et al*. 2001)
pUT18C-zip	Sequence coding for leucine zipper region of GCN4 (N-Terminal). Ampicillin resistance. IPTG inducible. Used as a positive control.	(Karimova *et al*. 2001)
pUT18-*cheY$_6$*	*cheY$_6$* cloned into pUT18.	This Study
pUT18C-*cheY$_6$*	*cheY$_6$* cloned into pUT18C.	This Study
pKNT25-*cheY$_6$*	*cheY$_6$* cloned into pKNT25.	This Study
pKT25-*cheY$_6$*	*cheY$_6$-loop* cloned into pKT25.	This Study
pUT18-*cheY$_6$-loop*	*cheY$_6$-loop* cloned into pU18.	This Study
pUT18C-*cheY$_6$-loop*	*cheY$_6$-loop* cloned into pUT18C.	This Study
pKNT25-*cheY$_6$-loop*	*cheY$_6$-loop* cloned into pKNT25.	This Study
pKT25-*cheY$_6$-loop*	*cheY$_6$-loop* cloned into pKT25.	This Study
pUT18-*fliM*	*fliM* cloned into pUT18.	This Study
pUT18C-*fliM*	*fliM* cloned into pUT18C.	This Study
pKNT25-*fliM*	*fliM* cloned into pKNT25.	This Study
pKT25-*fliM*	*fliM* cloned into pK25.	This Study

Table 2.2 – Plasmids

2.2 Growth Conditions

Growth conditions were dependent on the bacterial species and the specific experiment planned.

2.2.1 Antibiotics

Antibiotic	Concentration for *E. coli* (μg/ml)	Concentration for *R. sphaeroides* (μg/ml)
Nalidixic Acid	25	25
Kanamycin	25	25
Ampicillin	100	-
Tetracycline	25	-
Chloramphenicol	10	1

Table 2.3 – Antibiotic concentrations

2.2.2 Aerobic Growth of *E.coli*

E.coli were aerobically grown in LB medium (see Appendix A for recipe) containing the appropriate antibiotic/s, with shaking at 37°C.

2.2.3 Agar Plates for *E. coli*

E. coli were grown on solid agar plates made from LB medium, 2% agar, appropriate antibiotic/s and incubated at 37°C.

2.2.4 Photoheterotrophic Growth of *R. sphaeroides*

R. sphaeroides were grown photoheterotrophically in succinate medium (see Appendix A for recipe) containing the appropriate antibiotic/s. Growth containers were sealed with minimal air space and incubated under white light at 30°C.

2.2.5 Aerobic Growth of *R. sphaeroides*

R. sphaeroides were grown aerobically in succinate medium containing the appropriate antibiotic/s, with shaking overnight at 30°C.

2.2.6 Agar Plates for *R. sphaeroides*

R. sphaeroides were grown on solid agar plates made from LB medium, 2% agar, appropriate antibiotic/s and incubated at 30°C.

2.3 Genetic Techniques

2.3.1 Extraction of *R. sphaeroides* Chromosomal DNA

R. sphaeroides were grown aerobically to stationary phase (~48 hrs). Culture (1 ml) was centrifuged and flash frozen in liquid nitrogen. The frozen pellet was resuspended in lysis buffer (0.5 ml) (see Appendix A for recipe) and heated to 65°C. Proteinase K (100 μg) was added and the sample incubated at 45°C for 2 hours. Chromosomal DNA was extracted twice with phenol:chloroform:isoamyl-alcohol (0.5 ml, 25:24:1) and precipitated with ethanol (100%) at -20°C for 30 mins. The

sample was then centrifuged (16000 x g, 15 mins), the pellet washed with ethanol (70%), and centrifuged again as above. The pellet was dried overnight at 37°C, resuspended in sterile water (50 μl) and stored at -20°C.

2.3.2 Polymerase Chain Reaction (PCR)

Standard PCR

PCR reaction mixture is described in Table 2.4. Reaction mixture was placed in a thermocycler using the program settings in Table 2.5. The annealing temperature was dependent on the T_M of the specific primers used for each reaction.

Component	Quantity
Template DNA	0.5 μl
Primer 1	1 μl at 100 μM
Primer 2	1 μl at 100 μM
10x Pfu polymerase buffer (Promega)	5 μl
Pfu DNA polymerase (Promega)	1 μl (2.5 U)
dNTPs	5 μl at 2.5 mM
DMSO	2.5 μl for 5%
MilliQ	Make to a total of 50 μl

Table 2.4 – Composition of PCR reaction mixture

Stage	Time (mins)	Cycles	Temperature (°C)
Initial Denaturation	10	1	98
Denaturation	1	-	98
Annealing	1	30	T_M specific
Extension	2 per 1 kb	-	72
Final Extension	5	1	72

Table 2.5 – PCR reaction program

Overlap Extension PCR

Overlap extension PCR was employed to create plasmid constructs for protein purification. A schematic of the process is shown in Figure 2.1.

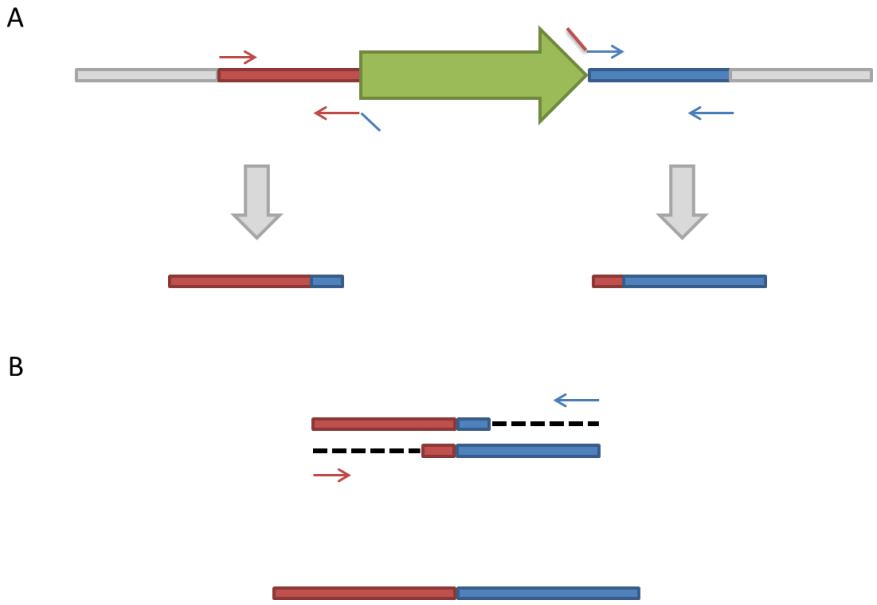

Figure 2.1 – Overlap extension PCR was used to create plasmid constructs containing residue deletions for protein purification. **A)** Two PCR reactions (grey arrows) are run using primers designed to amplify the flanking regions of the residues (red and blue) to be deleted. The inner primers contain an overlap region, corresponding to the other flanking region. The products are complimentary to each other. **B)** Second round of PCR. Outer primers and both products are used in a single reaction. The complimentary regions of both products act as primers and allow elongation of a single fused sequence.

2.3.3 Gel Electrophoresis

Gel electrophoresis was used to separate DNA fragments. Gels contained 0.8-2% multi-purpose agarose (Roche) in 0.5 x TBE (see Appendix A for recipe). Agarose percentage was dependent on the size of fragments being separated. Samples were

electrophoresed (80-140 V, 45 mins), stained in ethidium bromide (1 ng/ml) for 15 mins and visualised on a UV transilluminator.

2.3.4 Purification of DNA Fragments

DNA fragments were excised and purified from agarose gels using the Gel Extraction Kit (Qiagen), following the manufacturers protocol.

2.3.5 Restriction Enzyme Digest

Restriction enzyme digest reaction mixtures (see Table 2.6, Table 2.7) were incubated for at least 2 hours at 37°C.

Component	Quantity
DNA	25 μl of PCR product 10 μl of plasmid
10x Buffer	2 μl
Enzyme	0.5 μl
Bovine serum albumin	0.2 μl
MilliQ	Make to a total of 50 μl

Table 2.6 – Composition of restriction enzyme reaction mixture for digest of PCR products

Component	Quantity
Plasmid	5 μl
10x Buffer	2 μl
Enzyme	0.5 μl
Bovine serum albumin	0.2 μl
MilliQ	Make to a total of 20 μl

Table 2.7 – Composition of restriction enzyme reaction mixture for ligation confirmation

2.3.6 Dephosphorylation of DNA

Restriction enzyme digests were terminated via heating (80°C, 20 mins) and then cooling (4°C). Calf intestinal alkaline phosphatase (1 μl) (New England Biolabs) was added and the sample incubated for 1 hour at 37°C.

2.3.7 DNA Ligation

The composition of DNA ligation mixtures can be found in Table 2.8. The volume of insert DNA and plasmid was adjusted to reflect a specific molar ratio of 3:1.

Component	Quantity
Digested Insert	24 μl
Digested Plasmid	8 μl
T4 DNA ligase buffer (Invitrogen)	10 μl
T4 DNA ligase (Invitrogen)	1 μl
MilliQ	7 μl

Table 2.8 – Composition of DNA ligation mixture

2.3.8 Competent Cell Preparation

Chemically competent *E. coli* cell preparation - Rubidium chloride method

LB media (50 ml) was inoculated with stationary phase *E. coli* cells (1 ml) and incubated at 37°C until an OD_{600} of 0.4 was reached. The culture was transferred to a falcon tube, put on ice (15-30 mins) and then centrifuged (1000 x g, 10 mins, 4°C). The pellet was resuspended in TFB-I (16 ml, 4°C) (see Appendix A for recipe), incubated on ice (1 hour) and then centrifuged (750 x g, 10 mins, 4°C). The pellet was resuspended in TFB-II (4 ml, 4°C) (see Appendix A for recipe). Aliquots of resuspended cells (200 μl) were flash frozen in liquid nitrogen and stored at -80°C.

Electrocompetent *R. sphaeroides* cell preparation

R. sphaeroides (250 μl) were aerobically grown in succinate medium (500 ml) overnight, with shaking at 30°C. At OD_{700} 0.4, the culture was cooled (4°C, 10 mins) and centrifuged (1000 x g, 10 mins, 4°C). The pellet was resuspended in MilliQ (500 ml). The process was repeated three more times with resuspension in MilliQ (250 ml, 125 ml and 10 ml). Final resuspension was in MilliQ water (1 ml) with glycerol (10%). Aliquots (40 μl) were flash frozen in liquid nitrogen and stored at -80°C.

2.3.9 Electroporation

Fluorescent protein (desired amount) was added to *R. sphaeroides* electrocompetent cells (20 μl). The mixture was transferred to a pre-chilled cuvette and placed in a Bio-Rad Electroporator. Cells were electroporated on setting Manual (1.2 kV/cm). Succinate medium (500 μl) was added and cells left to recover (30°C, 5 mins) in a thermomixer (450 rpm). Cells were centrifuged (7000 x g, 1 min) and resuspended in succinate media (500 μl) four times to remove unelectroporated protein. Final resuspension was in succinate medium (100-200 μl).

2.3.10 Transformation of Plasmid DNA into Competent Cells

Plasmid DNA (0.5 μg for pure plasmid, 25 μl of ligation mixture) was added to *E. coli* XL-1 competent cells (100 μl) and incubated on ice (45 mins). Cells were heat shocked (42°C, 45 secs) and immediately put back on ice (1 min). LB medium (1 ml)

was added and the mixture was incubated at 37°C for 1 hour. Culture (100 μl) was plated on LB agar plates (see Appendix A for recipe) with appropriate antibiotic/s and incubated overnight (37°C).

2.3.11 Plasmid Purification

E. coli culture containing the desired plasmid was grown overnight in LB medium (5 ml) with the appropriate antibiotic/s at 37°C. The plasmid was extracted using the QIAGEN QIA DNA Mini or Midi kit following the manufacturer's instructions.

2.3.12 DNA Sequencing

DNA sequencing was performed using the Automated DNA Sequencing Service from Source Bioscience. The BigDye termination method (PE Biosystems) was used on a 3730 DNA sequencer (Applied Biosystems). Contigs were produced using the Staden software package and Clone Manager (Sci Ed Central) was used for analysis.

2.3.13 Conjugation of Plasmid DNA into *R. sphaeroides*

R. sphaeroides cannot be made competent, so *E. coli* S17-λpir cells were used to introduce plasmids via conjugation. *E. coli* S17-λpir cells had appropriate plasmid transformed into them as described in 2.3.9. *E. coli* cells (1 ml) in aerobic mid-log phase and *R. sphaeroides* (1 ml) in photoheterotrophic stationary phase were centrifuged (3500 x g, 3 mins). Both pellets were washed three times in LB medium (1 ml) without antibiotics. Resuspension was completed very carefully to avoid

shearing of the pili. *E. coli* (10 μl) were mixed with *R. sphaeroides* (100 μl) and the mixture pipetted onto a sterile nitrocellulose filter (Millipore 0.22 μm, surfactant free, GSTF 25 mm) on an LB agar plate with no antibiotic. The plate was incubated overnight at 30°C. Cells were washed off the filter paper in LB medium (800 μl) and spread onto an LB agar plate containing nalidixic acid and a selective antibiotic appropriate for the plasmid. The plate was incubated for two days at 30°C.

2.4 Phenotypical Analysis of *R. sphaeroides*

2.4.1 Swim Plate Assay

R. sphaeroides chemotactic ability was assessed with the use of swim plates. Semi-solid agar plates containing 0.25% agar (BiTek) in M22 minimal medium (see Appendix A for recipe) and appropriate antibiotic/s were produced. Propionate (100 μM) was used as a chemoattractant and was the only carbon source available. *R. sphaeroides* (5 μl) in photoheterotrophic stationary phase was spotted onto the plate. Plates were incubated for 48 hours at 30°C. Consumption of the propionate during growth creates a concentration gradient. If cells are chemotactic and motile, they will swim away from low concentrations of propionate. The diameter of the rings formed around the site of inoculation was measured and used to interpret chemotactic ability, relative to control strains.

2.4.2 Tethering Assay

R. sphaeroides cells were grown to stationary phase as described in 2.2.5. Sub cultures were grown (succinate medium) containing appropriate antibiotic/s and IPTG (1 mM) to mid-log phase (OD_{700} 0.4-0.6). Cells (1 ml) were centrifuged (3500 x g, 3 mins), washed three times and resuspended in PIPES buffer (1 ml, 10 mM, see Appendix A for recipe) containing chloramphenicol. Cells (10 μl) were tethered to a coverslip with anti-filament IgG (2 μl, 1:1000 dilution). The coverslip was placed into a flow cell. One run consisted of flowing PIPES buffer (3 mins), PIPES buffer (5 mins) with propionate (100 μM) and finally PIPES buffer (5 mins) with no propionate. Runs were imaged using a DALSA Genie HM640 black and white camera with a set frame rate (100 Hz, 10 ms) and exposure time (6000 ms). Image analysis was completed using BRAS and Click&Mean software. BRAS is an image segmentation program that was used to detect the rotation rate of individual cells every 50 ms. Cell rotation rate is detected by the difference in pixel intensity between the background and the cell. Click&Mean processes and displays coordinate data from BRAS output files. X-Y coordinate changes between each frame are converted into a rotational speed using a Fourier transformation (smoothing window of 128 frames).

2.5 Microscopy

2.5.1 Cell Preparation

R. sphaeroides were aerobically grown, as described in 2.2.5, to mid-log phase (OD_{700} 0.4-0.6).

2.5.2 Slide Preparation

Agarose pad slides were made using 1% agarose in succinate medium. A thin layer of this solution was applied to a microscope slide and cells (2 μl) were added. A cover slip was then placed on top.

2.5.3 Microscopes

Nikon Eclipse Ti

An inverted Nikon Eclipse Ti microscope using a differential interference contrast (DIC) enhancement was used to acquire fluorescence images of cells. Oil objectives (60X or 100X, Nikon) were used with an additional magnification (1.5X) applied inside the microscope. NIS Elements software (Nikon) was used to control the microscope. Epifluorescence mode is described below.

Nikon Eclipse Ti – Epifluorescence Mode

Epifluorescence imaging was achieved on the Nikon Eclipse Ti microscope using a mercury lamp and appropriate filters for YFP and CFP. A halogen lamp was used for brightfield images. An Andor iXON CCD camera was used to capture images.

Customized Olympus IX-71 Microscope

Single-molecule and single-cell fluorescence microscopy in live bacteria was completed using a customised inverted Olympus IX-71 microscope equipped with two lasers (638 nm diode laser (Cube; Coherent), 532 nm Nd:YAG laser (Samba; Cobolt AB)). Total internal reflection fluorescence (TIRF) microscopy was used for

cell imaging. Excitation power ranged from 0.5-3 mW with exposure times ranging from 15-100 ms. Fluorescence from cells was filtered (long-pass filter (HQ545LP: Chroma), notch filter (NF02-633S: Semrock)) to remove excitation light and spectrally separated using a dichroic mirror (630DRLP: Omega). Channels were imaged on separate halves of the chip of an electron-multiplying charge-coupled device camera (iXon+, BI-887: Andor). White light (WL) images were illuminated using a WL lamp (IX2-ILL100: Olympus) and condenser (IX2-LQUCD: Olympus) attached to the microscope. Images and movies were recorded using manufacturers' software.

2.6 Protein Expression, Purification, Labelling and Analysis

2.6.1 Overexpression and Purification of Non-isotopically Labelled Protein

E. coli BL21 (DE3) cells containing the appropriate plasmid were grown aerobically in 2TY medium (1 Litre) (see Appendix A for recipe) containing appropriate antibiotic/s, with shaking at 37°C. Cells were induced at OD_{600} 0.6-0.8 with the addition of IPTG (1 mM) at 18°C and left overnight. Cells were harvested by centrifugation (7000 x g, 20 mins) and resuspended in lysis buffer (containing protease inhibitor cocktail) (30 ml) (see Appendix A for recipe). Cells were lysed by a French Press (3 passes, 1000 psi) and lysate centrifuged (36000 x g, 1 hour) to remove cell debris and insoluble material. Supernatant was filtered (0.4 μm) and applied to a Nickel-NTA Agarose (Qiagen) column. All expressed proteins carry a His_6-tag which binds to the Nickel resin. The column was washed with 5 volumes of lysis buffer (no protease

inhibitor) and proteins eluted in appropriate buffer (no protease inhibitor) containing imidazole (200 mM). Protein purity was measured using SDS-PAGE gels stained with Coomassie Blue.

2.6.2 Overexpression of ^{15}N-labelled Protein for NMR Studies

E. coli BL21 (DE3) cells were grown aerobically as described in 2.6.1. At OD_{600} 0.6-0.8, cells were collected by centrifugation (7000 x g, 20 mins) and washed 3 times in M9 minimal medium (see Appendix A for recipe), exclusive of NH_4Cl. Cells were then resuspended in M9 minimal media containing ^{15}N labeled NH_4Cl, induced with IPTG (1 mM) and left overnight at 30°C. Cells were then harvested, lysed and purified as described in 2.6.1.

2.6.3 SDS-PAGE Electrophoresis for Protein Separation

Proteins of interest were identified by size comparison using SDS polyacrylamide gel electrophoresis (SDS-PAGE). Protein samples (20 μl) were added to 5x protein loading dye containing SDS (5 μl) and heated (100°C, 5 mins). Samples were run on an polyacrylamide gel (precast, 4-20%) with a Benchmark Prestained Protein Ladder (Invitrogen). SDS-PAGE running buffer (see Appendix A for recipe) was used and 165 V, 110 mA was applied (50 mins). The gel was stained using InstaBlue Coomassie blue.

2.6.4 Size Exclusion Chromatography

Size exclusion chromatography (gel filtration) was used to remove impurities from protein purified using a Nickel-NTA agarose column. Protein sample was centrifuged (10000 x g, 15 mins, 10°C) and injected onto a S75 gel filtration column (HiLoad 16/600 Superdex, GE Healthcare) attached to an AKTA system. Protein buffer was used at a flow rate of 1 ml/min. Void volume (50 ml) was discarded and fractions (1 ml) were collected for approximately 100 ml. UV absorption (280 nm) was used to identify protein containing fractions and SDS-PAGE gels were used for confirmation. Fractions containing protein of interest were combined and concentrated (centrifuge concentrator).

2.6.5 Protein-Dye Conjugation

$CheY_6$-(A134C) was expressed purified as described in Section 2.6.1, and stored in labelling buffer (see Appendix A for recipe at -80°C. $CheY_6$-(A134C) (200 μl, 50-100 μM) was thawed on ice, and maleimide dye Atto647 (resuspended in DMSO, 10x molar excess) was added. The reaction was left overnight at 4°C. Free dye was removed using size exclusion chromatography, as described in Section 2.6.4. Fractions were run on an SDS-PAGE gel and scanned for fluorescence using a UV-Vis Pharos FX Plus Molecular Imager (BioRad). Protein-dye fractions were collected, concentrated (2-60 μM) and stored at 4°C.

2.7 Circular Dichroism

Circular dichroism experiments were performed using a Jasco J-815 (JASCO) spectropolarimeter with a Peltier-thermostated cuvette holder. The CD instrument passes polarized light through the sample, to a photomultiplier detector. A nitrogen flow of 5 L/min was used to purge and cool the system. Measurements were taken in the far-UV (260-200 nm) spectrum, using a quartz cuvette (1 mm path length) at 20°C. The final spectrum was an average of ten scans using the following settings: 50 nm/min scan speed, 0.1 nm data pitch, 1 nm band width, 1 s response time and 0.5 nm step resolution. Blank (buffer) samples were taken and subtracted from the final spectra.

2.8 Phosphotransfer Assays

Phosphotransfer reactions from $CheA_3$ to $CheY_6$ were completed in TGMNKD buffer (see Appendix A for recipe) at 20°C. $CheA_3$ (5 μM) and $CheA_4$ (5 μM) were incubated with [γ-^{32}P] ATP (14.8 GBq/mmol, Amersham) for 15 mins before addition of $CheY_6$ (10 μM), to a final volume of 100 μl. Aliquots (10 μl) were taken at specific time intervals and quenched in 3x SDS/EDTA loading dye (5 μl, 4°C) (see Appendix A for recipe). Samples were kept on ice before SDS gel electrophoresis (4°C, 45 mins) on a polyacrylamide gel (15%). Gels were dried and exposed to phosphor screens (Kodak). Analysis was completed using a SF-phosphorimager with ImageQuant software (version 5.0, Molecular Dynamics). Corrections were made for background present in each lane.

2.9 Bacterial Two-Hybrid Assay

DHM1 (*E. coli*) competent cells were prepared using the protocol in Section 2.3.8. Appropriate T18 (0.5 μl) and T25 (0.5 μl) fusion plasmids were added to cells (30 μl) in a 96-well plate, and incubated on ice (20 mins). The cells were heat shocked (42°C, 1 minute), and immediately put back on ice. LB medium (150 μl) was added and the cells were left to recover (1 hour, 37°C). The cells were plated on LB agar containing appropriate antibiotics and incubated overnight. Colonies are picked and cultures grown overnight, with shaking at 37°C. The next day, the cells (10 μl) were plated on LB agar containing XGal (40 μg/ml), IPTG (100 μM) and appropriate antibiotics. Plates were imaged for up to seven days.

2.10 NMR Analysis of $CheY_6$

2.10.1 Sample Preparation

Isotopically labelled protein was made as described in Section 2.6.2. Nuclear magnetic resonance (NMR) experiments were collected at 20°C with the appropriate protein (0.2-2 mM - pH dependent) with the appropriate buffer (see Appendix A for recipes). D_2O (5%) was added to protein samples for deuterium locking. Shigemi NMR micro-tubes (Shigemi Inc.) required a minimum volume of 270 μl. For deuterium-hydrogen exchange experiments, protein was dialysed into water, lyophilised and dissolved in D_2O (100 %). A 10x stock of BeF_3^- (20 mM) was produced via reaction of $BeCl_2$ (20 mM) and NaF (200 mM) at room temperature. Final BeF_3^- concentration was 2 mM.

$CheY_6$ and $CheY_6$-Δloop buffer conditions

pH5.5 - Sodium Acetate (20 mM), $MgCl_2$ (2 mM) and D_20 (5 %)

pH7.5 - Tris.HCl (25 mM), $MgCl_2$ (15 mM) and D_2O (5 %)

2.10.2 Data Collection Parameters

NMR spectrometers situated in the Department of Biochemistry, University of Oxford with ^1H frequencies ranging from 500 MHz (Bruker Avance) to 950 MHz (Oxford Instruments, home built) were used for data collection. The 500 MHz spectrometer had a cryoplatform. Home-built spectrometers used magnets supplied by Oxford Instruments, UK. Home built triple-resonance pulsed-field gradient probe-heads and GE/OMEGA software.

Acquisition parameters for triple resonance experiments used for protein backbone assignment are shown in Table 2.9. Acquisition parameters for ^{15}N-edited experiments used for residual dipolar couplings and backbone dynamics are shown in Table 2.10. Acquisition parameters for ^{13}C-edited experiments used for side-chain assignments are shown in Table 2.11. NMRPipe (Delaglio *et al*. 1995) was used to process raw data. Analysis (CCPN) (Vranken *et al*. 2005) was used to plot and analyse data.

2.10.3 Residual Dipolar Coupling Measurements

Residual dipolar coupling experiments (RDCs) were calculated using the change in $^{1}J_{NH}$ scalar coupling values found in an IPAP (in-phase/antiphase) experiment of a partially aligned sample, relative to an isotropic sample. An anisotropic sample containing $C_{12}E_6$/hexanol (5% w/v) was prepared using the method of Ruckert and Otting (Rückert and Otting 2000).

Experiment	Spectrometer	Sweep Width (Hz)			Number of Complex Points			Spectrometer Frequency (MHz)	Centre Reference Chemical Shift (ppm)		
		^{1}H	^{15}N	^{13}C [^{1}H]	^{1}H	^{15}N	^{13}C [^{1}H]		^{1}H	^{15}N	^{13}C [^{1}H]
HNCO	Bruker 500	6666.67	1724.14	1886.24	512	32	64	500.012	4.8	117.2	172.5
HN(CA)CO	Bruker 500	6666.67	1724.14	1886.24	512	28	50	500.012	4.8	117.2	172.5
HNCA	Bruker 500	6666.67	1724.14	3521.13	512	28	50	500.012	4.8	117.2	53.0
HN(CO)CA	Bruker 500	6666.67	1724.14	3521.13	512	28	50	500.012	4.8	117.2	53.0
CBCANH	Bruker 500	6666.67	1724.14	7462.69	512	28	50	500.012	4.8	117.2	41.5
CBCA(CO)NH	Bruker 500	6666.67	1724.14	7462.69	512	28	50	500.012	4.8	117.2	41.5
HCC(CO)NH	Bruker 500	6666.67	1724.14	8298.35	512	32	64	500.012	4.8	117.2	39
HBHA(CO)NH	Bruker 500	6666.67	1724.14	[4761.9]	512	28	[89]	500.012	4.8	117.2	[4.8]
^{1}H,^{15}N-HSQC	Bruker 500	6666.67	1724.14	-	1024	128	-	500.012	4.8	117.2	-

Table 2.9– Acquisition parameters for triple resonance experiments used for protein backbone assignment

Experiment	Spectrometer	Sweep Width (Hz)			Number of Complex Points			Spectrometer Frequency (MHz)	Centre of Resonance Chemical Shift (ppm)			Mixing Time (ms)	Saturation time (s)
		^{1}H	^{15}N	^{1}H	^{1}H	^{15}N	^{1}H		^{1}H	^{15}N	^{1}H		
^{15}N-TOCSY-HSQC	Omega 500	6666.7	1666.7	6666.7	512	32	128	500.069	4.8	117.2	4.8	45	-
^{15}N-NOESY-HSQC	Omega 500	6666.7	1666.7	6666.7	512	32	128	500.069	4.8	117.2	4.8	150	-
Heteronuclear NOE	Omega 750	6666.7	1666.7	-	1024	110	-	749.914	4.8	117.2	-	-	4
^{1}H,^{15}N-IPAP	Omega 750	6666.7	1666.7	-	1024	128	-	749.914	4.8	117.2	-	-	-

Table 2.10 – Acquisition parameters for ^{15}N-edited NMR experiments.

Experiment	Spectrometer	Sweep Width (Hz)			Number of Complex Points			Spectrometer Frequency (MHz)	Centre Reference Chemical Shift (ppm)			Mixing Time (ms)
		^{1}H	^{13}C	^{1}H	^{1}H	^{13}C	^{1}H		^{1}H	^{13}C	^{1}H	
HCCH-TOCSY	Bruker 500	6666.7	8802.8	6666.7	512	46	128	500.012	4.8	41.8	4.8	15.2
^{13}C-NOESY-HSQC	Omega 750	10000	11876.5	8695.7	512	48	128	749.914	4.8	36.5	4.8	120
^{13}C-HSQC	Omega 750	10000	13192.6	-	1024	128	-	749.914	4.8	42.5	-	-

Table 2.11 – Acquisition parameters for ^{13}C-edited experiment

Chapter 3

Backbone and Side-chain Resonance Assignments in the NMR Spectra of $CheY_6$

3.1 Introduction

Nuclear Magnetic Resonance (NMR) spectroscopy has many useful applications. These include investigating and determining protein interactions, dynamics and structure. It is a unique technique for structure determination as it allows collection of atomic resolution data for proteins in solution. This is particularly useful when studying proteins that are difficult to crystallise. Studying proteins in solution also has the potential to remove artefacts created by crystallography. For example, structural changes as a result of crystal contacts.

NMR is also a powerful method for studying functional aspects of proteins in solution. Very weak protein-protein interactions (millimolar K_d) as well as protein-

ligand interactions can be studied to elucidate information on binding sites and affinities. This is very useful when studying structural changes of proteins upon binding of specific effectors. Most other techniques such as Surface Plasmon Resonance (SPR) and Isothermal Calorimetry (ITC) are not suitable for mM dissociation constant interactions.

To date, there is a crystal structure of $CheY_6$ in complex with the P1 domain of its cognate histidine kinase $CheA_3$ (Bell *et al*. 2010). However, it is not known if $CheY_6$ is in its active, inactive or an intermediate conformation. The switch mechanism of $CheY_6$ from its inactive to active conformation is also not known. Based on sequence alignments, $CheY_6$ may not have the classical Y-T switch mechanism seen in *E. coli* CheY, as it does not have an aromatic residue in the appropriate position in β5. NMR techniques will be used to characterise the structure of $CheY_6$ in solution to define both the active and inactive conformations. This could provide information about the switch mechanism. To achieve this, assignment of the backbone and side chain resonances of $CheY_6$ must be completed in order to interpret further NMR experiments that provide dynamic, structural and functional information. $CheY_6$ is activated via phosphorylation *in vivo*. $CheY_6$-Phosphate ($CheY_6$-P) has a short half-life, so a stable phosphate mimic was used instead. BeF_3^- has been extensively used as a phosphate mimic in CheY and related proteins, as it binds non-covalently to the aspartic acid residue in the active site which is phosphorylated by the histidine kinase CheA (Riepl *et al*. 2004).

3.2 Assignment Strategy

A general principle (Figure 3.1) was applied to the assignment of backbone and side chain resonances. Peaks in a 2D ^{1}H, ^{15}N-HSQC experiment were arbitrarily labelled and then used in conjunction with a series of triple resonance experiments to identify $^{1}H_{\alpha}$, $^{1}H_{\beta}$, $^{13}C_{\alpha}$, $^{13}C_{\beta}$ and ^{13}CO for each residue (i) and for each preceding residue (i-1). Given the known sequence, the 3D experiments could be used to link neighbouring residues based on through-bond information. The existence of unique residue sequences of known type (i.e. A-T-A) meant it was possible to unambiguously assign spin systems within the protein.

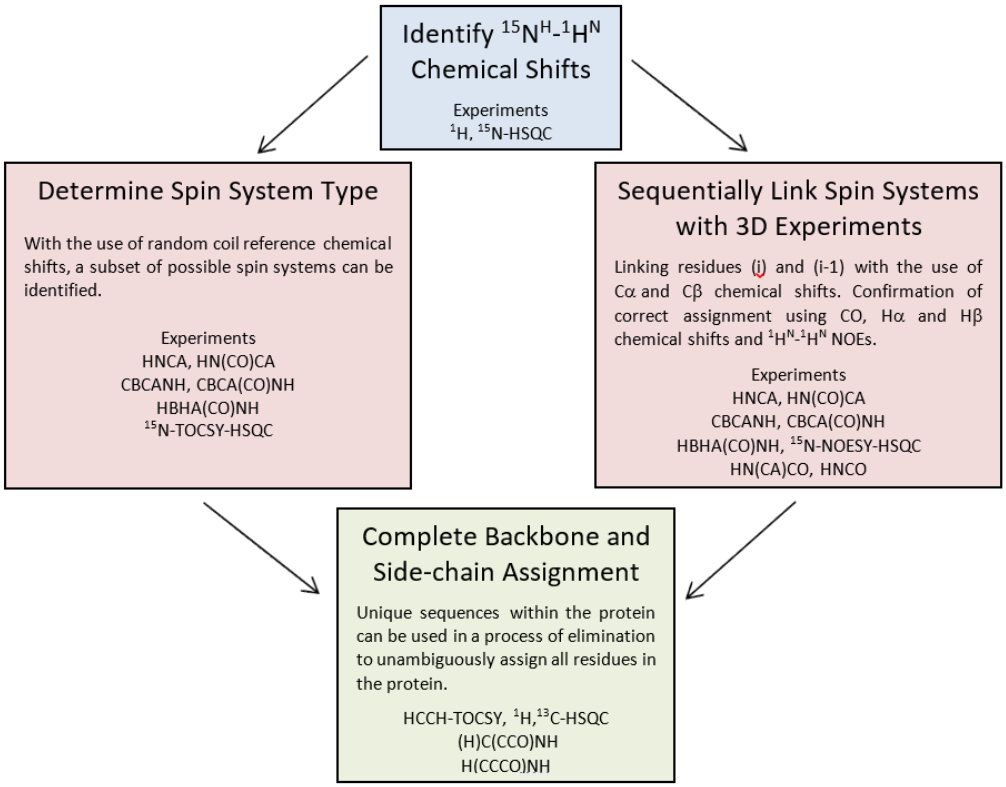

Figure 3.1 – Flow chart of the strategy used to assign backbone and side-chain resonances - NMR techniques used included ^{1}H, ^{15}N-HSQC, ^{15}N-edited TOCSY and a broad range of triple resonance experiments.

3.3 CheY$_6$ Sequence and Construct

cheY$_6$ was inserted into the expression plasmid pQE80 (N-terminal, His$_6$-tag) using the method described in Section 2.3 but using *Bam*HI and *Nco*I restriction enzymes. pQE80-*cheY$_6$* was transformed into *E. coli* BL21 (DE3) cells and induced in M9 minimal media containing $^{15}NH_4Cl$ for ^{15}N-labeled protein. $^{15}NH_4Cl$ and ^{13}C-glucose was used to produce ^{13}C, ^{15}N-labeled protein. Purification was achieved using a Nickel-NTA Agarose column and further purified using size exclusion chromatography. ^{13}C,^{15}N-CheY$_6$ was produced by C. H. Bell.

Purified CheY$_6$ used for NMR experiments contained 145 residues in total (Figure 3.2). The His$_6$-tag accounted for 11 residues. This chapter describes some of the experiments used for backbone and side-chain assignment work and shows some typical spectra for each experiment. It also describes how to interpret and assign these NMR spectra.

```
         10         20         30         40         50         60
MRGSHHHHHHGSPYNVMIVDDAAMMRLYIASFIKTLPDFKVVAQAANGQEALDKLAAQPN
         70         80         90        100        110        120
VDLILLDIEMPVMDGMEFLRHAKLKTRAKICMLSSVAVSGSPHAARARELGADGVVAKPS
       130        140
GTVSHDLEEKTGGELARTMRTLMAA
```

Figure 3.2 – Sequence of CheY$_6$ used for NMR experiments – The tag (red) required for purification contains a small linker (GlySer) between the His$_6$-tag and the protein.

3.4 Backbone Assignment Experiments

3.4.1 ^{1}H, ^{15}N-HSQC

A ^{1}H, ^{15}N heteronuclear single quantum coherence (HSQC) experiment results in a two dimensional spectrum, one axis for proton (^{1}H) and the other for the heteronucleus (^{15}N). It uses $^{1}J_{NH}$ coupling to transfer magnetisation between these two nuclei (Figure 3.3). Each peak in the spectrum corresponds to a proton attached to labelled nitrogen (^{15}N).

^{1}H, ^{15}N-HSQC

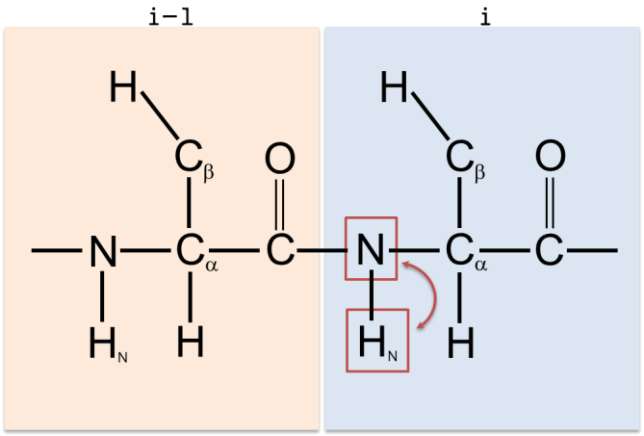

Figure 3.3 – ^{1}H, ^{15}N-HSQC coherence transfer schematic – Magnetisation is transferred from the proton to the adjacent nitrogen (^{15}N) through J-coupling. This is then evolved on the nitrogen before transfer back to the proton for detection. The ^{1}H, ^{15}N-HSQC spectrum contains one peak for each proton attached to labeled nitrogen.

A ^{1}H, ^{15}N-HSQC spectrum (Figure 3.4) was collected using a sample of ^{15}N-labeled $CheY_6$. The spectrum is generally well dispersed, however there is significant overlap in the central region (^{1}H 7.5-9.0 ppm, ^{15}N 115-125 ppm). This region has been magnified in Figure 3.5. The ^{1}H, ^{15}N-HSQC spectrum contained approximately

180 peaks which were arbitrarily labelled. These were then used as the basis of assignment where 3D experiments were used in tandem to achieve backbone and side-chain assignments.

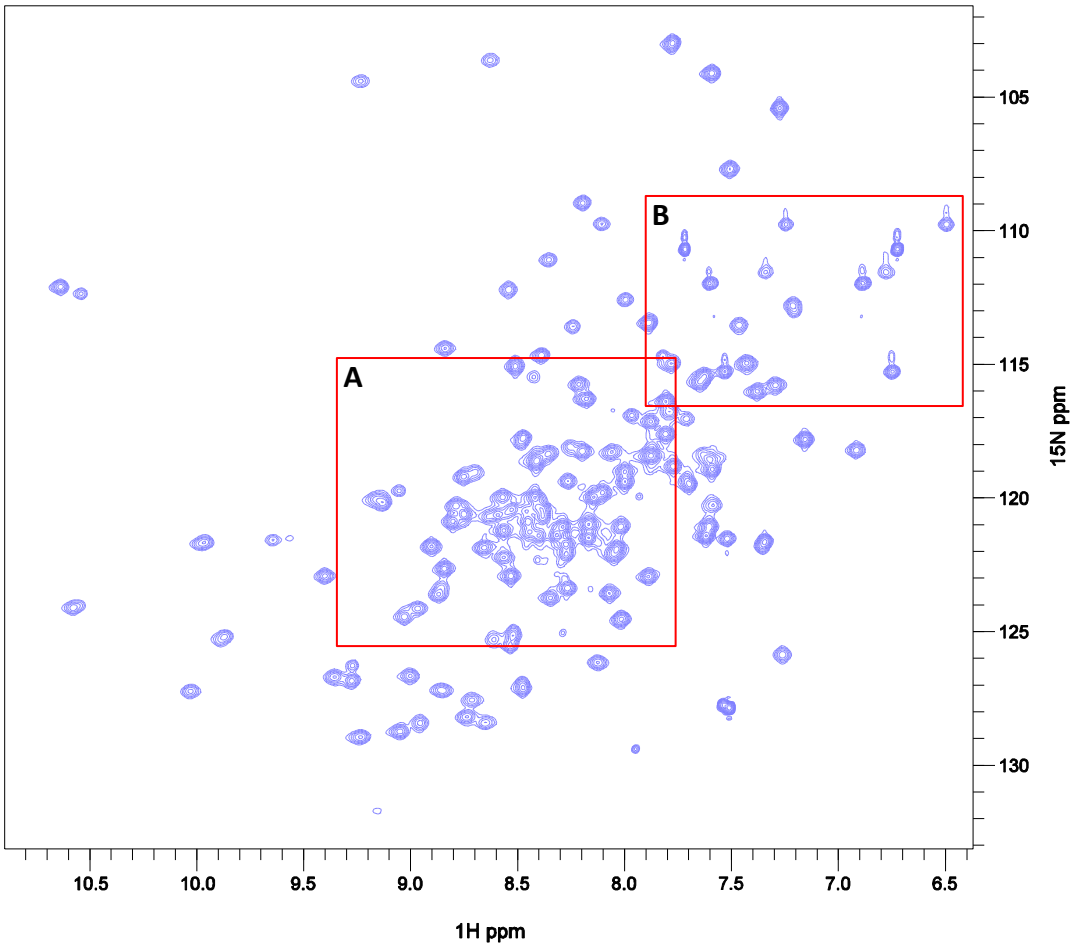

Figure 3.4 – 500 MHz ^{1}H, ^{15}N-HSQC spectrum of $CheY_6$ – **A)** Central region showing relatively poor dispersion of residues. Magnification of this region can be found in Figure 3.5. **B)** Region of spectrum that contains the NH_2 groups of N and Q.

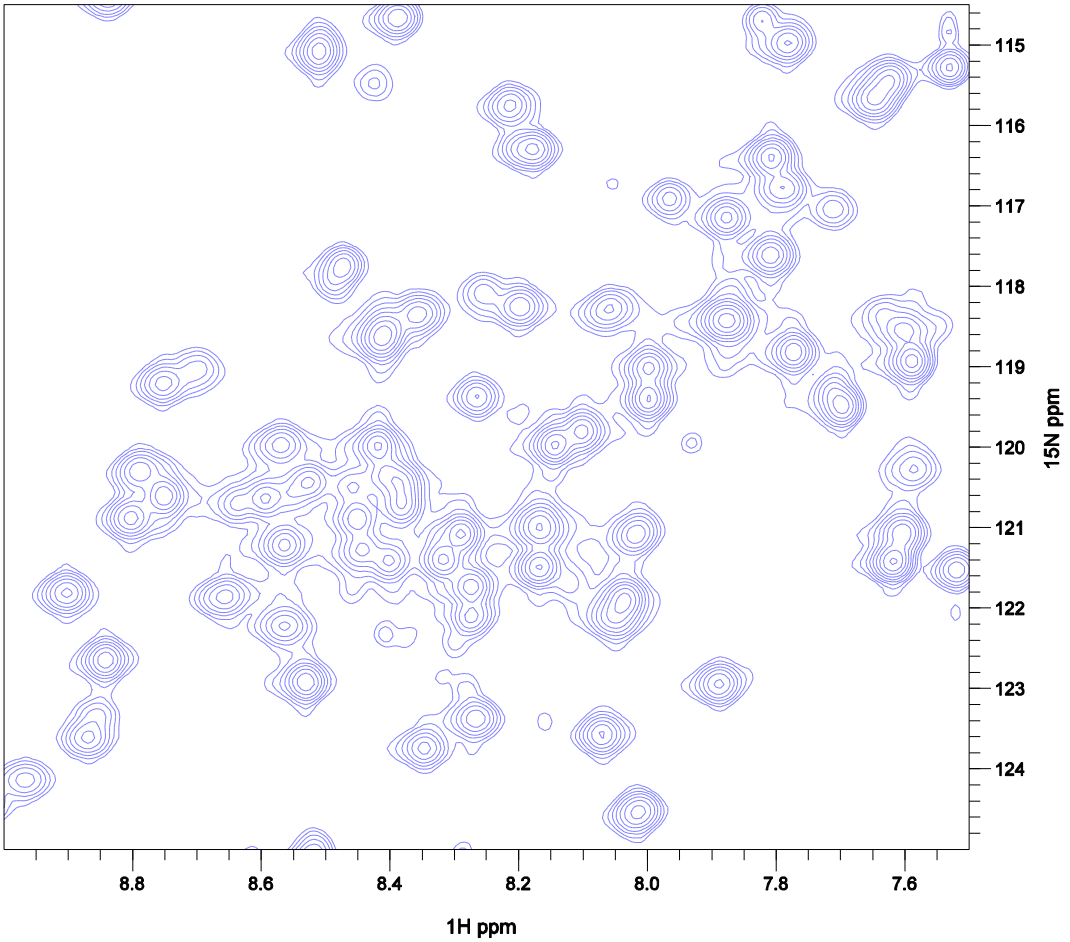

Figure 3.5 – Magnified central region of the ^{1}H, ^{15}N-HSQC spectrum of $CheY_6$ – Within the central region (^{1}H - 7.5-9 ppm, ^{15}N - 114.4-124.7 ppm), the peaks are less resolved and therefore more difficult to assign.

3.4.2 ^{1}H, ^{15}N-HSQC - Side-chain H^N identification

The side-chain NH_2 groups from asparagine and glutamine give peaks in the ^{1}H, ^{15}N-HSQC spectrum. Two peaks are seen for each NH_2 group. They have the same nitrogen chemical shift values, but with differing proton chemical shift values. These NH_2 peaks are relatively easy to identify because of the additional peaks (*) from the small amount of 'NHD' species present. The deuterium isotope effect on the ^{15}N chemical shift results in NHD peaks that are resolved from the NH_2 peaks. Once

these peaks were identified, they could be discounted from the backbone assignment process.

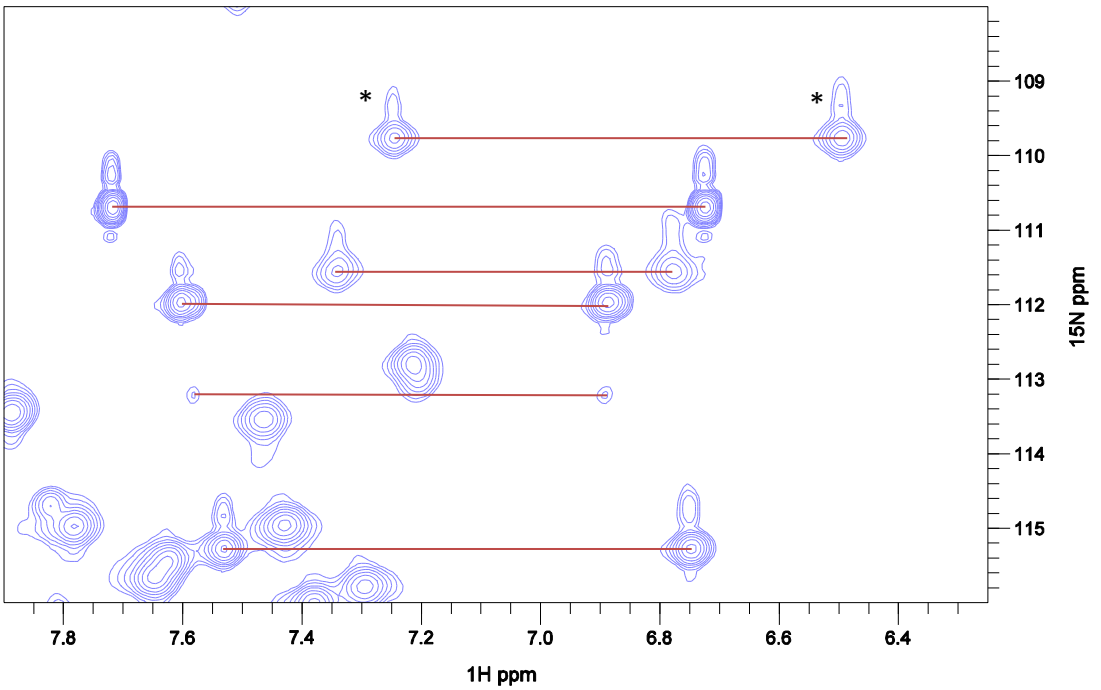

Figure 3.6 – Magnified region of the ^{1}H, ^{15}N-HSQC spectrum of $CheY_6$ containing the NH_2 side-chain groups. Each NH_2 group has two peaks with the same nitrogen chemical shift, but with differing proton chemical shifts.

3.4.3 3D Experiments – Triple Resonance Data

Triple resonance experiments were used to sequentially assign the backbone resonances of $CheY_6$. Double labeled protein (^{13}C, ^{15}N) was used to collect the appropriate spectra. Analysis of these 3D spectra (C_α and C_β in particular) allowed the linkage of sequential spin systems. Reference chemical shift values were used to determine the spin system type. Once the spin system type had been established, unique amino acid sequences within $CheY_6$ could be explored to unambiguously assign the spin system.

3.4.3.1 Analysing $^{13}C_{\alpha}$ chemical shifts to identify sequential connections

HNCA and HN(CO)CA experiments were used to measure and assign C_{α} chemical shifts. The HNCA experiment gives rise to two peaks in the carbon dimension of the spectrum. The experiment measures the chemical shift of the C_{α} attached to the NH group (i) that is directly measured and the C_{α} from the previous residue (i-1). In contrast, the HN(CO)CA only measures the C_{α} from the previous residue (i-1). The coherence transfer schematic (Figure 3.7) illustrates the transfer of magnetisation (Kay *et al*. 1990) (Grzesiek *et al*. 1992). An overlay of these two experiments (Figure 3.8) makes it possible to determine which C_{α} peaks are from the (i) and which are from the (i-1). These overlays can then be used to identify sequential spin systems.

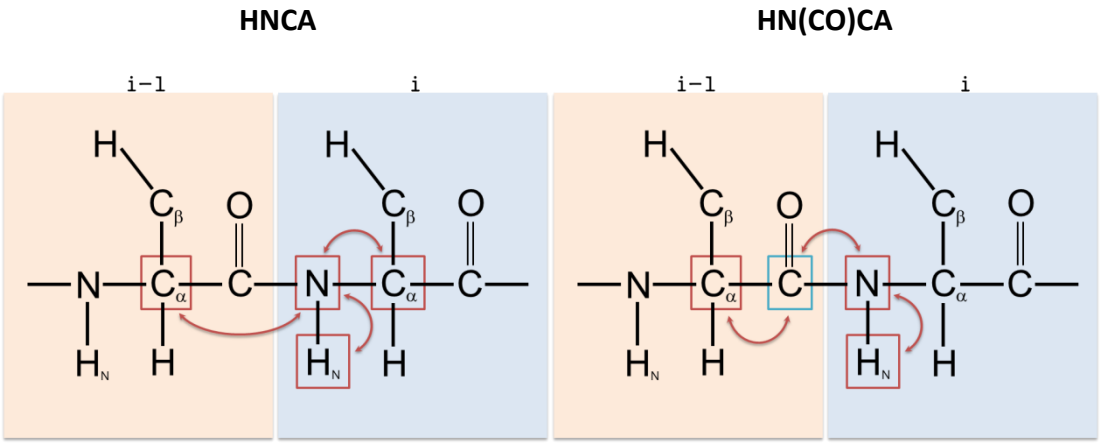

Figure 3.7 – HNCA and HN(CO)CA coherence transfer schematic – HNCA experiments select for the C_{α} for both the (i) and (i-1) residues whereas HN(CO)CA just selects for the C_{α} of the (i-1) residue (Grzesiek and Bax 1992). **HNCA** – Magnetisation is transferred from ^{1}H to ^{15}N, then to $^{13}C_{\alpha}$ via N-C_{α} J-coupling and then back to ^{15}N and ^{1}H for detection. **HN(CO)CA** – Magnetisation is transferred from ^{1}H to ^{15}N, then to ^{13}CO(i-1) and then to $^{13}C_{\alpha}$(i-1) where the chemical shift is evolved. Magnetisation is then passed back from $^{13}C_{\alpha}$(i-1) to ^{15}N (via ^{13}CO(i-1)) and finally to ^{1}H for detection. The chemical shift for ^{13}CO is not evolved.

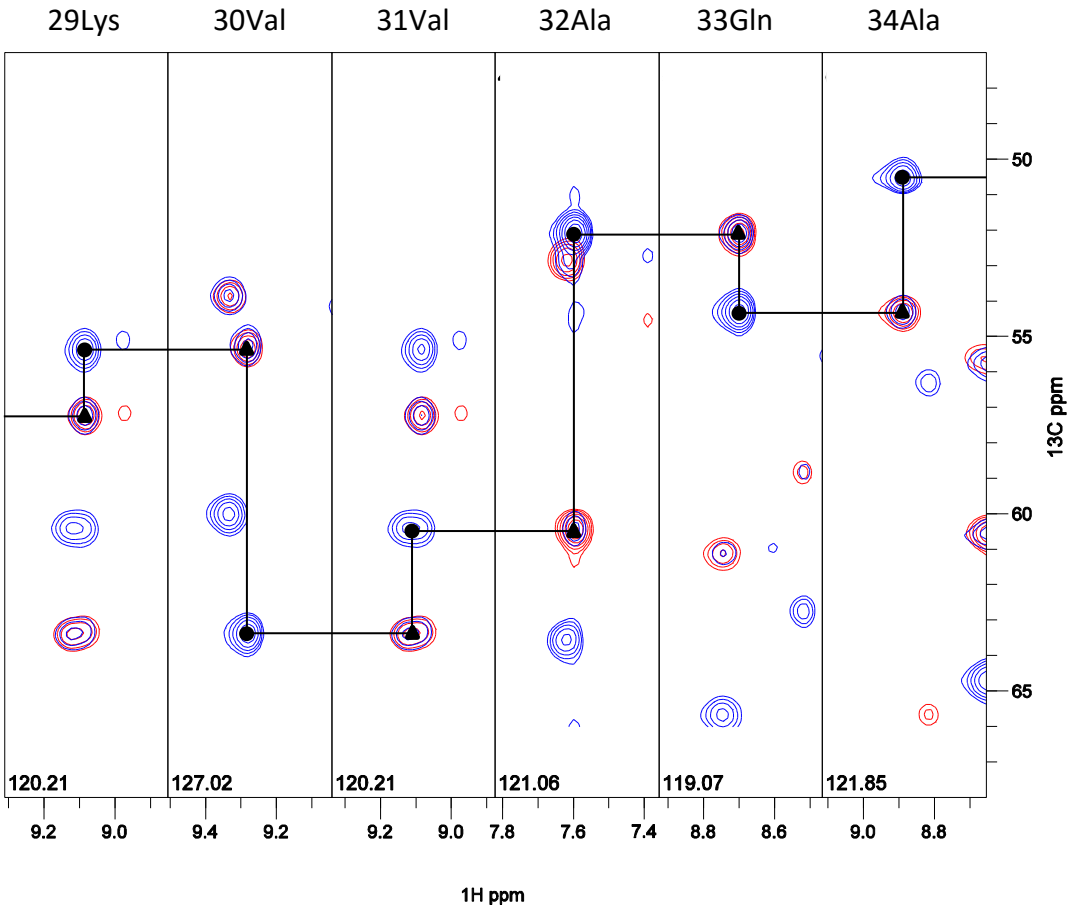

Figure 3.8 – HNCA (blue) and HN(CO)CA (red) spectra overlay of $CheY_6$ – HNCA gives two C_α peaks corresponding to residues (i) and (i-1). HN(CO)CA gives one C_α peak corresponding to the (i-1) residue. Circles (●) indicate C_α peaks from (i) and triangles (▲) indicate overlapped C_α (i-1) peaks from HNCA and HN(CO)CA. The strips shown for 29Lys-34Ala are an example of a well-dispersed region. In more complicated regions of the spectrum, other experiments were needed to unambiguously assign spin systems. The ^{15}N chemical shift (ppm) for each spin system can be found at the bottom of each strip.

3.4.3.2 Analysing $^{13}C_\beta$ chemical shifts to identify sequential connections

CBCANH and CBCA(CO)NH experiments were used to measure and assign C_β chemical shifts. The CBCANH experiment gives rise to two peaks in the C_β regions of

the spectrum. The experiment measures the chemical shift of the C_β attached to the NH group (i) that is directly measured and the C_β from the previous residue (i-1). The CBCANH experiment also measures the C_α chemical shifts. This allowed correlation with the HNCA and HN(CO)CA experiments for further verification of correct assignments. This was particularly useful when analysing residues such as S and T which have C_β chemical shifts that are within the C_α chemical shift region. In contrast, the CBCA(CO)NH only measures the C_α and C_β from the previous residue (i-1). The coherence transfer schematic (Figure 3.9) illustrates the transfer of magnetisation (Kay *et al*. 1990) (Grzesiek and Bax 1992). An overlay of these two experiments (Figure 3.10) makes it possible to determine which C_α and C_β peaks are from the (i) and which are from the (i-1). These overlays can then be used to identify sequential spin systems.

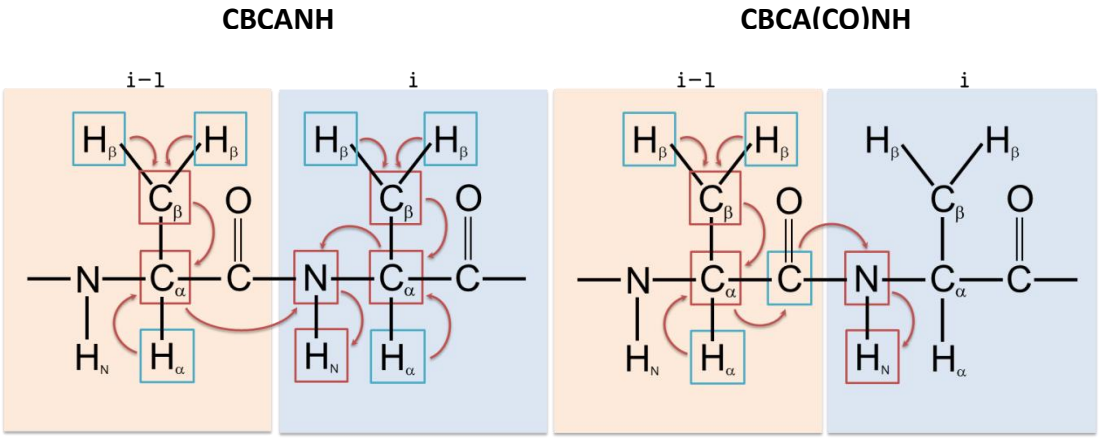

Figure 3.9 – CBCANH and CBCA(CO)NH coherence transfer schematic – CBCANH experiments select for the C_α and C_β for both the (i) and (i-1) residues whereas CBCA(CO)NH just selects for the C_α and C_β of the (i-1) residue (Grzesiek and Bax 1992). **CBCANH** – Magnetisation is transferred from $^{1}H_\alpha$ to $^{13}C_\alpha$ and from $^{1}H_\beta$ to $^{13}C_\beta$. Transfer then occurs from $^{13}C_\beta$ to $^{13}C_\alpha$, then to ^{15}N before transfer to $^{1}H^N$ for detection. Magnetisation can be transferred to $^{15}N(i)$ from both the $^{13}C_\alpha(i)$ and $^{13}C_\alpha(i-1)$ and both the $^{13}C_\beta(i)$ and $^{13}C_\beta(i-1)$. Hence, four peaks are visible for each NH group. **CBCA(CO)NH** – Magnetisation is transferred from $^{1}H_\alpha$ to $^{13}C_\alpha$ and from $^{1}H_\beta$ to $^{13}C_\beta$. Transfer then occurs from $^{13}C_\beta$ to $^{13}C_\alpha$, then to ^{15}N (via ^{13}CO) before transfer to $^{1}H^N$ for detection. The chemical shift for ^{13}CO is not evolved. As $^{13}C_\alpha$ and $^{13}C_\beta$ are evolved simultaneously in both experiments, they appear in one dimension. The chemical shifts of $^{1}H_\alpha$ and $^{1}H_\beta$ to are not evolved in either experiment.

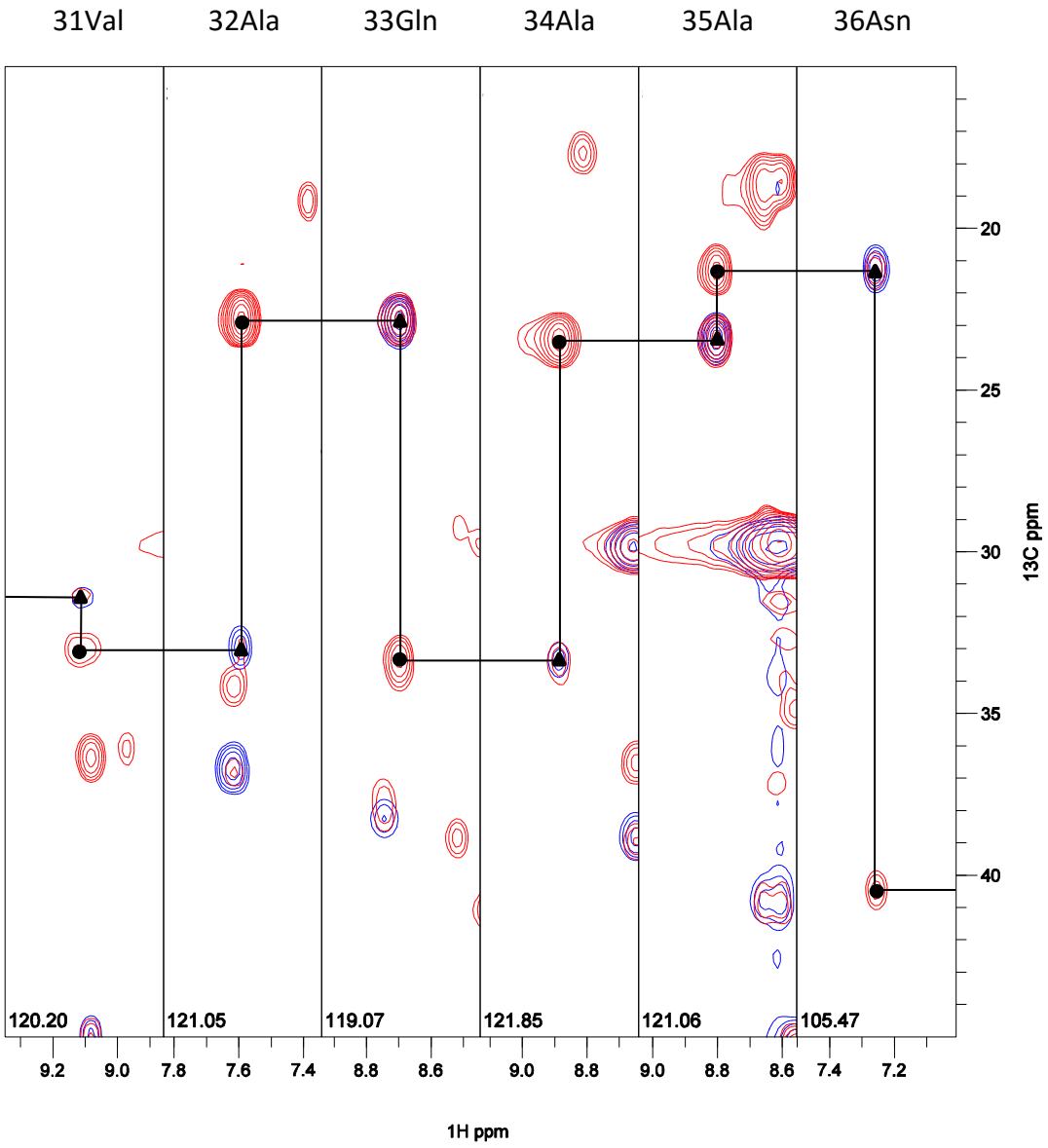

Figure 3.10 – CBCANH (red) and CBCA(CO)NH (blue) spectra overlay of $CheY_6$ – CBCANH gives two C_β peaks corresponding to residues (i) and (i-1). CBCA(CO)NH gives one C_β peak corresponding to the (i-1) residue. Circles (●) indicate C_β peaks from (i) and triangles (▲) indicate overlapped C_β(i-1) peaks from CBCANH and CBCA(CO)NH. Strips are shown for 31Val-36Asn which is an example of a well-dispersed region. In more complicated regions, other experiments were needed to unambiguously assign spin systems. The ^{15}N chemical shift (ppm) for each spin system can be found at the bottom of each strip.

3.4.3.3 Analysing ^{13}CO chemical shifts to identify sequential connections

HN(CA)CO and HNCO experiments were used to measure and assign the carbonyl carbon (CO) chemical shifts in the backbone of $CheY_6$. The HN(CA)CO experiment gives rise to two peaks in the CO region of the spectrum. The experiment measures the chemical shifts of the CO attached to the NH group (i) that is directly measured and the CO from the previous residue (i-1). In contrast, the HNCO only measures the CO from the previous residue (i-1). The coherence transfer schematic (Figure 3.11) illustrates the transfer of magnetisation (Clubb, Thanabal, and Wagner 1992). An overlay of these two experiments (Figure 3.12) makes it possible to determine which CO peaks are from the (i) and which are from the (i-1). As dispersion of the CO peaks is poor, it was difficult to use these experiments in isolation for sequential assignment. Instead, these experiments were used to verify assignments made by other experiments.

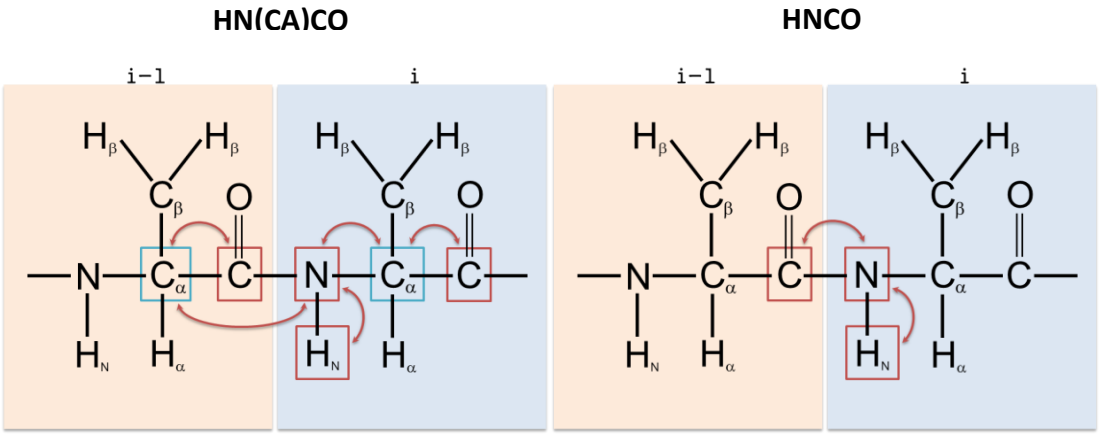

Figure 3.11 – HN(CA)CO and HNCO coherence transfer schematic – HN(CA)CO experiments select for the CO for both the (i) and (i-1) residues whereas HNCO just selects for the CO of the (i-1) residue (Clubb *et al*. 1992). **HN(CA)CO** – Magnetisation is transferred from $^{1}H^{N}$ to ^{15}N, then to $^{13}C_{\alpha}$ (via N-C_{α} J-coupling) and finally to ^{13}CO (via $^{13}C_{\alpha}$-^{13}CO J-coupling). Transfer then occurs in the reverse direction back to $^{1}H^{N}$ for detection. Magnetisation can be transferred to both $^{13}C_{\alpha}$(i) and $^{13}C_{\alpha}$(i-1) from the ^{15}N(i). Hence, two peaks are visible for each NH group. The chemical shifts for the $^{13}C_{\alpha}$ nuclei are not evolved. **HNCO** – Magnetisation is transferred from $^{1}H^{N}$ to $^{15}N^{H}$ and then to ^{13}CO(i-1) (via $^{15}N^{H}$-^{13}CO J-coupling). Transfer then occurs in the reverse direction back to $^{1}H^{N}$ for detection. The chemical shifts for $^{1}H^{N}$, ^{15}N and ^{13}CO are evolved in both experiments, leading to three dimensional spectra.

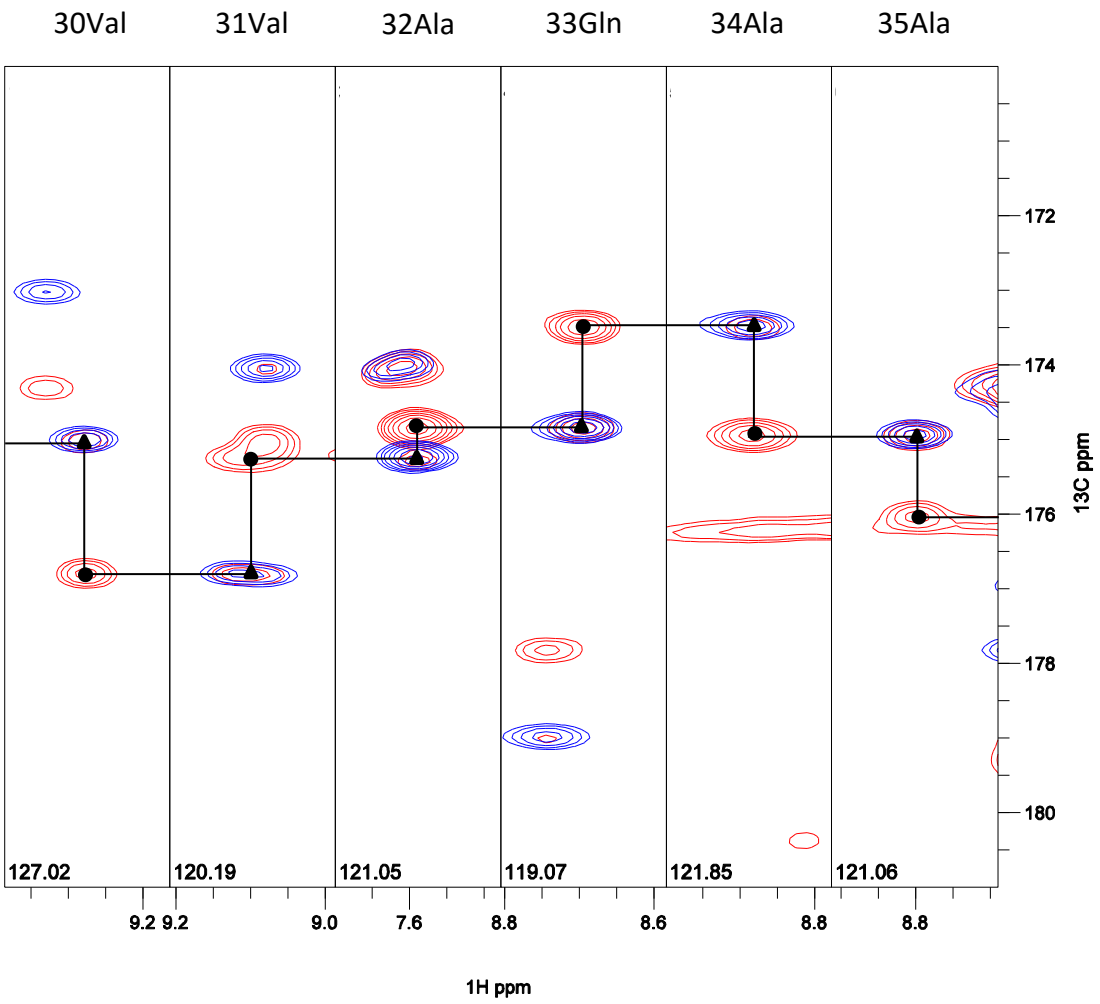

Figure 3.12 – HN(CA)CO (red) and HNCO (blue) spectra overlay of $CheY_6$ – HN(CA)CO gives two CO peaks corresponding to residues (i) and (i-1). HNCO gives one CO peak corresponding to the (i-1) residue. Circles (●) indicate CO peaks from (i) and triangles (▲) indicate (i-1) CO peaks in the two spectra. The strips shown for 30Val-35Ala are an example of a well-dispersed region. The ^{15}N chemical shift (ppm) for each spin system can be found at the bottom of each strip.

3.4.3.4 Analysing NH-NH chemical shifts to identify sequential connections

The 3D ^{15}N-NOESY-HSQC experiment shows peaks from pairs of protons that are close in space (through-space dipolar connections). The NOEs between NH groups can be used to identify neighbouring residues. This information is particularly useful when assigning sequential spins systems that have helical secondary structure. The coherence transfer schematic (Figure 3.13) illustrates the transfer of magnetisation (Messerle *et al*. 1989). A ^{15}N-NOESY-HSQC spectrum (Figure 3.14) can sometimes be overcrowded but it is a useful way to validate assignments.

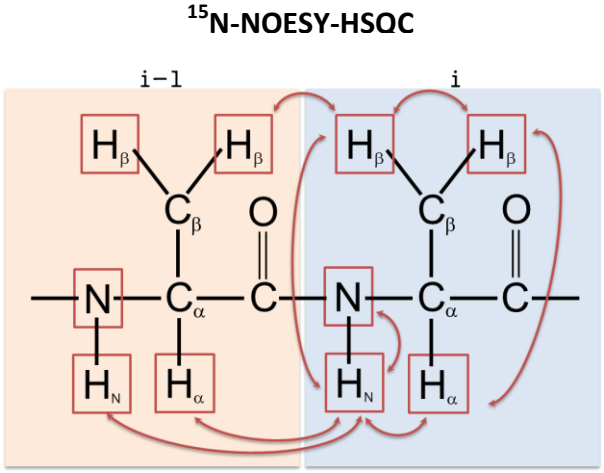

Figure 3.13 – ^{15}N-NOESY-HSQC coherence transfer schematic – Magnetisation is transferred between all protons using through-space NOE connections, before it is transferred in the HSQC step to the ^{15}N nuclei. Finally it is transferred back to the $^{1}H^{N}$ for detection (Messerle *et al*. 1989).

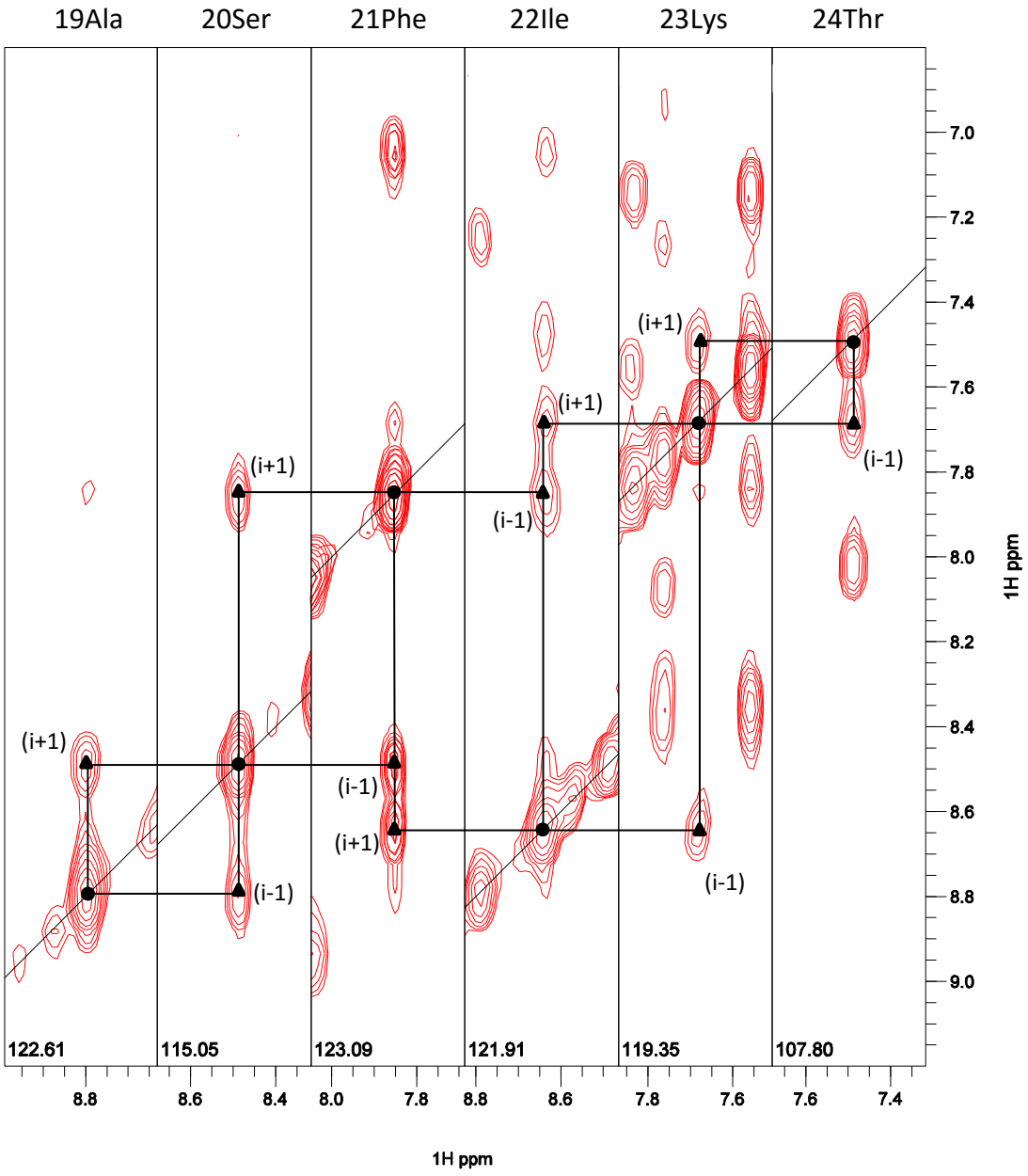

Figure 3.14 – ^{15}N-NOESY-HSQC spectrum of CheY$_6$ – The $^{1}H^{N}$ region of the spectrum is shown for residues 19Ala-24Thr which forms α-helix 1 in CheY$_6$. Circles (●) indicate strong diagonal peaks and triangles (▲) indicate peaks from connected protons (i+1) and (i-1). Spectrum shown is an example of a well-dispersed region. The ^{15}N chemical shift (ppm) for each spin system can be found at the bottom of each strip.

3.5 Side-chain Assignment Experiments

3.5.1 H_α, H_β Assignment

HBHA(CO)NH experiments were used to measure and assign the H_α and H_β chemical shifts of $CheY_6$. The experiment correlates the H_α and H_β chemical shifts of the preceding residue (i-1) to the NH group (i) that is directly measured. The coherence transfer schematic (Figure 3.15) illustrates the transfer of magnetisation (Zhang, Neal, and Wishart 2003). H_β chemical shifts were very useful in determining spin system type and aided in backbone assignment. Some regions of the spectrum (Figure 3.17) were crowded and some peaks too weak to resolve. A ^{15}N-edited TOCSY-HSQC measures the H_α and H_β chemical shifts of the NH group (i) that is directly measured and was used to confirm assignment in overlapped regions of the HBHA(CO)NH (Figure 3.18). The coherence transfer schematic (Figure 3.16) illustrates the transfer of magnetisation in the ^{15}N-TOCSY-HSQC.

HBHA(CO)NH

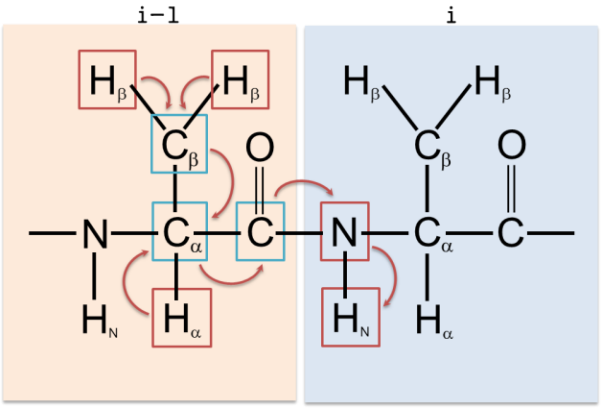

Figure 3.15 – HBHA(CO)NH coherence transfer schematic – Magnetisation is transferred from $^{1}H_{\alpha}$ to $^{13}C_{\alpha}$ and from $^{1}H_{\beta}$ to $^{13}C_{\beta}$. Then transfer occurs from $^{13}C_{\beta}$ to $^{13}C_{\alpha}$, then to ^{13}CO, then to ^{15}N and finally to $^{1}H^{N}$ for detection. Chemical shifts are only evolved for $^{1}H_{\alpha}$, $^{1}H_{\beta}$, ^{15}N and $^{1}H^{N}$ (Grzesiek and Bax 1992) (Wishart *et al*. 1995).

^{15}N-TOCSY-HSQC

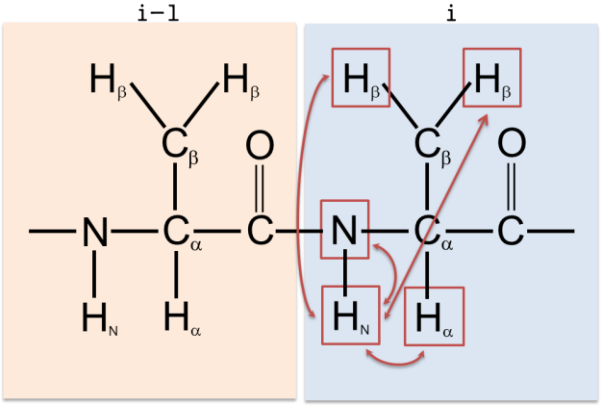

Figure 3.16 – ^{15}N-TOCSY-HSQC coherence transfer schematic – Magnetisation is transferred between ^{1}H spins with an isotropic mixing step. Transfer then occurs in the HSQC step to $^{1}H^{N}$ for detection.

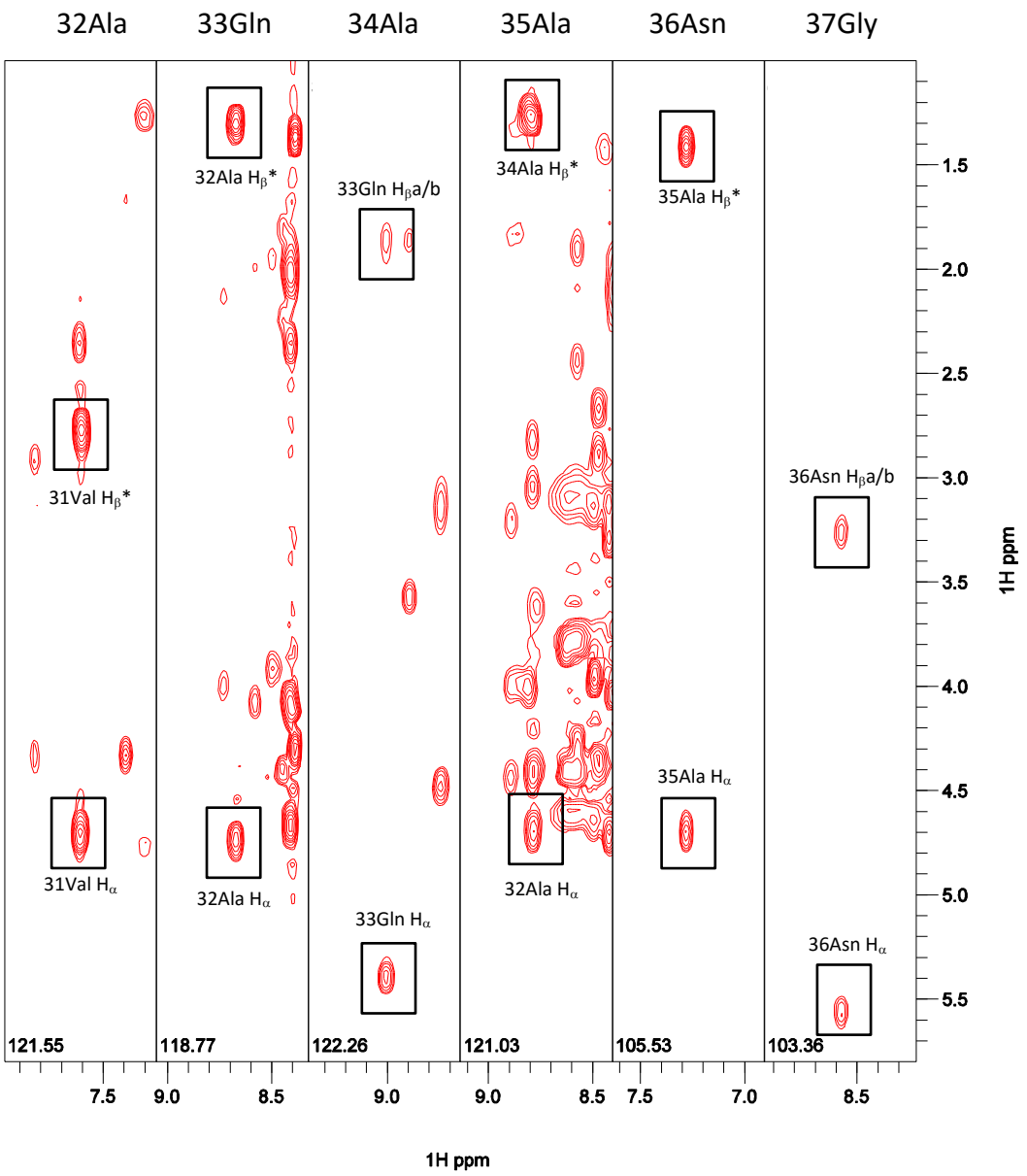

Figure 3.17 – HBHA(CO)NH spectrum of CheY$_6$ – The $^1H_\alpha$ and $^1H_\beta$ region of the spectrum is shown for residues 32Ala-37Gly. Boxes indicate peaks that correspond to the H_α and H_β chemical shifts of the previous residue (i-1). Spectrum shown is an example of a well-dispersed region. The ^{15}N chemical shift (ppm) for each spin system can be found at the bottom of each strip.

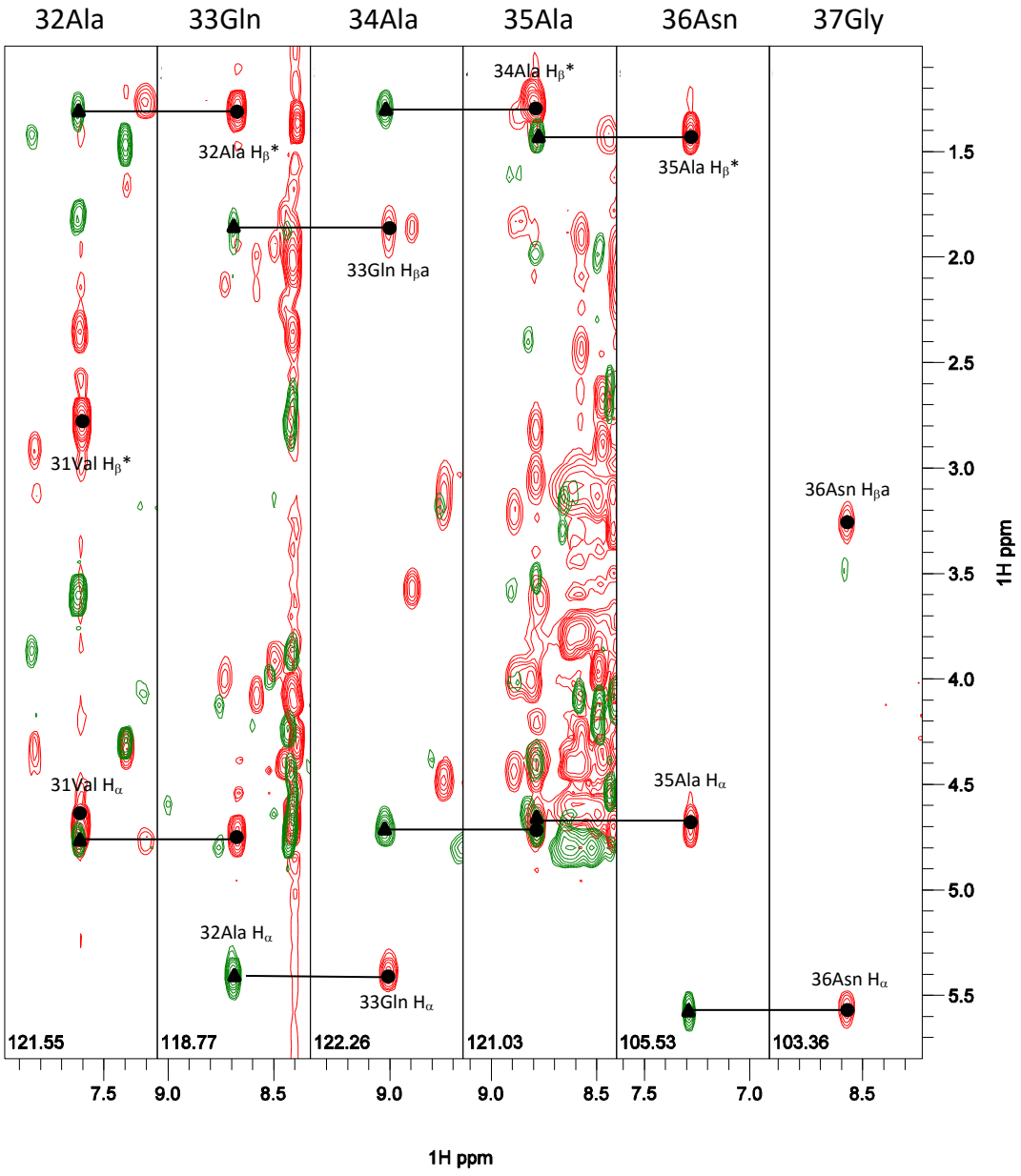

Figure 3.18 – ^{15}N-TOCSY-HSQC (green) and HBHA(CO)NH (red) spectra of CheY$_6$ – The $^{1}H_{\alpha}$ and $^{1}H_{\beta}$ region of the spectrum is shown for residues 32Ala-37Gly. Circles (●) indicate peaks that correspond to the H_{α} and H_{β} chemical shifts of the previous residue (i-1). Triangles (▲) indicate peaks that correspond to the H_{α} and H_{β} chemical shifts of residue (i). Spectrum shown is an example of a well-dispersed region. The ^{15}N chemical shift (ppm) for each spin system can be found at the bottom of each strip.

3.5.2 C_γ, C_δ, H_γ, H_δ – Additional Side-chain Assignments

(H)CC(CO)NH and HCCH-TOCSY experiments were used to make additional side-chain assignments that could be useful when carrying out structure determination. The coherence transfer schematics (Figure 3.19 and Figure 3.20 respectively) illustrate the transfer of magnetisation in both experiments (Fesik *et al*. 1990) (Bax, Clore, and Gronenborn 1990). The (H)CC(CO)NH experiment allows determination of the chemical shifts for side-chain carbon nuclei (e.g. C_γ, C_δ) of the residue (i-1) preceding the NH group (i) that is being directly measured. This can be used in conjunction with the HCCH-TOCSY experiment which yields strips at each carbon chemical shift where all proton resonances are visible. All aliphatic proton resonances can be linked to each other in the HCCH-TOCSY spectrum (Figure 3.22).

(H)CC(CO)NH

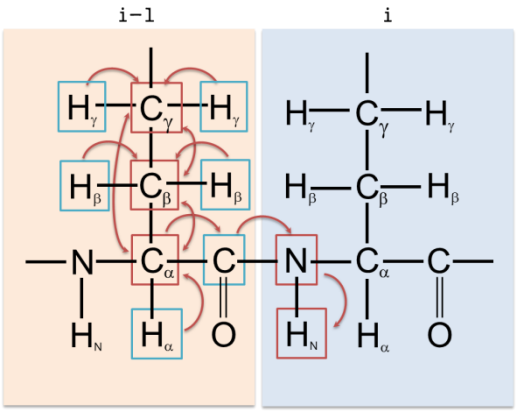

Figure 3.19 – (H)CC(CO)NH coherence transfer schematic – Magnetisation is transferred from the side-chain proton nuclei to the directly attached ^{13}C nuclei. Isotropic mixing is used to transfer magnetisation between ^{13}C nuclei. Transfer then occurs to ^{15}N (via ^{13}CO) and finally to $^{1}H^{N}$ for detection. Chemical shifts are evolved simultaneously for all ^{13}C nuclei. ^{13}CO and proton chemical shifts are not evolved.

HCCH-TOCSY

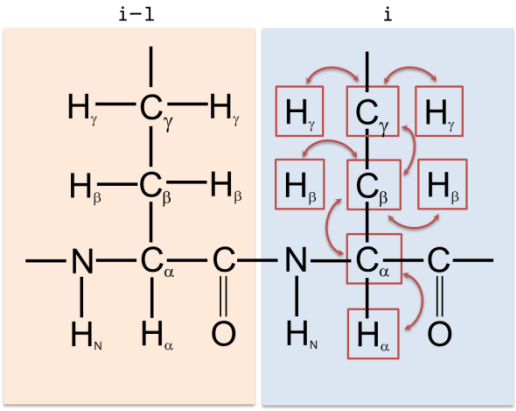

Figure 3.20 – HCCH-TOCSY coherence transfer schematic – Magnetisation is transferred from the H_α and side-chain ^{1}H nuclei to the directly attached ^{13}C nuclei. Isotropic mixing is used to transfer magnetisation between ^{13}C nuclei. Magnetisation is then transferred back to the H_α and side-chain ^{1}H nuclei for detection.

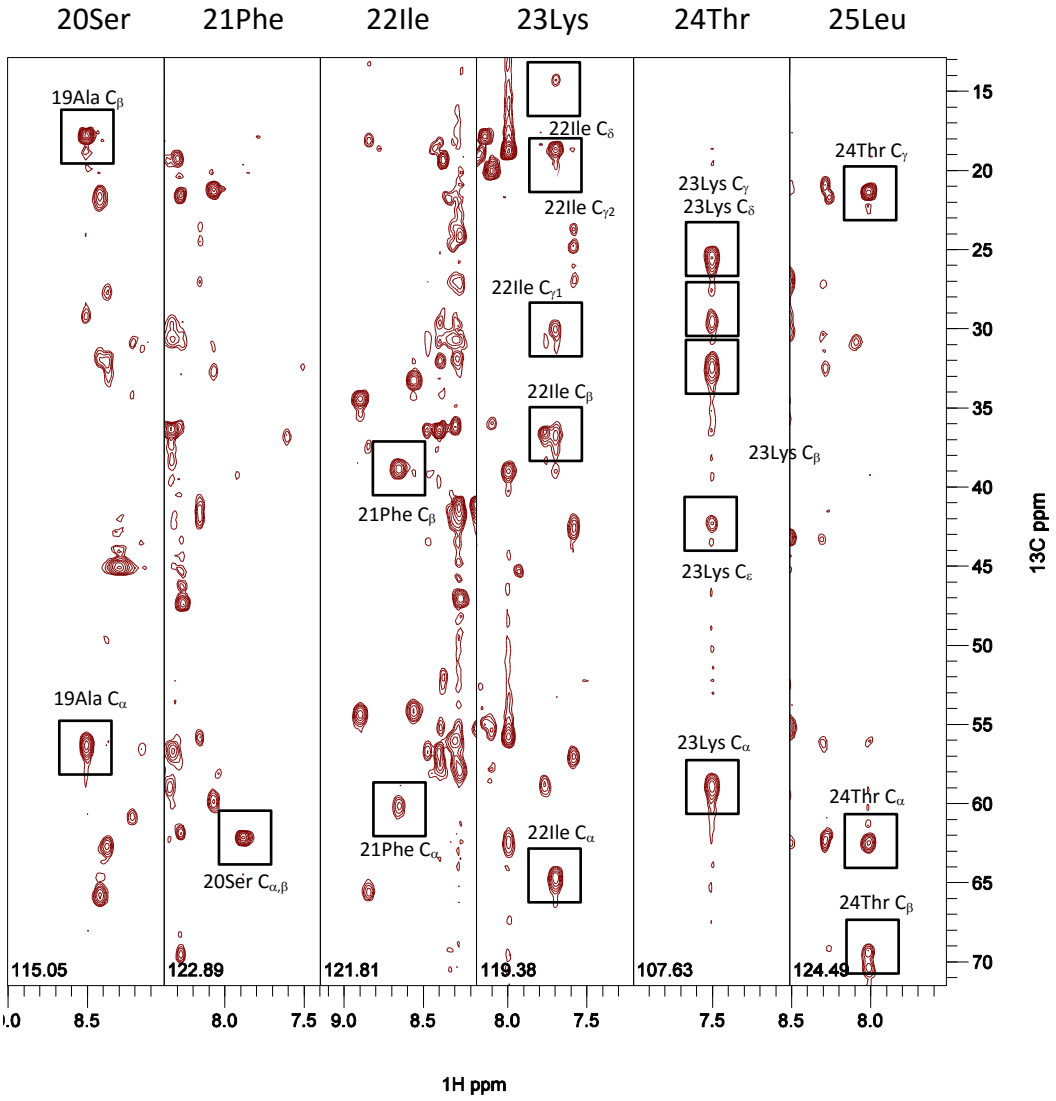

Figure 3.21 – (H)CC(CO)NH spectrum of CheY$_6$ – Boxes indicate peaks that correspond to the C_α, C_β, C_γ, C_δ, and C_ε chemical shifts of the previous residue (i-1). Spectrum shown is an example of a well-dispersed region (20Ser-25Leu). The ^{15}N chemical shift (ppm) for each spin system can be found at the bottom of each strip.

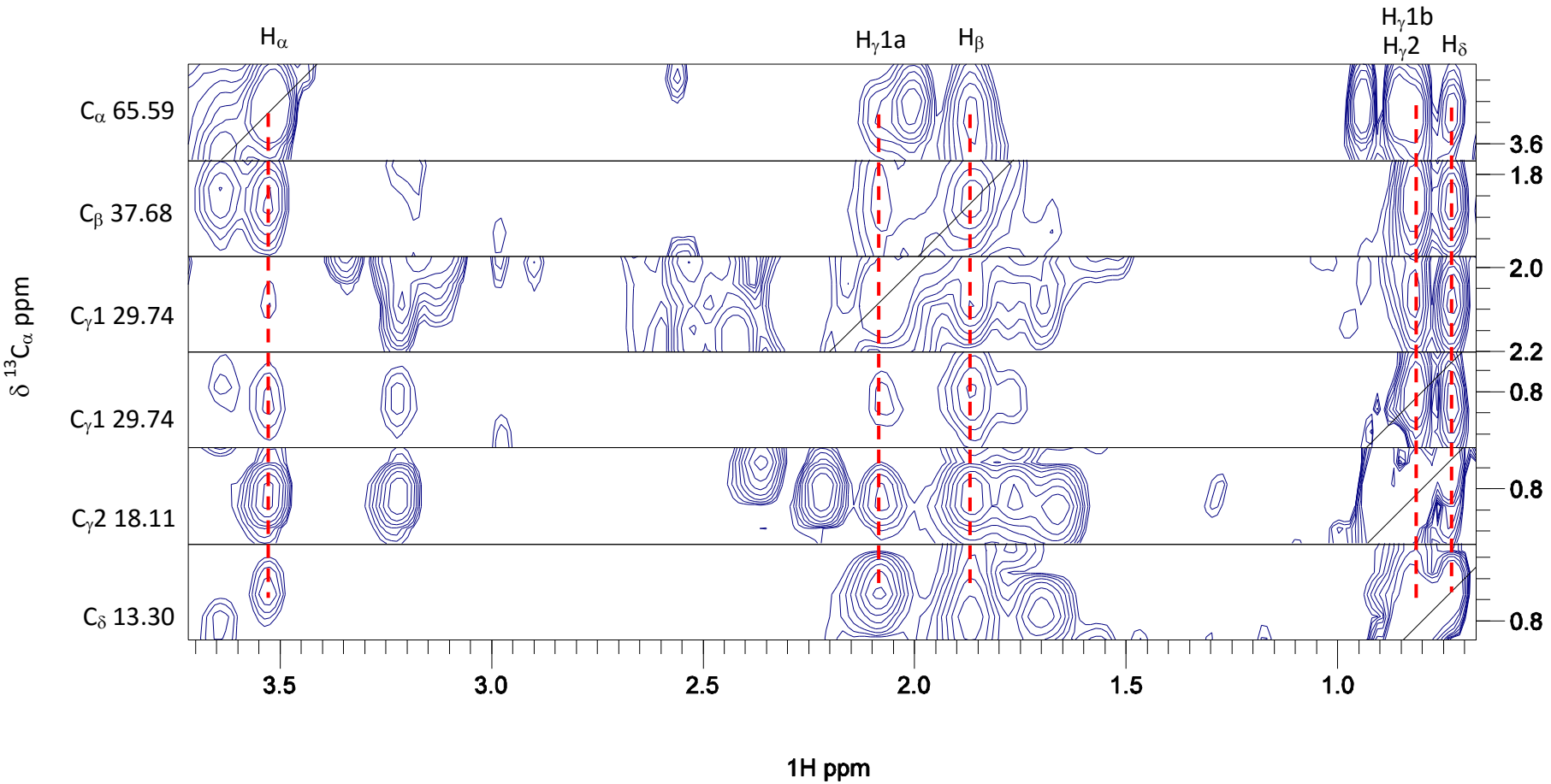

Figure 3.22 – Strips from the HCCH-TOCSY spectrum showing side-chain assignments of 18Ile – Peaks found at diagonal lines give the ^{1}H chemical shift for the proton connected to the ^{13}C nuclei of the carbon plane. Transfer of coherence allows strips to link up protons of the same spin system (dashed lines).

3.6 Statistics of Backbone and Side-chain Assignments

The $CheY_6$ construct used for data collection was comprised of 145 residues, 11 of these made up the N-terminal His_6-tag. Data were collected under four different conditions. Percentages of backbone and side-chain assignments can be found in Table **3.1** and

Table 3.2. Six proline residues are present in the $CheY_6$ construct which do not give a ^{15}N-$^{1}H^{N}$ correlations in the HSQC. Some NH backbone peaks broaden and are no longer visible at pH 7.2.

	Percentage Assigned			
Resonance	**$CheY_6$ pH 5.5**	**$CheY_6$ + BeF_3 pH 5.5**	**$CheY_6$ pH 7.2**	**$CheY_6$ + BeF_3 pH 7.2**
^{15}N	100	97.6	98.4	96.1
$^{1}H^{N}$	100	97.6	98.4	96.1
$^{13}C_{\alpha}$	98.5	98.5	100	97.7
$^{1}H_{\alpha}$	97.2	97.9	98.6	97.2
^{13}CO	94.0	97.0	95.5	96.2
Overall Backbone Assignment	97.0	96.6	97.0	95.4

Table 3.1 – Backbone assignment percentages of $CheY_6$ in different conditions. Percentages do not include ^{15}N proline residues.

	Percentage Assigned			
Resonance	**$CheY_6$ pH 5.5**	**$CheY_6$ + BeF_3 pH 5.5**	**$CheY_6$ pH 7.2**	**$CheY_6$ + BeF_3 pH 7.2**
$^{13}C_\beta$	98.4	98.4	99.2	97.6
$^{1}H_\beta$	95.2	97.1	98.1	95.2
$^{13}C_\gamma$	71.1	73.7	75.4	77.2
$^{1}H_\gamma$	77.3	80.9	82.3	83.0
$^{13}C_\delta$	72.6	68.5	69.9	67.1
$^{1}H_\delta$	75.6	78.9	73.3	75.6
$^{13}C_\varepsilon$	24.0	20.0	16.0	20.0
$^{1}H_\varepsilon$	39.1	34.8	34.8	30.4
Side-chain H	84.2	86.0	86.0	84.9
Side-chain non-H	68.7	68.5	69.2	69.0

Table 3.2 – Side-chain assignment percentages of $CheY_6$ in different conditions.

3.7 pH Effects on the NMR Spectra of $CheY_6$

Solution conditions at pH 5.5 (20 mM sodium acetate, 2 mM $MgCl_2$) were initially identified by Christian Bell, as conditions under which $CheY_6$ is stable and soluble. To study FliM interactions, pH 7.2 was required due to FliM stability, and it also provided more physiologically relevant conditions. $CheY_6$ shows precipitation when raising the pH to 7.2, additional Mg (15 mM) was found to improve stability.

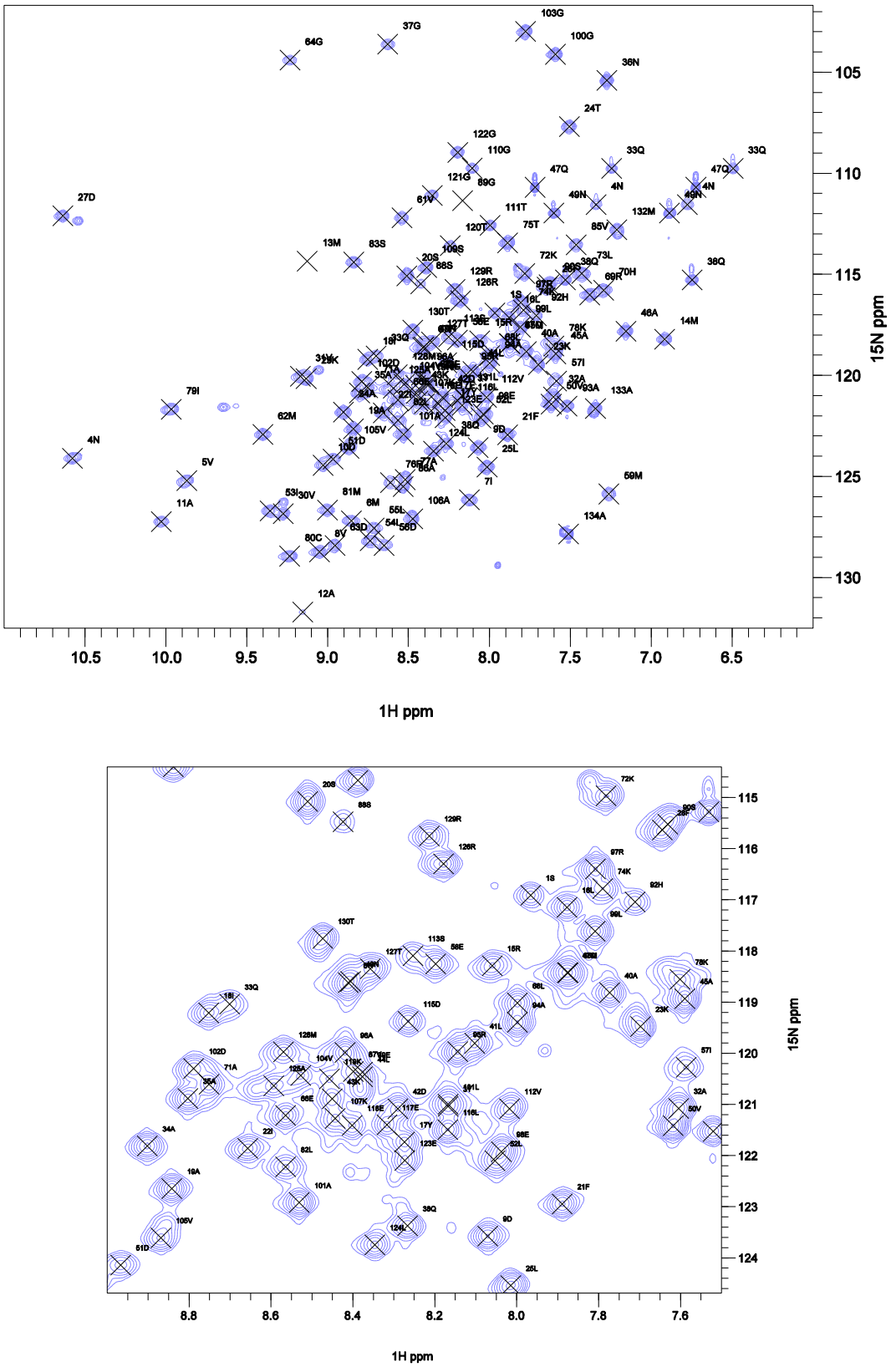

Figure 3.23 –500 MHz ^{1}H, ^{15}N-HSQC spectrum of $CheY_6$ at pH 5.5. A full chemical shift table is in Appendix B.

$CheY_3$ was shown to exhibit large chemical shift changes between pH 4.5 and 7 in the absence of BeF_3^- (Dr. Lorena Varela-Alvarez, personnel communication). Hence, assignments of $CheY_6$ with and without BeF_3^- at pH 5.5 and 7.2 were compared to investigate any pH dependent structural changes (Figure 3.24). The following equation was used to compare peak shift distances between different ^1H, ^{15}N-HSQC spectra, collected at different conditions. A shift larger than 0.4 ppm was considered significant (indicated by the dashed line).

$$\sqrt{(\Delta N * 0.15)^2 + \Delta H^2} \qquad \text{Equation 1}$$

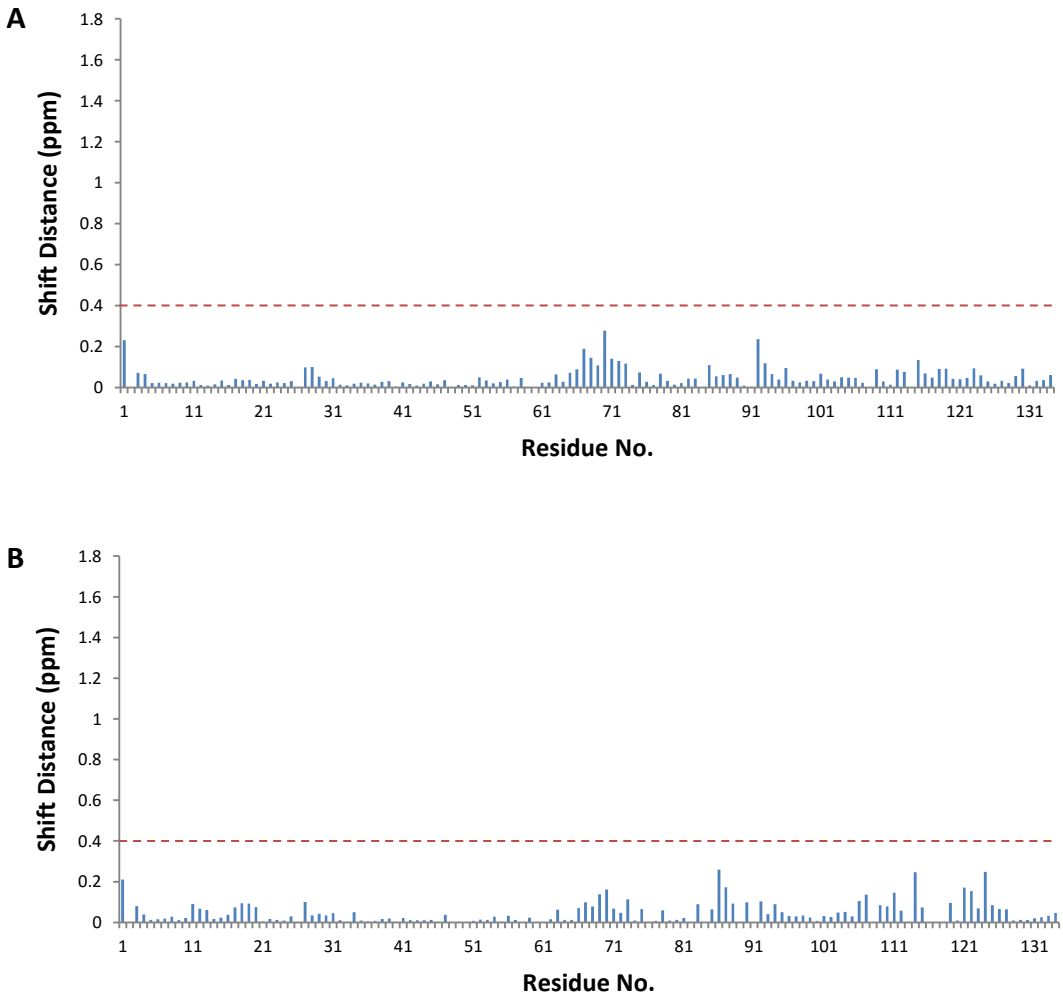

Figure 3.24 – Combined ($^1H^N$ +^{15}N) shift distances of $CheY_6$-BeF_3^- between pH 5.5 and 7.2 **A**) without and **B**) with BeF_3^-. The largest shifts are observed for F67, R69, H70, A86, H92 and H114.

$CheY_6$ does not exhibit large chemical shift changes (above 0.4 ppm) between pH 5.5 and 7.2. F67, H70, and H92 display the largest shifts. As histidine has a pK_a 6-7, a large shift might be expected between 5.5 and 7.2. The overall structure of $CheY_6$ does not appear to be pH dependent.

Conformation of Proline Residues

After close analysis of the $^{1}H,^{15}N$-HSQC, doubling of certain peaks was observed (Figure 3.25). All residues that exhibited peak doubling in the HSQC are close in space to P2 (Figure 3.26). It is thought that both cis and trans conformations are present in solution, giving rise to peak doubling due to slow interconversion on the NMR timescale.

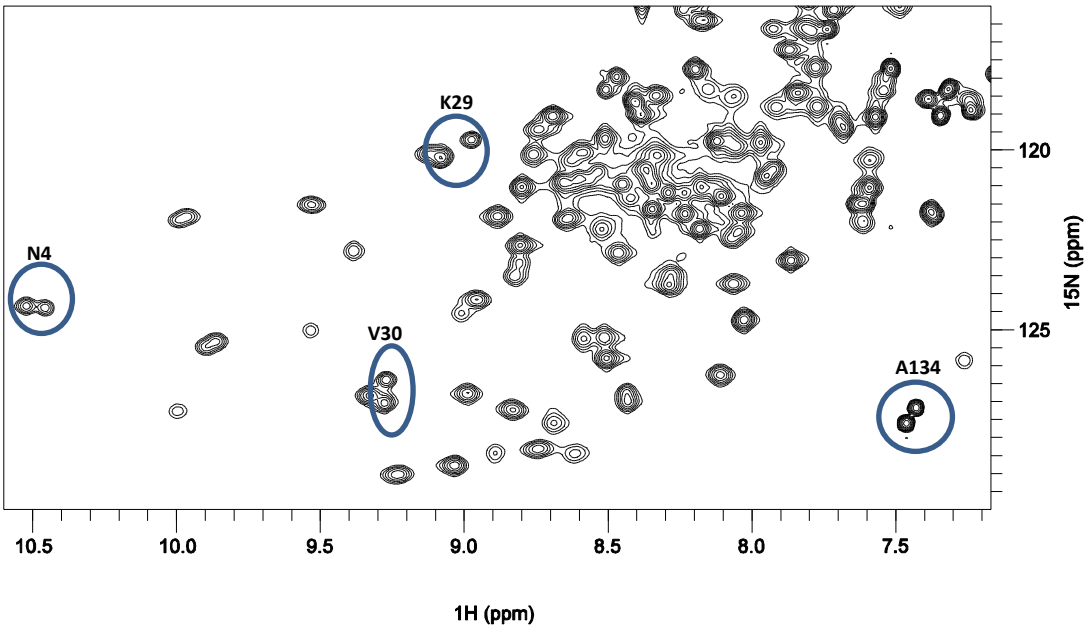

Figure 3.25 – $^{1}H,^{15}N$-HSQC of $CheY_6$. N4, K29, V30 and A134 are highlighted, showing the major and minor conformation peaks.

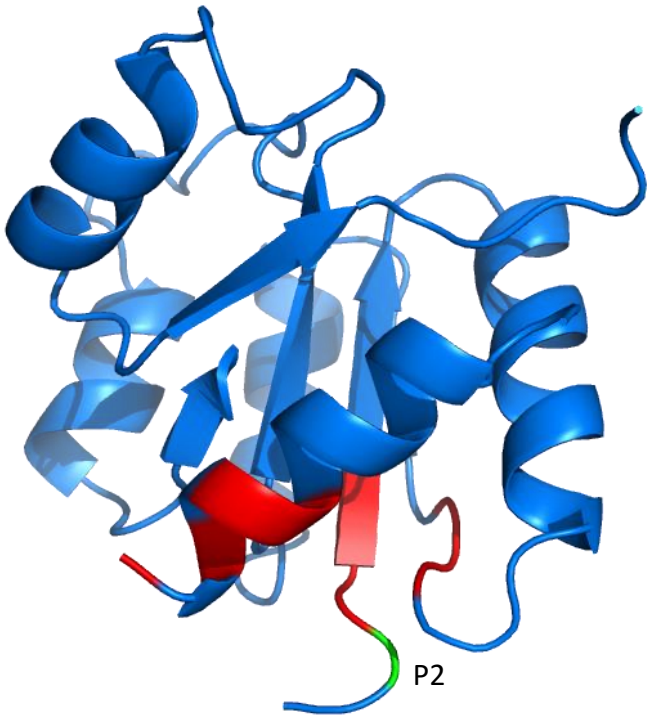

Figure 3.26 – Wild type $CheY_6$ structure, highlighting the residues (red) involved in the major and minor conformations in solution caused by the cis-trans isomerisation of P2 (green).

The Cβ and Cγ chemical shifts of cis and trans proline are different, and comparison of these values can be used to assign peaks to individual isomers (Figure 3.27) (Schubert *et al*. 2002). Analysis of the HSQC peak volumes indicates trans proline is the major conformation for P2 in solution (~60%).

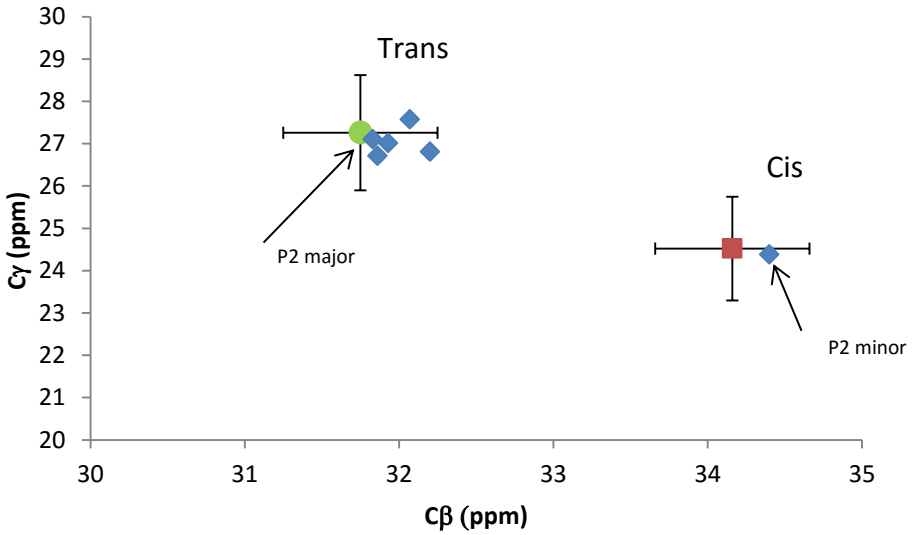

Figure 3.27 – The chemical shift values of Cβ and Cγ of proline residues found in $CheY_6$. P2 can be found in both cis and trans isomers. All other prolines are found to be trans isomers. P60 is not shown as the Cγ chemical shift could not be assigned (Cβ value indicates a trans isomer). The average values (of 1033 prolines) of both cis (red) and trans (green) conformations are indicated, with error bars indicating the standard deviation (Schubert *et al*. 2002).

In the crystal structure, P2 is in a cis conformation and hence different to the major conformation seen in solution by NMR. However, as the proline is very close to the N-terminus of the protein, it is unlikely to have any great effect on the overall protein structure. This may also be caused by the His_6-Tag present, although $CheY_6$ in the crystal structure also contained a His_6-Tag. Analysis of the chemical shifts for P108 indicates a trans conformation; this is also observed in the X-ray crystal structure of $CheY_6$. Interestingly, $CheY_{EC}$ and $CheY_{3RS}$ which lack the loop insertion, have a cis peptide bond at this proline. CheB which has an additional loop has a trans proline like $CheY_6$. The NMR assignments provide the starting point for characterising the structure, dynamics and FliM interactions of $CheY_6$ in solution.

Chapter 4

Structural Investigations of $CheY_6$ in its Active and Inactive States

The crystal structure of $CheY_6$ has been solved in complex with the P1 domain of the cognate histidine kinase $CheA_3$ (Bell *et al*. 2010). However, it is not known if this structure represents the active or inactive (or an intermediary) conformation. NMR studies were used to characterise the structure of $CheY_6$ in solution, and to investigate the switch mechanism of $CheY_6$ upon activation.

4.1 $^{1}H,^{15}N$-Heteronuclear NOE

Proteins often contain flexible regions that are not as well defined as regions of regular secondary (the root mean square deviation (rmsd) is higher). $^{1}H,^{15}N$-Heteronuclear NOE (hetNOE) experiments can be particularly useful in identifying mobile residues (Kay, Torchia, and Bax 1989). A hetNOE ratio is calculated by

collecting two spectra, one with ^{1}H saturation and one without. The spectrum without ^{1}H saturation is similar to an $^{1}H,^{15}N$-HSQC. The spectrum with ^{1}H saturation has lower peak intensities as a result of the ^{1}H-^{15}N NOE. The relative reduction in peak intensity can be linked to residue mobility on a fast (ps to ns) timescale. A hetNOE ratio of ~0.7-0.8 is indicative of a rigid backbone, whereas a ratio of <0.7 is indicative of backbone mobility. Steady state hetNOE experiments were used to investigate fast timescale backbone dynamics of $CheY_6$ (Figure 4.1).

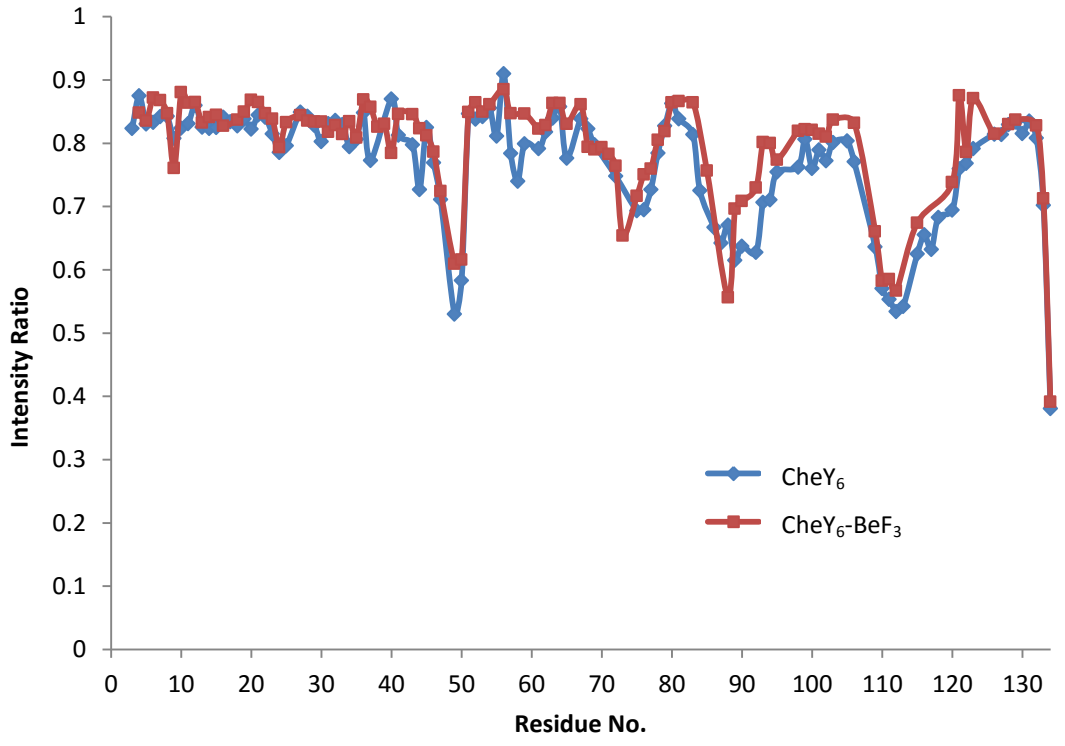

Figure 4.1 – 750 MHz $^{1}H,^{15}N$-heteronuclear NOE experiments of $CheY_6$, with (red) and without (blue) BeF_3.

HetNOE experiments for active (with BeF_3^-) and inactive $CheY_6$ show that residues S109-T120 have reduced hetNOE ratios (<0.7) (Figure 4.2). This indicates fast

timescale backbone dynamics (ps to ns) and is in agreement with the crystal structure where no electron density is observed for residues 113-118. Although S109 to V112 have electron density in the crystal structure, the corresponding hetNOE ratios are ~0.6. These residues are in contact with $CheA_3P1$ in the crystal structure of the complex and due to this interaction, the flexibility of these residues could be reduced in the complex.

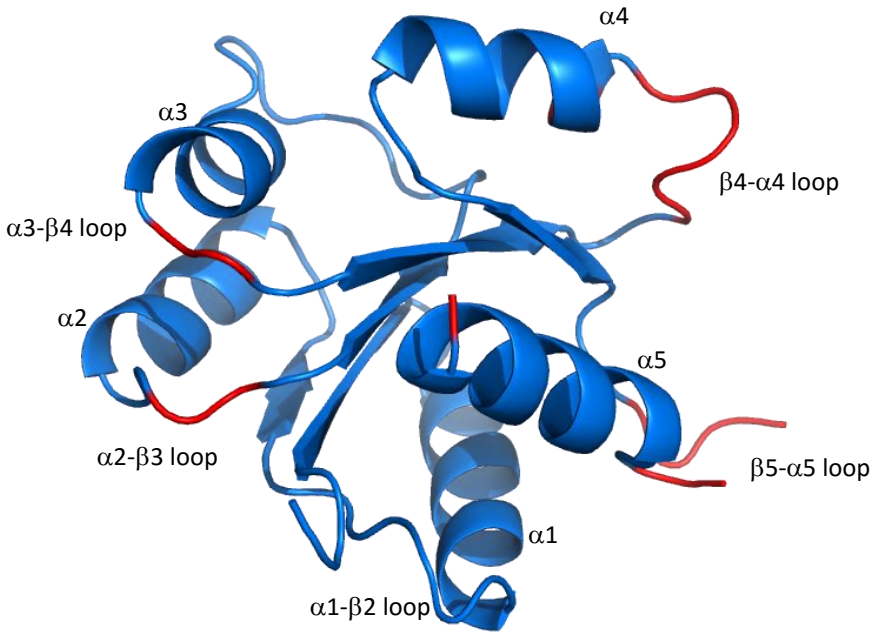

Figure 4.2 – The crystal structure of $CheY_6$ (PDB:3KYJ), highlighting residues with a reduced hetNOE ratio in red (<0.7). All residues with a reduced hetNOE ratio are located in loop regions.

Other regions of $CheY_6$ also showed reduced hetNOE ratios. These residues of $CheY_6$ are mainly located in loop regions between α-helix and β-strand secondary structure. Loop regions can be flexible in nature, and therefore a reduced hetNOE ratio it is not surprising. There are also a number of rigid loop regions, such as the α1-β2 loop (L25-V31), which display hetNOE ratios above 0.8.

4.2 Changes in the $^{1}H,^{15}N$-HSQC upon addition of BeF_3^-

$^{1}H,^{15}N$-HSQC spectra of $CheY_6$ with and without BeF_3^- were assigned in Section 3.6 and the spectra are overlaid in Figure 4.3. The $^{1}H^{N}/^{15}N$ chemical shift differences for each residue were compared to investigate structural changes upon activation (Figure 4.4).

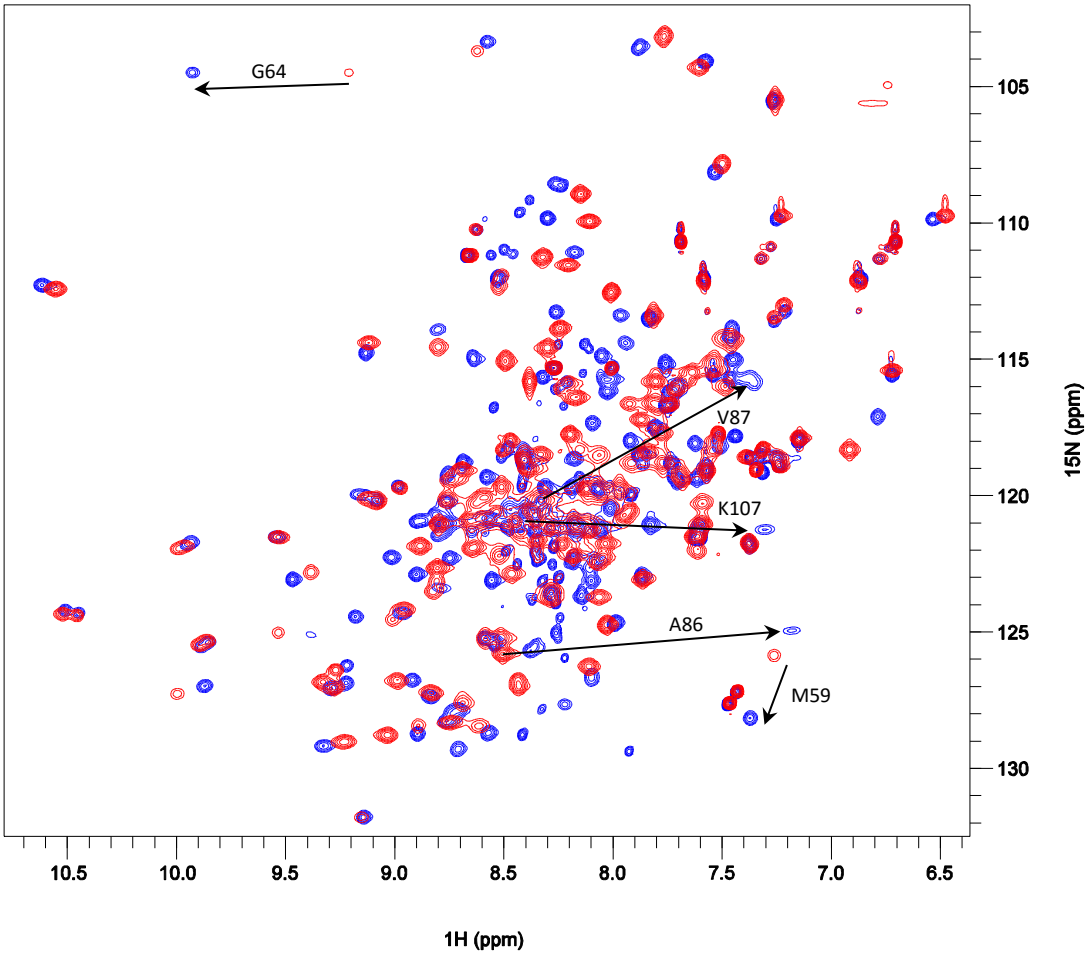

Figure 4.3 – 500 MHz ^{1}H, ^{15}N-HSQC spectra of $CheY_6$, with (blue) and without (red) BeF_3^- at pH 5.5. A full chemical shift table is in Appendix B.

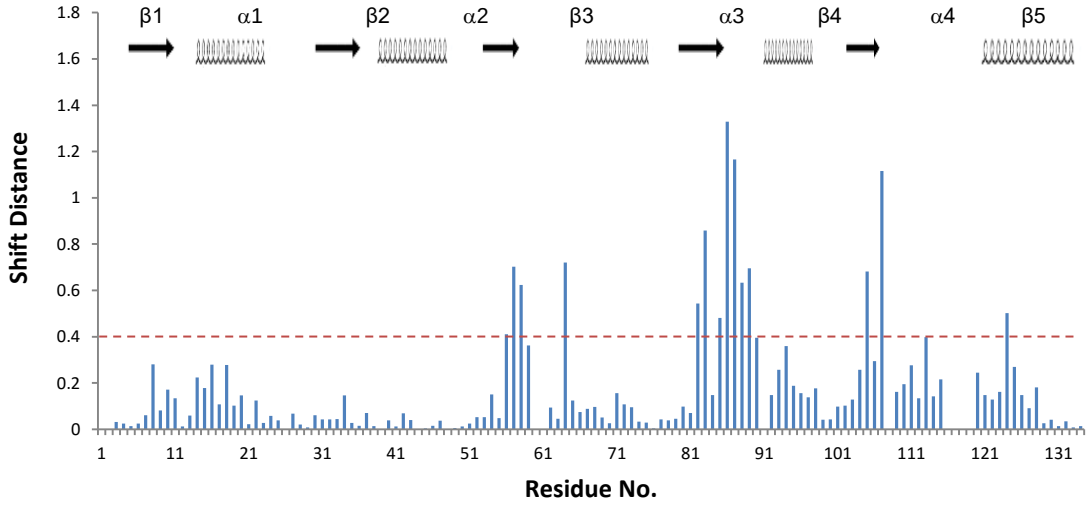

Figure 4.4 – Combined ($^{1}H^{N}$ + ^{15}N) chemical shift differences of $CheY_6$ with and without BeF_3 at pH 5.5. Shift distances were measured using Equation 1 (dashed line indicates significant shifts).

Most of the largest chemical shift changes are observed for residues located on one surface of $CheY_6$ (Figure 4.5). Large shifts are seen near the BeF_3^- binding site (D56 in β3) and in the β4-α4-loop region (A86, V87). These changes are similar to the changes reported for $CheY_{EC}$, where the β4-α4 loop plays an important role in the coupling mechanism between phosphorylation and conformational changes that increase the binding affinity to FliM (Dyer and Dahlquist 2006).

Many residues from the elongated β5-α5-loop region in $CheY_6$ could not be assigned following addition of BeF_3^-. This could infer structural changes in this loop that may be involved in the switch mechanism. The residues that have been assigned in this loop do show chemical shift changes upon addition of BeF_3^-. If the elongated loop

was completely unstructured in both states, chemical shift changes would not be expected.

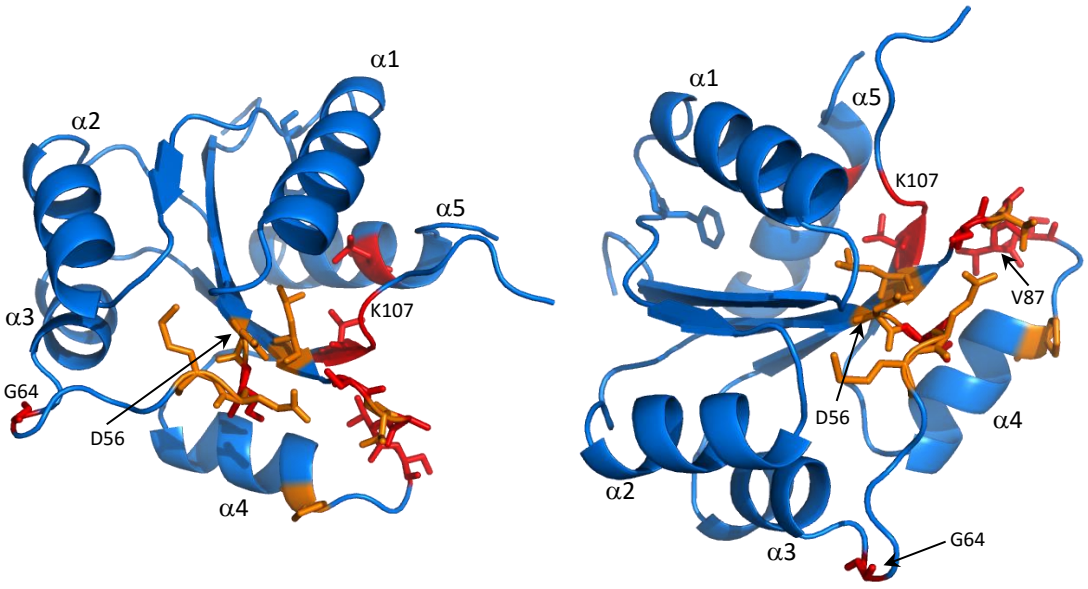

Figure 4.5 – $^{1}H,^{15}N$-HSQC shift distances of $CheY_6$ (PDB:3KYJ), larger than 0.4 (orange) and 0.6 (red) upon addition of BeF_3^-. Two different orientations are displayed.

A number of residues in $CheY_6$ that correspond to residues in the CheY switch mechanism, show large chemical shifts upon addition of BeF_3^-. For instance, larger chemical shift changes in the $^{1}H^{N}$ dimension are observed for $K107_{RS}$ compared with $K109_{EC}$. This is involved in a salt bridge with D56 ($D57_{EC}$), which breaks upon addition of BeF_3^- in $CheY_{EC}$. The perturbations of K107 in $CheY_6$ may affect the elongated loop region which follows it; this loop may be involved in the switch mechanism. Large chemical shift changes in the $^{1}H^{N}$ dimension are observed for G64. The same chemical shift changes are also seen in $CheY_{EC}$. The reason for this large chemical shift change is not known, as the residue is not near the site of phosphorylation or other residues that display perturbations.

$CheY_6$ does not have a homologous aromatic residue to Tyr106, which is involved in the $CheY_{EC}$ switch mechanism. If a similar mechanism is employed by $CheY_6$, sequence and structure alignment suggests S83 and V104 would facilitate the Y-T switch. Both S83 and V104 show chemical shift changes upon addition of BeF_3^-. The switch mechanism of $CheY_6$ is discussed in more detail in Section 4.6.

	E. coli		***R. sphaeroides***	
Nuclei	$^1H^N$	^{15}N	$^1H^N$	^{15}N
T87 / S83	8.50	115.20	8.80	114.55
T87 / S83 (A)	8.18	115.10	7.94	114.39
Y106 / V104	8.44	117.90	8.55	120.73
Y106 / V104 (A)	8.63	124.30	8.79	121.29
K107 / K109 (I)	8.45	122.50	8.42	121.34
K107 / K109 (A)	8.01	124.40	7.31	121.25

Table 4.1 – Chemical shift values for the residues thought to be involved in the switch mechanism of $CheY_{EC}$ (active – BMRB 4472, inactive – BMRB 4083), and the corresponding residues in $CheY_6$. (A) indicates the active state.

Similar upfield chemical shift changes are observed for $T87_{EC}$ and the corresponding $S83_{RS}$ upon addition of BeF_3^-; however, the shift for S83 $^1H^N$ is significantly larger than for T87 $^1H^N$. By contrast, $Y106_{EC}$ displays a much larger chemical shift change in the ^{15}N dimension (more than 6 ppm), than observed for $V104_{RS}$. This could indicate that $V104_{RS}$ does not undergo a similar conformational change to $Y106_{EC}$ upon activation.

4.3 Chemical Shift Analysis using TALOS-N

TALOS-N is an artificial neural network (ANN) based hybrid system for empirical prediction of backbone torsion angles (φ and ψ), side-chain torsion angles (χ_1) and secondary structure. Predictions are made using a combination of six (HN, H_α, C_α, C_β, CO and N) chemical shifts per residue from the protein of interest, which are then compared to a reference chemical shift library (Shen and Bax 2015). For each residue, φ and ψ torsion angles are predicted and the ten best fits from the database are displayed (Figure 4.6).

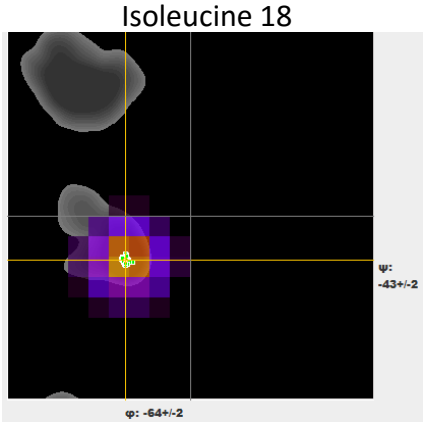

Figure 4.6 – Distribution of the ten nearest database matches for Isoleucine 18 on a Ramachandran plot. Clustered peaks (ten closest library predictions) predict a high confidence in the torsion angles (φ and ψ), indicative of α-helical secondary structure. The grey shaded areas show the allowed α and β regions of the Ramachandran plot.

TALOS-N secondary structure predictions for $CheY_6$ correlate well with the crystal structure (Figure 4.7). Five α-helices and five β-strands are predicted in the same regions shown in the crystal structure. Furthermore, reduced rigidity is predicted for the elongated loop (S109-E118) region that was shown to be flexible in the hetNOE experiments. TALOS-N predictions were also carried out for $CheY_6$-BeF_3^- (Figure 4.8).

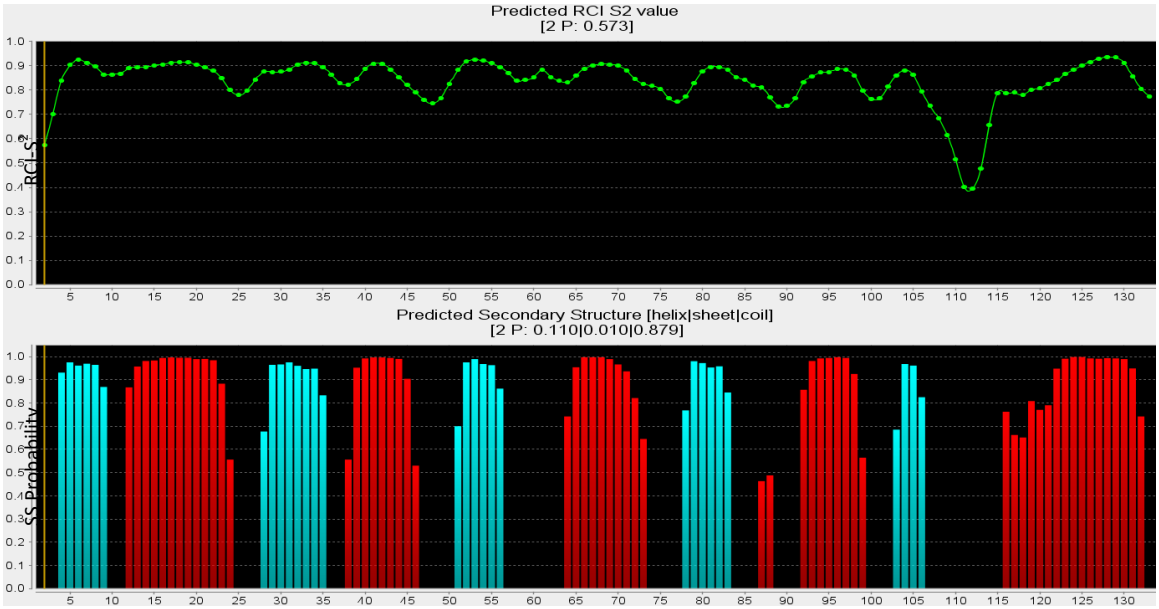

Figure 4.7 – TALOS-N predictions of $CheY_6$ secondary structure in its inactive state. A classic response regulator fold is seen with five α-helices (red) and five β-strands (blue). This is in good agreement with the crystal structure of the $CheY_6$-$CheA_3$ complex. RCI-S^2 (green) is a measure of the rigidity, based on the random coil index (Berjanskii and Wishart 2005).

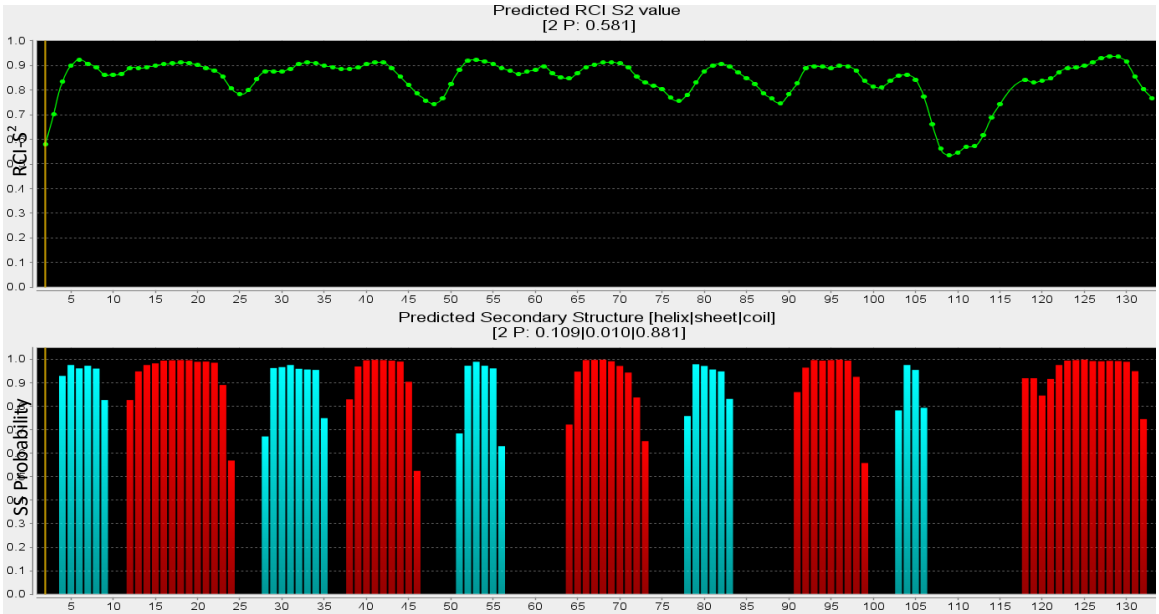

Figure 4.8 - TALOS-N predictions of $CheY_6$-BeF_3 secondary structure. Five α-helices and five β-strands are predicted in the same regions as $CheY_6$ without BeF_3^-.

$CheY_{EC}$ does not undergo large structural changes upon activation. TALOS-N shows an overall structure prediction for $CheY_6$-BeF_3^- that is very similar to $CheY_6$. Based on these predictions, $CheY_6$ is unlikely to undergo large conformational changes upon activation but instead, more subtle changes (such as a Y-T switch mechanism) are likely to occur to increase FliM binding affinity. Assignments for L116 and E117 were not made for $CheY_6$-BeF_3^-, so the prediction of a shorter α5 helix upon addition of BeF_3^- is likely the result of missing chemical shifts.

V87 and S88 are residues found in the β4-α4-loop region; these are additional residues not found in $CheY_3$, $CheY_4$ or $CheY_{EC}$ (refer to Figure 5.1 for alignment). TALOS-N predicts that both residues have helical structure without BeF_3^- (at both pH 5.5 and 7.2), but not with BeF_3^-. This turn agrees well with the crystal structure, but suggests that these residues undergo a conformational change upon addition of BeF_3^-. The β4-α4-loop was shown to be important in the switch mechanism of $CheY_{EC}$ (Dyer and Dahlquist 2006). The chemical shift changes of this loop upon addition of BeF_3^- were investigated.

Residue	$^1H^N$	^{15}N	H_α	C_α	C_β
V85	7.50	114.23	4.51	59.74	34.63
V85 (A)	7.97	113.41	4.45	61.00	32.24
A86	8.51	125.80	4.30	52.90	18.41
A86 (A)	7.18	124.92	4.43	51.13	17.63
V87	8.34	120.16	3.58	65.55	32.10
V87 (A)	7.39	115.67	4.01	61.85	33.15
S88	8.39	115.80	4.22	59.81	62.49
S88 (A)	8.76	119.21	4.11	60.41	62.53

Table 4.2 – Chemical shift values of $^1H^N$, ^{15}N, H_α, C_α and C_β for the β4-α4-loop region of $CheY_6$. (A) indicates the active state of $CheY_6$ via the addition of BeF_3^-.

Upfield shifted H_α with a downfield shifted C_α is indicative of helical structure. Based on the chemical shifts for V87, TALOS-N predicts helical structure in the absence of BeF_3^-. S90 is hydrogen bonded to V87 (S90 N – O V87) in the crystal structure of $CheY_6$. This in combination with the chemical shift values for V87 would suggest a 3_{10} helical turn. Other changes in $^1H^N/^{15}N$ chemical shifts may reflect differences in hydrogen bond lengths, or even rearrangements of hydrogen bonds.

A number of TALOS-N backbone (φ and ψ) torsion angle predictions do not agree well with the angles found in the crystal structure. Residues A35, V61, D63, M65, R76, G121 and A133 show discrepancies, both with or without BeF_3^- at both pH 5.5 and 7.2 These residues are located in loop regions of $CheY_6$, and close to the C-terminus (Figure 4.9). These residues could be involved in crystal contacts, and hence may have a different orientation in solution. TALOS-N is generally better for secondary structure predictions, compared with loop regions. Similar secondary structure predictions are found for both pH 5.5 and 7.2 (Shen and Bax 2015).

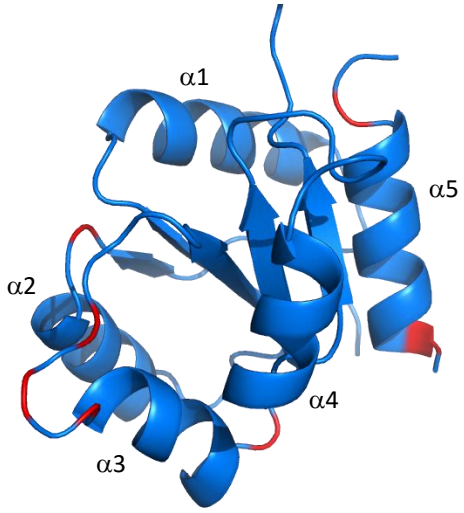

Figure 4.9 – TALOS-N and crystal structure backbone torsion angle disagreements for $CheY_6$, with and without BeF_3^-. Residues showing disagreements (red) are found in loop regions, and near the C-terminus of $CheY_6$.

There are a number of residues (D56, M59, V85 and V87) for which the TALOS-N predictions in the absence of BeF_3^- agree well with the crystal structure of $CheY_6$, but disagree with the predictions for $CheY_6$-BeF_3^-. These differences involve residues in close proximity to D56 and S83. M59 is hydrogen bonded to D56 (M59 N – O D56), and V85 to S83 (V85 O – OG S83). It is not surprising that D56 displays differences between $CheY_6$ and $CheY_6$-BeF_3^-, as this is the residue binding BeF_3^-. These changes in torsion angle upon activation may indicate residues involved in the switch mechanism upon phosphorylation.

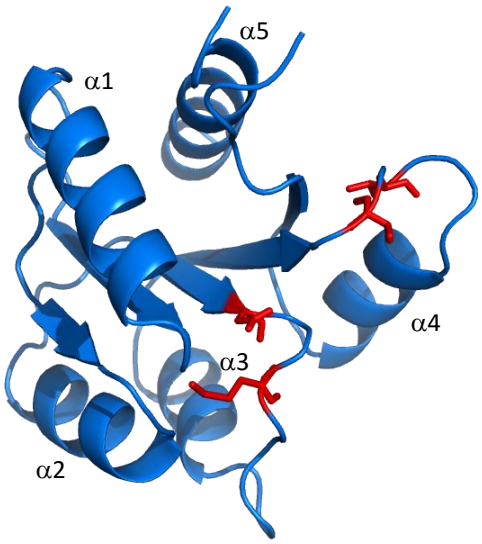

Figure 4.10 – TALOS-N and crystal structure backbone torsion angle disagreements of $CheY_6$. The highlighted residues (red) agree well with $CheY_6$, but disagree with $CheY_6$-BeF_3^-.

TALOS-N is also able to make predictions of $\chi 1$ torsion angles (Figure 4.11). As $\beta 1$ (4-8) is completely solvent inaccessible, the torsion angles from the crystal structure were compared against the predictions made by TALOS-N, to investigate their reliability.

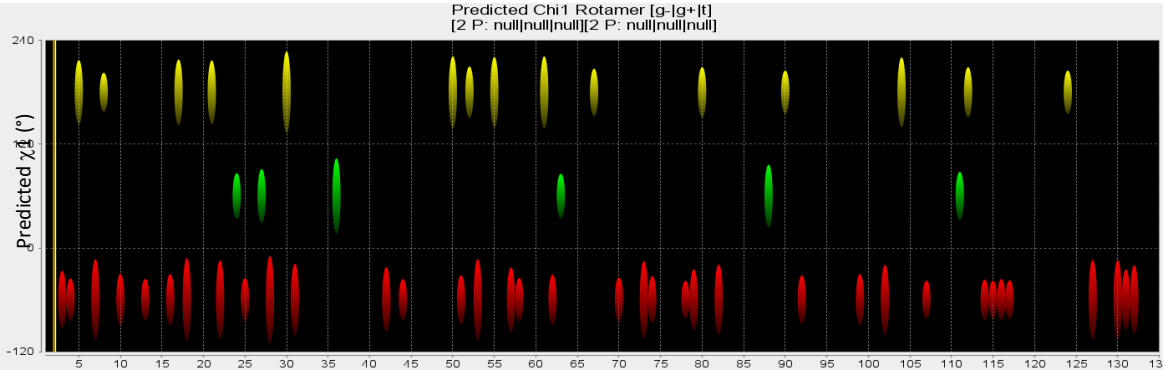

Figure 4.11 – TALOS-N $\chi 1$ torsion angle predictions of $CheY_6$ without BeF_3^-.

Residue	Crystal Structure χ1 (°)	TALOS-N χ1 (°)
N4	-64.4	-67.8
V5	-178.2	-176.1
M6	175.5	No prediction
I7	-55.8	-62.0
V8	-175.6	-177.7

Table 4.3 – Comparison of the χ1 torsion angles between the crystal structure and TALOS-N predictions of $CheY_6$.

With the exception of M6 for which χ1 is not predicted, the TALOS-N predictions agree well with the torsion angles found in the crystal structure. For M6, TALOS-N predicts the correct rotamer, but it does not reach the population threshold set for accurate predictions.

A number of χ1 torsion angle predictions for both $CheY_6$ and $CheY_6$-BeF_3^- disagree with the crystal structure (D10, M14, L16, D27, L44, I57, V61, D63, S88 and V104). With the exception of L44, the side-chains of these residues are solvent accessible, and hence χ1 angle predictions are less reliable due to possible crystal contacts or averaging in solution.

Torsion angle predictions are not made by TALOS-N for most residues in the β4-α4-loop region. This could suggest conformational averaging about the side chain C_α-C_β bond, as residues 84-87 all have some solvent accessibility.

4.4 Hydrogen-Deuterium Exchange

Hydrogen-deuterium exchange experiments were used to investigate hydrogen bonding, solvent accessibility and the tertiary structure of $CheY_6$. A sample of $CheY_6$ was lyophilised in buffer (25 mM Tris HCl, 15 mM $MgCl_2$, pH 7.2), and re-dissolved in D_2O (100%). A BeF_3^- stock solution was also produced in D_2O (100%). ^1H,^{15}N-HSQC spectra were collected every 40 minutes for 400 minutes, with and without BeF_3^-. A final ^1H,^{15}N-HSQC spectrum was collected after 5000 minutes.

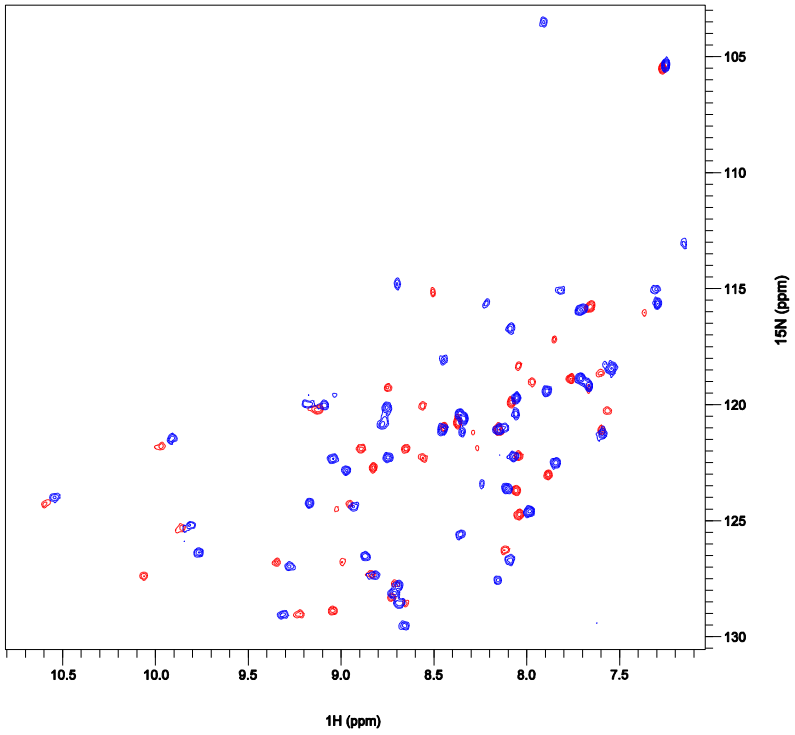

Figure 4.12 – ^1H,^{15}N-HSQC spectra of $CheY_6$ with (blue) and without (red) BeF_3^-, dissolved in D_2O. These spectra were collected 15 minutes after addition of D_2O. More peaks are observed for $CheY_6$-BeF_3^-.

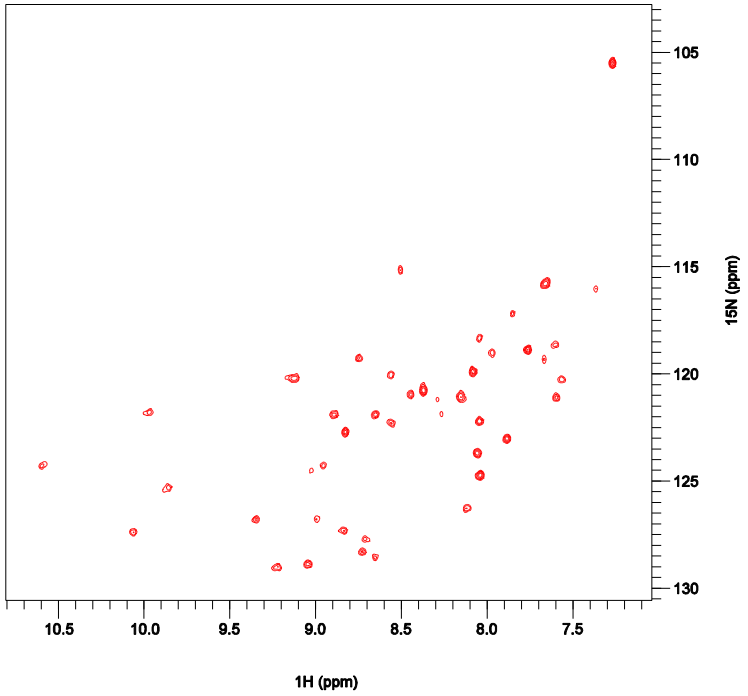

Figure 4.13 – $^{1}H,^{15}N$-HSQC spectrum of $CheY_6$ dissolved in D_2O. This spectrum was collected 15 minutes after addition of D_2O. Peaks from 39 residues are observed.

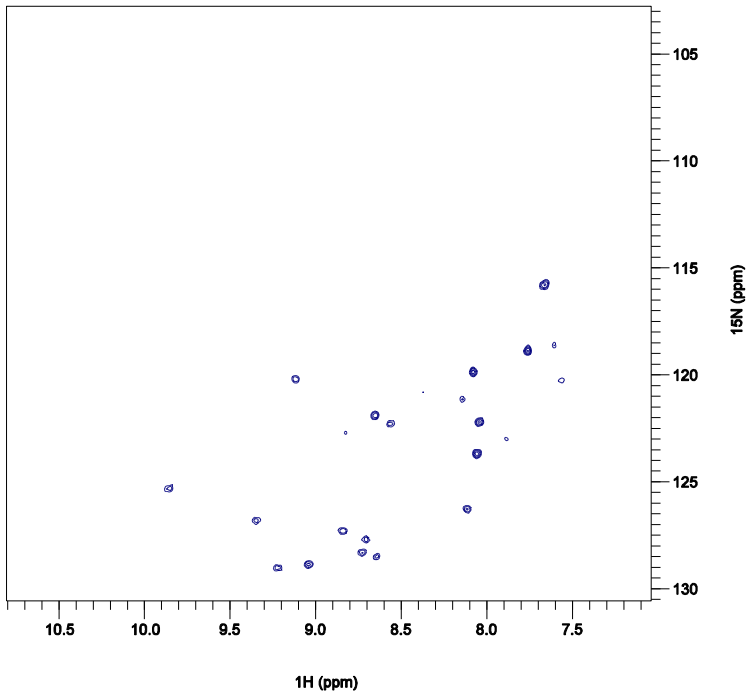

Figure 4.14– $^{1}H,^{15}N$-HSQC spectrum of $CheY_6$ dissolved in D_2O. This spectrum was collected 390 minutes after addition of D_2O. Peaks from 26 residues are observed. 13 residues have exchanged completely between 15 minutes and 390 minutes. These arise primarily from α-helices.

Signal decay throughout the time course of the experiment was examined, to investigate amide protection in regions of secondary structure. Different exchange behaviour was observed (Figure 4.15). Some amides such as D9 show no exchange during the course of the experiment while others, such as A19, N36 and L44, show a significant decrease in intensity.

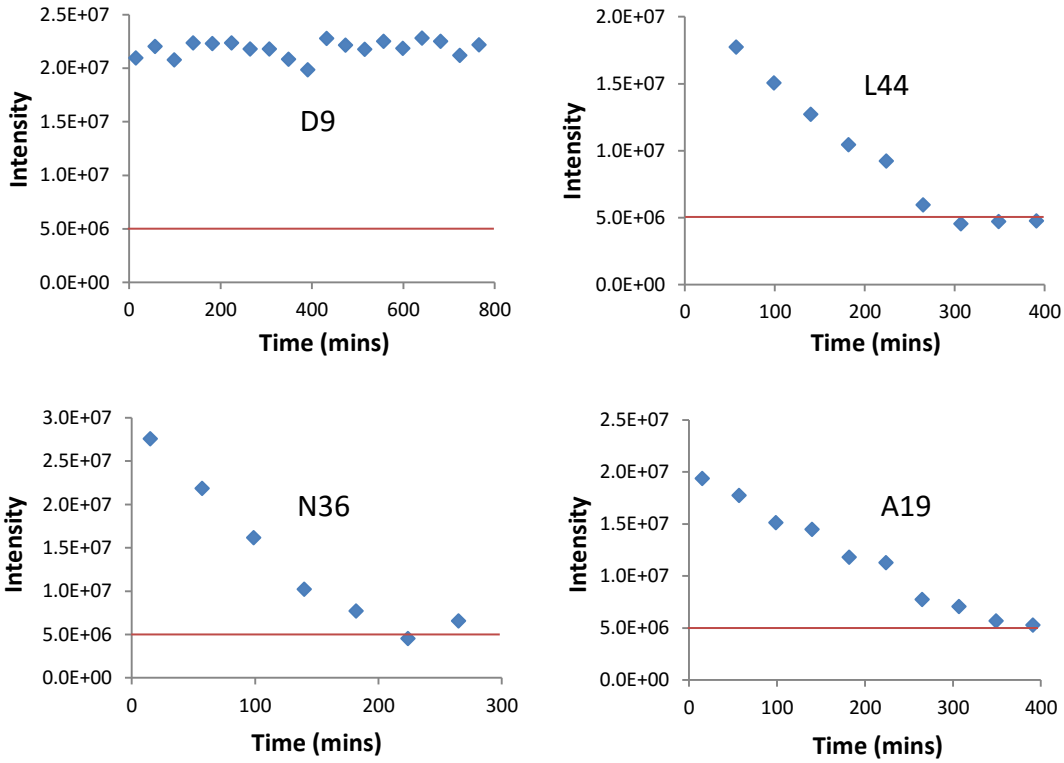

Figure 4.15 – Intensity changes of D9, L44, N36 and A19 as measured by a time course of $^{1}H,^{15}N$-HSQC spectra. L44, N36 and A19 display signal decay and hence hydrogen-deuterium exchange, whereas little or no exchange is observed for D9 (the red line indicates the noise intensity). Experimental exchange rates and protection factors for measurable residues are found in Appendix C.

The peak intensity changes over the time course were mapped onto the structure of $CheY_6$, without (Figure 4.16) and with BeF_3^- (Figure 4.17).

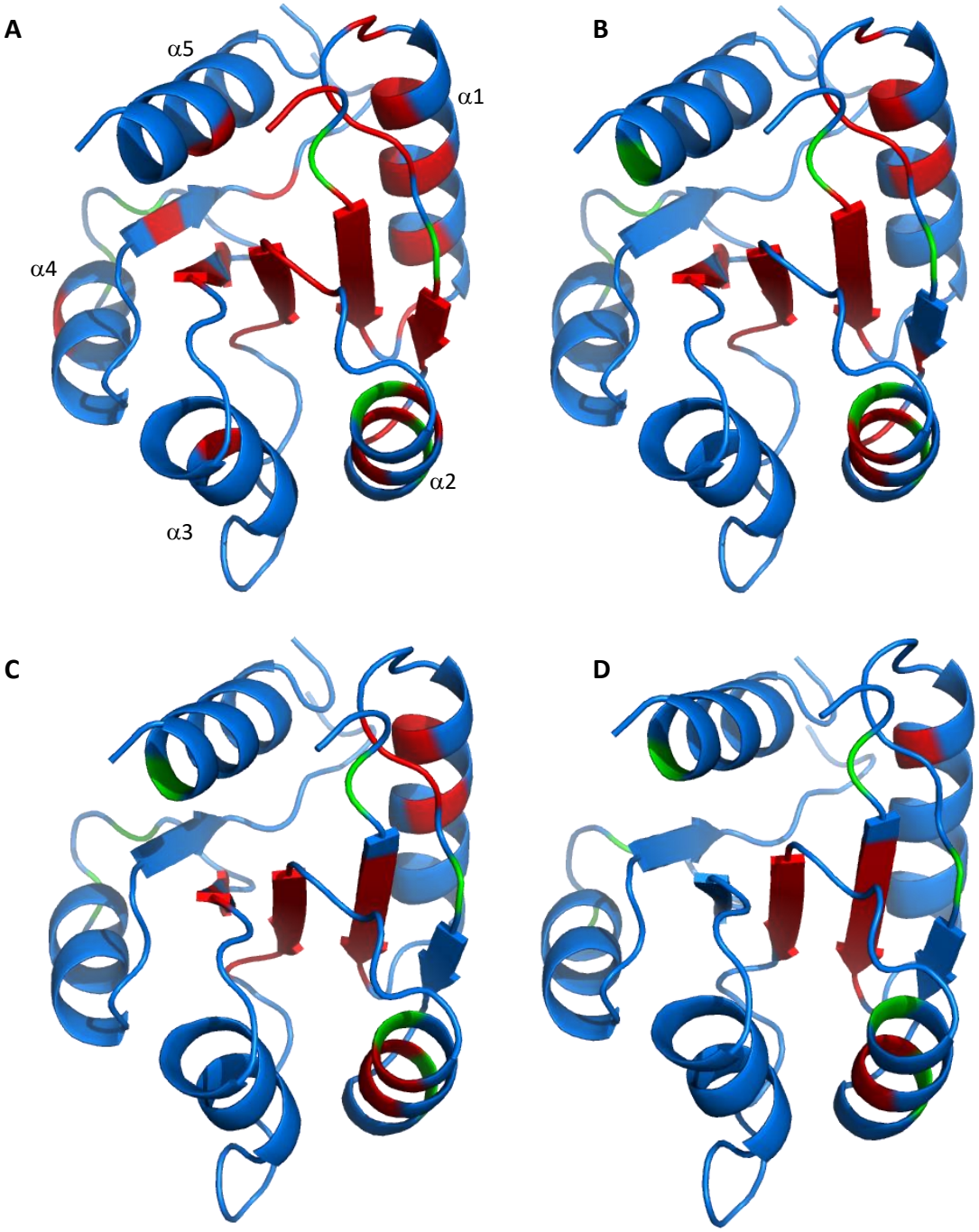

Figure 4.16 – Hydrogen-deuterium exchange experiments of $CheY_6$ without BeF_3^- at **A)** 15 **B)** 224 **C)** 390 and **D)** 5000 minutes after dissolving in D_2O (100%). In **A,** residues in blue do not show a peak in the $^1H,^{15}N$-HSQC spectrum, and hence the ^1H backbone amide rapidly exchanges with deuterium. In **A**, **B**, **C** and **D**; residues in red give a peak in the $^1H,^{15}N$-HSQC spectrum and hence exchange slowly with deuterium. Residues that showed overlapped peaks which cannot be assigned unambiguously, are highlighted in green.

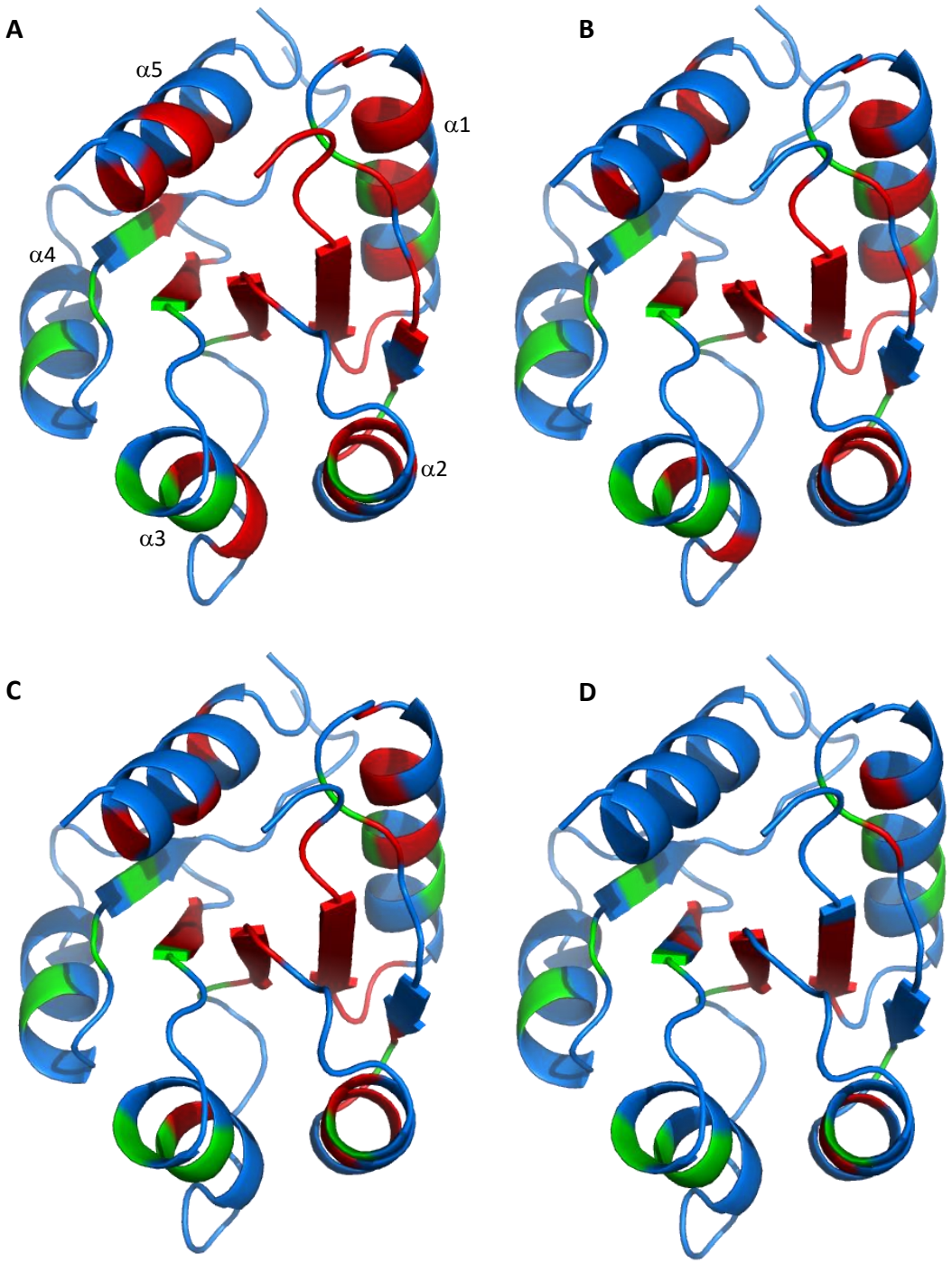

Figure 4.17 – Hydrogen-deuterium exchange experiments of $CheY_6$ with BeF_3^- at **A)** 15 **B)** 224 **C)** 390 and **D)** 5000 minutes after dissolving in D_2O (100%). In **A,** residues in blue do not show a peak in the $^{1}H,^{15}N$-HSQC spectrum, and hence the ^{1}H backbone amide rapidly exchanges with deuterium. In **A**, **B**, **C** and **D**; residues in red give a peak in the $^{1}H,^{15}N$-HSQC spectrum and hence exchange slowly with deuterium. Residues that showed overlapped peaks which cannot be assigned unambiguously, are highlighted in green.

In general, most protected amides are involved in hydrogen bonding. However, not all hydrogen bonded amides are slow to exchange, which is usually linked to surface accessibility. α-helices 1, 2 and 5 show protection on one face, and exchange on the other. The solvent accessible amides of these helices exchange more rapidly than the amides facing towards the core of the protein. $CheY_6$-BeF_3^- has more protected amides than $CheY_6$. This is especially evident after 390 minutes where $CheY_6$-BeF_3^- still has some α-helices displaying amide protection. The addition of BeF_3^- may offer more stability to certain regions of $CheY_6$. β1, 3 and 4 show high levels of amide protection with and without BeF_3^-, as many residues have not exchanged after 5000 minutes. As these residues have almost no main chain solvent accessibility, it is not surprising that these amides do not exchange.

Interestingly, S83 exchanges immediately in $CheY_6$, but gives a visible peak in the first 2-3 spectra collected for $CheY_6$-BeF_3^-. This could indicate a stronger hydrogen bond formed upon addition of BeF_3^-. In the crystal structure of $CheY_6$, S83 N has a hydrogen bond to V105 O. A similar hydrogen bond involving T87 and V107 is found in both active and inactive $CheY_{EC}$ (PDB:1CHN and 1FQW).

Investigation of the H_α chemical shift values of S83 show more β-sheet like values with BeF_3^- (5.32 ppm) compared with the absence of BeF_3^- (4.85 ppm). Thus, addition of BeF_3^- may stabilise the C-terminus of β4.

4.5 Residual Dipolar Couplings

Residual dipolar couplings (RDCs) provide useful information for structure determination. RDCs arise from weak alignment of a protein in an anisotropic medium, and can be used to produce long-range structural information. NH bonds ($^{1}H^{N}$-^{15}N RDCs) are oriented relative to a global alignment tensor. $^{1}J_{NH}$ splittings are measured in the ^{15}N dimension of an HSQC spectrum collected with the IPAP (in-phase and anti-phase) method (Yao, Ying, and Bax 2009). Anisotropic medium is produced using $C_{12}E_6$/hexanol (5% w/v) in isotropic buffer (Rückert and Otting 2000). Doublet peak separation was measured for both the isotropic and anisotropic samples, and the differences were used to calculate RDC sign and magnitude (Figure 4.18). RDC values for $CheY_6$ with and without BeF_3^- are plotted as a function of sequence (Figure 4.19), and the distribution of RDCs are plotted for comparison (Figure 4.20).

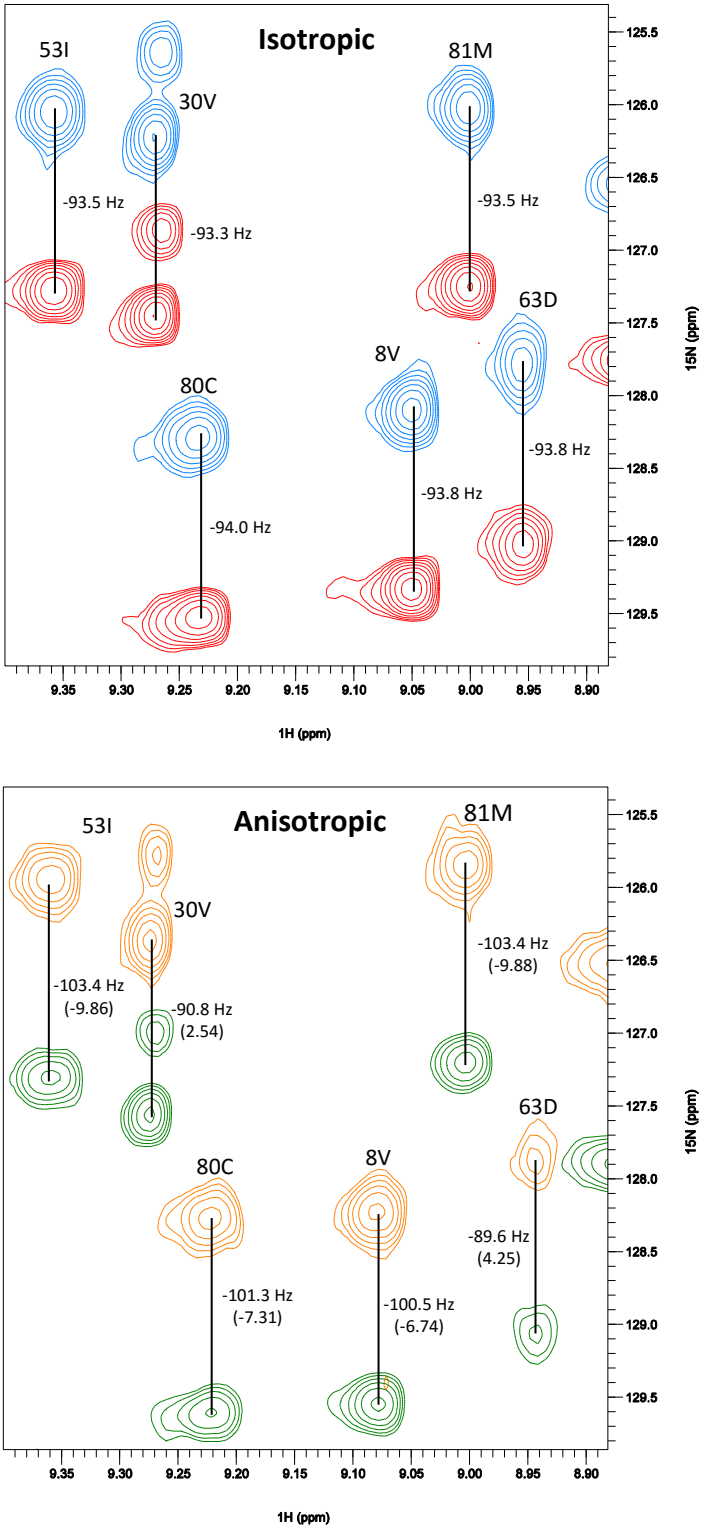

Figure 4.18 – HSQC-IPAP spectra of $CheY_6$. Doublet peak separations were measured and RDC values determined by the difference between isotropic (top) and anisotropic (bottom) splittings. No RDC contribution is seen for an isotropic sample, and splitting corresponds to the $^{1}J_{NH}$ scalar coupling (~-93 Hz). The anisotropic sample displays different splitting values and therefore observable RDCs.

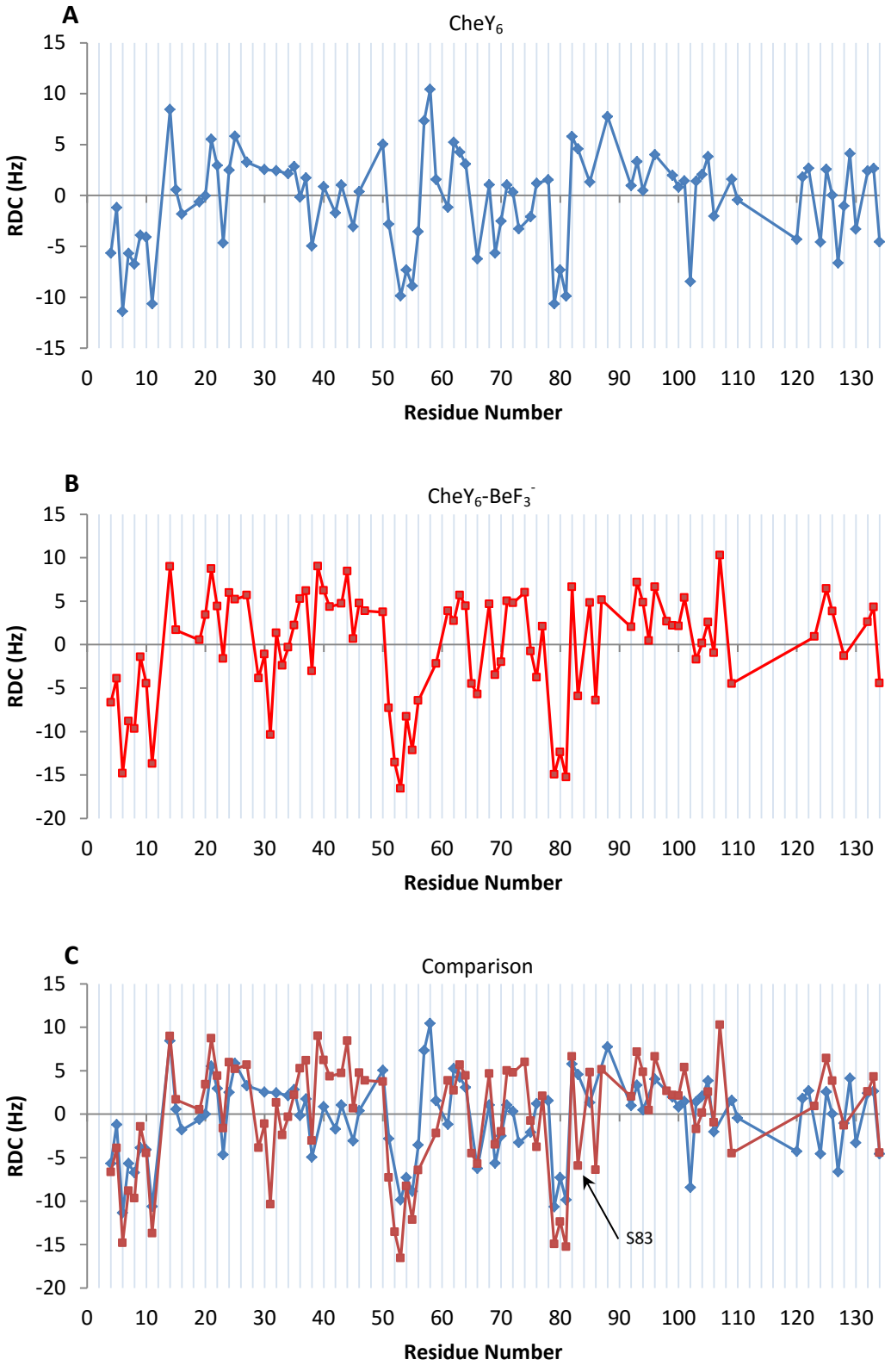

Figure 4.19 – Residual dipolar couplings are plotted against $CheY_6$ sequence for **A**) $CheY_6$, **B**) $CheY_6$-BeF_3^- and **C**) Comparison of both $CheY_6$ (red) and $CheY_6$-BeF_3 (black). S83 is highlighted.

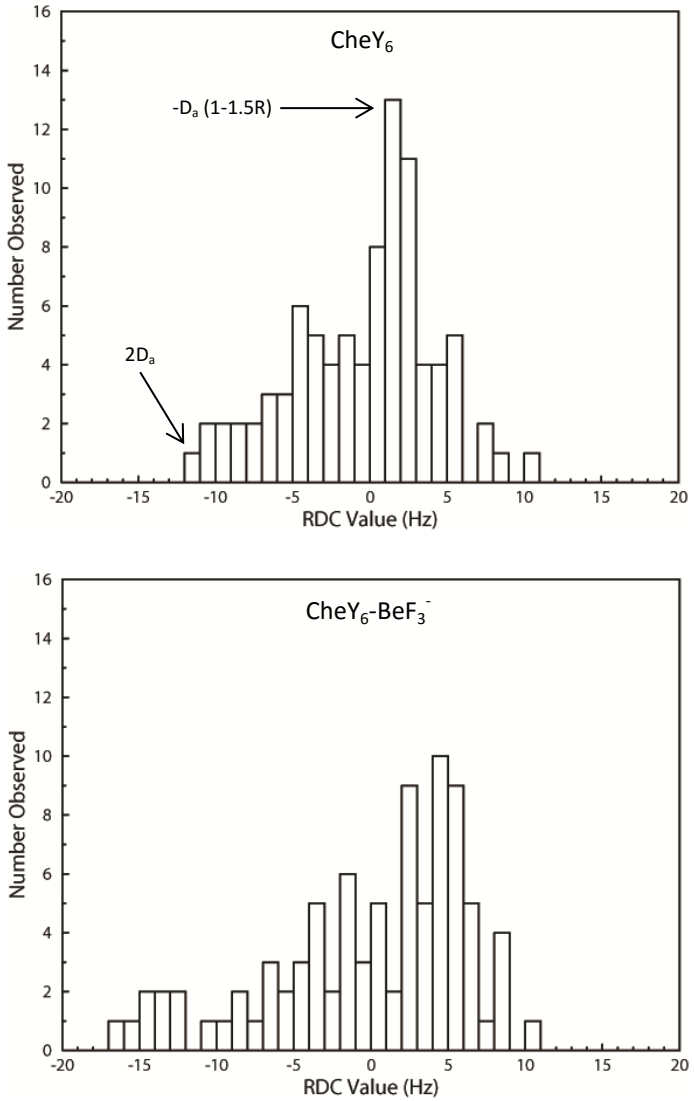

Figure 4.20 – Histogram of the residual dipolar coupling distribution for $CheY_6$, without (top) and with (bottom) BeF_3. The largest magnitude and most populated RDC values can be used to estimate the alignment parameters D_a and R.

A common method for estimating the axial (D_a^{NH}) and rhombic (R) ($R=D_a/D_r$) components of the alignment tensor is by using a histogram of the distribution of RDC values (Clore, Gronenborn, and Bax 1998). Using Equation 2 and 3 where D is the largest magnitude RDC in Eq. 2 and the most populated RDC in Eq. 3, it is possible to estimate D_a and R.

$$D = 2Da \quad \text{Equation 2}$$

$$D = -Da(1 - 1.5R) \quad \text{Equation 3}$$

	Estimated D_a	Estimated R
$CheY_6$	-5.5	0.424
$CheY_6$-BeF_3^-	-8.0	0.167

Table 4.4 – Estimated D_a and R values of $CheY_6$, with and without BeF_3^-. Values were calculated using data from the RDC histograms, and Equations 2 and 3.

The estimated D_a and R values agree well with the values obtained by fitting the experimental RDC values found in the following sections for both $CheY_6$, with and without BeF_3^-. The Simulation of Sterically Induced Alignment Tensor (SSIA) program (Zweckstetter and Bax 2000) predicts an R value of 0.554 from the X-ray coordinates. This is similar to the value for $CheY_6$ without BeF_3^-, and would suggest that the crystal structure is more similar to the inactive conformation of $CheY_6$.

The molecular alignment tensor for $CheY_6$ in the 3KYJ X-ray crystal structure was fitted to minimise the χ^2 between the calculated and experimental RDC data. Only residues with $\{^1H\}$-^{15}N NOEs greater than 0.7 were used.

$CheY_6$

88 backbone amide RDCs were measured for $CheY_6$ without BeF_3^-. Initially, RDCs for 56 residues located in secondary structure were fitted, and reasonable agreement between calculated and experimental RDC values was obtained with a Q value of

0.37. α3 displayed the poorest agreement between calculated and experimental RDCs and once removed from the fit, a much better agreement was observed with a Q value of 0.31. The fitted alignment tensor was then used to predict the RDCs for loop residues. These were compared with the experimental RDCs. Loop regions that agreed well were added to the fits, giving a Q value of 0.34 for 66 residues.

Residues fitted	No. Residues	D_a	R	Q
Residues in secondary structure	56	-5.16	0.59	0.37
Secondary structure (without α3)	49	-5.58	0.59	0.31
Secondary structure (without α3), with some loops	66	-5.55	0.52	0.34
All measured RDCs using alignment tensor from secondary structure calculations	88	-4.5	0.46	0.57

Table 4.5 – D_a, R and Q values for different sets of residues. The quality (Q) of the RDC fitting is calculated using the differences between calculated and experimental RDC (D) data: $Q = \{\Sigma_i (D_i^{meas} - D_i^{calc})^2 / \Sigma(D_i^{meas})^2\}^{1/2}$ (Cornilescu *et al*. 1998).

As α3 did not show good agreement for the RDCs, PDBePISA (Krissinel and Henrick 2007) was used to investigate crystal contacts that may alter its position. The results showed that a large proportion of α3 (R69, K72, L73, K74, T75 and R76) forms a crystal contact with $CheA_3P1$ (helix 1); in solution α3 may have a different orientation. Other regions that did not fit well include the β3-α3-loop (57-64) region and the β4-α4-loop (85-90) region. The varying degree of flexibility in loop regions may result in RDC disagreements, especially if they are solvent exposed.

$CheY_6$-BeF_3^-

89 backbone amide RDCs were measured for $CheY_6$-BeF_3^-. Initially, RDCs for 57 residues located in secondary structure were fitted, and showed reasonable agreement between calculated and experimental RDC values with a Q value of 0.37. S83 displayed a very poor agreement (exp. -5.95 Hz, calc. 5.37 Hz), and once removed a Q value of 0.30 was obtained. In a similar way to $CheY_6$ without BeF_3^-, removal of α3 further reduced the Q value to 0.27. This Q value indicates that for regions of secondary structure, except α3, the X-ray structure is an equally good model for the inactive and active states of $CheY_6$ in solution.

Residues fitted	No. Residues	D_a	R	Q
Residues in secondary structure	57	-7.42	0.12	0.37
Residues in secondary structure (without S83)	56	-7.65	0.15	0.30
Residues in secondary structure (without α3)	49	-7.77	0.18	0.27
Secondary structure with loop regions (without α3)	61	-7.61	0.17	0.29
Secondary structure with loop regions (with α3)	68	-7.53	0.15	0.32

Table 4.6 – D_a, R and Q values for different sets of residues for $CheY_6$-BeF_3^-.

The experimental data for S83 agrees well without BeF_3^- (expt. = +4.6 Hz, calc. = +5.8 Hz), but disagrees with BeF_3^- (expt. = -5.9 Hz, calc. = +5.4 Hz). As S83 may be involved in the switch mechanism, this may give an indication that the crystal structure is more like the inactive form. The large change in the experimental RDC for S83 may indicate a change in the orientation of its $^1H^N$-^{15}N bond upon activation. In the X-ray structures of active and inactive $CheY_{EC}$, there is a movement of the backbone of T87. This leads to a change in the position of T87 N, however the

hydrogen bond to V107 O is maintained. A similar movement of S83 N in $CheY_6$ could lead to the change in the RDC. The experimental RDC (-6.4 Hz) of A86 from $CheY_6$ with BeF_3^- does not fit well with the calculated RDC (+3.3 Hz) and hence, the crystal structure is not a good model for this residue in the β4-α4-loop region in solution; an RDC for A86 could not be measured in the absence of BeF3- due to spectral overlap.

4.6 Investigation of the Switch Mechanism of $CheY_6$

The crystal structure of $CheY_6$ displays a highly conserved overall conformation when compared to the crystal structure of $CheY_{EC}$ (Figure 4.21). Many of the residues thought to be involved in the switch mechanism of $CheY_{EC}$ are conserved in $CheY_6$ and superimpose in an overlay of the structures.

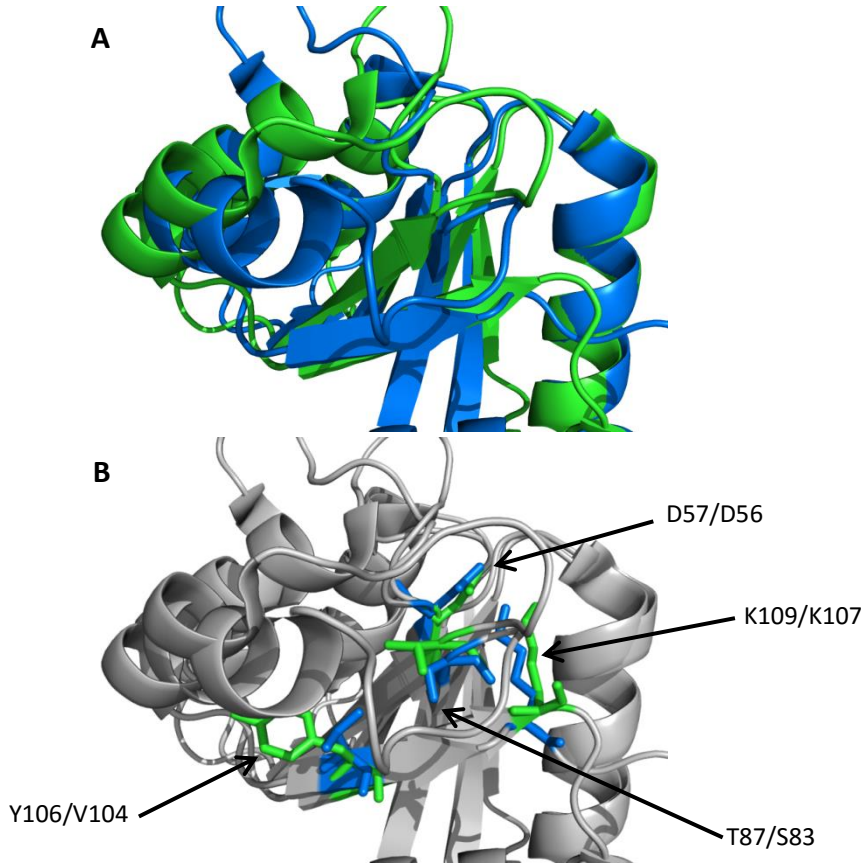

Figure 4.21 – Superposition of $CheY_{EC}$ (green, PDB:1CHN) and *R. sphaeroides* $CheY_6$ (blue, PDB:3KYI). **A**) Overall the secondary structure of $CheY_{EC}$ and $CheY_6$ display good agreement **B**) The important residues in the switch mechanism for $CheY_{EC}$ (D57, T87, Y106 and K109) and the corresponding residues in $CheY_6$ (D56, S83, V104 and K107) are highlighted. Residue labels (*E. coli* / *R. sphaeroides*).

High structural conservation is observed for D57, T87, Y106 and K109, along with the corresponding residues of $CheY_6$, particularly for D57, T87 and K109. As discussed, the $\beta4$-$\alpha4$-loop region has been suggested to play an important role in the $CheY_{EC}$ switch mechanism. This loop region in $CheY_6$ has an additional two residues (not found in $CheY_3$, $CheY_4$ or $CheY_{EC}$), and displays a very different conformation to $CheY_{EC}$ (Figure 4.22).

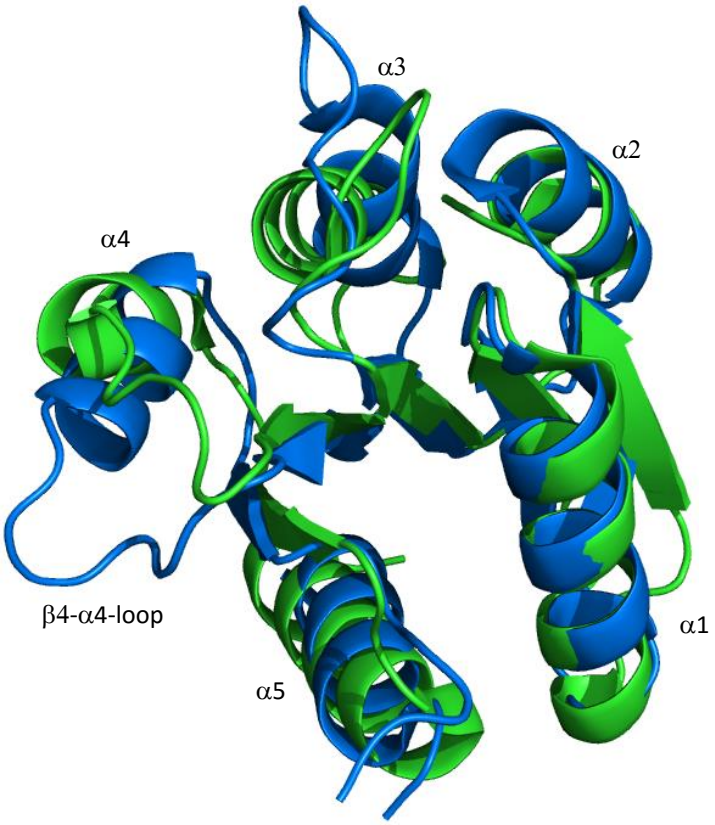

Figure 4.22 - Superposition of *E. coli* CheY (green) and *R. sphaeroides* $CheY_6$ (blue). The β4-α4-loop region is not well conserved between the two structures.

The β4-α4-loop region of $CheY_{EC}$ also undergoes structural changes upon activation (Figure 4.23).

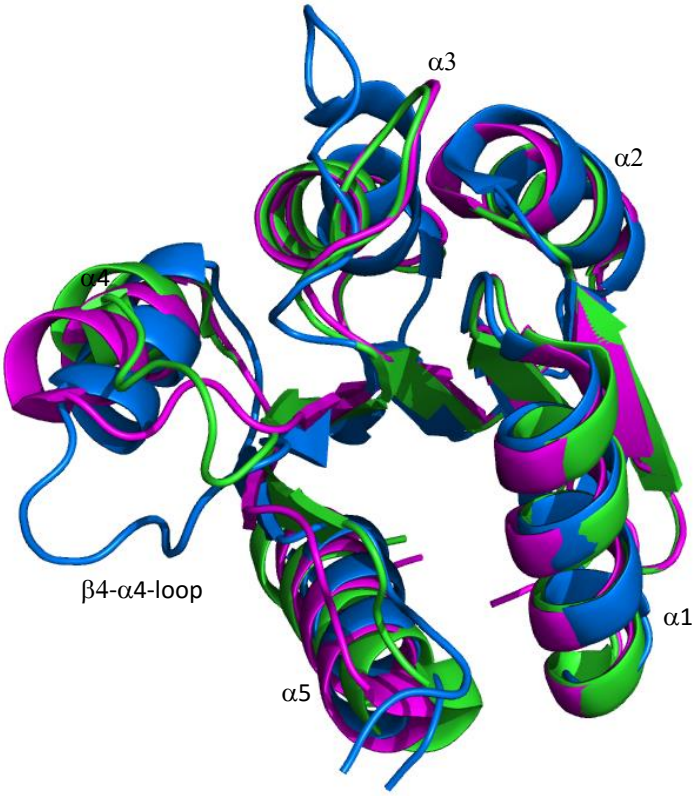

Figure 4.23 – Superposition of *E. coli* CheY in both the active (magenta; PDB:1FQW) and inactive state (green, PDB:1CHN), and *R. sphaeroides* $CheY_6$ (blue).

Based on the different position of the β4-α4-loop region in $CheY_6$ compared to $CheY_{EC}$, and chemical shift perturbations observed for this loop region, it is possible that the β4-α4-loop has an important role in the switch mechanism. Comparison of the residues involved in the $CheY_{EC}$ switch mechanism may elucidate information about the $CheY_6$ switch mechanism (Figure 4.24).

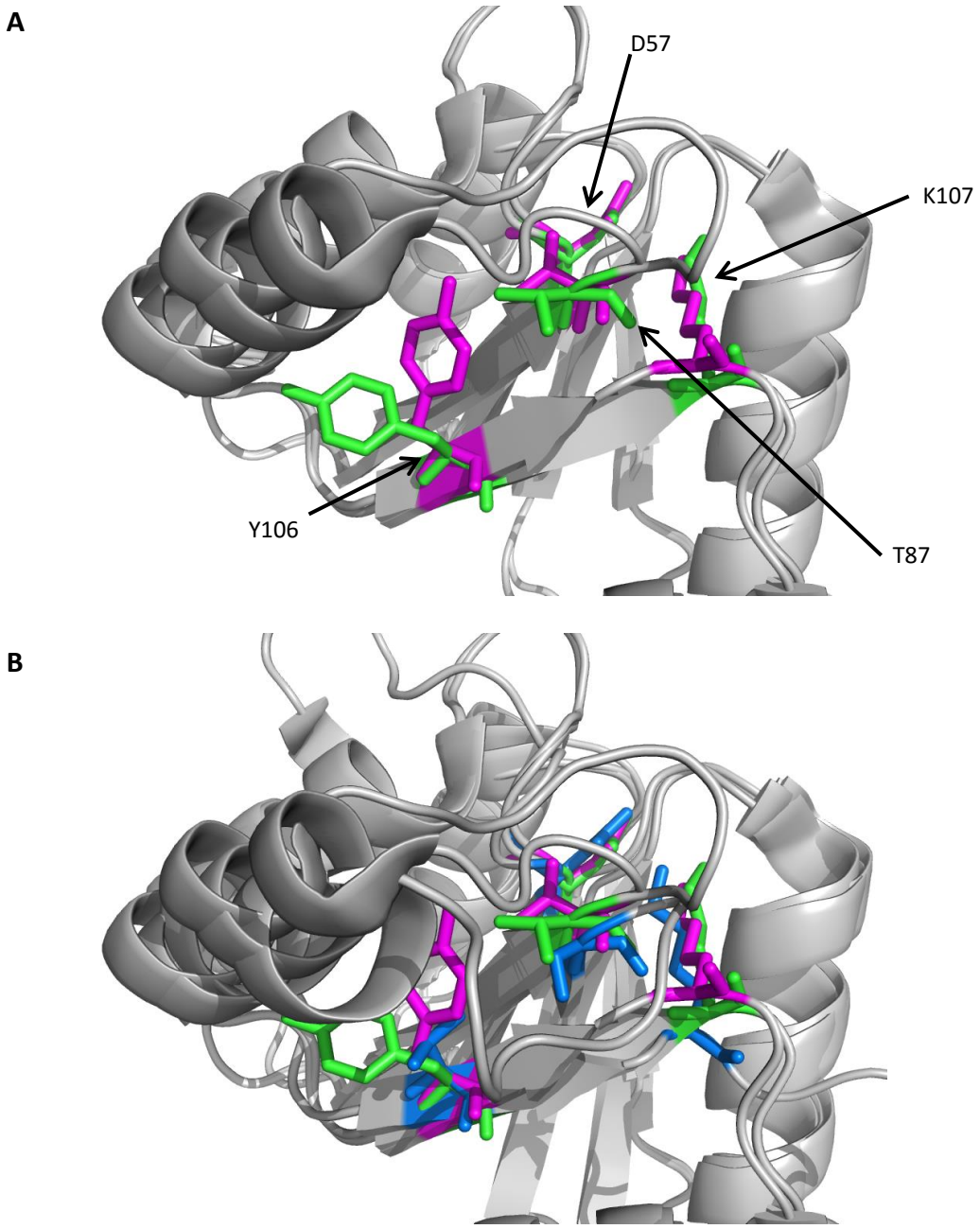

Figure 4.24 – A) Superposition of *E. coli* CheY in both the active (magenta) and inactive state (green). Residues highlighted are thought to be involved in the switch complex. **B**) Superposition of **A** and $CheY_6$ (blue). The corresponding residues of $CheY_6$ are highlighted.

Based on the positions of the $CheY_{EC}$ switch mechanism residues, the $CheY_6$ crystal structure is closer to the inactive conformation of $CheY_{EC}$. Although $Y106_{EC}$ (inactive)

and $V104_{RS}$ have similar backbone and C_α positions, the remaining side chain atoms of Y106 occupy a much larger space compared to V104 (Figure 4.25). It is unlikely that a similar Y-T switch mechanism is employed by $CheY_6$, as the V104 side chain is not large enough to interact with S83.

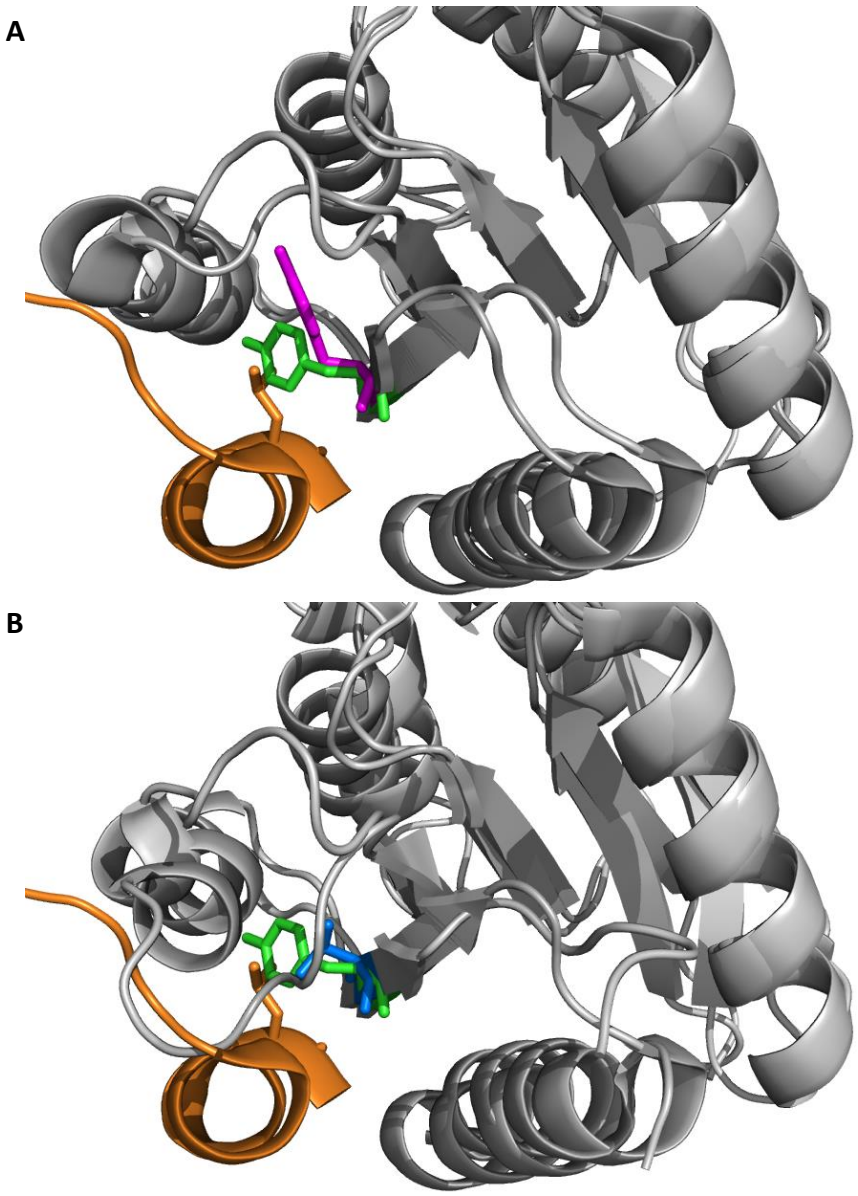

Figure 4.25 – Superposition of **A**) $CheY_{EC}$ (green) and $CheY_{EC}$-BeF_3^- (magenta) in complex with FliM (1-16, orange) **B**) $CheY_{EC}$ (green) and $CheY_6$ (blue). The side chains of residues $Y106_{EC}$, $V104_{RS}$ and Leu15 (FliM) are highlighted using a stick representation and colour.

In *E. coli*, the exposed side chain of Y106 would clash with L15 from the FliM N-terminal region; this leads to a lower affinity for FliM in the inactive state. The burial of Y106 upon activation removes the steric clash and leads to increased affinity for FliM. The much less bulky side chain of $V104_{RS}$ is unlikely to mimic $Y106_{EC}$; no steric clash with the N-terminal peptide of FliM is observed when the $CheY_6$ structure, which appears to resemble the inactive state, is superimposed on the $CheY_{EC}$-BeF_3^--FliM structure. However, the overlaid structure does highlight a significant steric clash with the β4-α4-loop region (Figure 4.26).

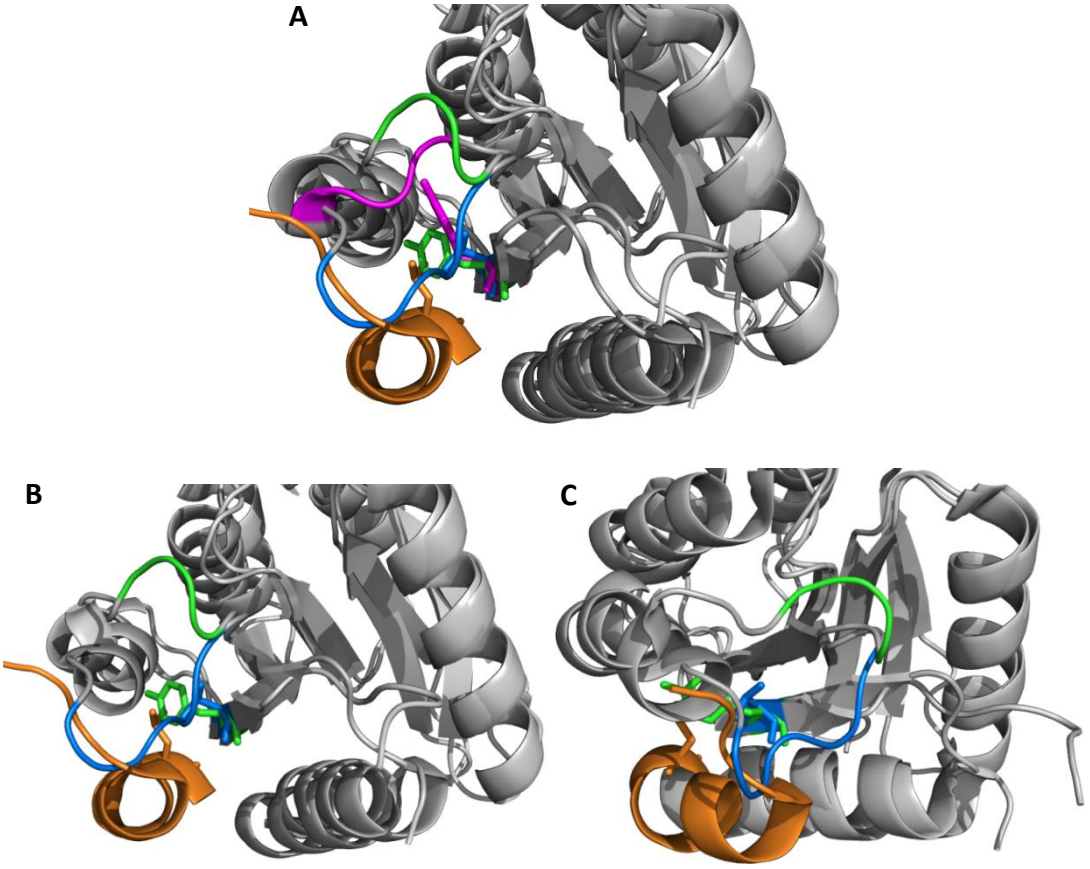

Figure 4.26 – Superposition of **A**) $CheY_{EC}$ (green) and $CheY_{EC}$-BeF_3^- (magenta) in complex with FliM (1-16, orange), and $CheY_6$ (blue) **B**) $CheY_{EC}$ (green) and $CheY_6$ (blue). **C**) A different orientation of **B**. The β4-α4-loop region and Leu15 (FliM) are highlighted.

The β4-α4-loop of inactive $CheY_6$ may sterically clash with the N-terminus of FliM. This loop region would have to reorient itself upon activation, to allow interaction with FliM. The large chemical shift changes observed for this loop region upon addition of BeF_3^- may suggest conformational changes that would allow interaction with FliM.

A conserved hydrogen bond is found between S83 and V105 (S83 N - O V105), which corresponds to the hydrogen bond found in $CheY_{EC}$ (T87 N - O V107). This is consistent with S83 being involved in the switch mechanism of $CheY_6$. There are a number of other conserved hydrogen bonds:

E. coli CheY	*R. sphaeroides* $CheY_6$
K109 N – O T87 (A and I)	K107 N – O S83
T87 OG – N E89 (A)	S83 OG – O V85
T87 OG – H_2O (I)	S83 OG – N V105

Table 4.7 – Comparison of the hydrogen bonds found in $CheY_{EC}$ and $CheY_6$. (A) indicates the active structure and (I) indicates the inactive structure of the corresponding CheY crystal structures.

In *E. coli* the T87 OG forms a hydrogen bond to E89 N, only in the activated state. In *R. sphaeroides* the comparable residue V85 O is found to have a hydrogen bond to S83 OG in the crystal structure, which is likely to represent the inactive state. The large observed chemical shift changes for the $^1H^N$ of A86 and V87, which represent an insertion in the sequence of the β4-α4-loop in $CheY_6$, may indicate a change in the hydrogen bonding of this loop to S83 OG. Changes in hydrogen bonds in the β4-

α4-loop, which lead to a movement of the loop away from the FliM binding site, may be involved in the switch mechanism of $CheY_6$.

4.7 Discussion and Future Work

HetNOE experiments confirmed the elongated loop (109-118) region of $CheY_6$ that showed no electron density in the crystal structure, is flexible in solution. It also highlighted other regions with reduced hetNOE ratios, however these regions were also found to be loops. NH peak shifts in the $^{1}H,^{15}N$-HSQC spectra upon addition of BeF_3^- provided some insight into the switch mechanism. Large shifts were seen for one surface of $CheY_6$, near the phosphorylatable D56 residue. This involved the β4-α4-loop region which has been observed to be important in the $CheY_{EC}$ switch mechanism. Similar chemical shift changes to $T87_{EC}$ were observed for $S83_{RS}$, which could indicate similar conformational changes upon activation. Although not all residues could be assigned, the elongated β5-α5-loop region showed chemical shift changes upon addition of BeF_3^-. This would not be expected if the region was completely unstructured. $K107_{RS}$ displays larger chemical shifts than $K109_{EC}$ upon addition of BeF_3^-, and is observed to be closer to D56 compared to the homologous residues in *E. coli*. This may suggest that $K107_{RS}$ has to undergo a larger conformational shift to accommodate BeF_3^-. The conformational shift of $K107_{RS}$ may cause the β5-α5-loop region to also change conformation.

TALOS-N provided evidence that no large secondary structure changes occur upon addition of BeF_3^-. TALOS-N also predicts a conformational change in the β4-α4-loop region, which may be important in the switch mechanism of $CheY_6$.

Hydrogen-deuterium exchange experiments showed core residues that did not exchange over the time course. β1, 3 and 4 displayed high levels of amide protection with and without BeF_3^-. As these β-strands have very low main chain solvent accessibility, it was not surprising to observe slow exchange. Interestingly, S83 displayed no amide protection without BeF_3^-, but showed slower signal decay upon addition of BeF_3^-. This could again indicate conformational changes involved in the switch mechanism. Residual dipolar coupling also data provided evidence that the crystal structure is more like the inactive conformation of $CheY_6$. These results also suggested that the conformation of S83 in crystal structure agrees well with inactive $CheY_6$ in solution, but does not match well with activated $CheY_6$. This provides further evidence that S83 is involved in the switch mechanism of $CheY_6$.

Superposition of the crystal structures of $CheY_{EC}$ and $CheY_6$ allowed investigation into the possible residues involved in the switch mechanism. $V104_{RS}$ is unlikely to play a similar role to $Y106_{EC}$, as it is not close (or large) enough to interact directly with $S83_{RS}$. This would suggest $CheY_6$ binds differently to FliM relative to $CheY_{EC,}$ and may be the cause of a stop rather than a rotational shift. The β4-α4-loop region displays large chemical shift changes upon addition of BeF_3^-, which would sterically clash with the N-terminus of FliM. A possible switch mechanism for $CheY_6$ may

involve movement of S83, which rearranges hydrogen bonds (such as K107 N - O S83) causing the β4-α4-loop to change conformation. This change in conformation would remove any steric clashes between $CheY_6$ and FliM, and therefore increase the binding affinity. It is apparent that the activation mechanism of the $CheY_6$ response regulator is complex and different to other studied CheY response regulators. Further analysis is needed to fully elucidate the complete switch mechanism of $CheY_6$.

Mutagenesis may provide insights into the switch mechanism of $CheY_6$. Removing the additional residues (V87 and S88) found the β4-α4-loop region of $CheY_6$ may remove the steric clash identified above and result in constitutively active $CheY_6$. If removal of V87 and S88 do not result in a constitutively active $CheY_6$ then the possible role of V104 could also be investigated. If V104 is involved in a steric clash with FliM, then its replacement with the smaller alanine, in addition to removal of V87-S88, might increase the affinity of active $CheY_6$ for FliM leading to a constitutively active phenotype.

Chapter 5

Investigation and Characterisation of the Loop Region in $CheY_6$

5.1 Structural Comparison of the CheYs of *R. sphaeroides*

The *che*Op_2 and *che*Op_3 chemotaxis signal transduction pathway contains three CheY response regulators, $CheY_3$, $CheY_4$ and $CheY_6$. *R. sphaeroides* requires at least two of these to be fully chemotactic, $CheY_6$ and either $CheY_3$ or $CheY_4$ (Porter *et al*. 2006). Without $CheY_6$, *R. sphaeroides* loses its chemotactic ability. This suggests $CheY_6$ plays a more important and unique role than the other CheYs.

A structure guided sequence alignment of $CheY_3$, $CheY_4$ and $CheY_6$ from *R. sphaeroides* and CheY from *E. coli*, highlighted an additional ten residues in $CheY_6$ (residues S109-E118) that are not present in the other CheYs (Figure 5.1). The CheBs of *R. sphaeroides* also have an additional ten residues.

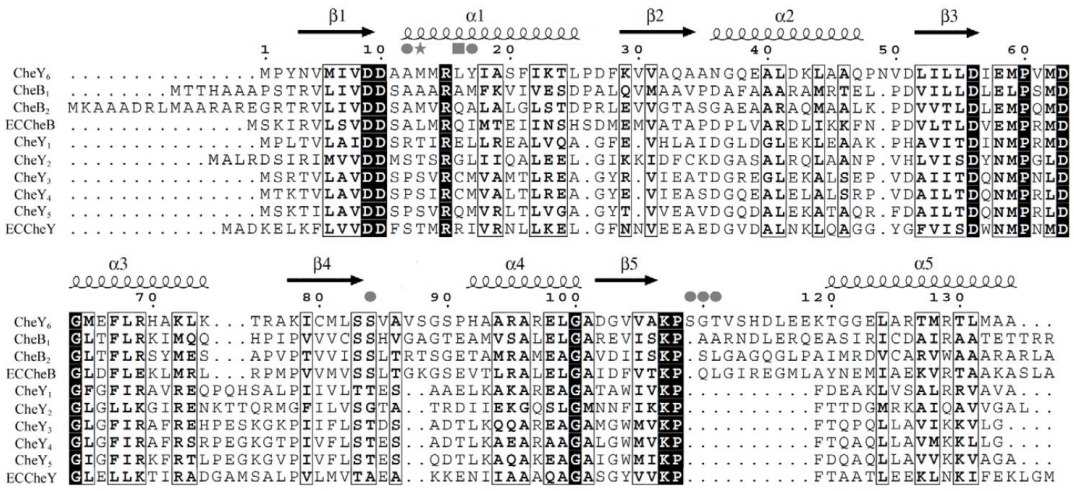

Figure 5.1 - Structure guided sequence alignment of the CheY and CheB response regulators from the *che*Op$_2$ and *che*Op$_3$ chemosensory network of *R. sphaeroides*. *E. coli* CheY and CheB are included for comparison (taken from (Bell *et al*. 2010)).

The crystal structure of CheY$_6$ in complex with CheA$_3$ showed missing electron density for the loop region, suggesting it is disordered in the crystal and might be flexible in solution (Bell *et al*. 2010). This flexible loop region might give CheY$_6$ its different function, compared to CheY$_3$ and CheY$_4$. It may also give insight into the stop-start mechanism of the flagellar motor of *R. sphaeroides*.

5.2 Protein Overexpression and Purification for NMR Studies

cheY$_6$-Δloop was created by overlap extension PCR (Section 2.3.2) of *cheY$_6$* from WS8N genomic DNA using four primers (see Appendix B). PCR products were confirmed using gel electrophoresis and purified via gel extraction. The resulting *cheY$_6$-Δloop* product and the expression plasmid pQE80 (Nterm, 6xHis-tag) were digested using *Bam*HI and *Nco*I. *cheY$_6$-Δloop* was ligated into pQE80 and a successful

insert was identified via digestion of mini-preps from transformed cells. Plasmids containing the correct sized insert were sequenced for confirmation, and checked for point mutations. pQE80-*cheY$_6$-Δloop* was transformed into *E. coli* BL21 (DE3) cells and induced with IPTG (1 mM) in 2TY media. Purification was achieved using a Nickel-NTA Agarose column and further purified using size exclusion chromatography (See Section 2.6). M9 minimal medium (containing $^{15}NH_4Cl$) was used when producing isotopically labelled protein.

5.3 NMR Studies Investigating the Loop Region of CheY$_6$

Protein structures are not always rigid and may contain flexible regions which are dynamic on a range of timescales. The {^{1}H}-^{15}N heteronuclear NOE experiment can be very useful for identifying residues that are mobile on a fast (ns to ps) timescale. For each residue, the relative decrease in peak intensity correlates with its mobility. A rigid backbone ^{15}N has an NOE ratio between 0.7-0.8 whereas a residue in a region of flexible backbone has a ratio of < 0.7 (Kay *et al*. 1989).

Steady state ^{1}H,^{15}N-heteronuclear NOE experiments (Figure 5.2) were used to identify the fast timescale mobility of residues in wild type CheY$_6$. In particular, the loop region was investigated.

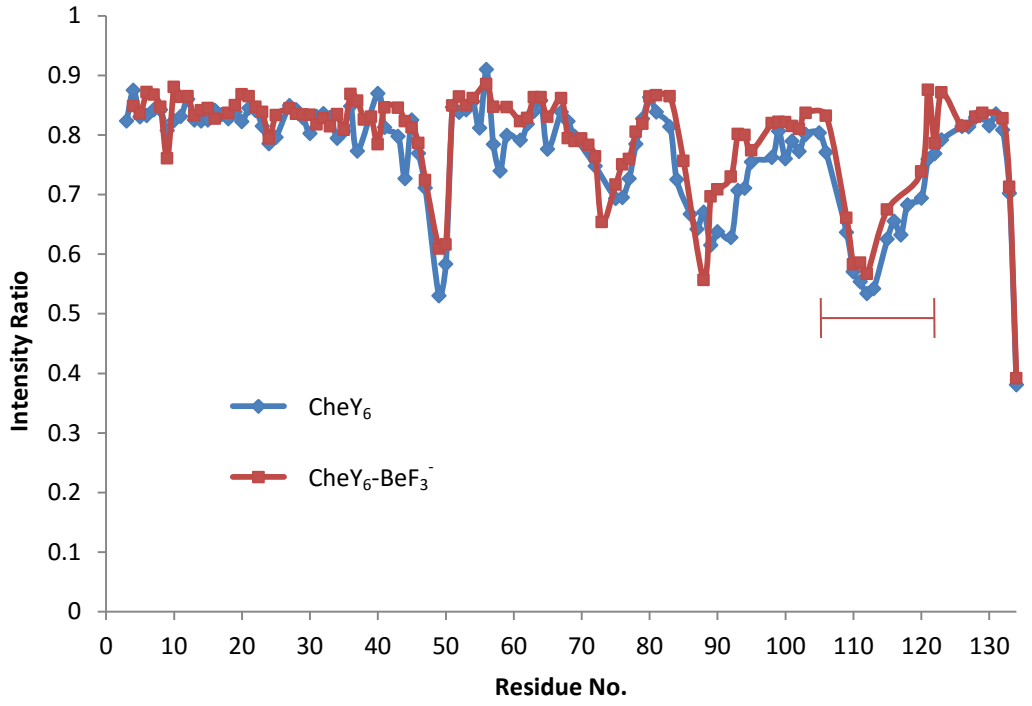

Figure 5.2 - Heteronuclear NOE data of $CheY_6$. A reduced heteronuclear NOE is observed for the loop region S109-E118, indicating that it is flexible on a fast timescale.

$CheY_6$ in both its active and inactive state shows a reduced hetNOE ratio (< 0.7) for residues S109-T120. This indicates fast timescale backbone dynamics (picosecond to nanosecond) and therefore infers a flexible region. This is in agreement with the crystal structure.

5.4 Modelling a $CheY_6$ Loop Deletion Mutant

To investigate the functional importance of this loop region, a deletion mutant was designed. Modelling (XPLOR-NIH, (Schwieters *et al*. 2003)) was first performed to determine whether the $CheY_6$ structure could accommodate the deletion of this loop. With the use of computer modelling, a peptide bond was created between the

CO of P108 and the NH of K119 and the structure was energy minimised using XPLOR-NIH. A low energy structure without any bond length or angle distortions suggested that $CheY_6$ can accommodate this loop deletion (Figure 5.3).

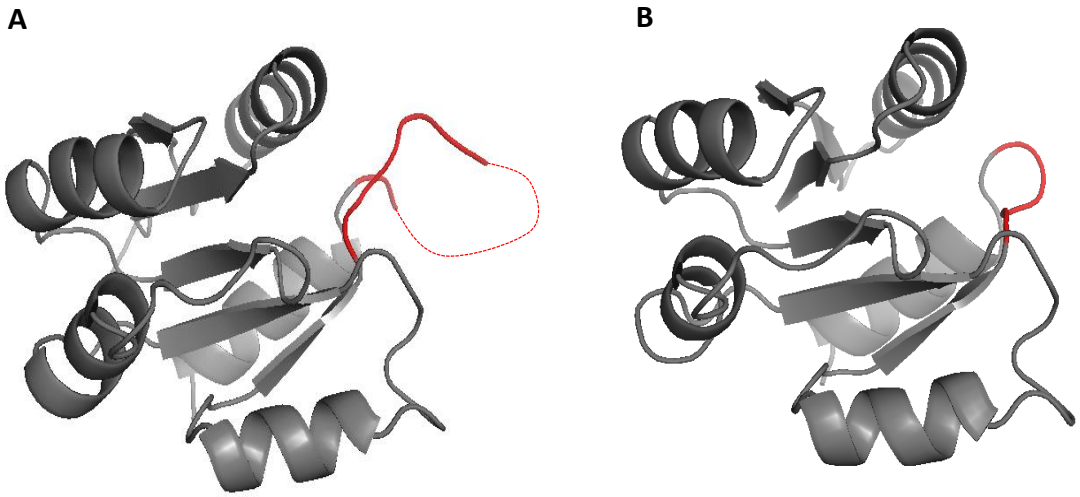

Figure 5.3 - **A)** Crystal structure of $CheY_6$. The red section indicates residues K107 to T120. Coordinates do not exist for residues S113-K119 as the crystal structure contained no electron density (Bell *et al*. 2010). **B)** Proposed $CheY_6$-Δloop structure. A pseudo peptide bond was made from P108 CO to K119 NH and energy minimisation calculations performed using XPLOR-NIH to determine if this was a suitable deletion. This resulting low energy structure suggests that deletion of residues 109-119 could result in stable and correctly folded protein.

Previous studies showed that deletion of $CheY_6$ from the genome created non-chemotactic strains. It was found that deletion of $CheY_6$ disrupted expression of downstream chemotaxis proteins such as $CheA_3$ (Pilizota *et al*. 2009) (Gould 2006) (Brown 2009). Inactivation of $CheY_6$ using a D56A mutation (JPA1216 strain) overcomes this problem and produces a smooth swimming phenotype(Brown 2009) (Porter *et al*. 2006).

5.5 Circular Dichroism

Purification of $CheY_6$-Δloop proved to be difficult, with many samples precipitating out of solution at various stages of purification. Circular dichroism was used to indicate whether $CheY_6$-Δloop was folded correctly (Figure 5.4). Wild type $CheY_6$ and $CheY_6$-Δloop were placed into a cuvette (1 mm), ellipticity (200-260 nm) was measured at 20°C and the traces were compared.

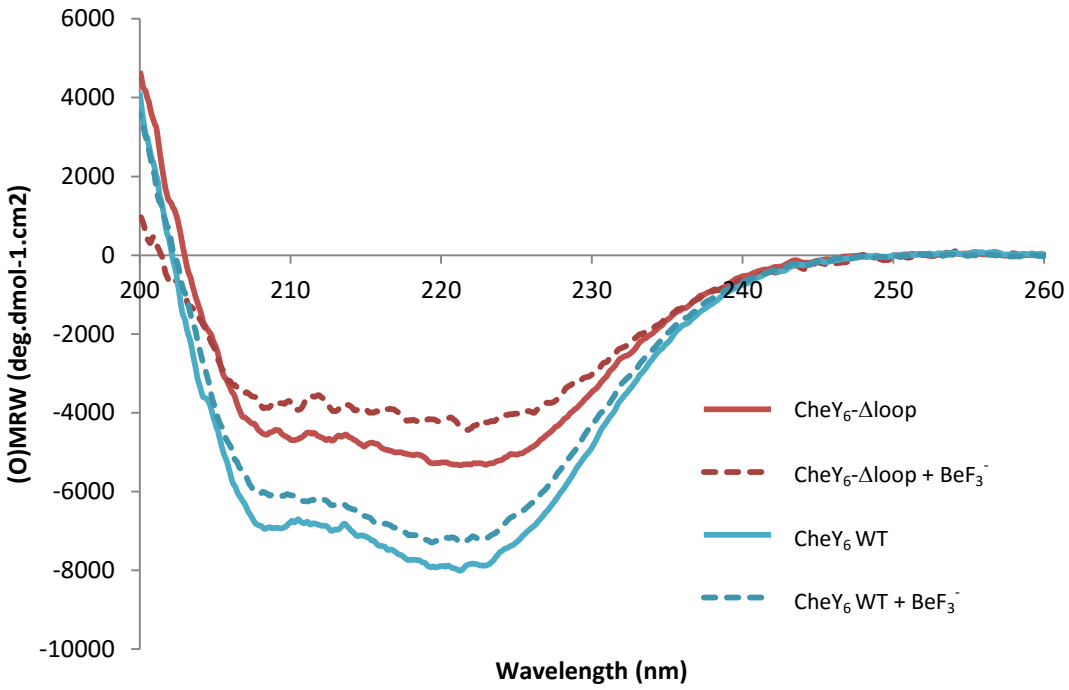

Figure 5.4 – Circular dichroism traces of wild type $CheY_6$ and $CheY_6$-Δloop with and without BeF_3^- at pH 7.2. Both proteins show minima at 208 and 222 nm which are indicative of α-helices and hence, folded protein.

$CheY_6$-Δloop traces show minima at 208 and 222 nm which is indicative of α-helices. This suggests that $CheY_6$-Δloop has secondary structure and could have a native fold.

5.6 pIND4 Plasmids for *in vivo* Studies

cheY$_6$-*Δloop* was created by overlap extension PCR (Section 2.3.2) of *cheY*$_6$ from WS8N genomic DNA using four primers (see Appendix B). PCR products were confirmed using gel electrophoresis and purified via gel extraction. The resulting *cheY*$_6$-*Δloop* product and pIND4 (Ind *et al*. 2009) were digested using *Nco*I and *Hind*III. *cheY*$_6$-*Δloop* was ligated into pIND4 and a successful insert was identified via digestion of mini-preps from transformed cells. Plasmids containing the correct sized insert were sequenced for confirmation and checked for point mutations. pIND4-*cheY*$_6$ was also produced for control strains.

5.7 Swim Plate Assays

Having demonstrated that CheY$_6$-Δloop can be expressed as folded protein, the second part of this project was to perform *in vivo* studies to determine whether chemotaxis was affected by deletion of this loop region (S109-E118) in CheY$_6$.

Swim plates (Section 2.4.1) were used to assess the chemotactic ability and motility of strains by quantifying how the bacteria swim through soft agar. Propionate is the only available carbon source on the plate. Cells are inoculated at a single point and as they grow the sodium propionate is consumed, generating a concentration gradient out from the site of inoculation. Motile and chemotactic cells are able to swim up this gradient creating a ring. The diameter of these swim rings were measured for each strain and compared to control strains. Three controls were

used; wild type (WS8N), a non-chemotactic strain (JPA1336, $\Delta cheY_6$) and a non-motile strain (JPA467, $\Delta\sigma 28$). The non-chemotactic strain has $CheY_6$ deleted from the genome. As the strain is still motile, it should exhibit a reduced swim diameter relative to wild type. The non-motile strain does not produce a flagellar motor and is therefore non-motile. This should result in the swim diameter not increasing very much over the course of the experiment. All swim diameters were normalised to wild type (Figure 5.5).

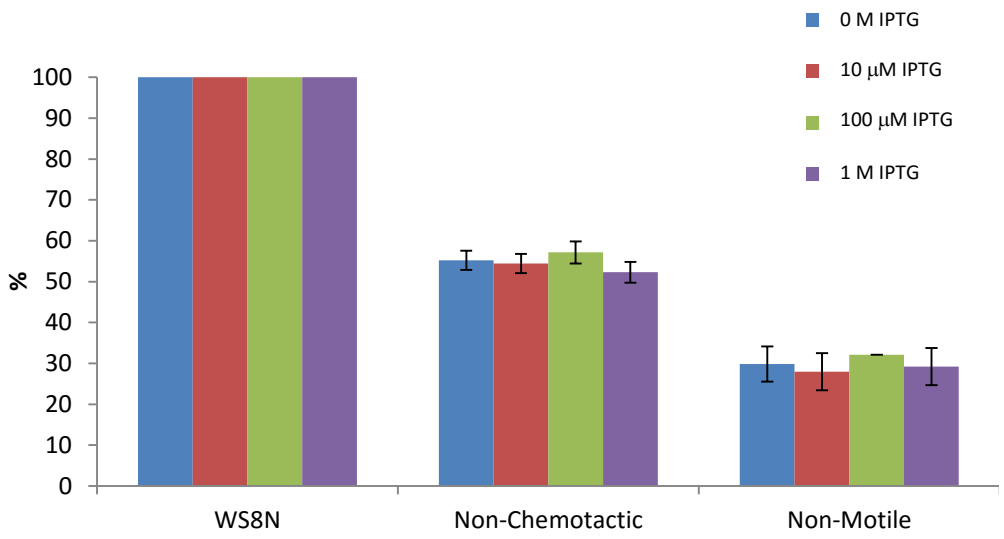

Figure 5.5 – Bar chart showing the swim diameters of the non-chemotactic (JPA1336) and non-motile (JPA467) control strains relative to wild type (WS8N). There is no IPTG dependence as there is no inducible plasmid present.

IPTG inducible expression plasmids pIND4-$cheY_6$-$\Delta loop$ and pIND4-$cheY_6$ were conjugated into a number of background strains. Protein expression levels were controlled by varying the concentration of IPTG (0 to 1 mM) within the plate. JPA1216 contains genomic *che*Y_6-D56A, which is inactive. If the loop plays an important role in chemotaxis, $CheY_6$-Δloop in strain JPA1216 (JPA2402) would

display a non-chemotactic phenotype whereas $CheY_6$ wild type in strain JPA1216 (JPA2401) would revert to a wild type phenotype. A representative swim plate is displayed below (Figure 5.6).

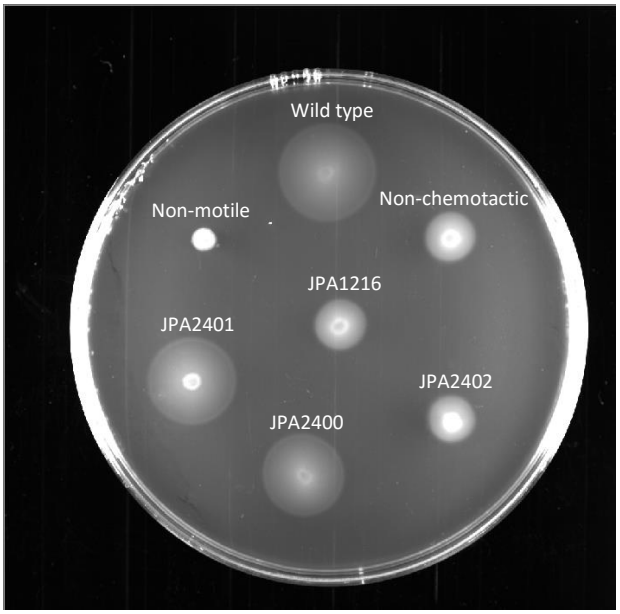

Figure 5.6 – A representative swim plate (1 mM IPTG) containing wild type (WS8N), non-motile control (JPA467), non-chemotactic control (JPA 1336), pIND4-*cheY*$_6$ in JPA1216 (JPA2401), pIND4-*cheY*$_6$-*Δloop* in JPA1216 (JPA2402 and *che*Y$_6$-Δloop in WS8N (JPA2400). Diameters were measured and normalised to WS8N.

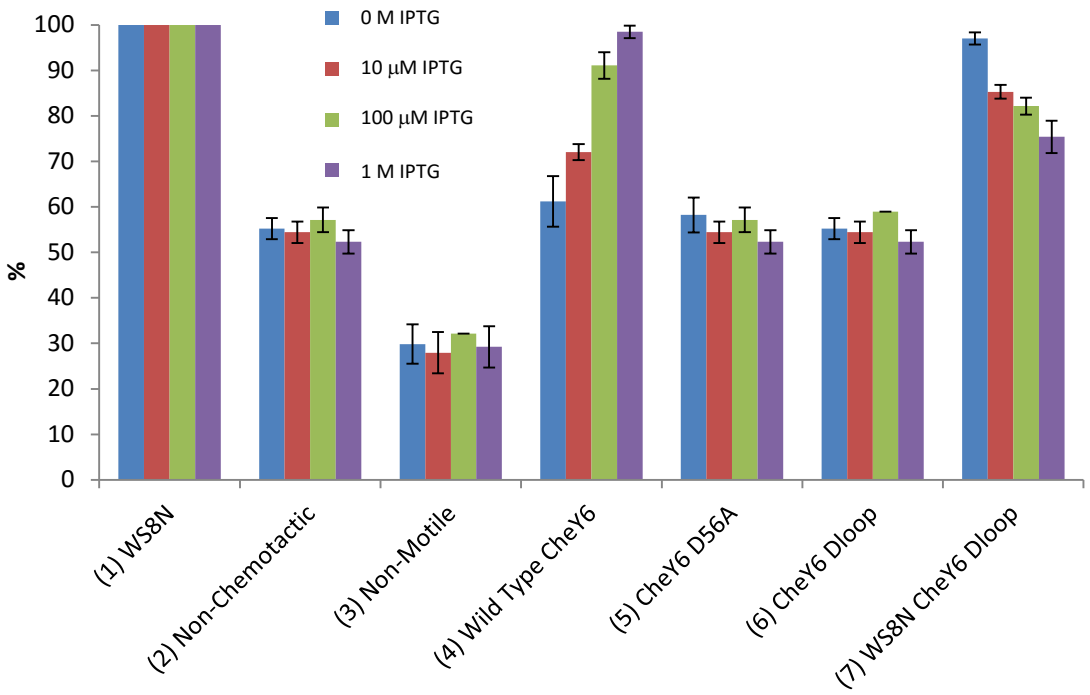

Figure 5.7 – Bar chart showing the swim diameters of mutant *R. sphaeroides* strains relative to wild type (1). Smooth swimming JPA1216 (*cheY*$_6$*-D56A*) shows a non-chemotactic phenotype (5). JPA1216 containing pIND4-*cheY*$_6$*-Δloop* (JPA2402) displays a non-chemotactic phenotype (6). JPA1216 containing pIND4-*cheY*$_6$ (JPA2401) however shows almost full restoration of chemotaxis with the addition of 1 mM IPTG (4). WS8N containing pIND4-*cheY*$_6$*-Δloop* (JPA2400) shows a reduction in swim diameter (7). Three repeats were performed in triplicate.

Smooth swimming strain JPA1216 shows a non-chemotactic phenotype, with a swim diameter of ~50% of wild type. JPA2401 cells, which express inducible wild type CheY$_6$, displayed a non-chemotactic phenotype at 0 M IPTG but showed almost complete restoration of chemotaxis to wild type levels when inoculated with 1 mM IPTG. However, JPA2402 cells, which express CheY$_6$-Δloop, had comparable swim diameters to the non-chemotactic control, suggesting a smooth swimming phenotype. Combining these two results suggest that deletion of the loop

(S109-E118) from $CheY_6$ renders it inactive. $CheY_6$-Δloop could be inactive for a number of reasons. Firstly, $CheY_6$-Δloop may not be folding correctly. However, CD and NMR studies (Section 5.11) indicated the protein is folding correctly. Secondly, $CheY_6$-Δloop may not be able to localise and interact with the cytoplasmic cluster. Fluorescence microscopy would test whether $CheY_6$-Δloop localises at the cytoplasmic cluster. Thirdly, $CheA_3$ may no longer be able to phosphorylate $CheY_6$-Δloop. Phosphotransfer assays would test whether $CheA_3$ is able to phosphorylate $CheY_6$-Δloop. Lastly, $CheY_6$-Δloop may not be able to bind to the motor. Tethering assays would test whether it has a smooth swimming phenotype. Interestingly, wild type cells expressing $CheY_6$-Δloop (JPA2400) showed a decrease in swim diameter as IPTG concentration increases. This suggests that $CheY_6$-Δloop is competing with wild type $CheY_6$ and reducing chemotactic ability. This further suggests $CheY_6$-Δloop is correctly folded, as it would be unlikely to compete with wild type $CheY_6$ if it was unfolded.

5.8 Tethering Assays

Cells were tethered to a glass cover slip using anti-flagellar antibody and placed in a flow cell (Figure 5.8). Wild type response consists of a stop in rotation after the removal of attractant. Rotation is recovered after ~40 s. This is the chemotactic response to the worsening of conditions, i.e. reduced attractant. In *E. coli*, the response is often measured by the addition of repellent, but except for the addition

of oxygen to photoheterotrophic cells, no repellent has been identified for *R. sphaeroides*.

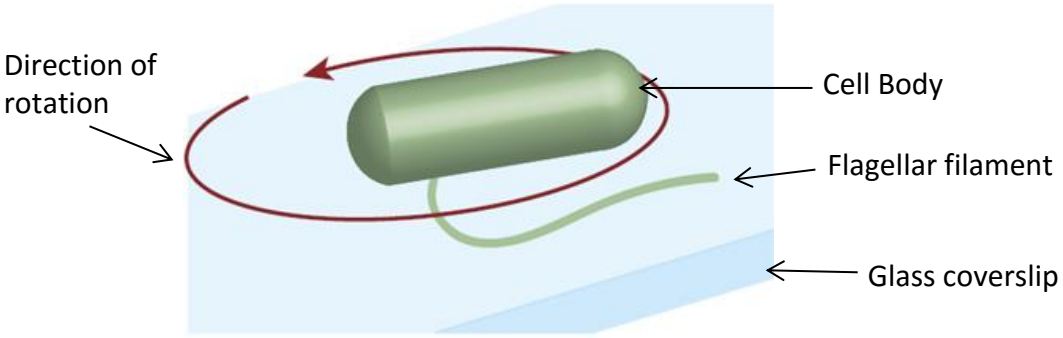

Figure 5.8 – Illustration of a tethered bacterium in a flow cell. Buffer is flowed through the cell at a constant flux. A single run consists of PIPES buffer containing no attractant for three minutes, PIPES buffer containing attractant (100 μM propionate) for five minutes and finally PIPES buffer containing no attractant. The flagellar filament is attached to the glass coverslip by anti-flagellin antibody.

Individually rotating cells were selected and image analysis was completed using BRAS and Click&Mean software (Kojadinovic *et al*. 2011). BRAS is an image segmentation program that was used to detect the rotation rate of individual cells every 50 ms. Cell rotation rate is detected by the difference in pixel intensity between the background and the cell. Click&Mean processes and displays coordinate data from BRAS output files. X-Y coordinate changes between each frame are converted into a rotational speed using a Fourier transformation (smoothing window of 128 frames). A typical wild type trace can be seen below (Figure 5.9).

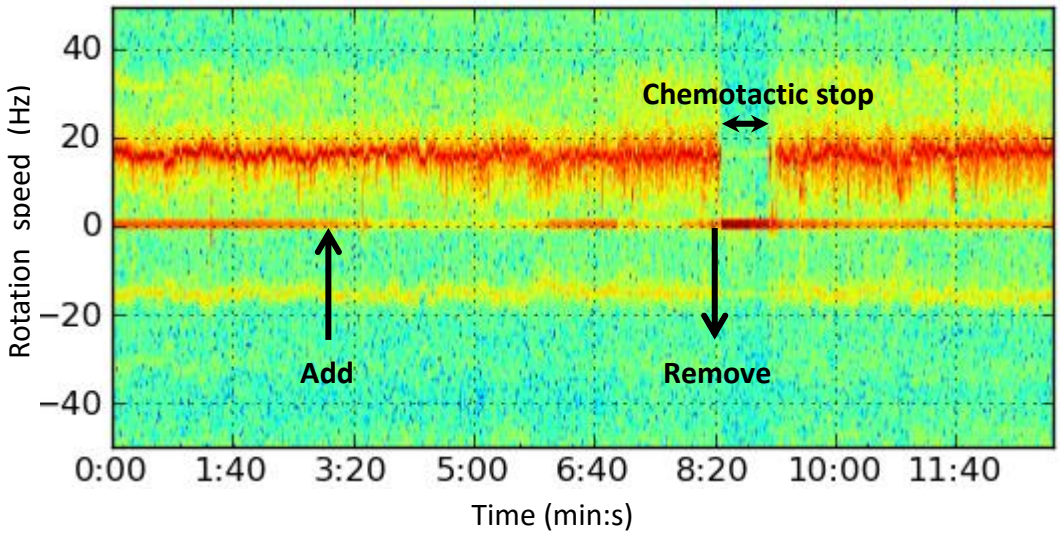

Figure 5.9 – Tethered cell trace of WS8N. Arrows denote addition and removal of attractant (100 μM sodium propionate). A run consisted of three minutes of PIPES buffer containing no attractant, followed by five minutes of PIPES with attractant and ending with five minutes of PIPES containing no attractant.

Upon addition of attractant after three minutes, there is no change in rotation speed. The removal of attractant after eight minutes causes a chemotactic stop in rotation. This stop lasts approximately 40 seconds, after which adaptation of the chemoreceptors occurs, and the bacterium starts rotating again.

Tethering assays were performed to assess the phenotypes of WS8N, a non-chemotactic control (JPA1216), the non-chemotactic strain containing wild type $CheY_6$ (JPA2401) and the non-chemotactic strain containing $CheY_6$-Δloop (JPA2402) (Figure 5.10). IPTG (500 μM) was used to induce protein expression. WS8N showed wild type behaviour as described above where 73% of 40 cells analysed stopped for an average of 39 ± 13 seconds. The non-chemotactic control retained smooth

swimming upon attractant removal (84% of 57 cells analysed). This was expected as $CheY_6$ could no longer be phosphorylated (i.e. D56A mutation).

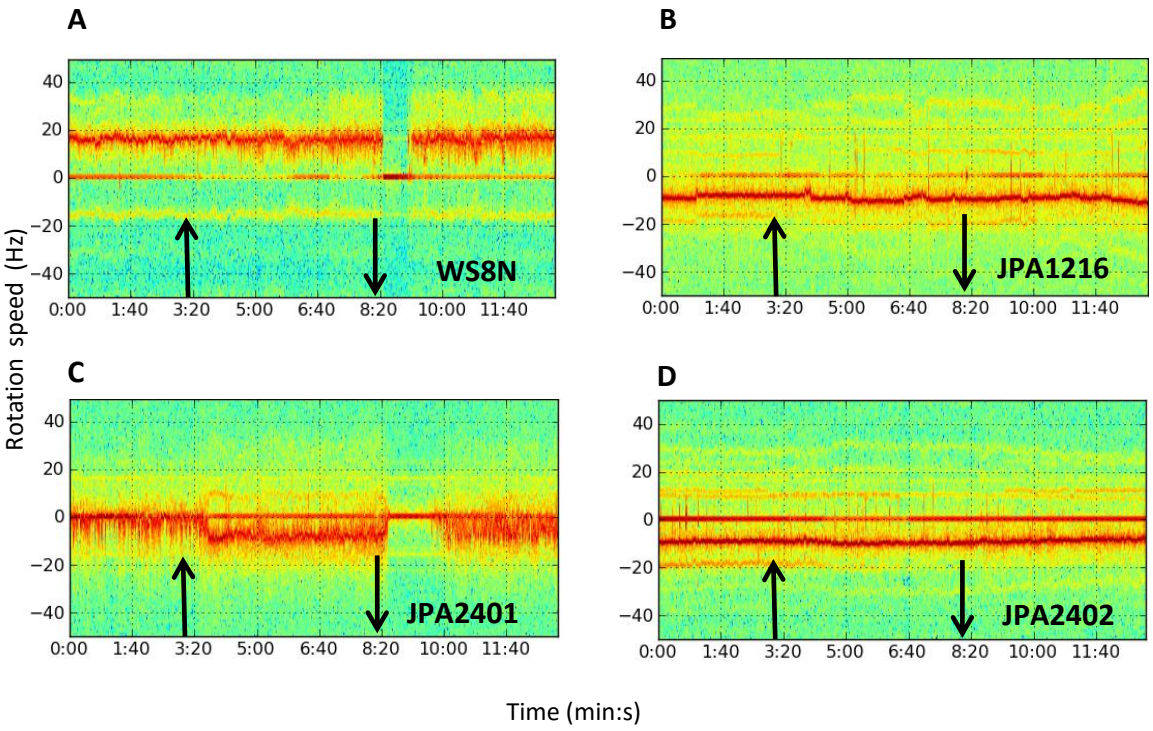

Figure 5.10 – Tethered cell assay traces of **A)** WS8N, **B)** Non-chemotactic (JPA1216), **C)** Wild type $CheY_6$ (JPA2401) and **D)** $CheY_6$-Δloop (JPA2402). Arrows denote addition and removal of attractant (100 μM propionate). The run consisted of three minutes of PIPES buffer containing no attractant, followed by five minutes of PIPES containing propionate and ending with five minutes of PIPES containing no attractant.

The non-chemotactic strain expressing wild type $CheY_6$ (JPA2401), displayed a wild type phenotype. 44% of 34 cells analysed stopped for an average of 60 ± 13 seconds. The stopping length was longer than for wild type. This was likely due to higher than wild type expression of $CheY_6$. A smooth swimming phenotype, similar to the non-chemotactic strain, was observed for JPA1216 (D56A) cells expressing $CheY_6$-Δloop.

88% of 58 cells analysed did not stop rotation. This result shows that $CheY_6$-Δloop is unable to trigger a chemotactic stop of the motor.

5.9 Microscopy

Previous studies have shown that wild type $CheY_6$ fused to Yellow Fluorescent Protein (YFP) localises approximately at mid-cell, where the cytoplasmic cluster has been shown to localise (Porter *et al*. 2006). Wild type $CheY_6$ and $CheY_6$-Δloop were fused to YFP on an inducible plasmid (pIND4) and expressed in a wild type background.

5.9.1 Epifluorescence Microscopy of $CheY_6$-Δloop

Two sets of images are collected during epifluorescence microscopy, brightfield images and epifluorescence images. Non-fluorescent brightfield images are collected to define the cell boundaries whereas epifluorescence images show signal from fluorescent protein.

pIND4-*cheY*$_6$-*Δloop-yfp* and pIND4-*cheY*$_6$-*yfp* were separately conjugated into WS8N. Cells were grown shaking overnight at 30°C, subcultured and induced with IPTG (100 μM) until OD_{700} 0.4-0.5.

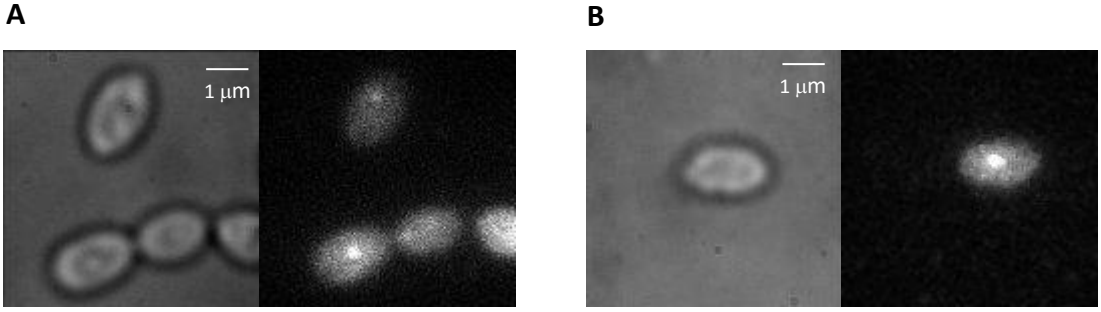

Figure 5.11 – Bright field and epifluorescence microscopy images of **A)** WS8N containing pIND4-*cheY-$_6$-yfp*. A diffuse pattern of localisation with a focus near the centre of the cell is observed. **B)** WS8N containing pIND4-*cheY$_6$-Δloop-yfp* shows a similar pattern of localisation to CheY$_6$-YFP. The images are 6x6 μm.

Epifluorescence microscopy images show a diffuse arrangement of CheY$_6$-YFP around the cell with a focus approximately at mid-cell (Figure 5.11). This is in agreement with the literature. CheY$_6$-Δloop-YFP shows the same pattern of localisation. This indicates that CheY$_6$-Δloop could be localising at the cytoplasmic cluster. Co-localisation experiments with double tagged strains containing CheY$_6$-Δloop-YFP and CheA$_3$-CFP would provide further evidence for this.

5.9.2 Co-localisation of CheY$_6$-Δloop-YFP with CheA$_3$-CFP

pIND4-*cheY$_6$-Δloop-yfp* and pIND4-*cheY$_6$-yfp* were conjugated separately into JPA1422 (*cheA$_3$-cfp*). Cells were grown shaking overnight at 30°C, subcultured and induced with IPTG (100 μM) until OD$_{700}$ 0.4-0.5 (Figure 5.12).

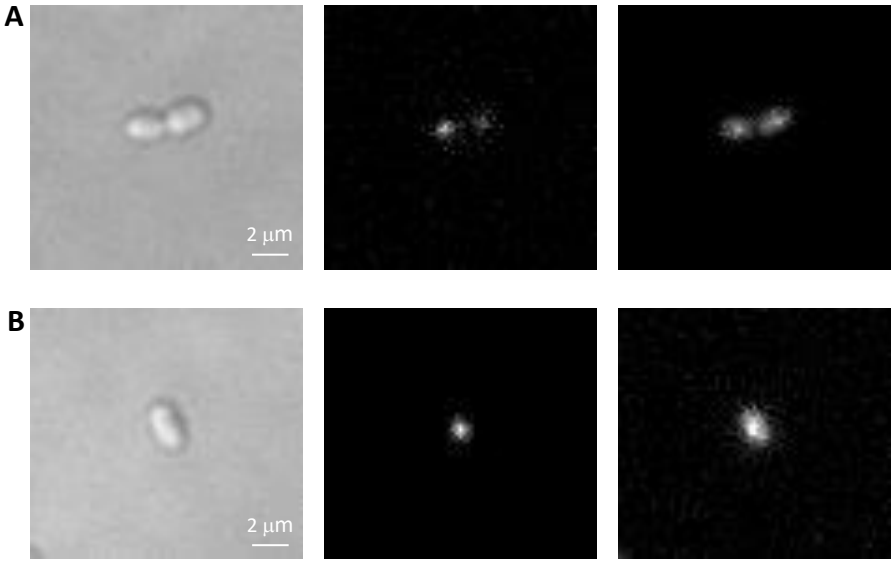

Figure 5.12 – A) Brightfield, CFP and YFP channels (respectively) of JPA1422 containing pIND4-*cheY$_6$-yfp*. **B)** Brightfield, CFP and YFP (respectively) channels of JPA1422 expressing CheY$_6$-Δloop-YFP. CheA$_3$-CFP localises approximately at mid-cell as expected. CheY$_6$-YFP and CheY$_6$-Δloop-YFP both show a diffuse pattern around the cell with a foci overlapping with CheA$_3$.

As expected, CheA$_3$-CFP localises approximately at mid-cell. This focus indicates the location of the cytoplasmic cluster. CheY$_6$-YFP and CheY$_6$-Δloop-YFP show a more diffuse pattern of fluorescence around the cell, with a focus overlapping with the cytoplasmic cluster. The fluorescence intensity profiles of individual cells (Figure 5.13) highlight the overlap of localisation.

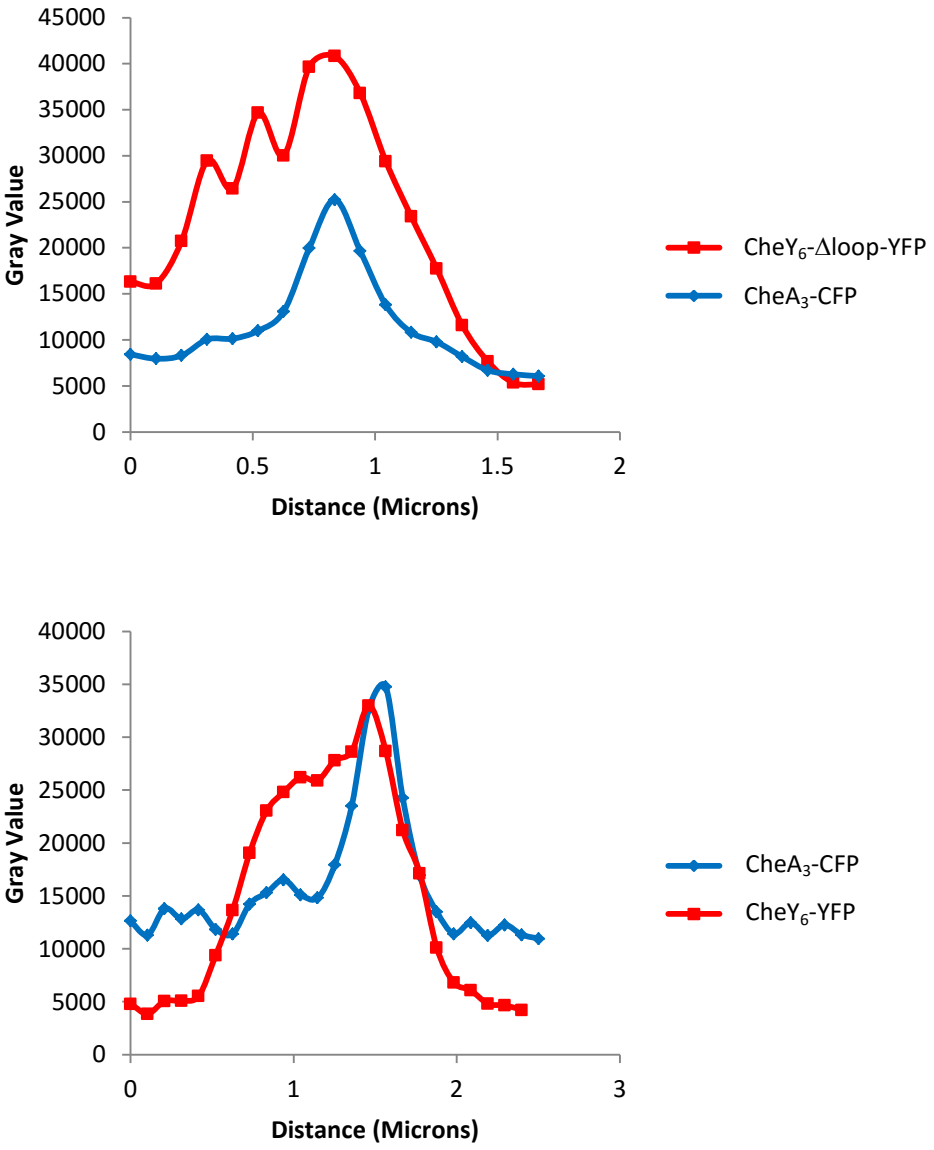

Figure 5.13 – Fluorescence profiles of individual cells **A)** JPA1422 containing pIND4-*che*Y_6-*Δloop-yfp* and **B)** JPA1433 containing pIND4-*che*Y_6-*yfp*. Both profiles show a sharp peak for $CheA_3$-CFP which indicates the location of the cytoplasmic cluster. $CheY_6$-ΔloopYFP and $CheY_6$-YFP illustrate a more diffuse pattern of localisation with a peak that overlaps with the cytoplasmic cluster.

The cell profiles show that $CheY_6$ and $CheY_6$-Δloop are diffuse around the cell. This is to be expected as $CheY_6$ is a cytosolic protein that interacts with multiple sites within the cell. A significant proportion of both are localised to the cytoplasmic cluster,

indicating $CheY_6$-Δloop is localising like wild type $CheY_6$. Interestingly, localisation is not seen at the polar cluster. Phosphotransfer assays would determine if $CheY_6$-Δloop can still interact with the cytoplasmic cluster and can still be phosphorylated by $CheA_3$.

5.10 Phosphotransfer Assays

$CheA_3$, $CheA_4$, $CheY_6$ and $CheY_6$-Δloop were inserted into the expression plasmid pQE80 (Nterm, 6xHis-tag) using the methods described in Section 2.3. pQE80 plasmids were transformed into *E. coli* BL21 (DE3) cells and induced with IPTG (1 mM) in 2TY media. Purification was achieved using a Nickel-NTA Agarose column and further purified using size exclusion chromatography (Section 2.6).

Phosphotransfer assays were used to observe phosphorylation of $CheY_6$ and $CheY_6$-Δloop by their cognate CheA histidine kinase complex, $CheA_3$-$CheA_4$. Both $CheA_3$ and $CheA_4$ are needed for phosphorylation of $CheY_6$. The kinase domain of $CheA_4$ phosphorylates the P1 domain of $CheA_3$, which in turn phosphorylates $CheY_6$ (Porter, Wadhams, and Armitage 2007). $CheA_3$-$CheA_4$ (5 μM) was preincubated with [γ-^{32}P] ATP (0.5 mM) to allow phosphorylation of the kinase complex before addition of $CheY_6$ (10 μM). Excess ATP was used to allow the CheA complex to autophosphorylate throughout the experiment. Progress of the reaction was recorded by quenching aliquots of the reaction at time points 15, 30, 60, 120 and 240 seconds. Quenched samples were gel electrophoresed, exposed to a phosphor

screen (Kodak) (Figure 5.14) and analysed using a SF-phosphorimager with ImageQuant software (version 5.0, Molecular Dynamics) (Figure 5.15). Band intensities were measured and background noise subtracted.

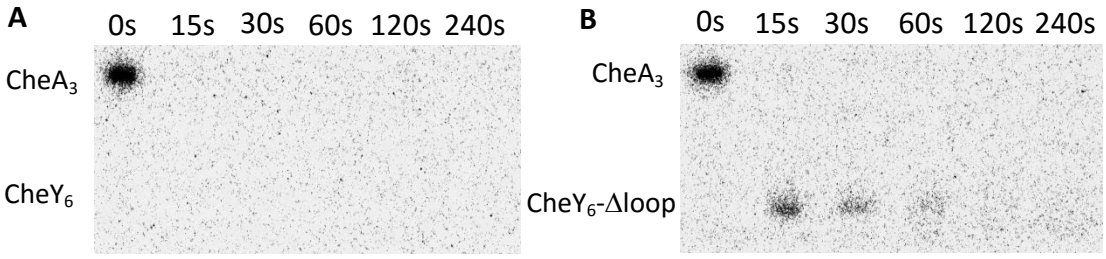

Figure 5.14 – Phosphotransfer reaction of **A)** $CheA_3$ to $CheY_6$. Within 15 seconds, no phosphorylated $CheA_3$ or $CheY_6$ is observed. This indicates $CheY_6$ has been phosphorylated by $CheA_3$ and auto-dephosphorylated faster than 15 seconds. As no $CheA_3$-P is observed for the entirety of the experiment, this indicates that $CheY_6$ auto-dephosphorylation is faster than phosphotransfer of $CheA_3$ to $CheY_6$. **B)** $CheA_3$ to $CheY_6$-Δloop. In contrast, $CheY_6$-Δloop-P is observed at 30 seconds, indicating a slower auto-dephosphorylation rate.

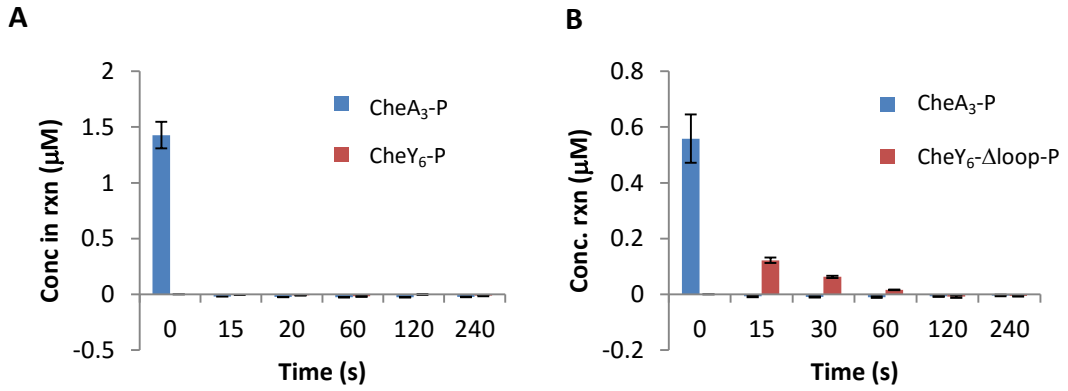

Figure 5.15 – Bar chart showing concentrations of γ-^{32}P with $CheA_3$ and **A)** $CheY_6$ and **B)** $CheY_6$-Δloop during the phosphotransfer reaction. Phosphorimaging of radiolabelled band intensities from SDS-PAGE gels was used to quantify concentration. Error bars are based on triplicate experiments and their standard deviation. Concentrations were measured using a standard curve.

The data are consistent with the literature and shows that wild type $CheY_6$ is phosphorylated by $CheA_3$-P (Porter *et al*. 2006). Wild type $CheY_6$ is phosphorylated and dephosphorylated within 15 seconds. $CheY_6$-Δloop is phosphorylated by CheA3-P which suggests a normal interaction. This would suggest that the loop deletion has not impaired its ability to interact with the cytoplasmic cluster. However, the rate of dephosphorylation is slower than wild type $CheY_6$. This could be due to stabilisation of $CheY_6$ in its active conformation by the removal of the disordered loop region. Another possible explanation could be that this loop region may be important in the interaction with the phosphatase domain of $CheA_3$. If $CheY_6$-Δloop could still interact and bind to the flagellar motor, a more stoppy phenotype would be expected. A stoppy phenotype has longer and more frequent chemotactic stops than a wild type phenotype. However, the tethering data shows a smooth swimming phenotype (no chemotactic stops). A combination of these results would suggest that deleting the loop region impairs the ability of $CheY_6$ to interact with the flagellar motor.

5.11 NMR Studies of $CheY_6$-Δloop

5.11.1 $^{1}H,^{15}N$-HSQC Experiments

HSQC data were collected for $CheY_6$-Δloop in the absence and presence of BeF_3^-. $CheY_6$-Δloop gives a well-dispersed spectrum, consistent with a folded protein. Chemical shifts of $CheY_6$-Δloop were compared with wild type $CheY_6$ (Figure 5.16) to

provide evidence of correctly folded protein and to highlight regions of possible changes in structure.

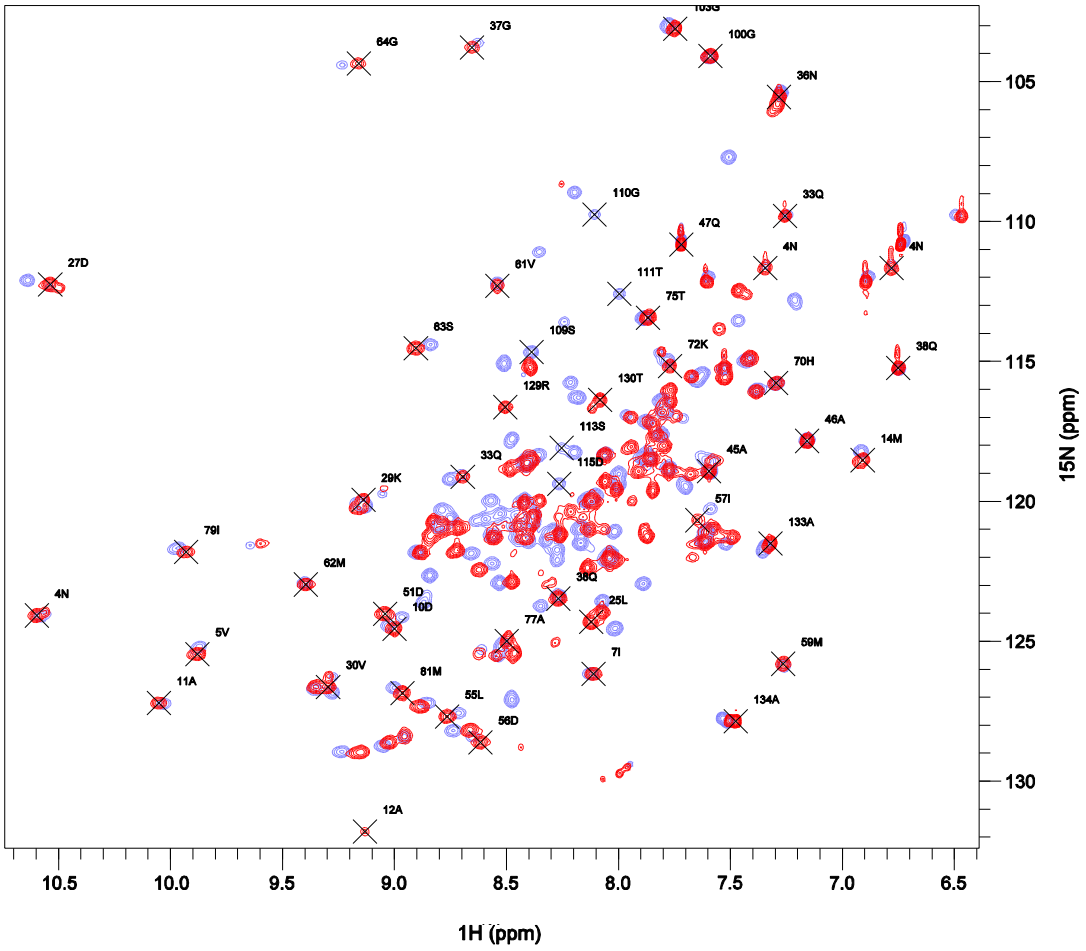

Figure 5.16 – ^{1}H, ^{15}N-HSQC spectra of $CheY_6$-Δloop (red) and wild type $CheY_6$ (blue). S109, G110, T111, S113 and D115 are labelled in the wild type spectrum to highlight successful deletion in $CheY_6$-Δloop; no peaks corresponding to these residues are observed for $CheY_6$-Δloop. Other labelled peaks indicate residues that do not shift significantly. Not all $CheY_6$-Δloop assignments are shown to reduce crowding.

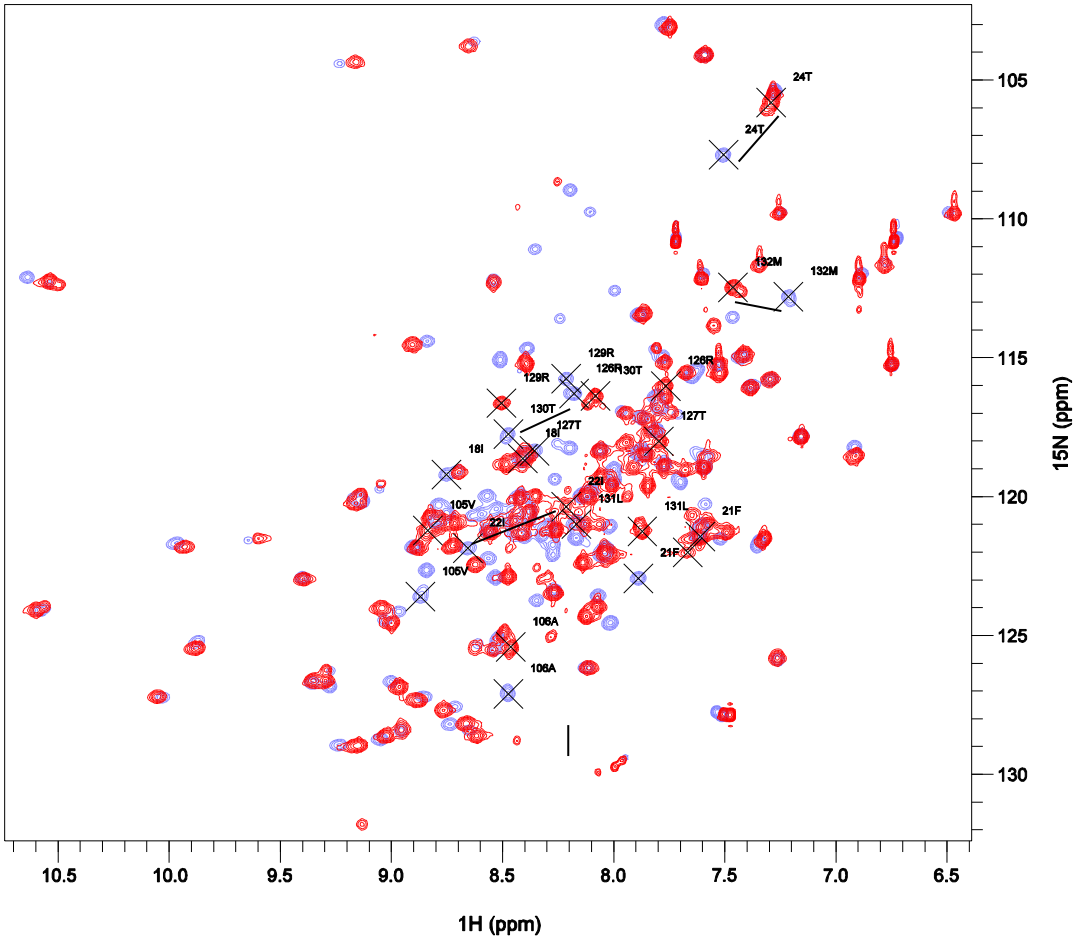

Figure 5.17 — ^{1}H, ^{15}N-HSQC spectra of $CheY_6$-Δloop (red) and wild type $CheY_6$ (blue). Spectra highlight peaks that have shifted more than 0.2 ppm.

The HSQC spectrum demonstrates successful deletion of the loop region from $CheY_6$. The $CheY_6$-Δloop spectrum shows good dispersion of peaks and is indicative of folded protein. Of the C-terminal helix, only residues A125-A134 could be identified. This region is thought to still be helical as the peaks are not found to have random coil chemical shifts, and ^{15}N-NOESY-HSQC data shows H^N-H^N connections indicative of helical structure. In total, peaks from ten residues were unassigned; three of these residues have peaks that broaden at pH 7.2 in wild type $CheY_6$ (S84, S88 and

G89), while the remaining seven residues could not be identified with the available spectra (K107, K119, T120, G121, G122, E123 and L124). A comparison of the chemical shifts was carried out to investigate any structural changes due to the loop deletion. Two regions of $CheY_6$-Δloop show chemical shift changes above 0.2 ppm using the equation shown in Section 3.1.6 (Figure 5.18).

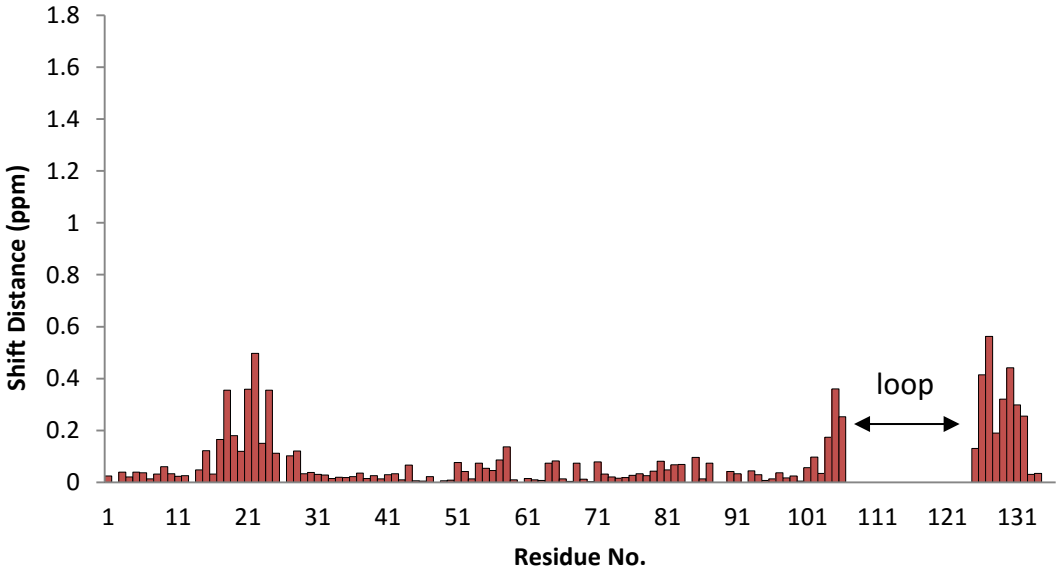

Figure 5.18 – The shift distance between wild type $CheY_6$ and $CheY_6$-Δloop. Peaks not found in $CheY_6$-Δloop are shown as blank. Wild type $CheY_6$ residue numbering is used.

The largest chemical shift differences are found for residues in α-helix 1 and 5 and before the loop region (Figure 5.19). These helices are in close proximity in the crystal structure of $CheY_6$ and hence, a slight change in one region could cause perturbations in the other. The rest of the protein structure appears to be unaffected.

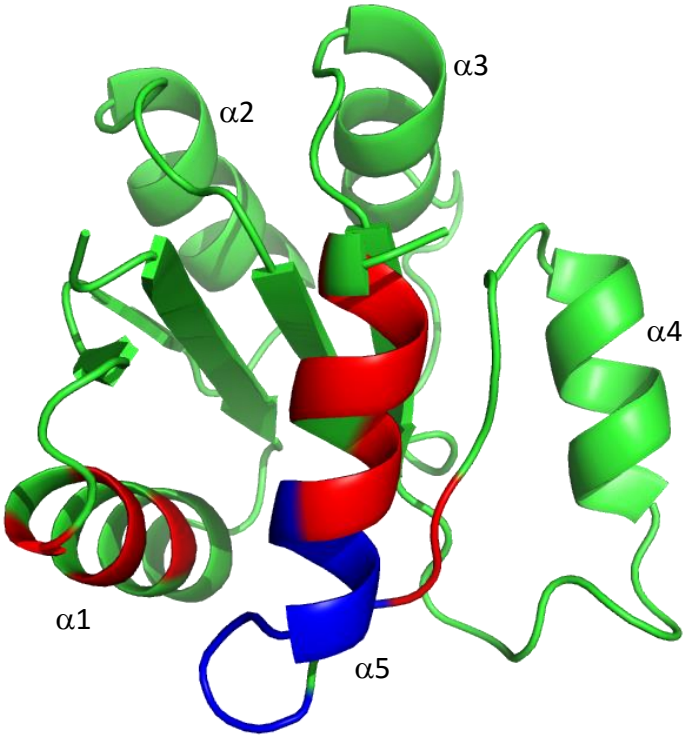

Figure 5.19– Shift differences above 0.2 ppm (red) between wild type $CheY_6$ and $CheY_6$-Δloop. Unassigned residues are coloured blue.

The ^{15}N-NOESY-HSQC spectrum of $CheY_6$-Δloop shows H^N-H^N NOES between neighbouring H^N groups of α1 (

Figure 5.20). It also shows H^N-H^N NOES between neighbouring H^N groups of α5 (Figure 5.21). Despite chemical shift changes in α1 and α5, this indicates helical secondary structure is maintained in α1 and α5 in $CheY_6$-Δloop.

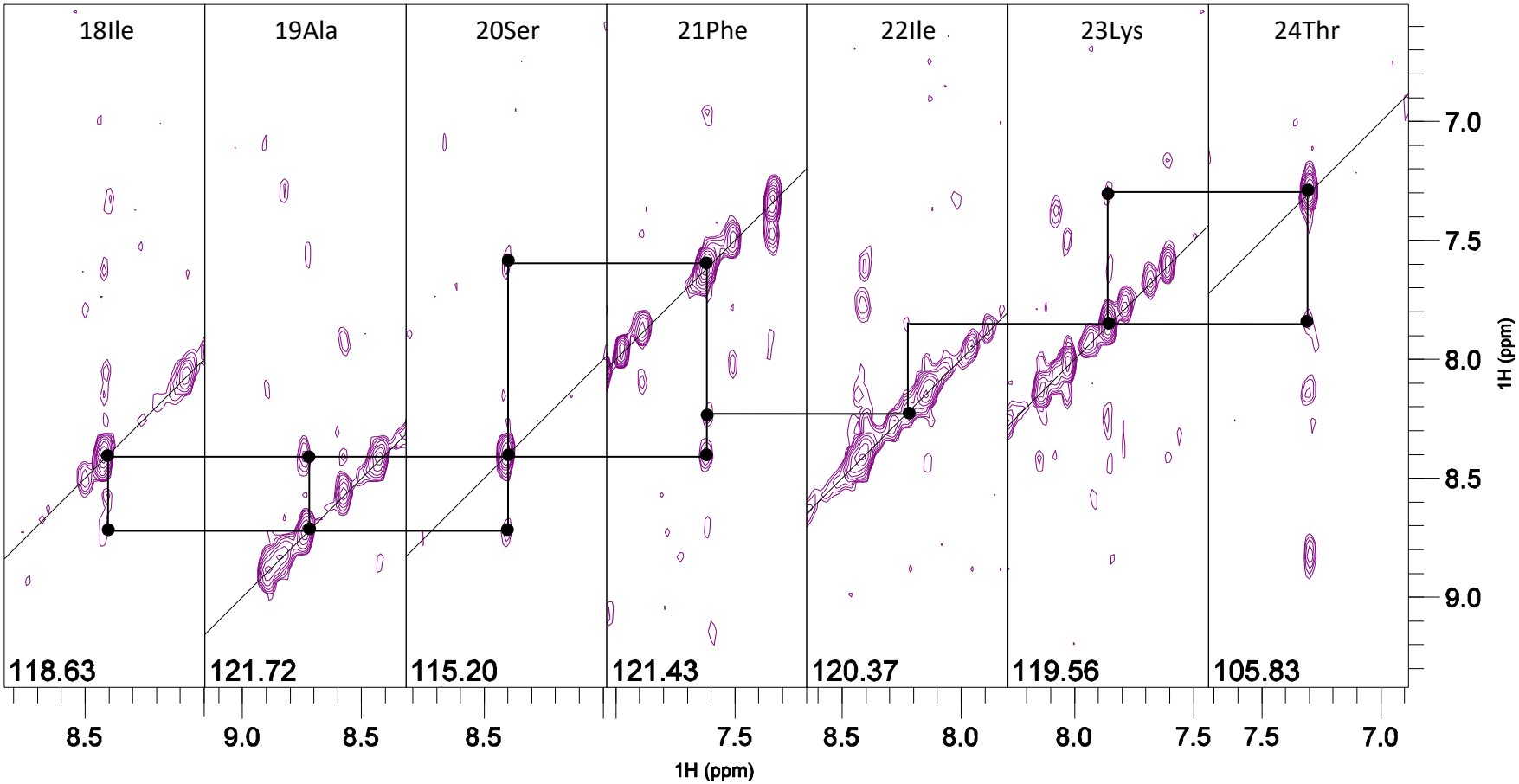

Figure 5.20 – ^{15}N-NOESY-HSQC spectrum of residues I18-T24 located in $\alpha 1$ of CheY$_6$-Δloop. Lines indicate connections between H^N-H^N groups. The ^{15}N chemical shift (ppm) for each spin system can be found at the bottom of each strip.

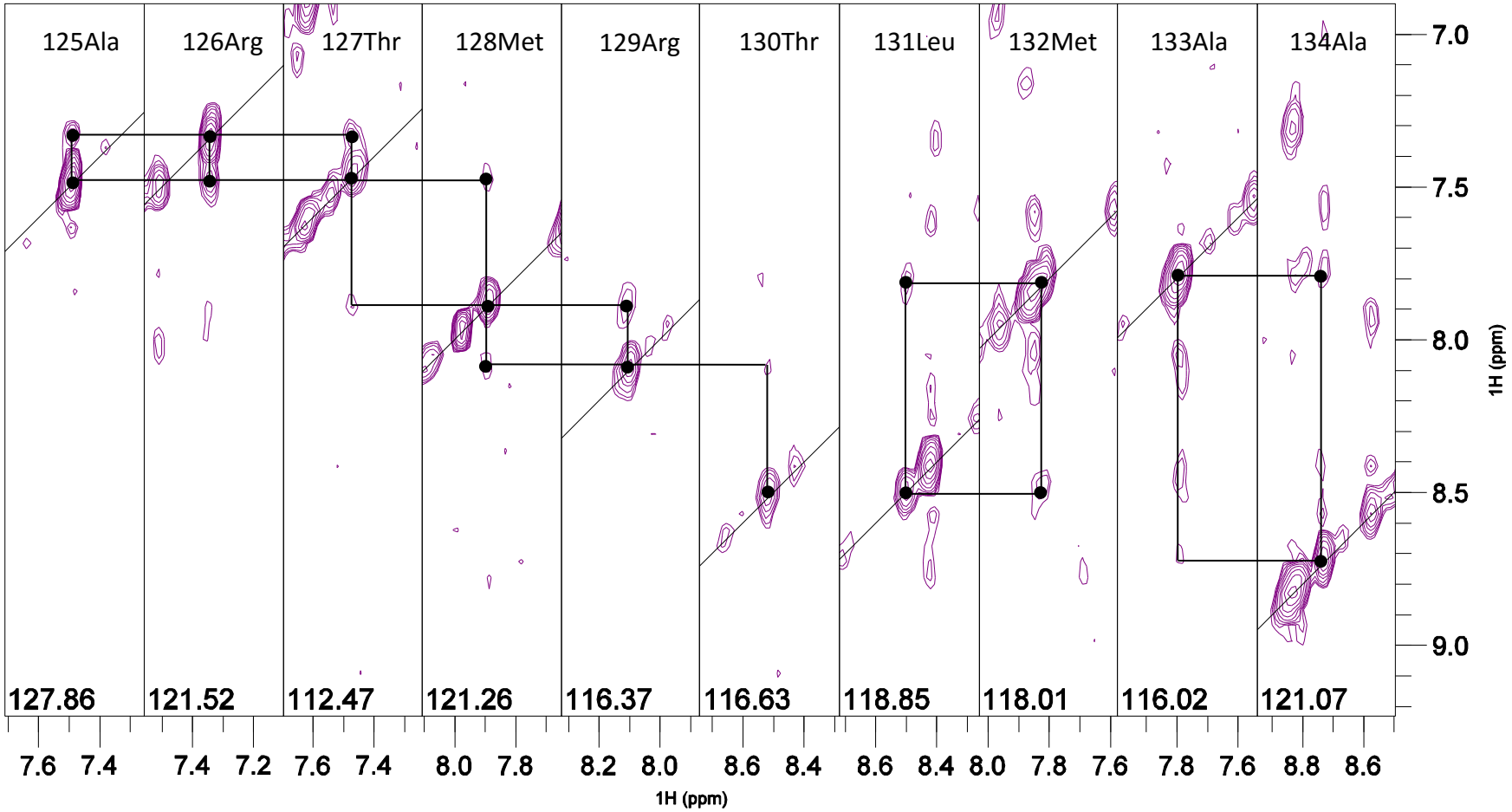

Figure 5.21 – ^{15}N-NOESY-HSQC spectrum of residues Ala125-Ala134 located in α5 of CheY$_6$-Δloop. Lines indicate connections between H^N-H^N groups. The ^{15}N chemical shift (ppm) for each spin system can be found at the bottom of each strip.

5.11.2 CheY$_6$-Δloop Activation via BeF_3^-

BeF_3^- was added to CheY$_6$-Δloop to investigate whether it could undergo activation (Figure 5.22).

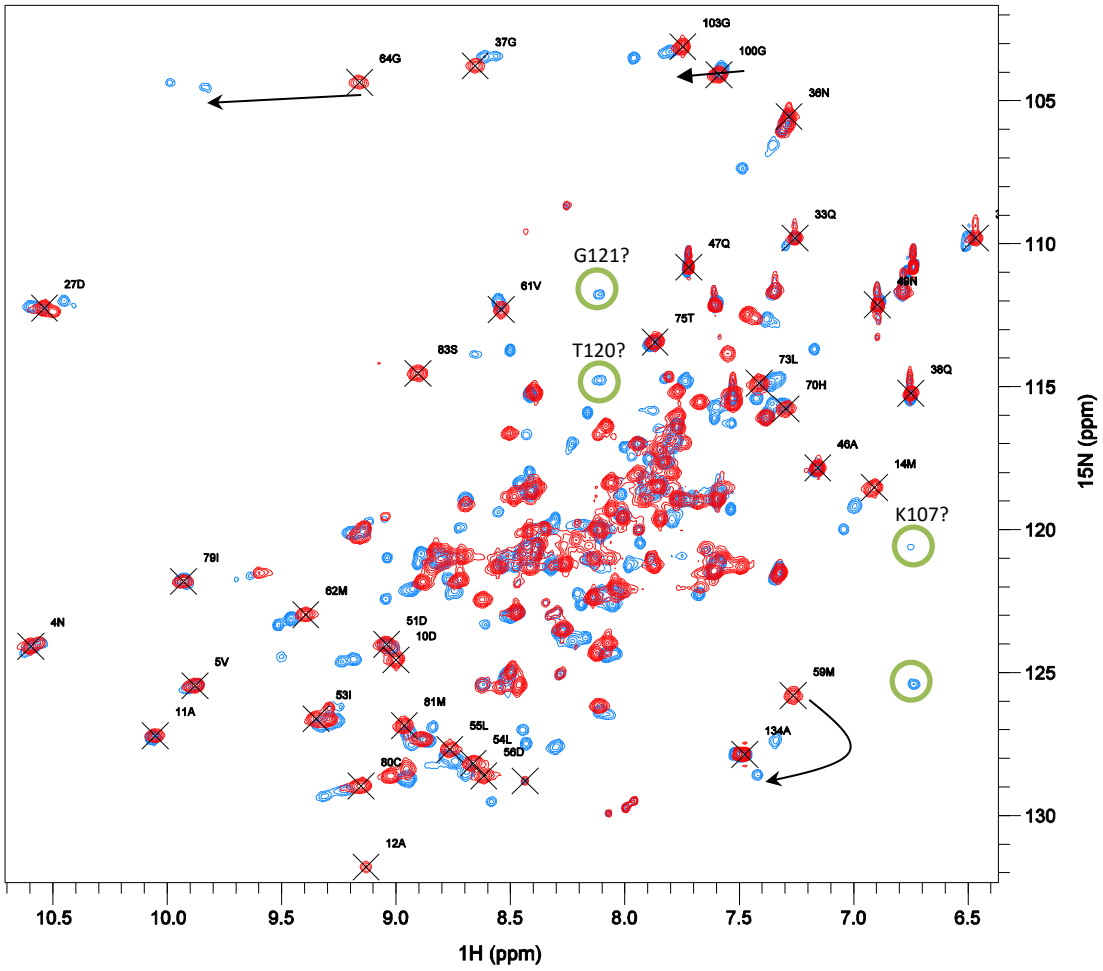

Figure 5.22 – ^1H, ^{15}N-HSQC spectra of CheY$_6$-Δloop (red) and CheY$_6$-Δloop-BeF_3^- (blue). Arrows indicate peak shifts that are similar to wild type CheY$_6$ activation. Green circles indicate peaks in the CheY$_6$-Δloop-BeF_3^- spectrum that could correspond to residues stabilised by BeF_3^-.

In comparison to wild type CheY$_6$, similar peak shifts are observed upon addition of BeF_3^- to CheY$_6$-Δloop, consistent with binding of BeF_3^- in the phosphorylation site. This is also in agreement with the results obtained from phosphotransfer assays.

Doubling of some peaks is observed upon addition of BeF_3^-, examples include G37, M62 and G64. With the available spectra, the reason for this is still unknown. A ^{15}N-NOESY-HSQC of $CheY_6$-Δloop-BeF_3^- was collected but due to protein concentration, the signal was too weak to interpret. New peaks also appear upon addition of BeF_3^- and could correspond to K107, T120 and G121. Further experiments are needed to assign the new peaks.

5.12 $CheY_3$ Loop Addition

To investigate the functional importance of the loop region of $CheY_6$ further, it was inserted into $CheY_3$ to see if it could confer $CheY_6$ function (Figure 5.23). An observation that F107 is conserved across $CheY_{1\text{-}5}$ and *E. coli* CheY but not $CheY_6$, led to the construction of three mutants. $CheY_3$-loop, $CheY_3$-loop-F107K and $CheY_3$-F107K were all overexpressed, purified and analysed to determine if they would fold correctly.

```
CheY6              MPYNVMIVDDAAMMRLYIASFIKTLPDFKVVAQAANGQEALDKLAAQPNVDLILLDIEMP
CheY3LA            MSRTVLAVDDSPSVRCMVAMTLREAG--YRVIEATDGREGLEKALSEP-VDAIITDQNMP
CheY3LA_F107K      MSRTVLAVDDSPSVRCMVAMTLREAG--YRVIEATDGREGLEKALSEP-VDAIITDQNMP
CheY3_F107K        MSRTVLAVDDSPSVRCMVAMTLREAG--YRVIEATDGREGLEKALSEP-VDAIITDQNMP
                   *. .*: ***:. :*  :*  ::       * :*::*:*.*:*  ::* ** *: * :**

CheY6              VMDGMEFLRHAKLKTRAK-ICMLSSVAVSGSPHAARARELGADGVVAKPSGTVSHDLEEK
CheY3LA            NLDGLGFIRAFREHPESKGKPIIFLSTDSADTLKQQAREAGAMGWMVKPSGTVSHDLEEF
CheY3LA_F107K      NLDGLGFIRAFREHPESKGKPIIFLSTDSADTLKQQAREAGAMGWMVKPSGTVSHDLEEK
CheY3_F107K        NLDGLGFIRAFREHPESKGKPIIFLSTDSADTLKQQAREAGAMGWMVKP----------K
                    :**: *:*  : :..:*   ::   : *...   :*** ** * :.**

CheY6              TGGELARTMRTLMAA 134
CheY3LA            TQPQLLAVIKKVLG- 131
CheY3LA_F107K      TQPQLLAVIKKVLG- 131
CheY3_F107K        TQPQLLAVIKKVLG- 121
                   *  :*  .::.::.
```

Figure 5.23 – Sequence alignment of $CheY_3$ and $CheY_6$ with proposed loop additions of $CheY_3$.

5.12.1 $CheY_3$ Loop Addition Overexpression and Purification

$cheY_3$-loop mutants were made using overlap extension PCR (Section 2.3.2), and inserted into the expression plasmid pQE80 (Nterm, 6xHis-tag) using the method described in Section 2.3, but using *Hind*III and *Bam*HI restriction enzymes. pQE80-*$cheY_3$-loop* was transformed into *E. coli* BL21 (DE3) cells and induced with IPTG (1 mM) in 2TY media. Purification was achieved using a Nickel-NTA Agarose column and protein was further purified using size exclusion chromatography (Section 2.6). M9 minimal medium (containing $^{15}NH_4Cl$) was used when producing isotopically labelled protein.

5.12.2 Circular Dichroism of $CheY_3$-loop Mutants

Circular dichroism was used to determine if the mutant $CheY_3$ proteins were folded. Individual mutants were placed into a cuvette (1 mm), ellipticity (200-260 nm) was measured at 20°C and the traces were compared to wild type $CheY_3$ (Figure 5.24).

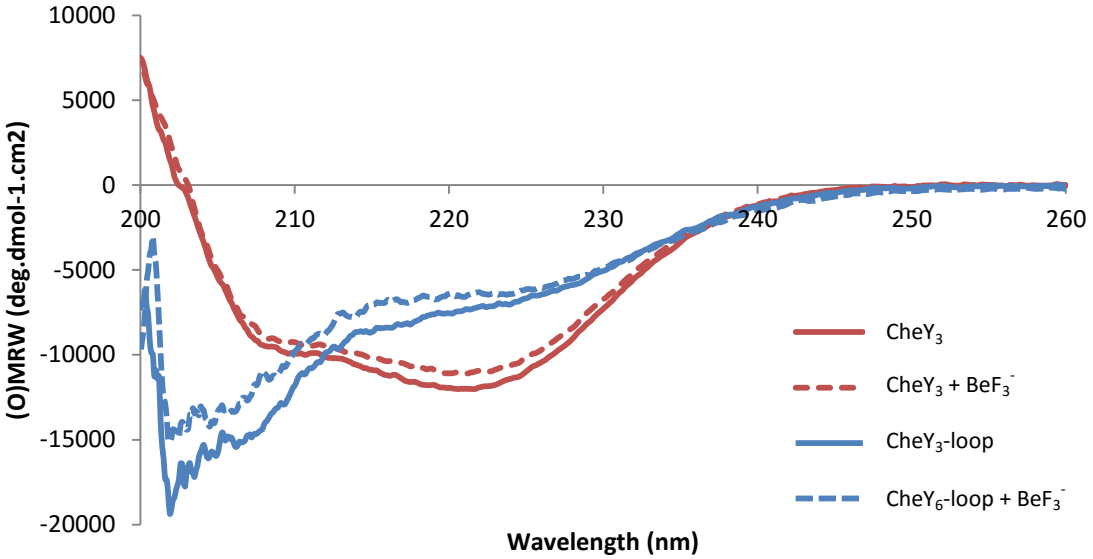

Figure 5.24 – Circular dichroism traces of $CheY_3$ (red) and $CheY_3$-loop (blue) at pH 7.2. Wild type $CheY_3$ shows minima at 208 nm and 222 nm, indicating folded α-helices. $CheY_3$-loop shows no minima at 208 nm or 222 nm and the trace is indicative of unfolded protein.

Wild type $CheY_3$ traces show characteristics of folded protein with strong minima around 208 and 222 nm. This is indicative of α-helix structure. Interestingly, addition of BeF_3^- seems to reduce the amount of protein structure. However, this could be an artefact caused by a change in concentration upon addition of BeF_3^-. $CheY_3$-loop traces show a distinctive random coil shape which indicates unfolded protein.

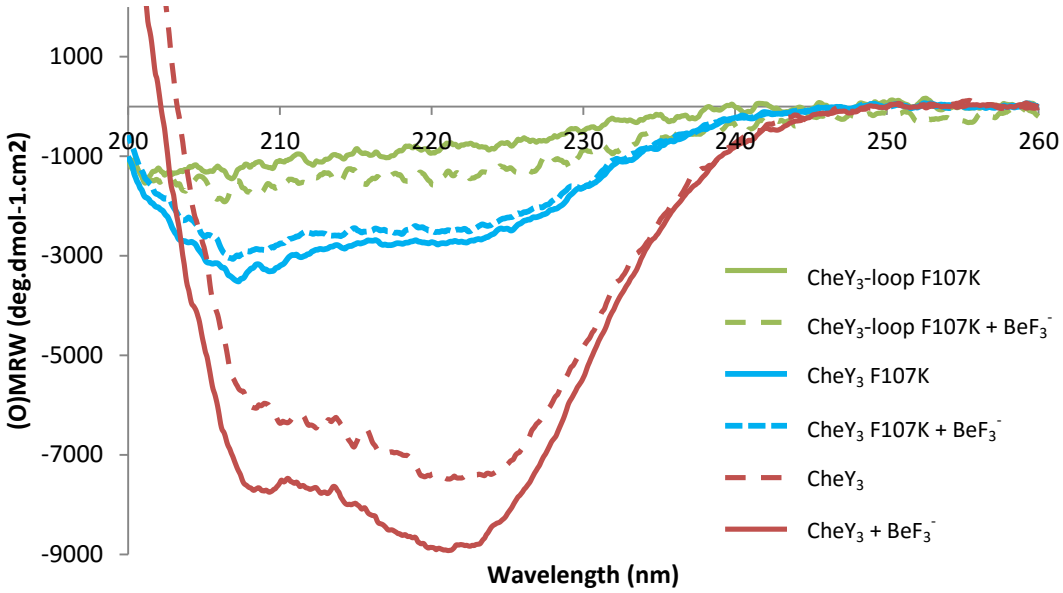

Figure 5.25 – Circular dichroism traces of wild type $CheY_3$ (green), $CheY_3$-F107K (green) and $CheY_3$-loop-F107K (orange) at pH 7.2. $CheY_3$-F107K shows some minima at 208 nm and 222 nm, indicating folded α-helices. $CheY_3$-loop-F107K shows no minima at 208 nm or 222 nm and the trace is indicative of unfolded protein

$CheY_3$-loop-F107K traces indicate unfolded protein (Figure 5.25). The combination of $CheY_3$-loop traces indicates $CheY_3$ cannot accommodate the insertion of the loop region from $CheY_6$. $CheY_3$-F107K traces show a more wild type like shape than the other mutants but do not indicate properly folded protein.

5.12.3 NMR Studies of $CheY_3$-loop Mutants

HSQC data was collected for $CheY_3$-loop (Figure 5.26) and $CheY_3$-F107K (Figure 5.28). This was completed to provide conclusive evidence these mutants do not fold correctly.

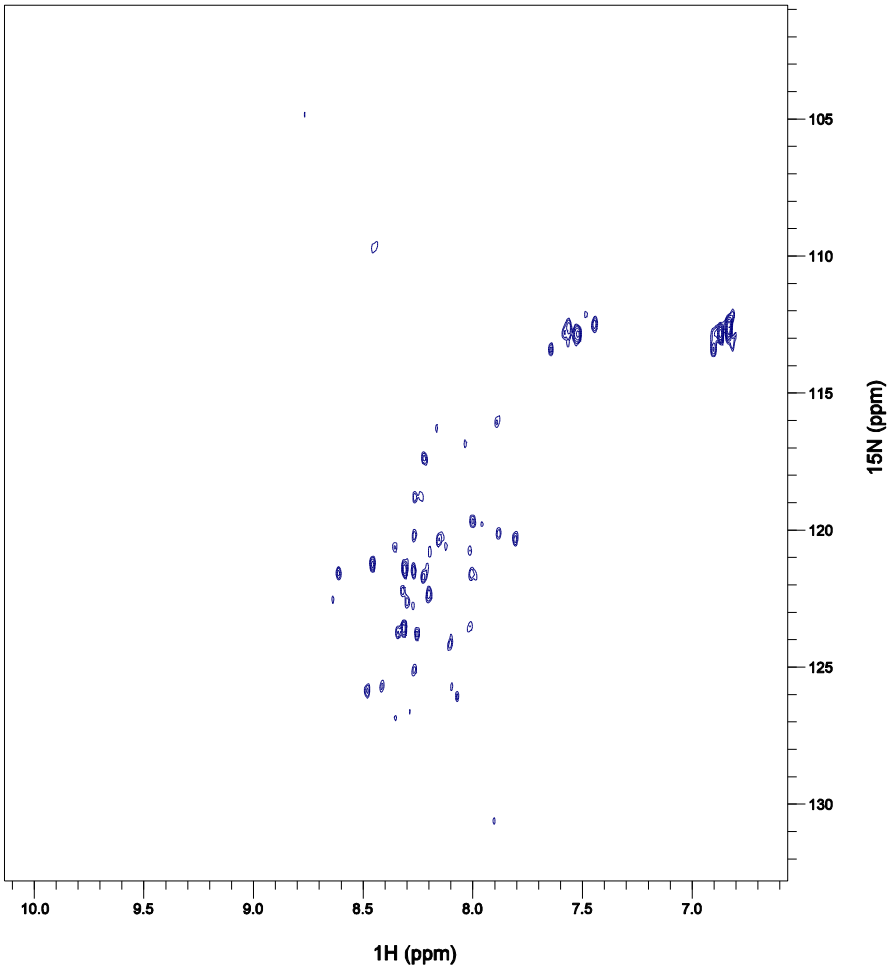

Figure 5.26 – ^{1}H, ^{15}N-HSQC of $CheY_3$-loop spectrum is indicative of an unfolded protein. Most peaks are found in the central region of the spectrum and no outlying peaks can be seen.

HSQC data for $CheY_3$-loop shows conclusively that it does not adopt a natively folded protein conformation. The peaks show poor dispersion in the ^{1}H dimension which is characteristic of unfolded protein. This is clearly evident when comparing the spectrum to wild type $CheY_3$ (Figure 5.27).

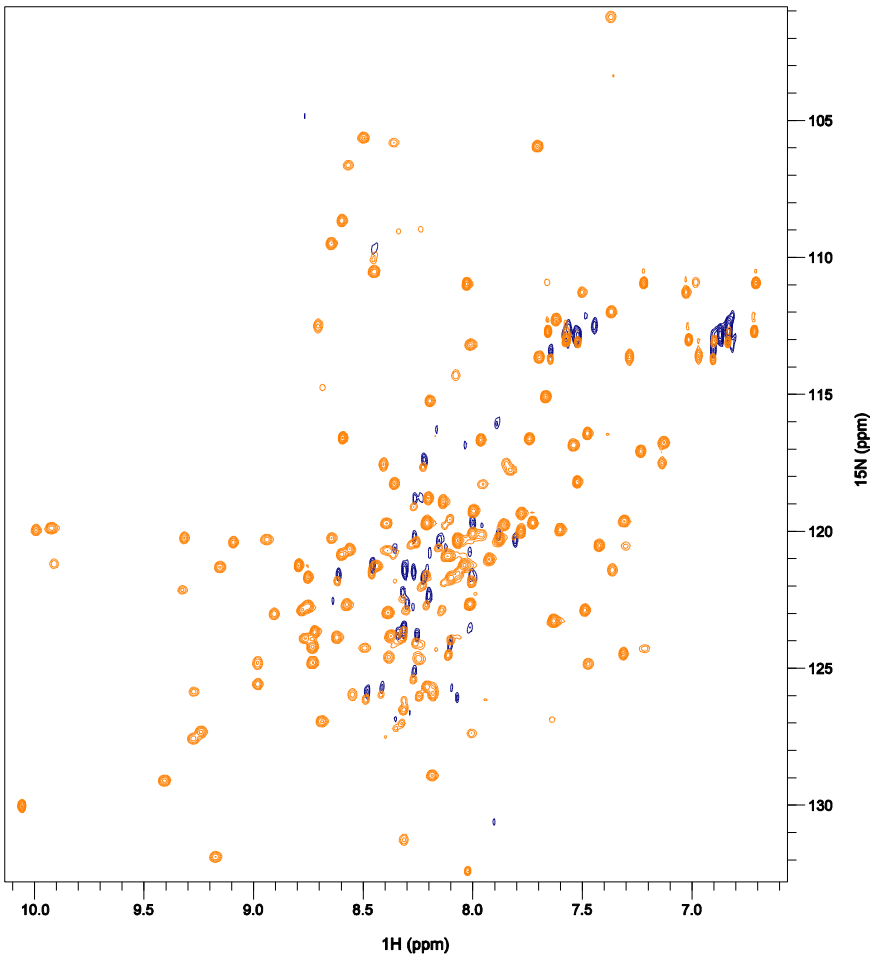

Figure 5.27 – ^{1}H, ^{15}N-HSQC of $CheY_3$-loop (blue) and wild type $CheY_3$ (orange). The spectra show that $CheY_3$-loop is indicative of unfolded protein.

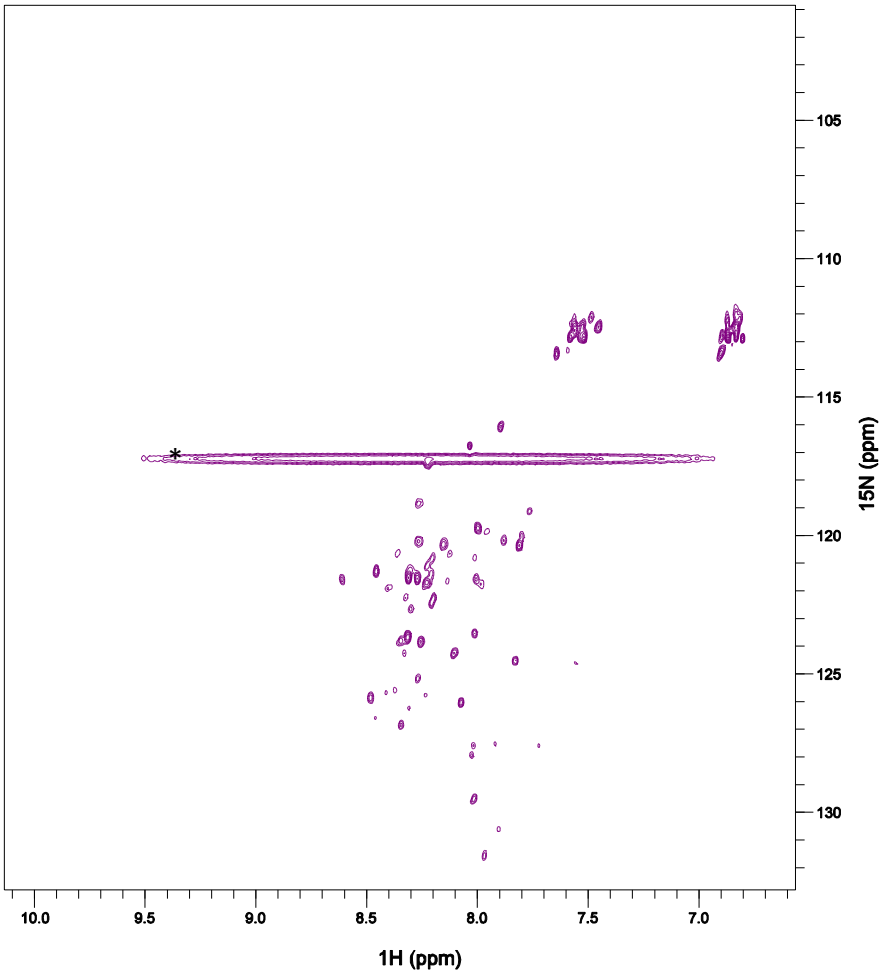

Figure 5.28 – ^{1}H, ^{15}N-HSQC of $CheY_3$-F107K is indicative of unfolded protein. Most peaks are found in the central region of the spectrum and no outlying peaks can be seen. * indicates an artefact observed in this spectrum.

HSQC data of $CheY_3$-F107K (Figure 5.28) shows conclusively that it does not fold correctly. The peaks are not dispersed in the ^{1}H dimension which is characteristic of unfolded protein. This is clearly evident when comparing the spectrum to wild type $CheY_3$.

5.13 Discussion

Circular dichroism data indicates that $CheY_3$ cannot accommodate the addition of the loop region from $CheY_6$ or the F107K mutation. This was further confirmed with the use of HSQC data. To further investigate the addition of this loop region, a more extensive series of mutants could be made. These could be conjugated into background strain JPA1216 which contains inactivated $CheY_6$ in the genome. If restoration of chemotaxis is observed with induction of a particular $CheY_3$-loop addition mutant, this mutant could then be analysed in more detail.

NMR studies reveal fast backbone dynamics for the loop region S109-E118. This loop region also shows some chemical shift changes upon binding of BeF_3^-. Swim plate assays provided evidence that removing the loop region S109-E118 from $CheY_6$ produces a non-chemotactic phenotype. It was shown that wild type $CheY_6$ could complement the inactivated $CheY_6$-D56A mutation whereas $CheY_6$-Δloop could not. Swim plates also indicated that $CheY_6$-Δloop could compete with wild type $CheY_6$, as a loss of chemotactic ability was observed when $CheY_6$-Δloop was expressed in a wild type background. This competition suggests that $CheY_6$-Δloop is expressed and correctly folded *in vivo*. Tethering data showed a smooth swimming phenotype for $CheY_6$-Δloop, suggesting either its ability to interact and bind to the flagellar motor was compromised or it could no longer be phosphorylated by the cytoplasmic cluster. Epifluorescence microscopy showed wild type $CheY_6$ and $CheY_6$-Δloop have a similar pattern of localisation within the cell. Double tagged strains showed $CheY_6$ and $CheY_6$-Δloop with a diffuse pattern of localisation around the cell with a focus

co-localising with $CheA_3$ in the cytoplasmic cluster. Phosphotransfer assays showed that $CheY_6$-Δloop can still be phosphorylated by the cognate histidine kinase $CheA_3$. The longer time seen for dephosphorylation might play a role but it remains unclear at this stage. Circular dichroism and NMR data suggest that $CheY_6$-Δloop is a folded protein that shows similar peak shifts upon activation. ^{15}N-NOESY-HSQC spectra also provided evidence of helical secondary structure for residues whose peaks are in perturbed in the HSQC. The reason for doubling of some peaks is not known and the appearance of new peaks upon addition of BeF_3^- needs further investigation.

The results suggest that the β5-α5-loop region does play an important role in the interaction of $CheY_6$ with the switch complex, however the exact function is still unknown. In future studies, mutagenesis of particular residues or sections of this loop in $CheY_6$ may elucidate the key residues involved in its function.

Chapter 6

The interactions of $CheY_6$ and FliM in *Rhodobacter sphaeroides*

A wide range of techniques have been used to probe the CheY-FliM interaction in a variety of different bacterial species. Techniques range from *in vivo* fluorescence microscopy such as FRET (Sourjik and Berg 2002), to *in vitro* techniques such as NMR (Dyer and Dahlquist 2006) and crystallography (Ahn *et al*. 2013). Some of these were discussed in the Introduction. The level of success of the different methods varied for reasons that are unclear.

Surface Plasmon Resonance (SPR) experiments have been performed previously, to try to identify an interaction between *R. sphaeroides* $CheY_6$ and FliM (Christian Bell, personal communication). $CheY_6$ was attached to a chip surface and FliM peptide (1-20) was flowed over the surface. No $CheY_6$-FliM binding was detected. To date, only pull down assays have provided evidence of $CheY_6$-FliM binding and in this case,

binding was weak and occurred whether $CheY_6$ was phosphorylated or not (Ferré *et al*. 2004). Knockout and tethering experiments provide evidence of the importance of $CheY_6$ in the *R. sphaeroides* chemosensory network. Deletion or inactivation of $CheY_6$ results in a non-chemotactic strain (smooth swimming), indicating $CheY_6$ is the only CheY able to trigger a stop in rotation, and therefore suggesting interaction with the flagellar motor (Porter *et al*. 2006). $CheY_3$ and $CheY_4$ are also known to be essential for chemotaxis, and are also thought to bind to the motor. The interaction between $CheY_6$ and FliM remains to be identified and defined at the molecular level; long-term the overall aim is to identify why only $CheY_6$ can stop the motor.

6.1 Bacterial Adenylate Cyclase Two Hybrid System

A number of two-hybrid systems have been engineered to investigate protein-protein interactions in bacteria. The bacterial adenylate cyclase two hybrid (BACTH) system (Karimova *et al*. 1998) was used in this study. The system is based on the reconstitution of a regulatory cascade involving cyclic adenosine 3',5'-monophosphate (cAMP). Adenylate cyclases are a family of enzymes that synthesise cAMP. *Bordetella pertussis* (a bacterium causing whooping cough) contains an adenylate cyclase (1706 residues) that elevates the level of cAMP in eukaryotic organisms (Confer and Eaton 1982). The cyclase becomes activated once bound to calmodulin (calcium-modulated protein). The enzymatic activity is found in the first 400 residues which can be divided into two sub-domains: the calmodulin binding domain (18 kDa – T18) and the main catalytic domain (25 kDa – T25) (Glaser *et al*. 1988) (Ladant 1988). Co-expression of these two domains, in the presence of

calmodulin, allows interaction and hence restores synthesis of cAMP (Ladant *et al*. 1989). Although the *B. pertussis* adenylate cyclase requires calmodulin to be fully active, a cryptic adenylate cyclase activity is detected in *E. coli*, without the presence of calmodulin (Glaser *et al*. 1988). This complementation is used in the BACTH system. Proteins of interest are fused to the T18 and T25 sub-units of adenylate cyclase. If these proteins interact, they replace the role of calmodulin and bring the T18 and T25 domains together (Figure 6.1). An *E. coli* strain (DMH1) containing an endogenous adenylate cyclase deletion (cya^- strain) is used to remove background enzymatic activity. The synthesised cAMP interacts with a catabolite activator protein (CAP). The cAMP/CAP complex is able to bind to promoter regions and regulate transcription of a number of genes. The catabolic operons of *lactose* and *maltose* are positively regulated. Within the *lac* operon, the *lac*Z gene encodes for β-galactosidase that hydrolyses β-galactosides. The method described below was used to investigate $CheY_6$-FliM interactions. Strains are plated on LB agar plates containing 5-bromo-4-chloro-3-indolyl-β-D-Galactopyranoside (X-Gal - galactose linked to a substituted indole) and incubated for several days. X-Gal is an analogue of lactose and can be hydrolysed by β-galactosidase. Once hydrolysed, the substituted indole turns a blue colour, indicating a protein-protein interaction.

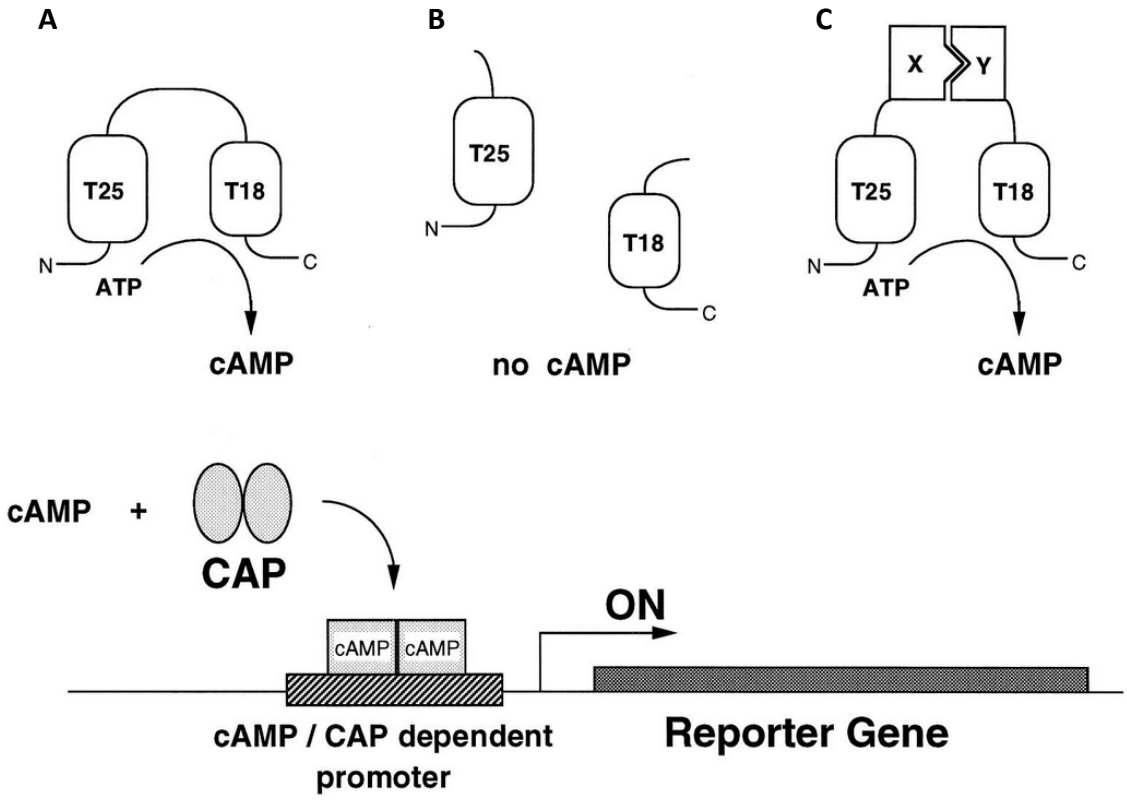

Figure 6.1 – The bacterial adenylate cyclase two hybrid (BACTH) system. (**Upper**) Basic principles of BACTH with T18 (225-399 AA) and T25 (1-224 AA) domains from *B. pertussis*. **A)** Full length catalytic domain. **B)** Co-expressed T18 and T25 domains are unable to interact, therefore no cAMP is synthesised. **C)** T18 and T25 are fused to two proteins of interest. If these proteins interact, the T18 and T25 domains are brought close together, resulting in an active adenylate cyclase and cAMP production. (**Lower**) cAMP binds to CAP and positively regulates transcription of the reporter gene. For instance in *E. coli*, *lac*Z and *mal* genes act as reporters (taken from (Karimova *et al*. 1998)).

6.1.1 Plasmid Production

A set of compatible plasmids has been created, with options to tag both the N- and C-terminus of the protein of interest with either the T18 or T25 domains (Karimova *et al*. 2001). $CheY_6$, $CheY_6$-Δloop and FliM were all tagged with either N- or C-terminal T18 or T25 tags. *$cheY_6$*, *$cheY_6$-Δloop* and FliM fragments were amplified by

PCR using WS8N genomic DNA and appropriate primers (See Appendix B). PCR products were confirmed using gel electrophoresis and purified via gel extraction. The resulting PCR products and appropriate plasmids were digested using *Xba*I and *Kpn*I restriction enzymes and ligated. Successful inserts were identified via digestion of mini-preps from transformed cells. Plasmids containing the correctly sized insert were sequenced and checked for point mutations. This led to the production of 12 plasmids: four $CheY_6$, four $CheY_6$-Δloop and four FliM plasmids (Figure 6.2).

6.1.2 Results

As the specific nature of the interaction between $CheY_6$ and FliM is not known, all combinations of T18 plasmids with T25 plasmids were investigated (Figure 6.3). Experiments were completed in triplicate. A strong positive control containing a leucine zipper motif was used to confirm the experiment was completed correctly (Karimova *et al*. 1998).

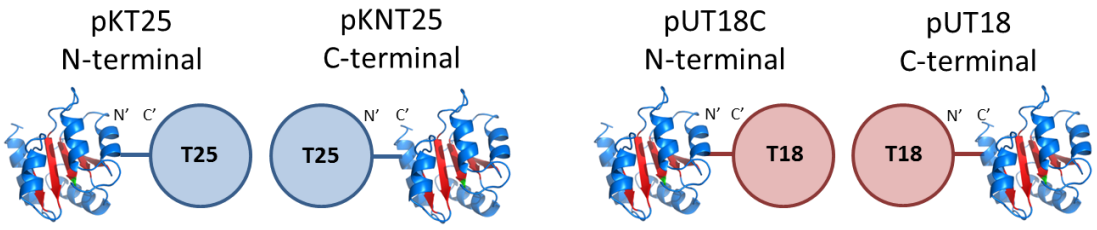

Figure 6.2 – $CheY_6$ tagged with either T18 or T25 tags. N- and C- terminal tags of both T18 and T25 were produced.

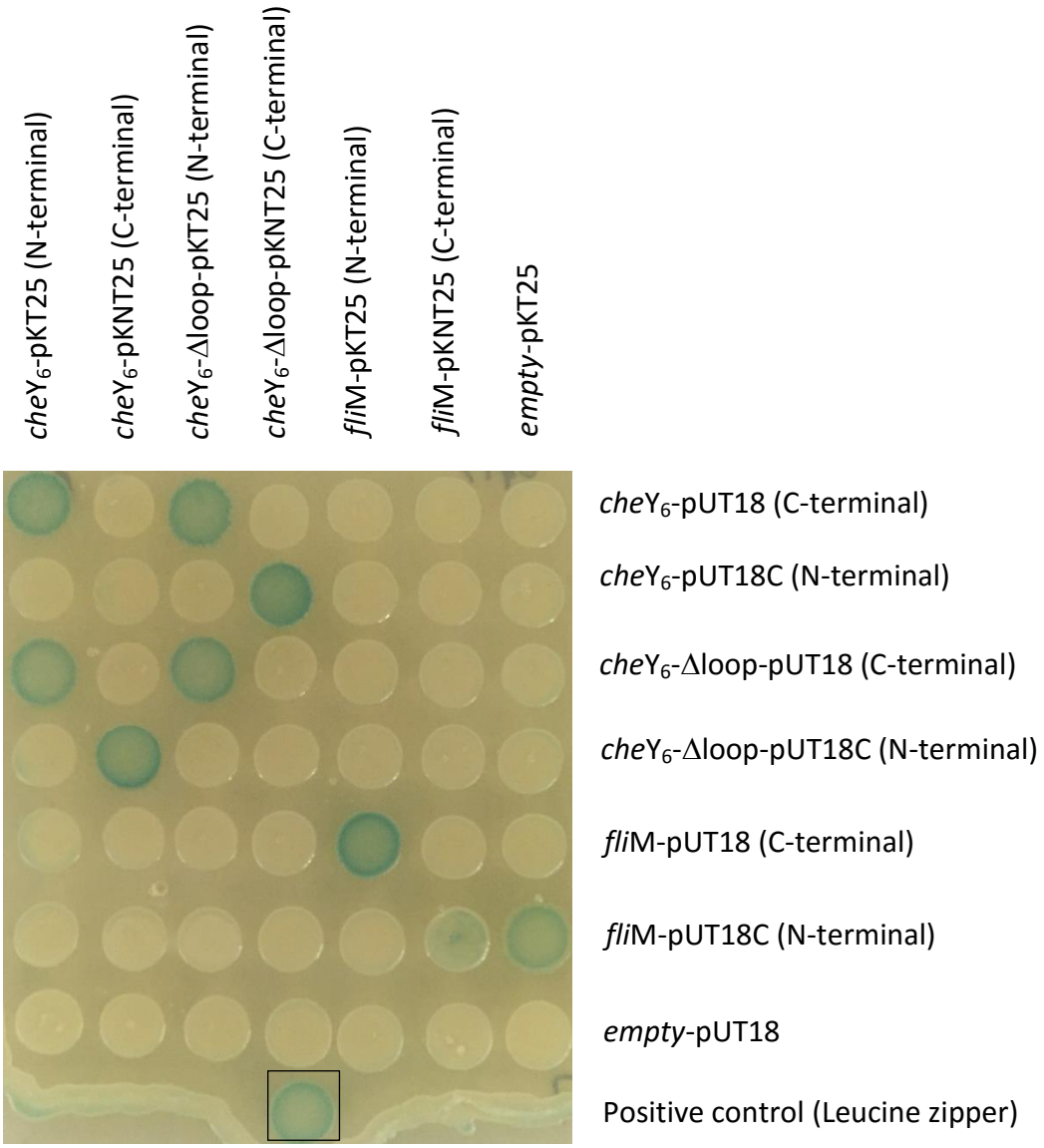

Figure 6.3 – The BACTH system of $CheY_6$, $CheY_6$-Δloop and FliM from *R. sphaeroides*. $CheY_6$ and $CheY_6$-Δloop are both shown to interact with themselves and each other. FliM is only shown to interact with its self. No $CheY_6$-FliM interaction is seen. The leucine zipper positive control (black box) also shows a positive interaction.

After completion of the experiment in triplicate, no interaction between either $CheY_6$ or $CheY_6$-Δloop with FliM was observed. FliM was shown to interact with

itself. This result was expected as FliM forms a 34-monomer ring in the switch complex. $CheY_6$ and $CheY_6$-Δloop also interact with themselves and each other. $CheY_6$ did not interact with itself in all of the possible T18-T25 combinations. Only combinations involving one N- and one C-terminal tag showed interaction. This could indicate dimerization between the N- and C-terminal regions of $CheY_6$. However, NMR spectra give sharp peaks consistent with a 15 kDa protein, rather than a 30 kDa dimer (Section 4.2). It is not surprising that $CheY_6$ and $CheY_6$-Δloop interact with each other as they both also interact with themselves. This is further evidence that $CheY_6$-Δloop is folded correctly. A possible interaction is seen between FliM and empty-pKT25. As there is no other interaction with empty-pK25 and this interaction was not seen in other repeats, it was assumed to arise from contamination. $CheY_6$ is not phosphorylated by *E. coli* CheA (Porter and Armitage 2004), which offers a possible explanation for the lack of interaction between $CheY_6$ and FliM. Although the affinity of unphosphorylated $CheY_{EC}$ is reduced relative to CheY-P, it has been shown to interact with FliM (Dyer and Dahlquist 2006). Hence, over the course of five days an interaction would be expected, regardless of the phosphorylation state of $CheY_6$. This evidence suggests that $CheY_6$ cannot interact with monomeric FliM, or at least not in BACTH. A mutated *E. coli* CheY (D13K Y106W) was shown to be constitutively active (mimicking the phosphorylated state) (Dyer *et al*. 2004). Unfortunately, the same mutations inactivate $CheY_6$ (Porter *et al*. 2006). This prevented further studies with $CheY_6$-P using the BACTH system.

6.2 Interactions Probed by NMR

NMR experiments have been used to define the CheY-FliM interaction interface in *E. coli*. A peptide from the N-terminal region (16 residues) of FliM was used, as it had been demonstrated (by molecular genetics) to form the main interaction site with CheY (Bren and Eisenbach 1998). In CheY, large chemical shift changes (greater than 95 Hz) were observed for a number of residues upon addition of FliM peptide (Figure 6.4) (McEvoy *et al*. 1999). V107, K109, Y106, A99, M85, V86, D57, L116, V108, N121, T87, E118, Y21, K91 and K126 (largest to smallest shift) showed the largest chemical shift changes. With the exception of the phosphorylation site (D57), these residues are situated in the fourth and fifth α-helices, and the fourth and fifth β-strands (C-terminal region) (McEvoy *et al*. 1999) (Figure 6.5).

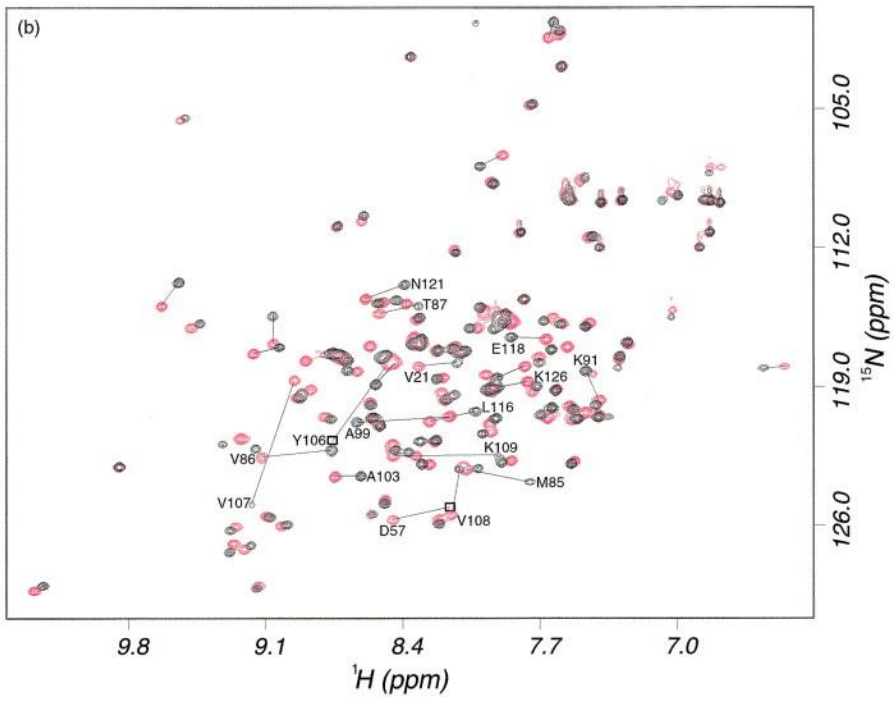

Figure 6.4 – ^{1}H,^{15}N-HSQC of *E. coli* CheY with (red) and without (black) FliM peptide. CheY was unphosphorylated. Residues with large chemical shift changes (above 95 Hz) are labelled, and shifts are indicated with a black lines (taken from (McEvoy *et al*. 1999)).

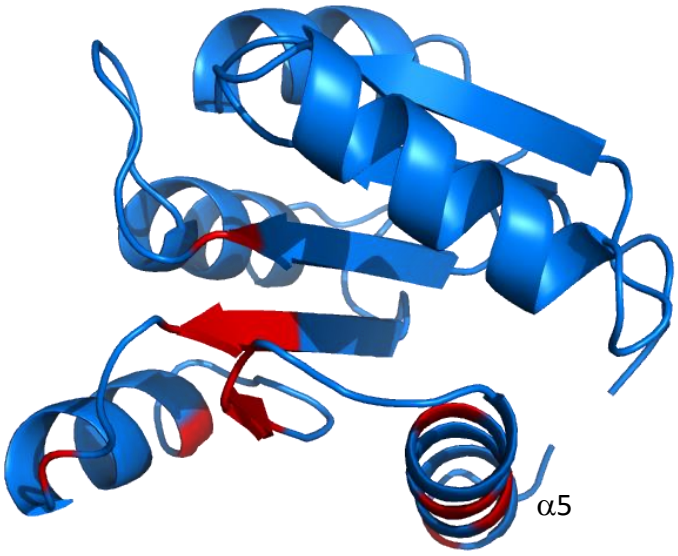

Figure 6.5 – The chemical shift changes (red, greater than 95 Hz) of *E. coli* CheY upon addition of FliM peptide. (Structural co-ordinates obtained from PDB:3CHY).

6.2.1 NMR Experiments Probing the FliM-CheY$_6$ Interaction

The interactions between FliM and CheY$_6$ were investigated using NMR techniques. FliM (N-terminal peptide 1-20, and truncated FliM (1-235, FliM$_{trunc}$) protein was provided by C. H. Bell (a former member of the Armitage group). NMR spectra were acquired by Prof. Christina Redfield.

6.2.1.1 FliM$_{pep}$-CheY$_6$ Interactions

NMR experiments were performed using an N-terminal peptide from FliM (FliM$_{pep}$, 1-20). FliM$_{pep}$ (660 μM) was added to CheY$_6$-BeF$_3^-$ (150 μM) and peak shifts investigated (Figure 6.6).

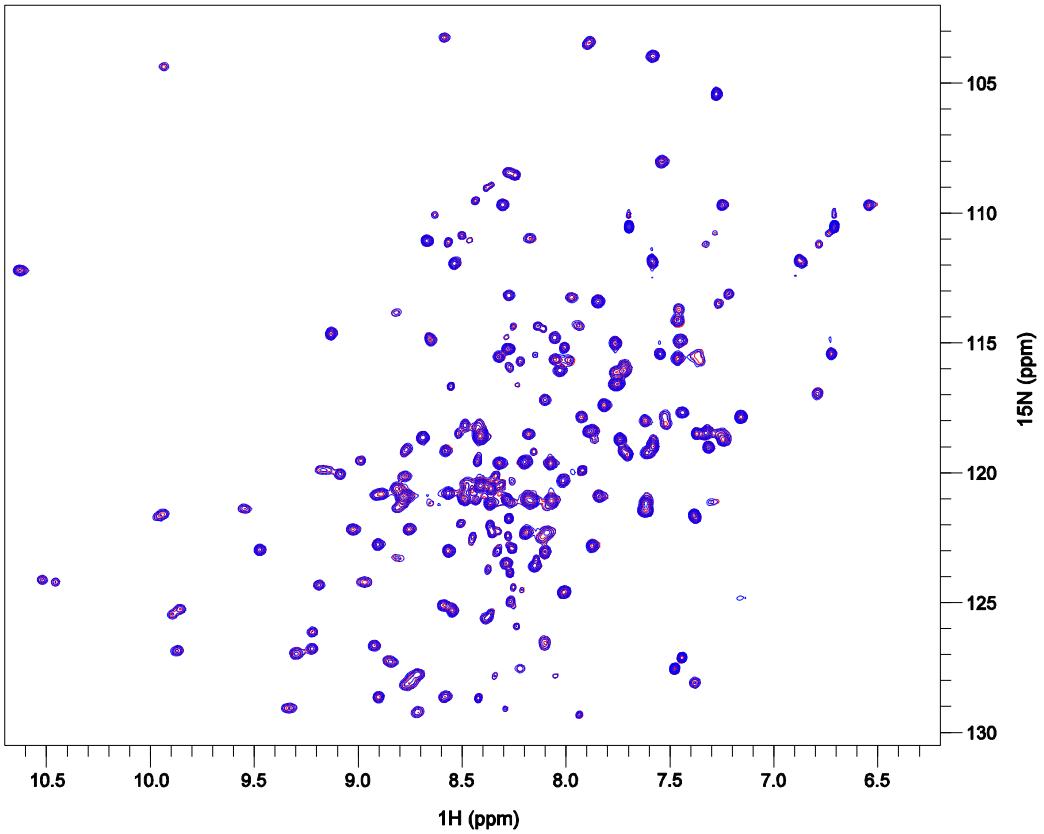

Figure 6.6 – $^{1}H,^{15}N$-HSQC of $CheY_6$-BeF_3^- with (blue) and without (red) $FliM_{pep}$ (10 mM HEPES, 300 mM NaCl, 2 mM TCEP, pH7.5). No noticeable changes are observed upon addition of $FliM_{pep}$, indicating no interaction between $CheY_6$-BeF_3^- and $FliM_{pep}$.

No chemical shift changes were observed upon addition of $FliM_{pep}$ to $CheY_6$-BeF_3^-. This indicates that there is no interaction between $CheY_6$ and $FliM_{pep}$. This could have been caused by the absence of other domains of FliM.

6.2.1.2 $FliM_{trunc}$-$CheY_6$ Interactions

Spectra were collected before and after FliM (1-235) (660 μM) was added to $CheY_6$ (150 μM) (Figure 6.7).

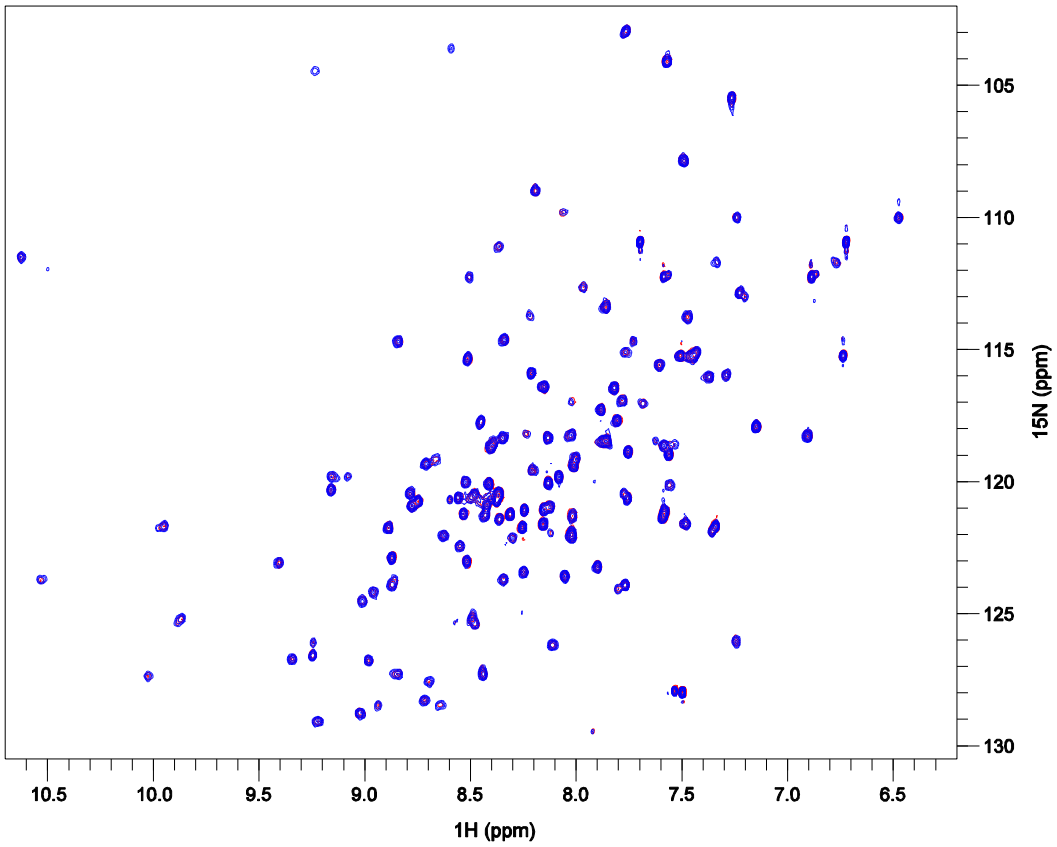

Figure 6.7 – $^{1}H,^{15}N$-HSQC of $CheY_6$ with (red) and without (blue) truncated FliM (10 mM HEPES, 300 mM NaCl, 2 mM TCEP, pH7.5). No discernible change could be seen upon addition of FliM.

No change was observed in $CheY_6$ upon addition of FliM. An expanded spectrum (Figure 6.8) shows that even in the crowded regions, no change is seen. This was somewhat surprising as *E. coli* CheY has been reported to interact with FliM (albeit with reduced affinity) without phosphorylation.

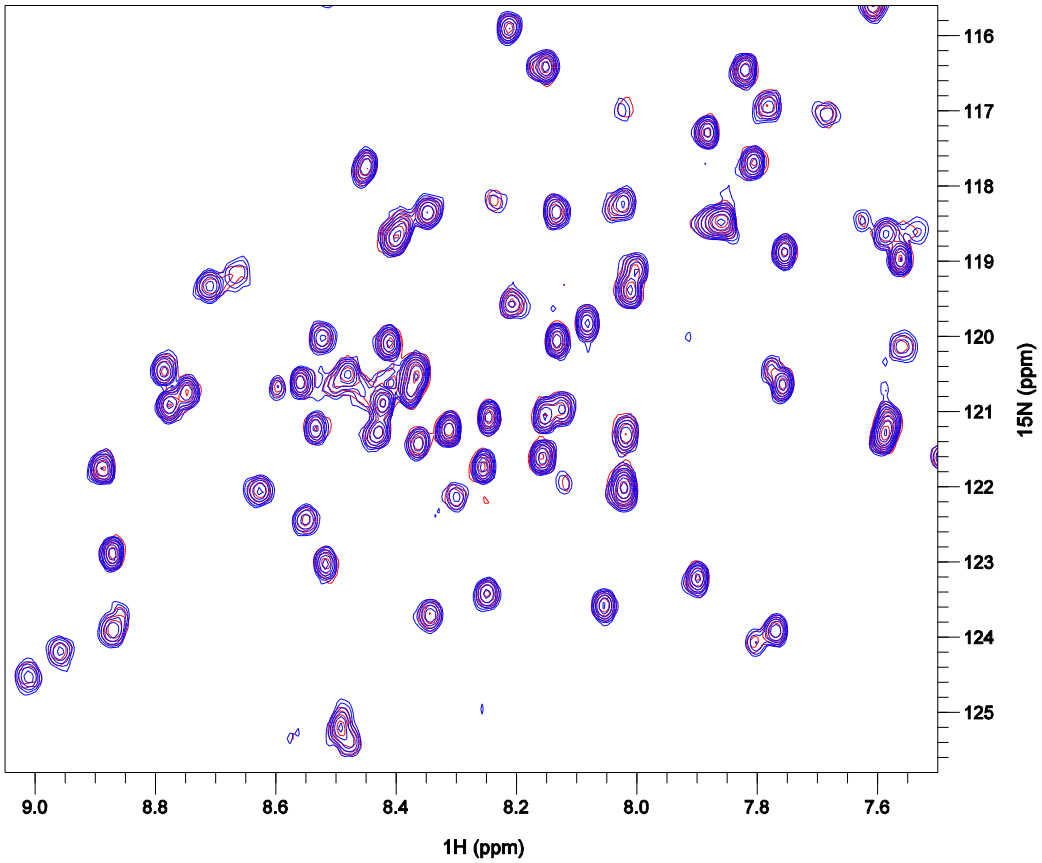

Figure 6.8 – $^{1}H,^{15}N$-HSQC of $CheY_6$ with (red) and without (blue) truncated length FliM. The spectrum is expanded to show the crowded central region, highlighting that no peak shifts are seen.

For an interaction to be seen, $CheY_6$ may need to be phosphorylated, as CheY-P has a greater affinity for FliM. As CheY-P is short lived, BeF_3^- was used as a stable phosphate mimic. It non-covalently binds to the phosphorylatable D56 residue of $CheY_6$ and has been shown to induce conformational changes, consistent with phosphorylation (Cho *et al*. 2001; Yan *et al*. 1999).

To investigate the residues important for interaction with FliM, comparisons must be made between $CheY_6$-BeF_3^- and FliM-$CheY_6$-BeF_3^- (Figure 6.9).

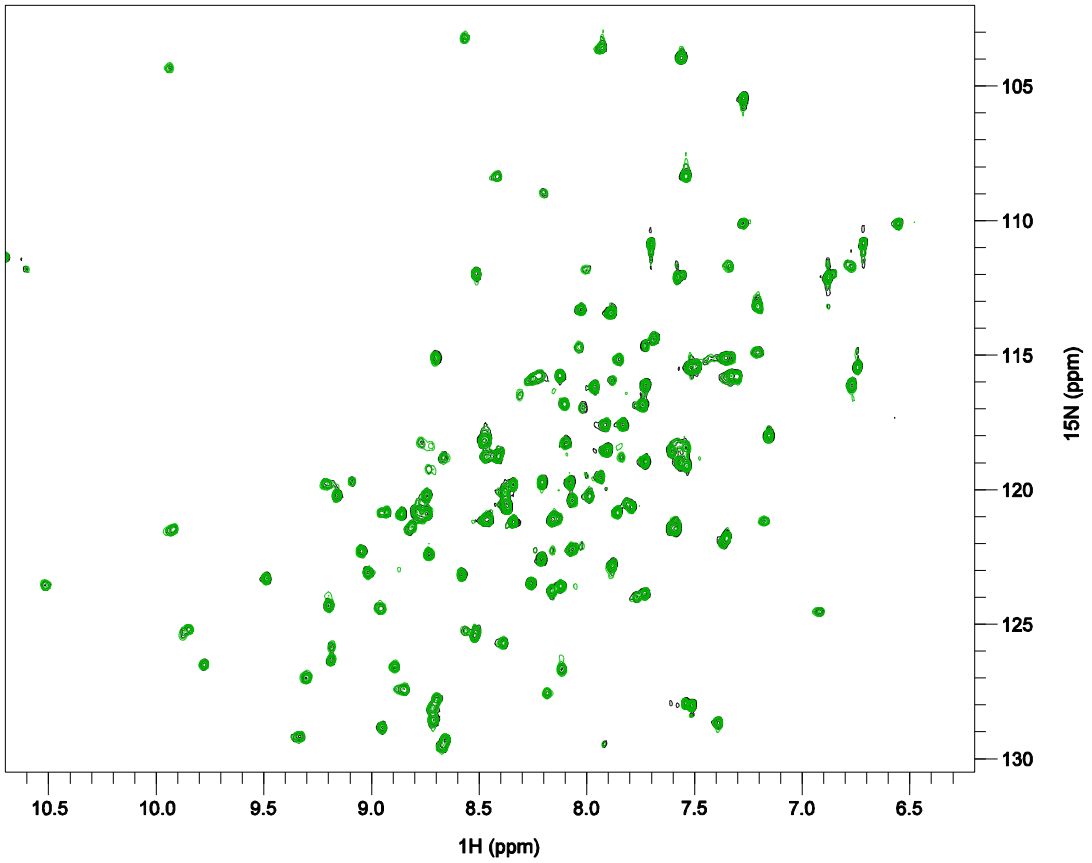

Figure 6.9 – $^{1}H,^{15}N$-HSQC of $CheY_6$-BeF_3^- (green) and FliM-$CheY_6$-BeF_3^- (black) (10 mM HEPES, 300 mM NaCl, 2 mM TCEP, pH7.5). No visible differences can be seen between the spectra, indicating no interaction between $CheY_6$ and FliM.

Again, no detectable chemical shift changes can be found between $CheY_6$-BeF_3^- and FliM-$CheY_6$-BeF_3^-. Even in the central crowded region (Figure 6.10), no changes are observed. This indicates that under the conditions used for NMR, $CheY_6$ does not interact with FliM, even in a conformation thought to mimic the phosphorylated state.

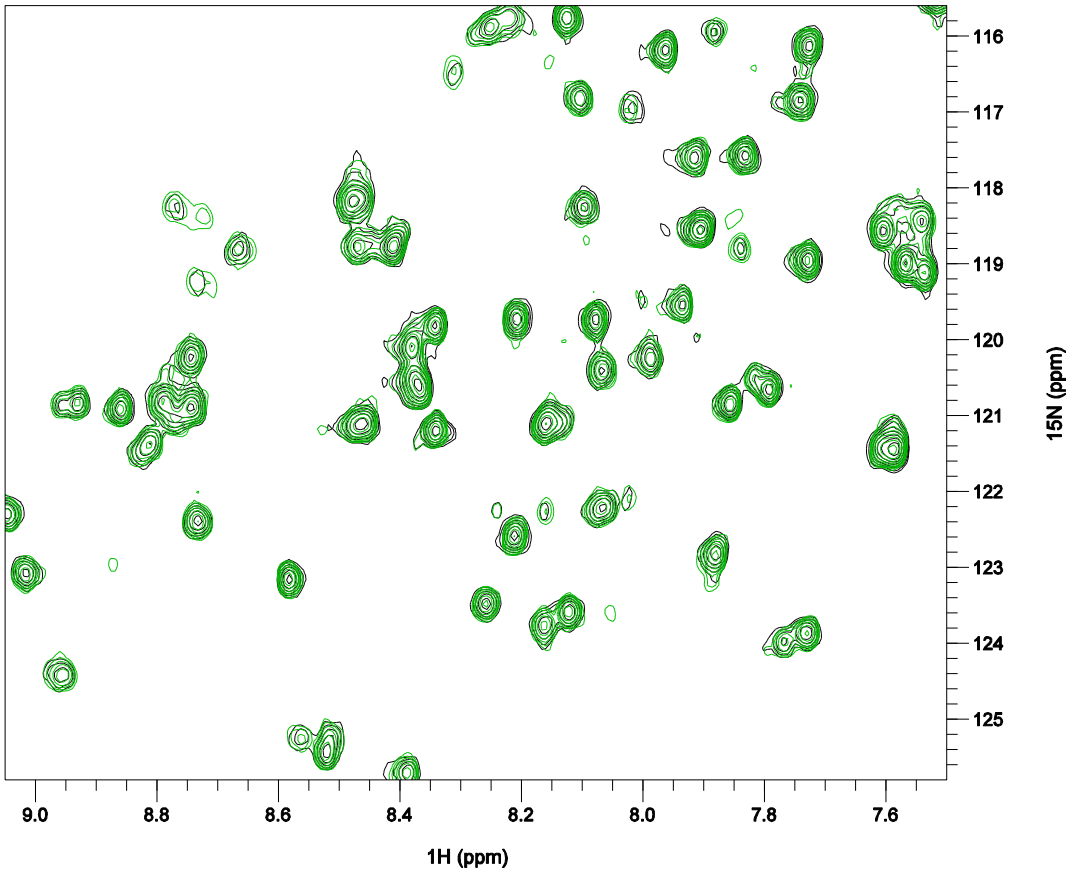

Figure 6.10 – $^{1}H,^{15}N$-HSQC of $CheY_6$- BeF_3 with (black) and without (green) FliM. The spectrum is expanded to show the crowded central region, highlighting that no peak shifts are seen.

6.2.2 Discussion

No interaction was observed between $CheY_6$ (in the absence or presence of BeF_3^-) and either the N-terminal peptide or truncated (1-235) FliM. A 1D NMR spectrum indicated FliM (1-235) was folded (Figure 6.11).

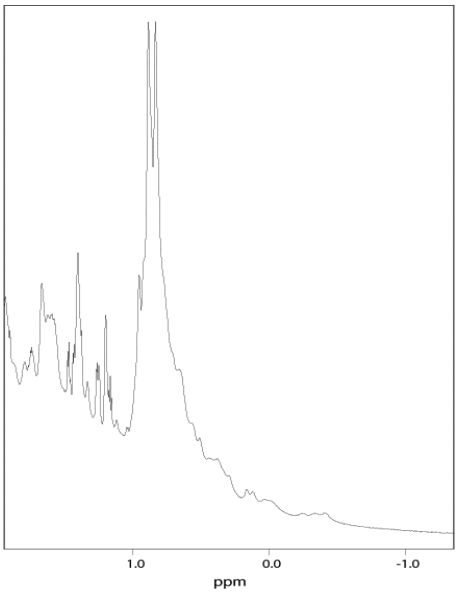

Figure 6.11 – Upfield region of the 750 MHz ^{1}H spectrum of FliM. The observed chemical shift dispersion (in particular, the peaks between 0.6 and -0.5 ppm) indicated FliM is folded and has a hydrophobic core in which methyl groups are in close proximity to one or more aromatic amino acids.

NMR studies were also used to investigate $CheY_3$-FliM interactions. No significant changes could be seen with $CheY_3$. Removing the His_6-tag of $CheY_3$ made no difference to FliM-$CheY_3$ interactions (Prof. C. Redfield and Dr. L. Varela-Alvarez, personal communication). Hence, the N-terminal His_6-tag located on $CheY_6$ is not thought to cause problems with FliM binding. As the BACTH system also showed no interaction between $CheY_6$ and FliM, a combination of these results suggest a few possibilities. Firstly, monomeric FliM may have a different conformation compared with FliM located in the switch complex, where it is part of a ring structure. These structural changes may not allow $CheY_6$ to bind to FliM in its monomeric state. Secondly, FliM may need the presence of FliN or FliG to allow $CheY_6$ binding. Finally, $CheY_6$ may bind to a different switch complex protein. The differences between the

FliM-CheY interactions of *E. coli* compared to *R. sphaeroides* could be attributed to the different mechanisms used for rotational switching i.e. stop-start vs rotation reversal.

The above studies were all performed *in vitro* with monomeric protein in solution. To identify whether $CheY_6$ can interact with at least some component of the motor *in vivo*, fluorescence microscopy was used.

6.3 Single Molecule Microscopy

Fluorescent proteins (FPs) have been extensively used in studies of cell biology, and to investigate the behaviour of proteins *in vivo*. Green Fluorescent Protein (GFP) (Yang, Moss, and Phillips 1996) and its mutated allelic forms (yellow, cyan and blue) can be fused to proteins of interest, expressed in living cells and fluorescence microscopy techniques can be used to investigate their behaviour (Day and Davidson 2009). These fusion proteins are particularly useful as difficulties in tagging and purifying the protein are avoided, and can be expressed as fusions in living cells. Diffusion patterns, cellular localisation and copy number have been determined using fusions (Cannistraro *et al*. 2011). This method has been used to determine the copy number and localisation of the CheYs of *R. sphaeroides* (Porter *et al*. 2006). $CheY_6$ fusions have demonstrated cytoplasmic cluster localisation. However, there are some serious limitations to this method. Fusion proteins are not always fully functional, and results can differ based on N- or C-terminal tagging. In some cases, such as CheY, the protein of interest can be much smaller than the FP. Fusion

proteins are also not useful for tracking single molecules, as spots often overlap and copy numbers are hard to determine. If only a small percentage of a large population bind to the site of interest, it can be difficult to discriminate due to this high background.

Organic dyes are widely used as fluorophores for *in vitro* studies. Organic dyes are small (up to 100-fold smaller than FPs), exceptionally photostable (up to 100-fold more stable than FPs) and easily added to the protein of interest (e.g. by cysteine cross-linking) (Shaner, Steinbach, and Tsien 2005) (Dempsey *et al*. 2011). These organic dyes can fluoresce for minutes, compared to tens of seconds for FPs. However, genetic tagging is not possible with these organic dyes, making *in vivo* studies difficult. A method, recently developed in Oxford, allows bacterial cells to take up small numbers of organically tagged proteins (Crawford *et al*. 2013) (Aigrain *et al*. 2015). The method takes advantage of electroporation, a well-established technique used to achieve cellular uptake of DNA. An external electric field is applied to cells suspended in water with glycerol (10%) (low ionic strength), producing transient pores in the cell membrane. This allows uptake of macromolecules (such as organic dye-labelled protein) and DNA. Cells that have internalised proteins tagged with organic dye can be visualised using microscopy techniques such as near Total Internal Reflection Fluorescence Microscopy (nTIRF). To date, although this has been tried in *E. coli* (Diana Di Paolo, unpublished), electroporation of proteins tagged with organic dyes and specifically, localisation of the CheYs to the flagellar motor has not been visualised in *R. sphaeroides*.

Electroporation poses a number of potential problems. Cell death is common among electroporated cells, especially due to unsealed pores, and only a small percentage of cells show normal growth afterwards. Other issues include the electroporation itself, which must be performed in water. *R. sphaeroides* displayed good cell growth after electroporation.

6.3.1 Protein Expression, Purification and Labelling

cheY_6(A134C)-pQE80 was produced via quick-change PCR of *che*Y_6-pQE80 using specific primers (See Appendix B). The PCR product was digested (*Dpn*I), transformed into *E. coli* (XL1-Blue) and sequenced. $CheY_6$(A134C) was expressed and purified using the protocol found in Section 2.6.1. A 10x molar excess of Atto647-maleimide dye (dissolved in DMSO, excitation wavelength 647 nm) was added to purified $CheY_6$(A134C), and left overnight at 4°C (Figure 6.12). Free dye was removed using size exclusion chromatography.

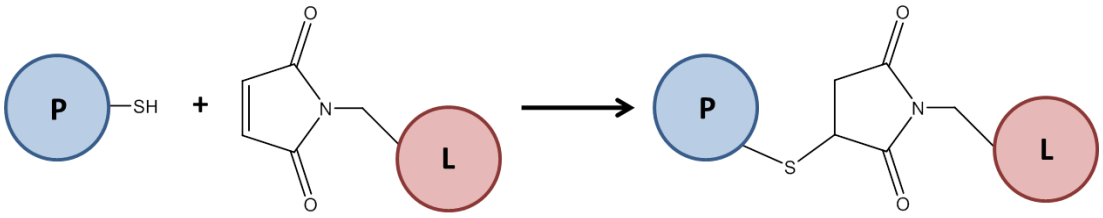

Figure 6.12 – Reaction mechanism between a maleimide dye and a protein sulfhydryl group. The labelling group (L) is attached to a maleimide group that reacts with the target cysteine (SH) of the protein (P). The Atto chromophore has a rigid structure which does not allow cis-trans isomerisation.

6.3.2 Electroporation of $CheY_6$(A134C)-Atto647 into *R. sphaeroides*

R. sphaeroides were made electrocompetent using the protocol found in Section 2.3.9. This increases membrane permeability and reduces the ionic strength of the cell culture (to avoid arcing during electroporation). Cells were incubated with $CheY_6$(A134C)-Atto647 (15 pM, lysis buffer) and an electric field was applied to internalise the fluorescent protein (Figure 6.13). Non-internalised fluorescent protein was removed via washing and cells were allowed to recover in succinate medium for one hour.

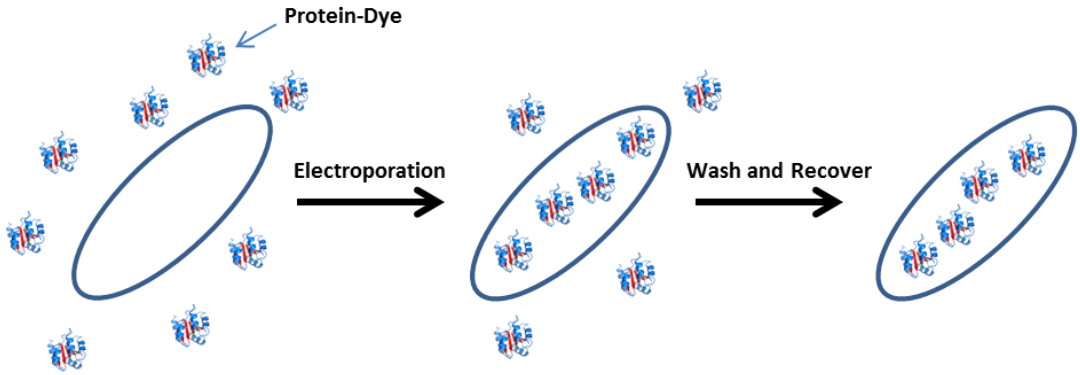

Figure 6.13 – Electroporation schematic. Cells are incubated with fluorescent protein before an electric field is applied. This internalises the fluorescent protein. Cells are then washed and left to recover before imaging.

6.3.3 nTIRF Microscopy

Electroporated, non-electroporated and empty cells (no fluorescent protein) were placed onto agarose pads, and imaged using nTIRF microscopy. Imaging was performed in collaboration with Diana Di Paolo, (Armitage and Berry Lab, University of Oxford). As expected, empty cells showed no fluorescence at 647 nm.

Approximately 10% of non-electroporated cells contained $CheY_6$(A134C)-Atto647, highlighting that the electrocompetent *R. sphaeroides* cells were exceptionally permeable. Approximately 70% of electroporated cells contained $CheY_6$(A134C)-Atto647 (measured by eye). Cells were imaged (excitation - λ637 nm (red), frame rate - 10 ms) until photobleaching occurred. In some cases, $CheY_6$(A134C)-Atto647 was fluorescent for more than a minute. To identify the position of the motor and to determine whether $CheY_6$ interacts with the motor, experiments with either FliM-YFP (genomic) or FliM-YPet (genomic) were completed. YPet is an improved version of YFP (improved brightness and faster maturation time) (Nguyen and Daugherty 2005). Due to the low copy number of FliM in the switch complex, FliM-YFP was not sufficiently bright to determine the motor location. FliM-YPet proved to be substantially brighter. The FliM-YPet channel was stacked into one image to improve motor visibility (Figure 6.14) (movies are provided on CD).

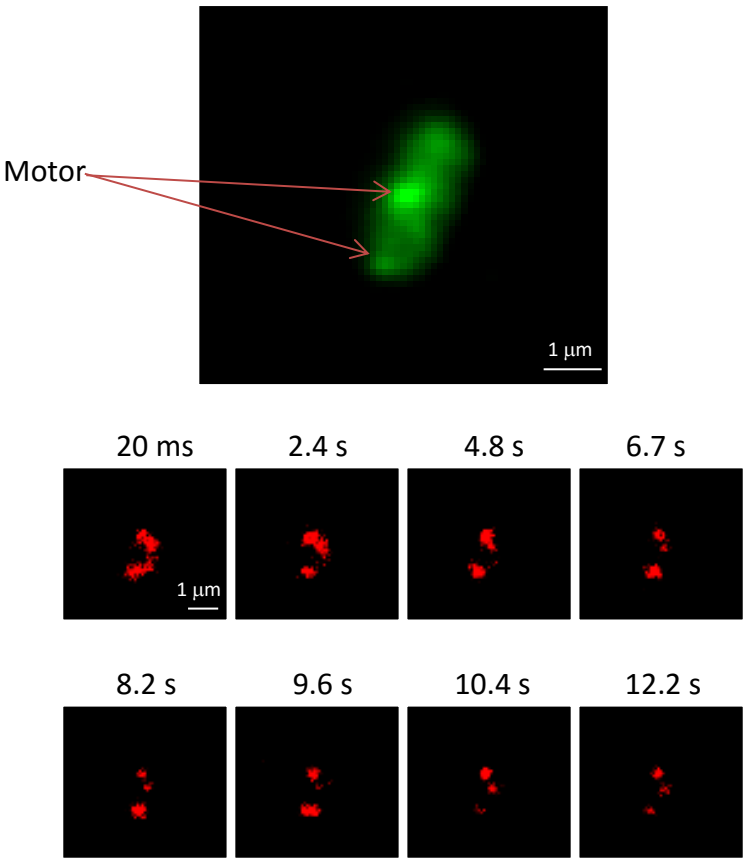

Figure 6.14 – nTIRF microscopy images of *R. sphaeroides* (FliM-YPet) containing $CheY_6$(A134C)-Atto647 (red). Images are from specified time points throughout the video (full videos found on CD).

Three main foci are observed for $CheY_6$(A134C)-Atto647 and two main foci are observed for FliM-YPet. It has been previously shown that *R. sphaeroides* often has more than one focus for FliM, especially if the cell is dividing (Dr. C. W. Jones, personal communication). Some cells show possible interactions with the cytoplasmic cluster (Figure 6.15).

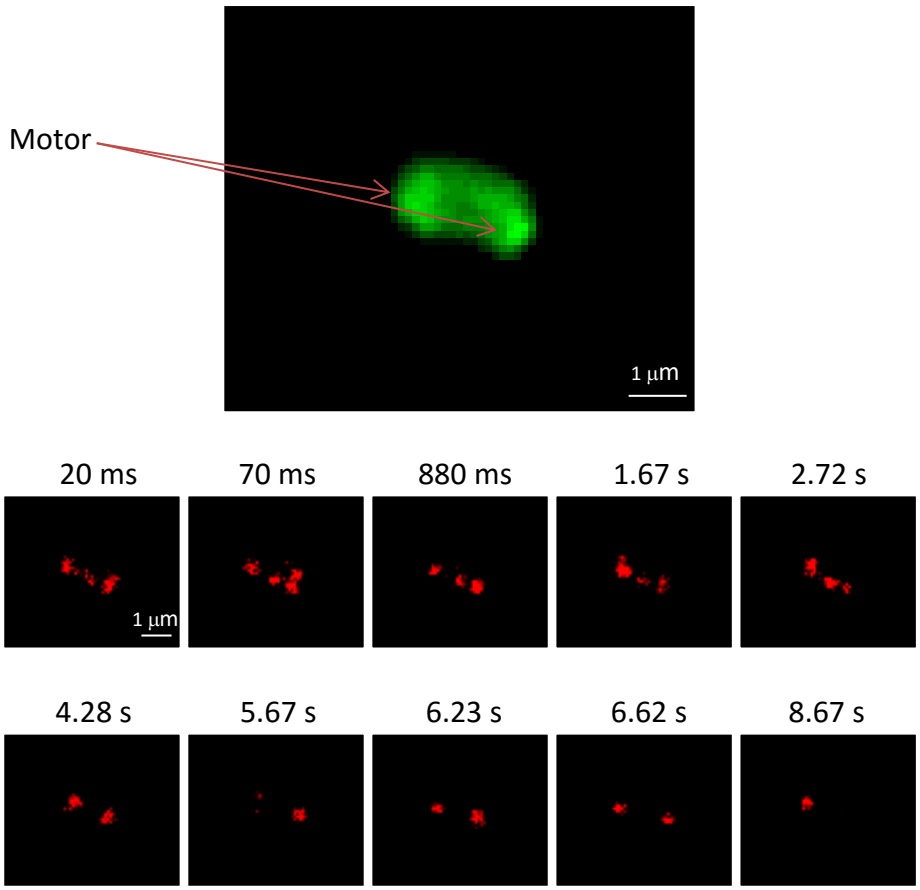

Figure 6.15 – nTIRF microscopy images of *R. sphaeroides* (FliM-YPet - green) containing $CheY_6$(A134C)-Atto647 (red). Images show specific time points of the video. A central focus gives evidence of cytoplasmic cluster localisation.

$CheY_6$ foci are shown to overlap with FliM foci for extended periods of time (Figure 6.16). A $CheY_6$ focus overlaps with a FliM focus at approximately mid-cell and the cell pole. Unfortunately due to the overlap of more than one $CheY_6$ molecule, individual tracking was not possible.

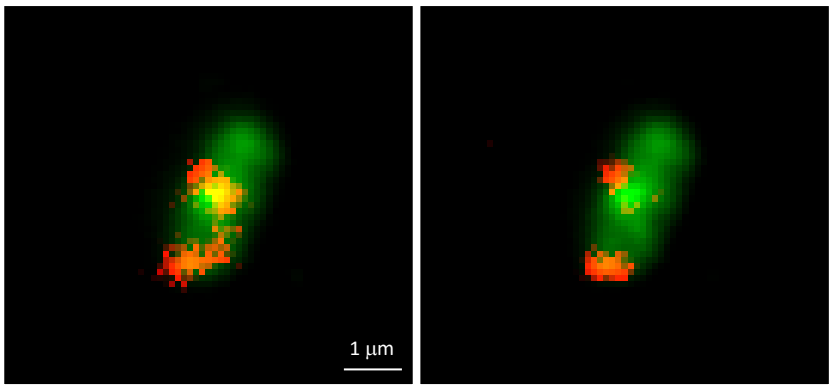

Figure 6.16 – Combined nTIRF microscopy images of $CheY_6$(A134C)-Atto647 (red) and FliM-YPet (green) after 20 ms (left) and 9.55 s (right) respectively.

Some cells show foci that localise to something that does not contain a FliM focus, approximately at mid-cell (Figure 6.17). This is probably the cytoplasmic cluster, shown to be the site of $CheY_6$ localisation in earlier studies.

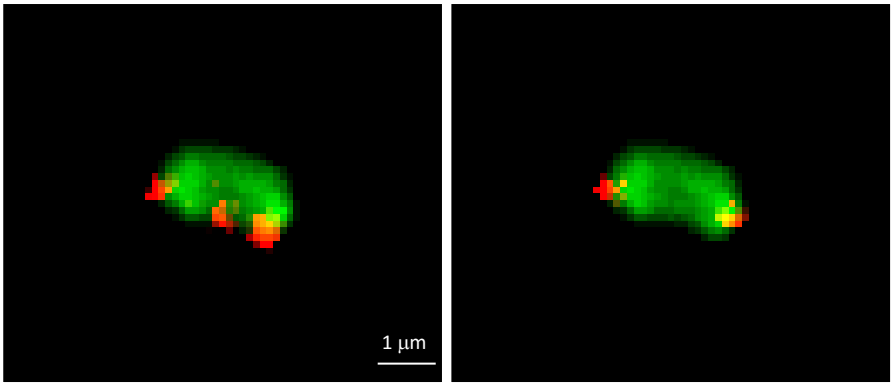

Figure 6.17 – Combined nTIRF microscopy images of $CheY_6$(A134C)-Atto647 (red) and FliM-YPet (green) after 2.72 s (left) and 6.62 s (right) respectively.

nTIRF microscopy of $CheY_6$(A134C)-Atto647 with FliM-YPet suggest that $CheY_6$ might interact with the flagellar motor. There is also evidence that shows probable

interaction with the cytoplasmic cluster. *R. sphaeroides* containing both $CheA_3$ and FliM tagged with FP is the next step to confirm $CheY_6$ transducing a signal from the cytoplasmic cluster to the flagellar motor.

6.4 Conclusions

The BACTH system showed no interaction between $CheY_6$ and FliM. NMR experiments also showed no interaction *in vitro*. However, *in vivo* nTIRF microscopy with organic dyes showed $CheY_6$ colocalising with FliM foci and hence, the flagellar motor. In previous experiments with fluorescently tagged fusion proteins, it was not possible to distinguish $CheY_6$-FliM binding. This was principally a copy number and background issue. There are thousands of $CheY_6$ and $CheA_3$ proteins within a cell, so the relatively small amount of $CheY_6$ interacting with the flagellar motor could not be visualised. Electroporation provided control of the number of fluorescent $CheY_6$ molecules, and hence removed background issues. Single molecule microscopy provides strong evidence that shows probable interaction of $CheY_6$ with the flagellar motor. There are a number of possibilities that would explain why no interaction is seen *in vitro*. FliM may need the presence of FliG and/or FliN for interaction to occur with $CheY_6$. FliM may have two different conformations, a monomeric conformation and a switch complex conformation. $CheY_6$ may only be able to interact with the switch complex conformation. The interaction between FliM and CheY has been investigated in several bacterial species, and these data suggest monomeric FliM can interact with CheY in those species. The *R. sphaeroides* flagellar motor has an unusual stop-start mechanism. The reason for the lack of interaction *in vitro* could

be due to a different mode of interaction between FliM and $CheY_6$, which in turn disrupts the FliG-Stator interface in a way that does not allow a reversal of rotation. As $CheY_3$ or $CheY_4$ is also necessary for a fully chemotactic strain, electroporation of either $CheY_3$ or $CheY_4$ and $CheY_6$ could provide further insight into their different functions.

Chapter 7

Discussion

7.1 Structural Investigations of $CheY_6$ in its Active and Inactive States

R. sphaeroides, unlike most studied bacterial species, requires two CheYs to control its stop-start flagellar motor, $CheY_6$ and either $CheY_3$ or $CheY_4$. $CheY_6$-P is the only CheY able to stop the motor. The crystal structure of $CheY_6$ in complex with the cognate histidine kinase has been solved (Bell *et al*. 2010), however, it is not known whether this represents the active, inactive or an intermediary conformation. The structure of $CheY_6$ displays a classic response regulator fold, consisting of five α-helices and five β-strands, where the α-helices surround a β-sheet. The overall $CheY_6$ structure is well conserved in comparison to $CheY_{EC}$. The conserved site of phosphorylation, D56, forms a Mg^{2+}-binding acid pocket with D9 and D10, and a salt bridge is formed between the highly conserved K107 and the carboxylic acid group of D56. The key residues involved in the switch mechanism of $CheY_{EC}$ have been identified (Dyer and Dahlquist 2006), however $CheY_6$ does not contain all of the

residues involved. Superposition of the crystal structures of $CheY_{EC}$ (active and inactive) and $CheY_6$ allowed investigation into the possible residues involved in the switch mechanism (Figure 7.1). $V104_{RS}$ is unlikely to play a similar role to $Y106_{EC}$, as it is not close (or large) enough to interact directly with $S83_{RS}$. The $CheY_6$ switch mechanism upon phosphorylation was probed using NMR studies.

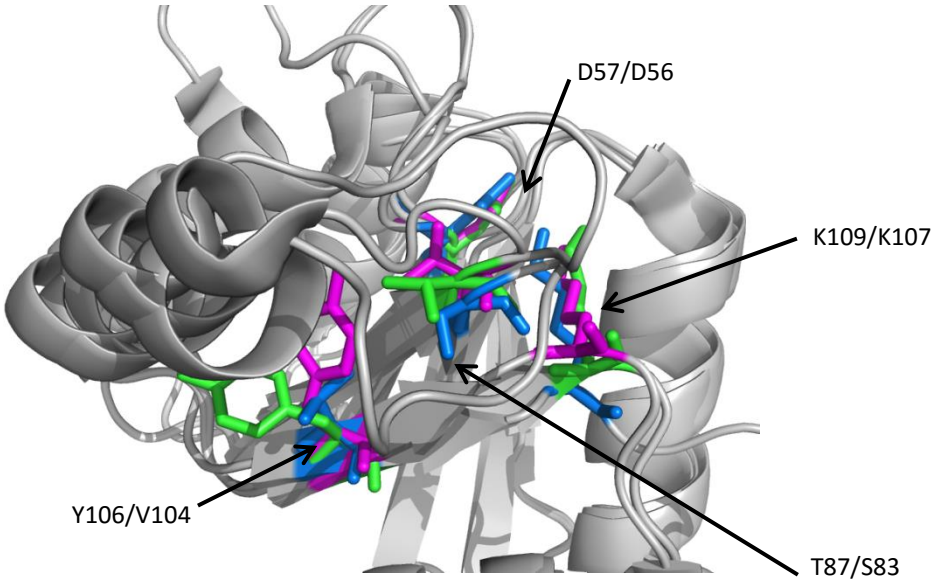

Figure 7.1 - Superposition of *E. coli* CheY in both the active (magenta) and inactive state (green), with $CheY_6$ (blue). Residues important for activation are highlighted (*E. coli*/*R. sphaeroides*).

$^{1}H,^{15}N$-Heteronuclear NOE experiments confirmed the elongated loop (109-118) region of $CheY_6$ not present in other CheYs that showed no electron density in the crystal structure, is flexible in solution. TALOS-N provided evidence that no scale large conformational changes are observed upon activation, although predictions suggested conformational changes for the $\beta4$-$\alpha4$-loop region which has been shown to be important in the $CheY_{EC}$ switch mechanism. NH peak shifts in the $^{1}H,^{15}N$-HSQC spectra upon addition of the phosphoryl mimic BeF_3^- provided some insight into the

switch mechanism. Large shifts were seen for one surface of $CheY_6$, near the phosphorylatable D56 residue which involved the β4-α4-loop region. Similar chemical shift changes to $T87_{EC}$ were observed for $S83_{RS}$, which could indicate similar conformational changes upon activation. Although not all residues could be assigned, the elongated β5-α5-loop region showed chemical shift changes upon addition of BeF_3^-. This would not be expected if the region was completely unstructured and suggests that a conformational change occurs in this loop upon activation.

Hydrogen-deuterium exchange experiments showed high amide protection in β1, 3 and 4, with and without BeF_3^-. This was not surprising as these β-strands have very low main chain solvent accessibility. Interestingly, S83 displayed slower exchange upon addition of BeF_3^-. This could indicate conformational changes involved in the switch mechanism. Further evidence from residual dipolar coupling data suggested that the conformation of S83 in the crystal structure agrees well with inactive $CheY_6$ in solution, but does not match with that in activated $CheY_6$. RDC data also provided evidence that the crystal structure is more like the inactive conformation of $CheY_6$.

Investigation into the β4-α4-loop position and superposition with $CheY_{EC}$ and FliM suggested that this loop region may sterically clash with the N-terminus of FliM (Figure 7.2).

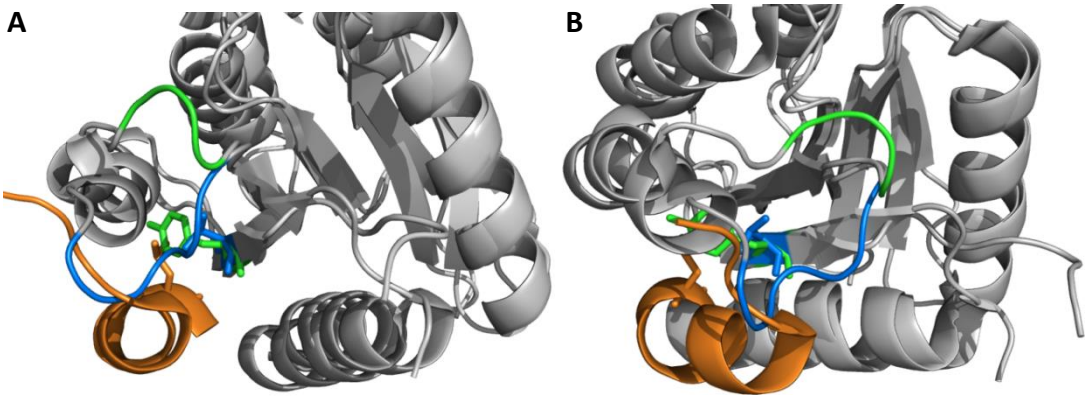

Figure 7.2 - Superposition of **A**) $CheY_{EC}$ (green) in complex with FliM (1-16, orange), and $CheY_6$ (blue) **B**) A different orientation of **A**. The β4-α4-loop region and L15 (FliM) are highlighted.

A possible switch mechanism for $CheY_6$ may involve movement of S83, which rearranges hydrogen bonds (such as K107 N - O S83) causing the β4-α4-loop to change conformation. This change in conformation may remove any steric clashes between $CheY_6$ and FliM, and therefore increase the binding affinity. It is apparent that the activation mechanism of the CheY response regulator is complex and not conserved across all CheY response regulators. Further analysis is needed to fully elucidate the complete switch mechanism of $CheY_6$.

7.2 Investigation and Characterisation of the Loop Region in $CheY_6$

NMR studies reveal fast (ps to ns) backbone dynamics for the elongated loop region S109-E118. This loop region was deleted ($CheY_6$-Δloop) and the effects investigated *in vivo* and *in vitro*. Circular dichroism and NMR experiments (Figure 7.3) provided evidence that $CheY_6$-Δloop is a folded protein. Swim plate and tethering assays provided evidence that removal of this loop inactivates $CheY_6$-Δloop. Epi-

fluorescence and phosphotransfer assays however, indicated that $CheY_6$-Δloop localised to the cytoplasmic cluster, and is still phosphorylated by $CheA_3$. This indicates that $CheY_6$-Δloop can still interact with $CheA_3$ in a wild type manner, and hence the loop deletion is likely to affect the interaction with the switch complex of the flagellar motor. A reduced auto-dephosphorylation time was observed for $CheY_6$-Δloop compared with wild type $CheY_6$. The loop deletion may have disrupted the interaction of $CheY_6$ with the phosphatase domain of $CheA_3$, and hence increased the half-life of $CheY_6$-Δloop-P.

The results suggest that the β5-α5-loop region does play an important role in the interaction of $CheY_6$ with the switch complex. Mutagenesis of specific residues or groups of residues of this loop in $CheY_6$ may elucidate the key residues involved in its function.

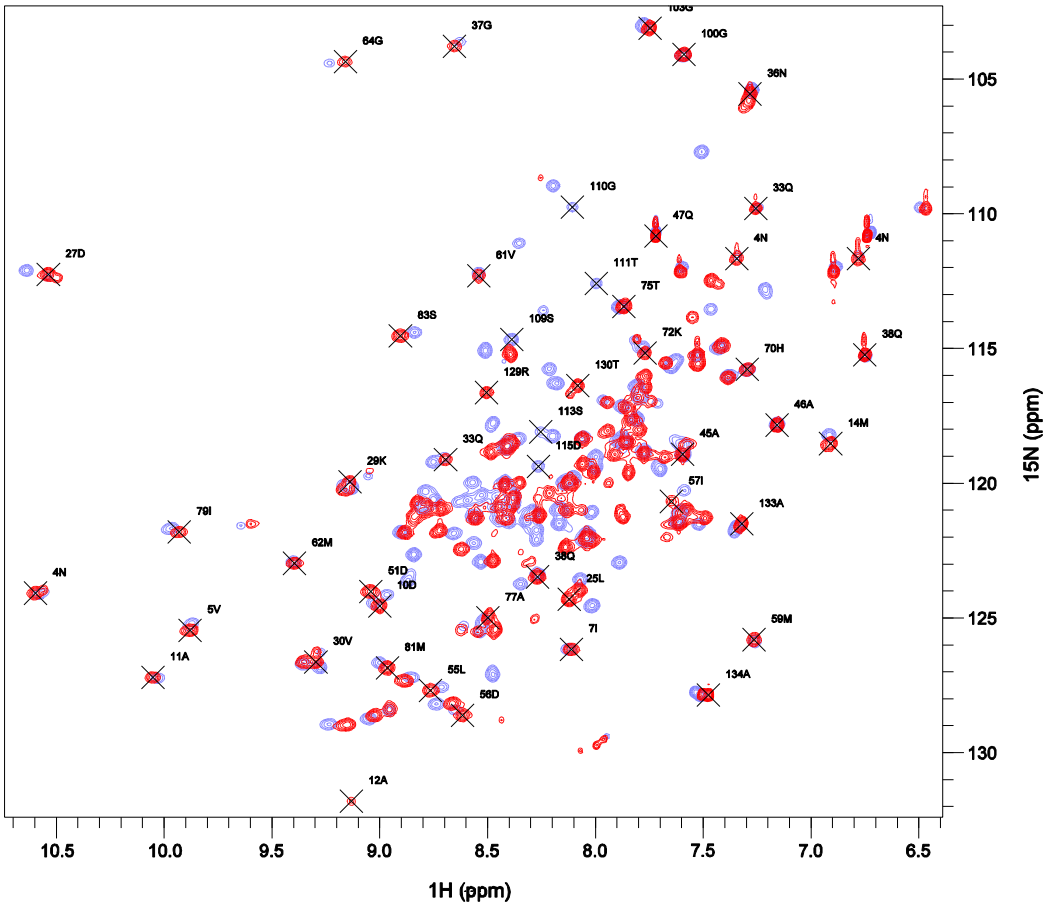

Figure 7.3 – ^{1}H, ^{15}N-HSQC spectra of $CheY_6$-Δloop (red) and wild type $CheY_6$ (blue). S109, G110, T111, S113 and D115 are labelled in the wild type spectrum to highlight successful deletion in $CheY_6$-Δloop; no peaks corresponding to these residues are observed for $CheY_6$-Δloop. Other labelled peaks indicate residues that do not shift significantly. Not all $CheY_6$-Δloop assignments are shown to reduce crowding.

7.3 The interactions of $CheY_6$ and FliM in *Rhodobacter sphaeroides*

All six CheYs of *R. sphaeroides* have been shown to interact with FliM *in vitro* (Ferré *et al*. 2004). However, further studies with $CheY_6$ have not been able to reproduce these results. Bacterial two hybrid assays provided no evidence of interaction. NMR studies probing the interaction between $CheY_6$ and FliM also indicated that no

interaction occurs *in vitro*. This evidence suggests that $CheY_6$ cannot interact with monomeric FliM. It is likely that FliM adopts a different conformation when in the switch complex. This different conformation could be caused by interactions with itself, or interactions with other components of the switch complex (FliG or FliN). In contrast, studies have provided *in vitro* evidence of the interaction between CheY and FliM of *E. coli* (McEvoy *et al*. 1999) (Toker and Macnab 1997). This may be relevant to the behavioural differences seen between the flagellar motors of *E. coli* and *R. sphaeroides*, and could be linked to the stop-start phenotype observed in *R. sphaeroides*. There is also the possibility that $CheY_6$ does not interact with FliM, and instead interacts with other components of the switch complex such as FliN.

nTIRF microscopy experiments have provided the first evidence of $CheY_6$ interacting with the flagellar motor *in vivo* (Figure 7.4). Electroporation of $CheY_6$ with a chemically bonded organic dye, removed background fluorescence problems observed with previous microscopy experiments that used genomic fusions of $CheY_6$ with fluorescent protein. It also allowed the visualisation of single molecules of $CheY_6$ for prolonged periods within a cell.

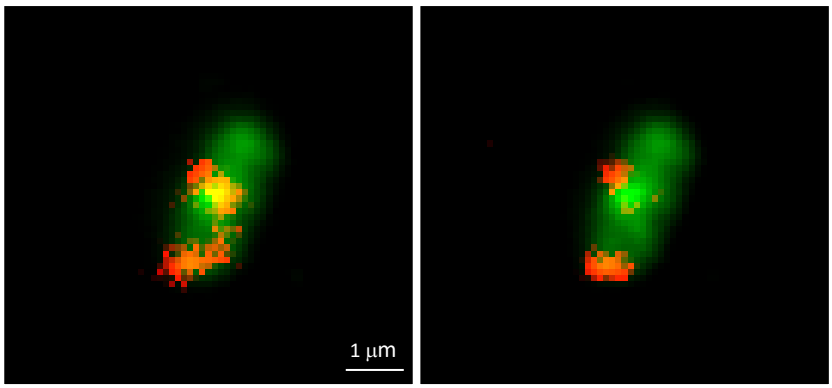

Figure 7.4 – Combined nTIRF microscopy images of $CheY_6$(A134C)-Atto647 (red) and FliM-Ypet (green) after 20 ms (left) and 9.55 s (right) respectively.

$CheY_6$ is observed to co-localise with FliM for extended periods of time. Although the specifics of the interaction are still unknown, this suggests that $CheY_6$ does interact with the flagellar motor. Further experiments are required to determine if $CheY_6$ is interacting with FliM (in a ring conformation), or another component of the switch complex. Electroporation of either $CheY_3$ or $CheY_4$ with $CheY_6$ may provide insight into their different functions.

$CheY_6$-P stops the *R. sphaeroides* flagellar motor and a combination of molecular, biophysical and imaging techniques have identified a role for a loop region not identified in CheYs of other species in the interaction with the flagellar switch, and a role for S83 in controlling the switch mechanism between active and inactive states.

Appendix A

LB Medium

Ingredient	Quantity per litre
Tryptone	10 g
Yeast Extract	5 g
NaCl	5 g

Made up to 1 litre (MilliQ water), adjusted to pH 7.0 and autoclaved.

10x TBE Medium

Ingredient	Quantity per litre
Tris base	108 g
Boric acid	55 g
EDTA pH 8.0	7.4 g

Made up to 1 litre (MilliQ water), adjusted to pH 8.3 and autoclaved.

TFB I

Ingredient	Concentration
$RbCl_2$	100 mM
$MnCl_2$ $4H_2O$	50 mM
Potassium acetate	30 mM
$CaCl_2$ $2H_2O$	10 mM
Glycerol	15% (v/v)

Adjusted to pH 5.8 (0.2 M acetic acid) and filter sterilised.

TFBII

Ingredient	Concentration
$CaCl_2$ $2H_2O$	75 mM
$RbCl_2$	10 mM
PIPES	10 mM
Glycerol	15% (v/v)

Adjusted to pH 6.8 (HCl) and filter sterilised.

5x DNA loading dye

Ingredient	Concentration
Glycerol	70%
MilliQ water	29.5%
Bromophenol blue	0.25%
Xylene cyanol	0.25%

M22

Ingredient	Quantity per litre
Conc. Base	20 ml
Phosphate buffer (1 M)	20 ml
Growth factor	2 ml
$(NH_4)_2SO_4$	0.5 g
NaCl	0.5 g

Made up to 1 litre (MilliQ water), adjusted to pH 7.2 (KOH) and autoclaved.

Succinate Media

Ingredient	Quantity per litre
Conc. Base	20 ml
Phosphate buffer (1 M)	20 ml
Growth factor	2 ml
Sodium succinate	2 g
Casamino acids	1 g
$(NH_4)_2SO_4$	0.5 g
NaCl	0.5 g

Made up to 1 litre (MilliQ water), adjusted to pH 7.2 (KOH) and autoclaved.

Phosphate buffer pH 7.0 (1 M)

Ingredient	Quantity per litre
K_2HPO_4 (1 M)	174.18 g
KH_2PO_4 (1 M)	136.09 g

Adjusted to pH 7.0 (KOH), autoclaved and stored at 4 °C.

Concentrated base

Ingredient	Quantity per litre
Metals 44 solution	25 ml
$MgSO_4$ $7H_2O$	14.5 g
Nitrilotriacetic acid (diNa salt)	5.94 g
$CaCl_2$ $2H_20$	1.67 g
$FeSO_4$ $7H_2O$	50 mg
Ammonium molybdate $4H_2O$	4.6 mg

Dissolved diNa first and adjusted to pH 5.0 (KOH). This allowed $FeSO_4$ to dissolve. Added all other ingredients, adjusted to pH 6.8 (KOH), autoclaved and stored at 4 °C.

Metals 44 solution

Ingredient	Quantity per litre
$ZnSO_4$ $7H_2O$	11 g
$FeSO_4$ $7H_2O$	5 g
$MnSO_4$ $4H_2O$	3 g
Tetrasodium versenate (EDTA)	2.5 g
Sulphuric acid (3 M)	1.5 ml
$CuSO_4$ $5H_2O$	0.39 g
$CoCl_2$ $6H_2O$	0.2 g
H_3BO_3	0.12 g

Filter sterilised and stored at 4 °C.

Growth factor

Ingredient	Quantity per litre
Niacin	1 g
$NaHCO_3$	500 mg
Thiamine HCl	500 mg
Biotin	20 mg

Autoclaved and stored at 4 °C.

2TY Media

Ingredient	Quantity per litre
Tryptone	16 g
Yeast Extract	10 g
NaCl	5 g

Made up to 1 litre (MilliQ water), adjusted to pH 7.0 and autoclaved.

Lysis Buffer

Ingredient	Quantity
Tris-HCl pH 8.0	10 mM
NaCl	200 mM
EDTA	1 mM
SDS	1%

Dissolved in MilliQ water and filter sterilised.

M9 Minimal Media

Ingredient	ml per litre
10x M9 Salts	100
20% w/v Glucose	10
1 M $MgSO_4$	1
1 M Thiamine.HCl	1
0.1 M $CaCl_2$	1

Made up to 1 litre (MilliQ water) and autoclaved.

10x M9 Salts

Ingredient	Quantity per litre
$NaHPO_4$ $2H_2O$	75.2 g
KH_2PO_4	30 g
NH_4Cl	10 g
NaCl	5 g

Made up to 1 litre (MilliQ water) and autoclaved.

TGMNKD buffer

Ingredient	Concentration
NaCl	150 mM
Tris-HCl	50 mM
KCl	50 mM
$MgCl_2$	5 mM
DTT	1 mM
Glycerol	10%

Made up to 1 litre (MilliQ water) and adjusted to pH 8.0.

SDS/EDTA Loading Dye

Ingredient	Quantity per litre
EDTA	90 mM
Tris HCl (pH 6.8)	37.5 mM
Glycerol	37.5%
SDS	7.5%
β-mercaptoethanol	3%

SDS-PAGE running buffer

Ingredient	Quantity per litre
Glycine	188 g
Tris HCl (pH 6.8)	30.2 g
SDS	10 g

Labelling buffer

Ingredient	Concentration
Tris-HCl	50 mM
NaCl	150 mM
TCEP	0.1 mM

Made up to 1 litre with MilliQ water and adjusted to pH7.2.

Appendix B

Primer List

Primer Name	Sequence (5'-3')	Feature
MS-Y6-A	CCGGACCGGCCCCTTTCGGG	Upstream of *cheY*$_6$
MS-Y6-B	CACGCCTCGGAAGGCTCCGC	Downstream of *cheY*$_6$
MS-Y6-1	CGCG CCATGGCGCCCTACAATGTCATGATC	*ncoI* site
MS-Y6-2	CAAGCTCGCCGCCGGTCTTGGGCTTGGCCACCA CGCC	Upstream of loop region in *cheY*$_6$
MS-Y6-3	GGCGTGGTGGCCAAGCCCAAGACCGGCGGCGA GCTTG	Downstream of loop region in *cheY*$_6$
MS-Y6-4	CGCGAAGCTTTCAGGCGGCCATCAGC	*hindIII* site
MS-R-Y6-pQE60	ATATGGATCCGGCGGCCATCAGCGTCCGCA	*bamHI* site
FliM-F-pQE60	ATATCCATGGCCGCCACTCCGCGCAAACTCTCG	*ncoI* site
FliM-R-pQE60	ATATGGATCCGCCCCGGACATGGCGGCGCG	*bamHI* site
Y6_A134C_F	CGGACGCTGATGGCCTGCTGAAAGCTTAATTAG	Quick change mutation
Y6_A134C_R	CTAATTAAGCTTTCAGCAGGCCATCAGCGTCCG	Quick change mutation
Y6_YFP_6	CGCGAAGCTTGGCGGCCATCAGCGTCCGCATG	*hindIII*
FliM_pKNT25_F	ATATTCTAGAAATGGCCGCCACTCCGCGCAAAC	*xbaI*
FliM_pKNT25_R	ATATGGTACCGCGCCCCGGACATGGCGGCGCG	*kpnI*
FliM_pKT25_F	ATATTCTAGACATGGCCGCCACTCCGCGCAAAC T	*xbaI*
FliM_pKT25_R	ATATGGTACCCTAGCCCCGGACATGGCGGCGC GT	*kpnI*
FliM_pUT18_F	ATATTCTAGACATGGCCGCCACTCCGCGCAAAC T	*xbaI*
FliM_pUT18_R	ATATGGTACCGCGCCCCGGACATGGCGGCGCG TC	*kpnI*
FliM_pUT18C_F	ATATTCTAGACATGGCCGCCACTCCGCGCAAAC	*xbaI*

	TCT	
FliM_pUT18C_R	ATATGGTACCCTAGCCCCGGACATGGCGGCGC GTCA	*kpnI*
Y6_pKNT25_F	ATATTCTAGAAATGCCCTACAATGTCATGATCGT GG	*xbaI*
Y6_pKNT25_R	ATATGGTACCGCGGCGGCCATCAGCGTCCGCAT GGT	*kpnI*
Y6_pKT25_F	ATATTCTAGACATGCCCTACAATGTCATGATCGT	*xbaI*
Y6_pKT25_R	ATATGGTACCTCAGGCGGCCATCAGCGTCCGCA T	*kpnI*
Y6_pUT18_F	ATATTCTAGACATGCCCTACAATGTCATGATCGT	*xbaI*
Y6_pUT18_R	ATATGGTACCGCGGCGGCCATCAGCGTCCGCAT G	*kpnI*
Y6_pUT18C_F	ATATTCTAGACATGCCCTACAATGTCATGATCGT GG	*xbaI*
Y6_pUT18C_R	ATATGGTACCTCAGGCGGCCATCAGCGTCCGCA TGG	*kpnI*

Appendix C

Chemical Shifts – $CheY_6$ pH 5.5

		H	N	HA	HB	HG	HD	HE	C	CA	CB	CG	CD	CE	
-9	Arg	-	-	4.41	1.85,1.85	1.67,1.67	3.21,3.21		-	176.43	56.61	30.95	26.94	43.30	-
-8	Gly	8.67	111.20	3.97,4.07	-	-	-	-	173.87	45.24	-	-	-	-	
-7	Ser	8.27	115.36	4.42	3.80,3.80	-	-	-	174.46	58.25	64.06	-	-	-	
-1	His	-	-	4.41	3.12,3.12	-	-	-	175.07	56.59	28.85	-	-	-	
0	Gly	8.52	111.90	3.66,3.98	-	-	-	-	173.79	45.27	-	-	-	-	
1	Ser	7.74	116.66	4.71	3.74,3.64	-	-	-	171.97	56.46	63.06	-	-	-	
2	Pro	-	-	3.94	1.40,1.83	1.91,1.91	3.75,3.58		-	176.23	62.44	31.83	27.10	50.43	-
3	Tyr	8.24	121.27	4.44	2.71,2.71	-	6.43	6.45	175.36	58.34	38.66	-	133.20	117.88	
4	Asn	10.52	124.32	5.45	3.08,2.60	-	7.32,6.78		-	176.84	52.98	40.01	-	-	- 111.31:Nd2
5	Val	9.87	125.32	5.52	2.02	0.86,1.20	-	-	175.07	60.79	35.55	21.72,24.13	-	-	
6	Met	8.83	127.22	5.57	1.93,1.80	2.03,2.07	-	-	173.97	53.23	37.90	31.29	-	-	
7	Ile	8.11	126.27	4.51	1.68	0.86,0.83,1.71	0.94		-	173.64	60.93	41.19	18.05,27.52	15.72	-
8	Val	9.03	128.77	4.83	2.08	0.47,0.33	-	-	173.47	60.00	32.55	21.07,21.17	-	-	
9	Asp	8.07	123.70	4.63	2.40,2.25	-	-	-	175.05	55.67	43.84	-	-	-	
10	Asp	9.01	124.51	4.87	2.87,2.93	-	-	-	175.42	55.78	41.03	-	-	-	
11	Ala	10.00	127.29	4.68	1.39	-	-	-	177.22	50.78	18.32	-	-	-	
12	Ala	9.15	131.79	3.78	1.50	-	-	-	180.44	56.13	18.25	-	-	-	
13	Met	9.11	114.35	4.25	2.12,1.94	2.64,2.53	-	-	178.77	57.99	31.81	32.34	-	-	
14	Met	6.92	118.29	4.68	2.20,2.06	2.65,2.39	-	-	178.35	56.05	30.81	31.70	-	-	
15	Arg	8.06	118.49	3.76	2.00,1.84	-	2.94,2.94		-	177.97	61.69	29.97	-	43.53	-
16	Leu	7.87	117.21	4.14	1.75,1.74	-	0.92,0.92		-	179.84	58.08	41.79	-	24.10	-
17	Tyr	8.23	121.84	4.30	3.33,3.17	-	7.01	6.61	179.02	61.10	38.30	-	132.64	118.00	
18	Ile	8.74	119.44	3.54	1.89	0.85,0.83,2.08	0.75		-	177.83	65.63	37.46	18.18,29.89	13.24	-
19	Ala	8.81	122.62	3.85	1.49	-	-	-	180.37	56.33	17.68	-	-	-	
20	Ser	8.50	115.10	4.04	3.98,3.94	-	-	-	175.97	62.02	63.18	-	-	-	
21	Phe	7.87	123.09	4.40	3.10,3.17	-	-	-	178.62	60.53	38.95	-	-	-	
22	Ile	8.65	121.91	3.24	1.79	0.84,1.88,0.86	0.63		-	177.34	64.65	36.54	18.46,29.82	13.98	-
23	Lys	7.69	119.37	4.15	1.98,2.03	-	1.73,1.73	2.99,2.99	177.41	58.88	32.41	25.31	29.38	42.19	

24	Thr	7.50	107.81	4.28	4.37	1.30	-	-	173.98	62.68	69.69	21.12	-	-					
25	Leu	8.03	124.73	4.86	1.69,2.37	1.45	0.63,0.55	-	174.92	51.47	41.19	25.89	21.93,26.62	-					
26	Pro	-	-	4.50	2.31,1.97	2.06	3.68,4.04	-	177.20	64.38	31.93	27.01	50.57	-					
27	Asp	10.56	112.49	4.22	2.55,2.66	-	-	-	174.17	52.63	37.06	-	-	-					
28	Phe	7.71	116.06	5.49	2.84,2.67	-	-	-	174.03	57.21	45.00	-	-	-					
29	Lys	9.08	120.21	4.57	1.80,1.64	1.16,1.34	1.64,1.64	2.93,2.93	175.02	55.39	36.21	24.44	29.24	42.04					
30	Val	9.28	126.95	4.43	2.16	0.99,0.98	-	-	176.79	63.40	31.47	21.56,23.67	-	-					
31	Val	9.11	120.15	4.71	2.38	0.90,0.75	-	-	175.25	60.43	33.04	18.47,21.61	-	-					
32	Ala	7.59	121.06	4.77	1.32	-	-	-	174.85	52.17	22.84	-	-	-					
33	Gln	8.70	119.08	5.41	1.97,1.85	2.30,2.05	-	6.48,7.23	173.50	54.25	33.42	34.27	-	-	109.73:Ne2				
34	Ala	8.89	121.85	4.73	1.30	-	-	-	174.95	50.57	23.35	-	-	-					
35	Ala	8.80	121.05	4.68	1.43	-	-	-	176.03	51.38	21.28	-	-	-					
36	Asn	7.26	105.48	5.60	3.32,3.19	-	-	-	176.27	53.11	40.48	-	-	-					
37	Gly	8.63	103.64	3.98,3.98	-	-	-	-	173.57	47.66	-	-	-	-					
38	Gln	8.28	123.56	-	-	-	-	6.73,7.54	-	-	-	-	-	-	115.40:Ne2				
39	Glu	8.37	120.56	4.15	2.06,1.99	2.57,2.23	-	-	178.89	58.78	30.52	36.32	-	-					
40	Ala	7.77	118.78	3.77	1.23	-	-	-	178.65	55.48	20.12	-	-	-					
41	Leu	8.08	119.77	4.04	1.51,2.10	2.15	0.53,0.68	-	179.95	58.44	41.31	26.47	22.75,26.38	-					
42	Asp	8.29	121.18	4.38	2.68,2.92	-	-	-	179.84	57.50	39.81	-	-	-					
43	Lys	8.45	120.99	4.17	1.93,1.70	-	-	-	178.99	59.34	32.60	26.51	-	-					
44	Leu	8.37	120.58	4.02	1.82,1.68	-	0.94,0.91	-	178.56	57.08	42.48	-	24.40,23.48	-					
45	Ala	7.57	119.08	4.13	1.51	-	-	-	178.89	54.29	18.11	-	-	-					
46	Ala	7.15	117.88	4.38	1.52	-	-	-	177.41	52.85	19.82	-	-	-					
47	Gln	7.84	118.43	4.76	1.88,2.09	2.20,2.28	-	7.69,6.71	171.67	53.10	29.53	34.07	-	-	110.70:Ne2				
48	Pro	-	-	4.68	2.04,2.38	1.99,1.87	3.66,3.39	-	178.07	63.74	32.20	26.81	50.02	-					
49	Asn	8.41	118.67	4.74	2.80,2.79	-	7.59,6.88	-	174.02	52.85	36.74	-	-	-	112.21:Nd2				
50	Val	7.61	121.50	3.62	1.82	0.86,0.79	-	-	174.10	63.60	34.12	22.28,23.09	-	-					
51	Asp	8.96	124.15	4.99	2.85,2.94	-	-	-	175.77	56.41	44.54	-	-	-					
52	Leu	8.05	122.27	5.23	1.63,1.64	1.33	0.78,0.75	-	173.03	53.79	45.18	27.70	27.59,23.91	-					
53	Ile	9.33	126.82	4.76	1.76	1.57,0.63	0.91	-	174.31	60.08	40.41	17.72,28.17	13.91	-					
54	Leu	8.74	128.32	5.12	1.22,1.81	1.49	0.82,0.75	-	173.86	53.12	42.36	26.85	22.97,26.49	-					
55	Leu	8.69	127.61	4.64	0.73,1.94	1.58	0.31,0.98	-	173.75	53.67	47.61	26.08	23.44,28.65	-					
56	Asp	8.62	128.43	4.86	3.03,3.27	-	-	-	174.50	54.59	43.29	-	-	-					
57	Ile	7.59	120.28	3.66	1.89	0.72	0.84	-	-	65.99	38.41	17.64	13.13	-					
58	Glu	8.17	118.27	4.61	1.95,2.29	2.28,2.28	-	-	-	57.22	28.24	35.54	-	-					

59	Met	7.26	125.86	-	-	-	-	-	-	54.04	38.34	-	-	-
60	Pro	-	-	4.52	2.38,2.07	-	-	-	-	62.34	32.78	-	-	-
61	Val	8.53	112.35	3.12	2.61	0.91,0.91	-	-	177.65	69.47	30.06	21.31,21.29	-	-
62	Met	9.39	122.81	4.37	2.24,1.64	2.64,2.60	-	-	174.53	56.48	35.50	31.29	-	-
63	Asp	8.89	128.44	4.57	3.93,3.00	-	-	-	175.53	53.54	40.55	-	-	-
64	Gly	9.21	104.47	4.12,3.67	-	-	-	-	175.70	47.61	-	-	-	-
65	Met	7.92	118.84	4.27	2.39,1.92	2.47,2.66	-	-	178.64	57.58	30.49	33.33	-	-
66	Glu	8.64	120.90	4.10	2.00,2.19	2.43,2.56	-	-	179.65	58.70	29.28	36.01	-	-
67	Phe	8.51	119.65	4.22	3.34,2.84	-	-	-	177.03	62.74	38.82	-	-	-
68	Leu	8.06	119.87	3.69	1.65,2.15	2.01	1.03,0.88	-	178.50	58.65	42.25	26.86	26.08,24.51	-
69	Arg	7.48	115.98	3.99	1.83,1.73	1.80,1.50	3.16,3.16	-	178.34	59.15	30.13	27.93	43.54	-
70	His	7.46	114.29	4.43	2.84,3.09	-	-	-	176.97	57.37	30.90	-	-	-
71	Ala	8.65	121.37	3.58	0.56	-	-	-	179.02	54.80	19.24	-	-	-
72	Lys	7.81	115.79	4.14	1.93,1.88	1.60,1.60	-	-	177.42	58.24	31.14	24.27	27.90	-
73	Leu	7.54	115.12	4.33	1.77,1.70	-	0.93,0.87	-	177.98	55.66	41.99	26.98	24.85,23.07	-
74	Lys	7.79	116.71	4.48	1.93,1.62	1.40,1.40	1.61,1.61	2.98,2.97	175.65	55.85	34.85	24.48	28.54	41.89
75	Thr	7.82	113.41	4.80	4.14	1.11	-	-	172.19	60.22	69.60	18.57	-	-
76	Arg	8.59	125.27	4.60	2.10,1.77	1.70,1.70	3.20,3.20	-	176.34	55.27	29.83	26.84	43.17	-
77	Ala	8.52	125.21	4.06	1.15	-	-	-	177.80	53.20	19.33	-	-	-
78	Lys	7.54	118.35	4.54	1.78,1.40	1.57,1.57	-	3.11,3.11	176.42	54.67	33.94	24.92	-	-
79	Ile	9.98	121.88	4.73	1.72	0.85	0.81	-	174.33	61.00	41.00	19.10,27.75	13.80	-
80	Cys	9.23	128.98	4.84	1.80,2.93	-	-	-	173.49	56.37	28.58	-	-	-
81	Met	8.99	126.83	5.47	2.03,2.03	2.45,2.55	-	-	175.46	54.18	32.24	33.01	-	-
82	Leu	8.52	122.21	5.08	1.83,1.08	1.50	0.68,0.78	-	175.17	52.48	44.10	26.05	23.16,26.08	-
83	Ser	8.80	114.58	4.85	3.46,3.67	-	-	-	175.74	56.17	64.99	-	-	-
84	Ser	9.54	125.03	4.54	3.98,4.07	-	-	-	173.38	60.14	63.62	-	-	-
85	Val	7.50	114.23	4.51	2.20	0.84,0.92	-	-	175.77	59.74	34.63	18.49,21.24	-	-
86	Ala	8.51	125.83	4.30	1.37	-	-	-	177.80	52.90	18.41	-	-	-
87	Val	8.34	120.16	3.58	2.03	0.90,0.93	-	-	178.00	65.55	32.10	21.74,22.52	-	-
88	Ser	8.39	115.85	4.21	3.88,3.86	-	-	-	175.36	59.81	62.49	-	-	-
89	Gly	8.21	111.58	3.94,4.07	-	-	-	-	174.18	45.08	-	-	-	-
90	Ser	7.64	115.58	4.77	3.98,3.98	-	-	-	174.99	55.47	63.76	-	-	-
91	Pro	-	-	4.51	1.72,2.29	1.98	4.04	-	178.02	64.36	31.86	26.71	50.95	-
92	His	7.93	116.62	4.61	2.93,3.22	-	-	-	176.33	57.34	31.21	-	-	-
93	Ala	7.61	121.98	4.02	1.51	-	-	-	178.39	55.65	19.03	-	-	-
94	Ala	7.98	119.76	4.11	1.46	-	-	-	180.47	55.20	17.93	-	-	-
95	Arg	8.12	119.74	4.14	1.94,1.94	-	3.34,3.18	-	177.82	57.92	29.98	-	43.22	-
96	Ala	8.33	120.16	3.91	1.41	-	-	-	179.60	55.19	17.65	-	-	-

97	Arg	7.82	116.59	4.27	1.93,1.98	1.84,1.83	3.19,3.19	-	180.25	59.13	29.39	27.44	42.66	-				
98	Glu	8.04	121.75	4.06	2.19,2.27	2.43,2.30	-	-	178.57	59.23	29.42	36.07	-	-				
99	Leu	7.78	117.69	4.27	1.64,1.89	1.77	0.90,0.86	-	176.57	55.19	43.37	-	22.60,26.02	-				
100	Gly	7.61	104.26	3.74,4.42	-	-	-	-	174.68	45.19	-	-	-	-				
101	Ala	8.47	122.86	4.11	1.31	-	-	-	176.76	53.30	18.98	-	-	-				
102	Asp	8.76	120.12	4.65	2.38,2.75	-	-	-	175.59	56.13	43.82	-	-	-				
103	Gly	7.77	103.25	3.73,4.34	-	-	-	-	171.06	45.26	-	-	-	-				
104	Val	8.55	120.70	4.76	1.97	0.84,0.84	-	-	173.23	61.71	34.82	20.98,20.98	-	-				
105	Val	8.82	123.46	4.51	1.92	0.78,0.82	-	-	173.02	59.30	35.85	21.09,21.09	-	-				
106	Ala	8.43	126.97	4.64	1.31	-	-	-	177.31	51.81	18.89	-	-	-				
107	Lys	8.42	121.34	-	-	-	-	-	176.33	54.93	-	-	-	-				
108	Pro	-	-	4.42	1.83,2.15	1.70,1.70	3.49,3.66	-	174.85	62.96	32.07	27.57	49.79	-				
109	Ser	8.30	114.57	4.29	3.75,3.84	-	-	-	-	58.01	64.51	-	-	-				
110	Gly	8.11	109.96	3.66,3.77	-	-	-	-	174.02	45.08	-	-	-	-				
111	Thr	8.01	112.55	4.27	4.19	1.10	-	-	174.78	61.68	69.53	21.40	-	-				
112	Val	7.95	120.72	4.14	2.10	0.90,0.89	-	-	175.88	62.43	32.65	21.01,19.94	-	-				
113	Ser	8.20	117.74	4.42	3.99,3.86	-	-	-	174.68	58.12	63.93	-	-	-				
114	His	8.62	120.25	4.60	3.30,3.33	-	-	-	174.93	57.13	28.43	-	-	-				
115	Asp	8.39	118.99	4.49	2.61,2.72	-	-	-	177.10	55.64	41.08	-	-	-				
116	Leu	8.11	121.29	4.21	1.60,1.51	-	0.75,0.79	-	178.13	56.34	41.69	26.97	25.04,23.42	-				
117	Glu	8.35	121.65	-	-	-	-	-	178.50	58.10	29.76	36.07	-	-				
118	Glu	8.35	120.93	4.24	-	-	-	-	-	-	29.75	36.07	-	-				
119	Lys	8.37	120.56	4.26	1.93,1.82	1.46,1.46	-	2.99,2.99	178.54	58.68	32.75	24.88	29.17	42.31				
120	Thr	8.25	113.84	4.17	4.16	1.16	-	-	176.70	64.43	69.10	21.86	-	-				
121	Gly	8.32	111.27	3.51,3.35	-	-	-	-	174.98	46.55	-	-	-	-				
122	Gly	8.15	108.94	3.93,4.02	-	-	-	-	176.30	47.24	-	-	-	-				
123	Glu	8.18	122.20	4.18	2.08,2.10	2.29,2.29	-	-	179.21	58.93	29.46	36.16	-	-				
124	Leu	8.29	123.75	4.01	1.88,1.47	-	0.76,0.69	-	177.89	59.47	40.87	-	23.22,25.66	-				
125	Ala	8.60	120.85	3.98	1.60	-	-	-	179.32	55.80	18.48	-	-	-				
126	Arg	8.17	116.39	4.08	1.93,1.98	1.58,1.79	3.25,3.25	-	179.85	59.87	30.44	27.18	43.25	-				
127	Thr	8.33	118.48	3.90	4.22	1.12	-	-	-	67.63	68.82	20.89	-	-				
128	Met	8.59	120.07	3.48	1.61,1.84	2.72,1.88	-	-	177.54	60.98	33.99	30.62	-	-				
129	Arg	8.23	116.08	3.94	1.99,1.95	-	-	-	179.67	61.04	29.73	-	43.26	-				
130	Thr	8.48	117.99	4.00	4.36	1.30	-	-	177.14	66.70	68.84	21.50	-	-				
131	Leu	8.18	121.03	4.10	1.86,1.12	1.94	0.70,0.59	-	178.55	57.66	41.82	26.76	25.43,23.97	-				
132	Met	7.22	113.03	4.35	1.68,1.26	2.75,2.74	-	-	176.51	54.52	31.94	-	-	-				
133	Ala	7.38	121.71	4.32	1.48	-	-	-	176.58	52.69	19.20	-	-	-				
134	Ala	7.46	127.66	4.14	1.41	-	-	-	182.66	54.13	20.10	-	-	-				

Chemical Shifts – $CheY_6$-BeF_3^- pH 5.5

		H	N	HA	HB	HG	HD	HE	C	CA	CB	CG	CD	CE	
-9	Arg	-	-	4.39	1.83,1.83	-	-	-	176.44	56.69	30.87	27.09	43.37	-	
-8	Gly	8.67	111.20	4.00,4.00	-	-	-	-	173.89	45.20	-	-	-	-	
-7	Ser	8.27	115.29	4.42	3.80,3.80	-	-	-	174.47	58.21	64.00	-	-	-	
-1	His	-	-	4.41	3.09,3.09	-	-	-	-	56.67	29.02	-	-	-	
0	Gly	8.52	112.00	3.95,3.64	-	-	-	-	173.82	45.21	-	-	-	-	
1	Ser	7.75	116.64	4.70	3.63,3.72	-	-	-	171.99	56.48	63.09	-	-	-	
2	Pro	-	-	3.93	1.86,1.39	1.91	3.58,3.74	-	176.23	62.38	31.92	27.21	50.47	-	
3	Tyr	8.27	121.29	4.41	2.68,2.70	-	6.44	-	175.37	58.38	38.69	-	-	-	
4	Asn	10.51	124.20	5.41	3.07,2.58	-	6.78,7.32	-	176.84	53.06	40.08	-	-	-	111.28:Nd2
5	Val	9.86	125.37	5.53	2.00	1.19,0.86	-	-	175.22	60.87	35.56	24.18,21.71	-	-	
6	Met	8.84	127.39	5.52	1.95,1.77	2.00,2.09	-	-	173.73	53.31	37.85	31.34	-	-	
7	Ile	8.10	126.66	4.42	1.68	0.95,1.68,0.89	0.90	-	173.93	61.07	41.54	17.73,27.44	15.74	-	
8	Val	8.76	128.24	4.81	2.13	0.26,0.46	-	-	173.70	60.19	32.53	21.09,21.35	-	-	
9	Asp	8.15	123.64	4.58	2.61,2.24	-	-	-	174.85	55.60	43.78	-	-	-	
10	Asp	9.18	124.46	4.86	2.82,2.82	-	-	-	175.53	55.81	40.88	-	-	-	
11	Ala	9.87	127.03	4.64	1.35	-	-	-	177.25	50.87	18.32	-	-	-	
12	Ala	9.14	131.80	3.73	1.47	-	-	-	180.70	56.15	18.41	-	-	-	
13	Met	9.13	114.79	4.18	1.84,2.02	2.58,2.50	-	-	178.17	57.42	31.69	31.69	-	-	
14	Met	6.79	117.11	4.59	2.08,2.24	-	-	-	178.33	56.37	32.08	-	-	-	
15	Arg	8.10	117.33	3.81	2.02,1.76	2.01,1.03	2.88,2.88	-	177.96	61.75	29.82	29.31	43.45	-	
16	Leu	7.63	118.04	4.12	1.70,1.70	-	0.87,0.85	-	180.01	58.30	41.47	-	24.16,24.16	-	
17	Tyr	8.17	121.20	4.46	3.21,3.21	-	7.07	-	179.68	60.46	37.75	-	-	-	
18	Ile	8.90	120.93	3.57	1.86	0.83,0.81,1.92	0.80	-	177.91	65.50	37.87	18.77,29.40	14.31	-	
19	Ala	8.90	122.86	3.86	1.47	-	-	-	180.65	56.29	17.67	-	-	-	
20	Ser	8.64	114.96	4.15	4.01,4.01	-	-	-	176.09	62.15	63.34	-	-	-	
21	Phe	7.87	122.95	4.48	3.18,3.10	-	7.05	-	178.58	60.43	38.90	-	-	-	
22	Ile	8.75	122.34	3.17	1.79	0.94,0.82,1.79	0.61	-	177.57	64.56	36.27	29.71,18.37	13.51	-	
23	Lys	7.71	119.42	4.13	2.00,2.00	1.61,1.61	1.72,1.72	3.00,3.00	177.50	58.92	32.41	25.35	29.56	42.22	
24	Thr	7.53	108.15	4.26	4.37	1.34	-	-	173.94	62.84	69.94	21.39	-	-	
25	Leu	8.00	124.68	4.86	2.35,1.66	1.36	0.47,0.59	-	174.81	51.37	41.23	25.75	26.64,22.06	-	
26	Pro	-	-	4.47	2.31,1.93	2.04,2.04	4.05,3.67	-	177.15	64.45	31.92	-	50.61	-	
27	Asp	10.61	112.30	4.20	2.57,2.55	-	-	-	174.15	52.61	37.03	-	-	-	
28	Phe	7.73	116.28	5.48	2.83,2.66	-	-	-	174.06	57.25	44.90	-	-	-	
29	Lys	9.08	120.16	4.57	1.62,1.77	1.16,1.31	1.62,1.62	2.91,2.91	174.99	55.32	36.32	24.48	29.45	42.10	

30	Val	9.22	126.75	4.41	2.14	0.99,0.96	-	-	176.93	63.46	31.71	23.81,21.50	-	-							
31	Val	9.16	119.99	4.71	2.37	0.75,0.89	-	-	175.26	60.38	33.11	21.63,18.54	-	-							
32	Ala	7.61	121.35	4.73	1.30	-	-	-	174.85	52.07	22.84	-	-	-							
33	Gln	8.68	118.80	5.40	1.87,1.85	2.30,2.09	-	7.25,6.53	173.51	54.35	33.21	34.19	-	-	109.83:Ne2						
34	Ala	9.01	122.24	4.70	1.28	-	-	-	174.97	50.58	23.47	-	-	-							
35	Ala	8.77	121.01	4.71	1.42	-	-	-	176.10	51.18	21.23	-	-	-							
36	Asn	7.27	105.53	5.57	3.26,3.26	-	-	-	176.21	53.14	40.57	-	-	-							
37	Gly	8.58	103.35	3.45,3.57	-	-	-	-	173.60	47.68	-	-	-	-							
38	Gln	8.28	123.59	4.04	2.22,2.22	2.19,2.34	-	7.55,6.72	177.77	58.24	29.14	33.85	-	-	115.50:Ne2						
39	Glu	8.41	120.63	4.13	1.97,1.97	2.55,2.24	-	-	178.81	58.79	30.56	36.34	-	-							
40	Ala	7.74	118.86	3.76	1.17	-	-	-	178.69	55.47	20.27	-	-	-							
41	Leu	8.07	119.76	4.05	2.09,1.51	2.18	0.56,0.68	-	179.99	58.55	41.37	26.51	22.74,26.39	-							
42	Asp	8.36	121.30	4.36	2.67,2.90	-	-	-	179.88	57.54	39.84	-	-	-							
43	Lys	8.48	121.10	4.11	1.71,1.93	-	-	-	179.00	59.41	32.52	26.55	29.43	-							
44	Leu	8.36	120.89	4.00	1.83,1.64	1.81	0.94,0.91	-	178.60	57.13	42.52	26.65	23.50,24.86	-							
45	Ala	7.57	119.07	4.12	1.50	-	-	-	178.91	54.28	18.16	-	-	-							
46	Ala	7.15	117.97	4.37	1.51	-	-	-	177.44	52.85	19.90	-	-	-							
47	Gln	7.88	118.51	4.76	1.87,2.09	2.25,2.19	-	7.69,6.71	171.68	53.06	29.58	34.16	-	-	110.61:Ne2						
48	Pro	-	-	4.68	2.36,2.02	1.86,2.00	3.66,3.38	-	178.07	63.75	32.18	26.82	50.09	-							
49	Asn	8.41	118.66	4.71	2.78,2.78	-	7.58,6.87	-	174.03	52.85	36.74	-	-	-	111.93:Nd2						
50	Val	7.61	121.46	3.60	1.80	0.86,0.78	-	-	174.18	63.67	34.11	22.64,23.19	-	-							
51	Asp	8.96	124.28	4.96	2.87,2.87	-	-	-	175.82	56.41	44.49	-	-	-							
52	Leu	8.10	122.49	5.24	1.60,1.60	1.35	0.78,0.75	-	173.03	53.83	45.23	28.03	27.85,24.25	-							
53	Ile	9.30	127.09	4.78	1.76	0.67,1.57,1.57	0.92	-	174.34	60.01	40.58	17.90,28.18	14.10	-							
54	Leu	8.71	129.27	5.15	1.48,1.72	1.45	0.78,0.80	-	174.82	53.59	42.68	27.17	26.39,23.52	-							
55	Leu	8.71	127.85	4.72	2.02,0.71	1.81	0.42,1.03	-	174.04	54.21	47.95	25.91	23.78,28.49	-							
56	Asp	8.22	127.67	5.09	3.57,3.03	-	-	-	174.49	53.13	43.77	-	-	-							
57	Ile	7.36	115.89	3.89	1.74	0.67,1.73,0.80	0.77	-	176.80	65.43	38.47	17.60,30.50	13.53	-							
58	Glu	8.77	118.13	4.39	2.00,2.26	2.11	-	-	173.46	57.54	27.75	35.99	-	-							
59	Met	7.37	128.18	4.63	2.10	3.11	-	-	171.98	54.04	38.10	33.69	-	-							
60	Pro	-	-	4.52	2.05,2.36	-	-	-	-	62.40	32.70	-	-	-							
61	Val	8.53	112.04	3.10	2.60	0.88,0.89	-	-	177.70	69.56	30.08	21.39,21.40	-	-							
62	Met	9.47	123.06	4.37	2.24,1.62	2.58,2.67	-	-	174.43	56.46	35.70	31.23	-	-							
63	Asp	8.89	128.72	4.61	2.89,3.94	-	-	-	176.06	53.76	40.86	-	-	-							
64	Gly	9.93	104.48	4.33,3.71	-	-	-	-	175.82	47.38	-	-	-	-							
65	Met	7.93	117.97	4.29	1.90,2.44	2.56,2.71	-	-	178.65	57.20	30.73	33.58	-	-							
66	Glu	8.57	120.90	4.08	1.99,2.16	2.56,2.56	-	-	179.70	58.83	29.13	35.90	-	-							
67	Phe	8.58	119.36	4.21	2.84,3.29	-	-	-	176.95	62.86	38.86	-	-	-							

68	Leu	8.02	120.47	3.63	1.60,2.18	1.99	1.03,0.85	-	178.47	58.82	42.37	27.09	26.02,24.75	-	
69	Arg	7.46	115.65	3.98	1.68,1.80	1.82,1.48	3.14,3.14	-	178.38	59.35	30.08	28.30	43.69	-	
70	His	7.46	114.19	4.42	2.83,3.06	-	-	-	177.18	57.47	31.12	-	-	-	
71	Ala	8.79	121.44	3.51	0.49	-	-	-	179.18	55.04	19.04	-	-	-	
72	Lys	7.76	115.19	4.12	1.88,1.88	-	-	-	177.46	58.03	30.90	24.69	27.76	-	
73	Leu	7.45	115.02	4.33	1.71	-	0.93,0.86	-	178.02	55.76	42.05	27.11	25.05,23.36	-	
74	Lys	7.75	116.63	4.47	1.60,1.92	1.39,1.39	1.61,1.61	2.97,2.97	175.63	55.99	34.94	24.62	28.63	42.07	
75	Thr	7.84	113.50	4.80	4.11	1.09	-	-	172.18	60.18	69.63	18.70	-	-	
76	Arg	8.59	125.22	4.58	1.76,2.08	1.69,1.69	3.19,3.19	-	176.44	55.30	29.86	26.98	43.22	-	
77	Ala	8.54	125.42	4.04	1.14	-	-	-	177.76	53.28	19.24	-	-	-	
78	Lys	7.51	118.14	4.53	1.40,1.75	1.56,1.56	-	-	176.38	54.44	33.79	24.78	-	-	
79	Ile	9.95	121.71	4.73	1.65	0.86	0.83	-	174.37	61.06	41.17	27.81,19.10	13.89	-	
80	Cys	9.33	129.18	4.83	1.75,2.97	-	-	-	173.60	56.14	28.75	-	-	-	
81	Met	8.92	126.77	5.44	2.02,2.02	2.36,2.69	-	-	175.94	53.96	30.62	33.37	-	-	
82	Leu	8.38	125.68	5.37	1.07,1.62	1.28	0.78,0.62	-	175.03	53.72	42.95	27.52	25.81,23.77	-	
83	Ser	7.95	114.37	5.32	3.97,3.39	-	-	-	175.94	56.01	65.55	-	-	-	
84	Ser	9.39	125.11	4.46	4.00,3.88	-	-	-	174.62	60.97	63.18	-	-	-	
85	Val	7.97	113.42	4.45	2.14	0.60,0.79	-	-	176.17	61.00	32.24	18.93,21.03	-	-	
86	Ala	7.19	124.96	4.43	1.10	-	-	-	175.34	51.13	17.63	-	-	-	
87	Val	7.39	115.73	4.01	2.15	0.93,0.91	-	-	177.25	61.85	33.15	19.66,21.14	-	-	
88	Ser	8.76	119.23	4.11	3.86,3.86	-	-	-	175.96	60.41	62.53	-	-	-	
89	Gly	8.80	113.90	3.83,4.14	-	-	-	-	174.34	45.51	-	-	-	-	
90	Ser	8.04	115.73	-	-	-	-	-	174.84	-	64.43	-	-	-	
91	Pro	-	-	4.47	2.31,1.75	1.87	3.95	-	179.01	64.62	31.77	27.77	51.06	-	
92	His	8.01	115.68	4.34	2.92,2.92	-	-	-	177.35	59.22	30.89	-	-	-	
93	Ala	7.83	121.04	3.86	1.42	-	-	-	178.54	55.57	18.62	-	-	-	
94	Ala	7.62	119.41	4.07	1.47	-	-	-	180.70	55.07	17.89	-	-	-	
95	Arg	8.31	119.69	4.09	1.90,1.90	-	3.13,3.28	-	177.90	58.23	29.95	26.88	43.29	-	
96	Ala	8.19	119.72	3.92	1.39	-	-	-	179.67	55.28	16.88	-	-	-	
97	Arg	7.72	115.95	4.23	1.91,1.91	1.49,1.86	3.16	-	180.37	59.52	29.42	27.97	42.91	-	
98	Glu	8.18	122.39	4.02	2.15,2.27	-	-	-	178.70	59.30	29.51	36.07	-	-	
99	Leu	7.81	117.51	4.23	1.90,1.61	-	0.91,0.83	-	176.52	55.22	43.46	-	22.56,26.35	-	
100	Gly	7.58	104.05	3.70,4.42	-	-	-	-	174.65	45.14	-	-	-	-	
101	Ala	8.56	123.08	4.01	1.26	-	-	-	176.87	53.72	18.65	-	-	-	
102	Asp	8.81	120.77	4.64	2.74,2.38	-	-	-	175.61	56.08	44.08	-	-	-	
103	Gly	7.88	103.53	4.41,3.63	-	-	-	-	171.32	45.00	-	-	-	-	
104	Val	8.78	121.13	4.38	1.98	0.78,0.78	-	-	173.15	62.67	35.60	21.61,21.61	-	-	171.31:789
105	Val	8.75	128.01	4.18	1.83	0.76,0.75	-	-	173.48	60.81	35.02	21.69,21.78	-	-	

106	Ala	8.57	128.70	4.78	1.27	-	-	-	178.31	51.05	19.30	-	-	-				
107	Lys	7.31	121.28	4.05	1.20,1.92	1.15	-	2.79	174.97	54.90	33.44	27.54	-	42.18				
108	Pro	-	-	4.40	2.17,1.83	-	3.39,3.69	-	176.54	63.18	32.02	-	50.06	-				
109	Ser	8.32	115.64	4.45	3.86,3.83	-	-	-	174.55	57.84	63.92	-	-	-				
110	Gly	8.30	109.81	3.81,4.12		-	-	-	174.40	44.77	-	-	-	-				
111	Thr	8.26	113.27	4.16	4.22	1.19	-	-	175.07	62.94	69.38	21.57	-	-				
112	Val	8.06	121.22	4.11	2.07	0.87,0.87	-	-	175.68	61.97	32.29	20.91,20.91		-	-			
113	Ser	7.98	119.91	4.42	3.80,3.79	-	-	-	-	57.86	64.36	-	-	-				
114	His	8.48	120.57	4.17	3.14,3.15	-	-	-	174.16	56.59	28.65	-	-	-				
115	Asp	8.18	118.62	4.39	2.46,2.59	-	-	-	176.23	54.23	40.33	-	-	-				
118	Glu	-	-	-	-	-	-	-	-	59.14	30.02	-	-	-				
119	Lys	8.42	118.58	4.24	1.87,1.87	1.45,1.45	1.66,1.66	2.97,2.97	-	58.62	32.87	25.19	29.16	42.29				
120	Thr	8.06	114.90	4.23	3.93	1.14	-	-	175.77	64.30	69.54	22.46	-	-				
121	Gly	8.18	111.03	3.15,3.57		-	-	-	175.15	47.35	-	-	-	-				
122	Gly	8.26	108.56	3.92,3.92		-	-	-	176.31	51.11	-	-	-	-				
123	Glu	8.10	123.10	4.12	2.07,2.07	2.24,2.24	-	-	179.38	58.89	29.63	36.18	-	-				
124	Leu	8.79	123.36	4.00	1.32,1.84	1.61	0.78,0.66	-	177.78	58.70	41.53	27.13	23.11,25.71		-			
125	Ala	8.89	120.96	4.01	1.60	-	-	-	179.38	55.86	18.43	-	-	-				
126	Arg	8.03	116.20	4.09	1.96,1.96	1.76	3.25,3.25	-	179.82	59.83	30.37	26.95	43.33	-				
127	Thr	8.41	118.75	3.88	4.21	1.12	-	-	-	67.68	68.85	20.73	-	-				
128	Met	8.77	120.31	3.45	1.81,1.62	1.90,2.70	-	-	177.62	60.95	34.09	30.58	-	-				
129	Arg	8.21	115.83	3.91	1.97,1.97	-	3.25,3.11	-	179.68	61.03	29.69	-	43.31	-				
130	Thr	8.49	118.38	3.99	4.35	1.28	-	-	177.12	66.80	68.85	21.56	-	-				
131	Leu	8.18	121.14	4.07	1.89,1.11	1.95	0.69,0.60	-	178.50	57.61	41.66	27.09	24.14,25.14		-			
132	Met	7.22	113.25	4.33	1.66,1.21	2.70,2.70	-	-	176.45	54.60	32.58	31.67	-	-				
133	Ala	7.38	121.79	4.29	1.46	-	-	-	176.70	52.75	19.20	-	-	-				
134	Ala	7.47	127.67	4.13	1.40	-	-	-	182.64	54.08	20.13	-	-	-				

Chemical Shifts – $CheY_6$ pH 5.5 (minor conformation)

		H	N	HA	HB	HG	HD	C	CA	CB	CG	CD
2	Pro	-	-	4.14	2.03,1.51	1.77,1.77	3.41,3.41	174.80	61.10	34.41	24.38	50.60
3	Tyr	8.14	121.03	4.68	2.67,2.87	-	-	175.18	57.28	38.93	-	-
4	Asn	10.46	124.41	-	-	-	-	176.84	53.03	39.90	-	-
27	Asp	-	-	4.24	-	-	-	-	-	-	-	-
28	Phe	7.67	115.80	-	-	-	-	174.19	57.06	44.93	-	-
29	Lys	8.98	119.76	-	-	-	-	175.22	55.15	36.06	-	-
30	Val	9.27	126.40	-	-	-	-	-	-	-	-	-
52	Leu	8.06	122.41	-	-	-	-	-	-	-	-	-
125	Ala	8.65	120.90	-	-	-	-	-	-	-	-	-
129	Arg	8.21	115.87	-	-	-	-	-	-	-	-	-
130	Thr	8.51	118.34	-	-	-	-	-	-	-	-	-
132	Met	7.26	113.44	-	-	-	-	-	-	33.04	-	-
133	Ala	7.37	121.89	-	-	-	-	-	-	-	-	-
134	Ala	7.43	127.38	4.06	1.34	-	-	-	-	-	-	-

Chemical Shifts – $CheY_6$ pH 7.2

		H	N	HA	HB	HG	HD	HE	C	CA	CB	CG	CD	CE
0	Gly	-	-	3.70,3.89	-	-	-	-	173.75	45.07	-	-	-	-
1	Ser	7.96	116.83	4.65	3.72,3.61	-	-	-	171.91	56.44	63.11	-	-	-
2	Pro	-	-	3.86	1.79,1.35	1.89,1.89	3.54,3.70	-	176.16	62.38	31.09	27.24	50.39	-
3	Tyr	8.17	121.02	4.45	2.72,2.67	-	-	-	175.42	58.18	38.78	-	-	-
4	Asn	10.57	124.07	5.41	3.06,2.57	-	7.34,6.78	-	176.88	53.07	40.07	-	-	- 111.55:Nd2
5	Val	9.87	125.16	5.50	1.99	1.19,0.84	-	-	175.14	60.79	35.52	21.76,24.30	-	-
6	Met	8.85	127.16	5.56	1.90,1.78	2.05,2.05	-	-	173.93	53.22	37.90	31.29	-	-
7	Ile	8.12	126.09	4.49	1.65	1.73,0.85,0.80	0.93	-	173.60	60.87	41.27	27.56,18.07	15.90	-
8	Val	9.05	128.68	4.80	2.06	0.30,0.45	-	-	173.39	59.90	32.70	21.26,21.30	-	-
9	Asp	8.07	123.53	4.59	2.22,2.38	-	-	-	175.09	55.71	43.94	-	-	-
10	Asp	9.03	124.38	4.83	2.80,2.88	-	-	-	175.38	55.78	41.10	-	-	-
11	Ala	10.03	127.20	4.65	1.37	-	-	-	177.20	50.77	18.36	-	-	-

12	Ala	9.15	131.64	3.75	1.48	-	-	-	180.53	56.04	18.32	-	-	-	
13	Met	9.13	114.28	4.24	2.09,1.92	2.62,2.53	-	-	178.65	57.87	31.73	32.28	-	-	
14	Met	6.91	118.14	4.65	2.03,2.20	2.63	-	-	178.45	55.92	30.72	31.79	-	-	
15	Arg	8.06	118.21	3.75	1.81,2.00	-	2.91,2.91	-	178.00	61.66	30.05	-	43.49	-	
16	Leu	7.88	117.09	4.13	1.76,1.71	-	0.90,0.90	-	179.86	58.08	41.84	-	24.13,24.13	-	
17	Tyr	8.27	121.67	4.26	3.32,3.16	-	-	-	179.06	61.17	38.45	-	-	-	
18	Ile	8.75	119.16	3.53	1.86	0.82,0.82,2.09	0.73	-	177.81	65.69	37.68	29.74,18.11	13.30	-	
19	Ala	8.84	122.56	3.85	1.47	-	-	-	180.45	56.31	17.64	-	-	-	
20	Ser	8.51	115.05	4.03	3.91,3.91	-	-	-	175.95	61.87	62.62	-	-	-	
21	Phe	7.89	122.89	4.34	2.98,3.03	-	-	-	178.62	60.38	38.94	-	-	-	
22	Ile	8.65	121.81	3.22	1.77	0.82,0.82,1.86	0.61	-	177.38	64.68	36.56	18.54,30.02	14.22	-	
23	Lys	7.70	119.38	4.13	2.02,1.95	1.64,1.56	1.71,1.71	2.98,2.98	177.44	58.84	32.48	25.54	29.63	42.24	
24	Thr	7.51	107.64	4.27	4.35	1.29	-	-	173.98	62.63	69.76	21.39	-	-	
25	Leu	8.02	124.49	4.84	1.69,2.33	1.43	0.53,0.60	-	174.93	51.44	41.19	25.79	26.65,21.93	-	
26	Pro	-	-	4.45	1.89,2.27	2.02	4.02,3.64	-	177.12	64.37	32.02	27.19	50.49	-	
27	Asp	10.63	112.04	4.12	2.51,2.40	-	-	-	174.08	52.54	37.14	-	-	-	
28	Phe	7.65	115.61	5.46	2.83,2.63	-	-	-	174.11	57.10	45.12	-	-	-	
29	Lys	9.13	120.08	4.56	1.61,1.77	1.31,1.15	1.63,1.63	2.91,2.91	174.98	55.39	36.36	24.54	29.43	42.12	
30	Val	9.27	126.71	4.40	2.13	0.95,0.98	-	-	176.85	63.39	31.51	23.83,21.72	-	-	
31	Val	9.15	119.95	4.69	2.36	0.89,0.74	-	-	175.21	60.41	33.05	18.60,21.75	-	-	
32	Ala	7.61	121.03	4.73	1.30	-	-	-	174.87	52.15	22.78	-	-	-	
33	Gln	8.70	118.93	5.39	1.93,1.82	2.04,2.29	-	7.25,6.49	173.50	54.34	33.29	34.35	-	-	109.77:Ne2
34	Ala	8.90	121.75	4.71	1.28	-	-	-	174.94	50.54	23.44	-	-	-	
35	Ala	8.80	120.86	4.65	1.42	-	-	-	176.05	51.29	21.24	-	-	-	
36	Asn	7.27	105.37	5.59	3.22,3.29	-	-	-	176.26	53.13	40.54	-	-	-	
37	Gly	8.63	103.58	3.92,4.00	-	-	-	-	173.54	47.72	-	-	-	-	
38	Gln	8.27	123.36	4.03	2.19,2.22	2.30,2.25	-	7.53,6.75	177.90	58.32	28.97	33.94	-	-	115.28:Ne2
39	Glu	8.38	120.48	4.13	1.95,2.02	2.55,2.22	-	-	178.96	58.87	30.56	36.36	-	-	
40	Ala	7.77	118.81	3.75	1.17	-	-	-	178.68	55.40	20.13	-	-	-	
41	Leu	8.10	119.78	4.04	2.08,1.48	2.13	0.53,0.66	-	180.04	58.51	41.40	26.26	22.97,26.35	-	
42	Asp	8.29	121.07	4.35	2.89,2.66	-	-	-	179.92	57.59	39.89	-	-	-	
43	Lys	8.45	120.85	4.11	1.70,1.93	-	-	-	179.01	59.33	32.53	26.73	-	-	
44	Leu	8.38	120.42	4.00	1.65,1.80	-	0.94,0.89	-	178.93	57.05	42.55	-	23.80,24.83	-	
45	Ala	7.59	118.85	4.11	1.49	-	-	-	178.88	54.33	18.28	-	-	-	
46	Ala	7.16	117.75	4.36	1.51	-	-	-	177.42	52.90	19.79	-	-	-	
47	Gln	7.88	118.37	4.74	1.87,2.08	2.26,2.19	-	6.72,7.72	178.85	53.05	29.64	34.20	-	-	110.70:Ne2
48	Pro	-	-	4.67	2.36,2.02	1.85,1.99	3.64,3.36	-	178.75	63.81	32.25	26.83	50.04	-	
49	Asn	8.41	118.59	4.71	2.80,2.76	-	6.89,7.60	-	173.91	53.02	36.82	-	-	-	111.97:Nd2

50	Val	7.62	121.41	3.60	1.78	0.84,0.76	-	-	174.04	63.47	34.28	22.39,23.24	-	-					
51	Asp	8.96	124.08	4.96	2.81,2.87	-	-	-	175.73	56.56	44.50	-	-	-					
52	Leu	8.05	122.07	5.21	1.65,1.57	1.30	0.72,0.78	-	173.06	53.84	45.22	27.73	23.70,27.73	-					
53	Ile	9.36	126.70	4.75	1.76	0.63,1.57	0.90	-	174.37	60.04	40.52	28.31,17.87	13.85	-					
54	Leu	8.74	128.16	5.09	1.21,1.80	1.47	0.82,0.74	-	173.84	53.26	42.39	27.00	26.45,23.17	-					
55	Leu	8.72	127.55	4.63	0.72,1.93	1.58	1.00,0.32	-	173.74	53.72	47.73	25.94	28.53,23.37	-					
56	Asp	8.65	128.42	4.83	3.05,3.24	-	-	-	174.52	54.59	43.38	-	-	-					
57	Ile	7.59	120.33	3.64	1.85	0.64	0.81	-	177.22	66.00	38.27	17.56	13.03	-					
58	Glu	8.20	118.23	4.56	2.25,1.93	2.22,2.22	-	-	173.21	57.34	28.51	35.73	-	-					
59	Met	7.26	125.83	-	-	-	-	-	172.24	53.79	38.30	-	-	-					
60	Pro	-	-	4.51	2.36,2.05	1.96,2.08	-	-	-	62.24	32.83	26.74	-	-					
61	Val	8.54	112.16	3.10	2.60	0.89,0.89	-	-	175.31	69.55	30.05	21.39,21.39	-	-					
62	Met	9.40	122.86	4.37	2.23,1.63	2.60,2.60	-	-	174.56	56.39	35.72	31.16	-	-					
63	Asp	8.95	128.39	4.56	2.97,3.92	-	-	-	175.52	53.66	40.65	-	-	-					
64	Gly	9.23	104.35	3.66,4.14	-	-	-	-	175.56	47.67	-	-	-	-					
65	Met	7.88	118.40	4.28	2.38,1.92	2.66,2.47	-	-	177.41	57.16	30.59	33.30	-	-					
66	Glu	8.56	121.21	4.17	2.17	-	-	-	179.06	58.82	29.29	36.24	-	-					
67	Phe	8.41	118.55	4.24	2.86,3.28	-	-	-	176.74	62.51	39.13	-	-	-					
68	Leu	8.00	119.00	3.67	1.65,2.08	1.98	1.00,0.87	-	178.39	58.62	42.53	27.09	26.16,25.02	-					
69	Arg	7.38	115.98	3.95	1.68,1.76	1.71,1.44	3.11,3.11	-	178.47	59.14	29.95	27.83	43.57	-					
70	His	7.30	115.69	4.37	2.89,2.74	-	-	-	178.27	58.03	32.98	-	-	-					
71	Ala	8.75	120.53	3.50	0.54	-	-	-	179.36	54.92	19.03	-	-	-					
72	Lys	7.78	114.93	4.13	1.89,1.93	1.61,1.61	-	-	177.54	57.91	30.86	24.28	27.85	-					
73	Leu	7.43	114.91	4.35	1.66,1.78	1.65	0.86,0.93	-	178.10	55.67	42.10	27.17	24.98,22.74	-					
74	Lys	7.79	116.76	4.46	1.57,1.90	1.38,1.38	1.58,1.58	2.96,2.96	175.63	56.00	35.20	24.69	28.76	42.06					
75	Thr	7.89	113.39	4.81	4.12	1.09	-	-	172.18	60.08	69.58	18.70	-	-					
76	Arg	8.61	125.22	4.58	2.07,1.77	1.68,1.68	3.20,3.20	-	176.38	55.24	29.93	26.91	43.23	-					
77	Ala	8.52	125.12	4.03	1.13	-	-	-	177.89	53.25	19.33	-	-	-					
78	Lys	7.60	118.52	4.51	1.79,1.37	1.57,1.57	-	3.09,3.09	176.59	54.74	33.97	25.09	-	-					
79	Ile	9.97	121.56	4.72	1.68	0.84	0.79	-	174.37	61.04	41.08	19.20,27.93	13.50	-					
80	Cys	9.24	128.91	4.80	1.78,2.92	-	-	-	173.51	56.25	28.53	-	-	-					
81	Met	9.00	126.63	5.45	1.98,2.06	2.51,2.41	-	-	175.47	54.16	32.34	33.26	-	-					
82	Leu	8.56	122.15	5.06	1.82,1.06	1.48	0.75,0.64	-	175.17	52.61	44.41	26.17	26.16,23.37	-					
83	Ser	8.84	114.36	4.81	3.69,3.43	-	-	-	175.86	56.18	65.11	-	-	-					
84	Ser	-	-	4.48	4.08,3.98	-	-	-	-	59.68	63.49	-	-	-					
85	Val	7.47	113.50	4.53	2.22	0.81,0.90	-	-	175.72	59.46	34.83	18.07,21.33	-	-					
86	Ala	8.53	125.49	4.12	1.36	-	-	-	178.67	53.10	18.35	-	-	-					
87	Val	8.40	120.35	3.51	2.00	0.85,0.93	-	-	-	65.86	32.01	22.79,21.70	-	-					

88	Ser	8.42	115.44	4.18	3.88,3.85	-	-	-	-	59.89	62.24	-	-	-				
89	Gly	8.16	111.35	4.13,3.88	-	-	-	-	-	45.09	-	-	-	-				
90	Ser	7.63	115.50	4.71	4.05,3.97	-	-	-	175.23	55.44	63.77	-	-	-				
91	Pro	-	-	4.52	2.24,1.67	1.96,1.54	3.82,4.01	-	177.80	64.09	31.94	26.73	51.14	-				
92	His	7.71	116.97	4.56	2.79,3.18	-	-	-	176.73	57.98	32.51	-	-	-				
93	Ala	7.52	121.49	3.88	1.49	-	-	-	178.44	55.82	19.10	-	-	-				
94	Ala	8.00	119.38	4.08	1.45	-	-	-	180.66	55.13	17.67	-	-	-				
95	Arg	8.14	119.92	4.11	1.89,1.94	1.73,1.73	3.16,3.34	-	177.89	58.17	29.94	-	43.24	-				
96	Ala	8.42	119.95	3.89	1.38	-	-	-	179.72	55.20	17.60	-	-	-				
97	Arg	7.81	116.35	4.25	1.93,1.68	1.82	3.18,3.10	-	180.43	59.11	29.30	27.54	42.68	-				
98	Glu	8.04	121.90	4.03	2.16,2.25	2.42,2.25	-	-	178.69	59.39	29.70	36.23	-	-				
99	Leu	7.81	117.57	4.24	1.62,1.88	1.76	0.82,0.89	-	176.60	55.22	43.59	26.93	26.26,22.76	-				
100	Gly	7.59	104.09	4.42,3.71	-	-	-	-	174.75	45.24	-	-	-	-				
101	Ala	8.53	122.88	4.06	1.28	-	-	-	176.84	53.32	18.68	-	-	-				
102	Asp	8.79	120.30	4.62	2.35,2.74	-	-	-	175.58	56.15	43.81	-	-	-				
103	Gly	7.78	102.94	4.31,3.72	-	-	-	-	171.01	45.27	-	-	-	-				
104	Val	8.53	120.42	4.74	1.95	0.83,0.83	-	-	173.19	61.74	34.90	21.18,21.18	-	-				
105	Val	8.87	123.58	4.51	1.87	0.82,0.75	-	-	172.83	59.29	36.10	21.26,21.25	-	-				
106	Ala	8.47	127.07	4.63	1.30	-	-	-	177.32	51.75	18.99	-	-	-				
107	Lys	8.44	121.27	-	-	-	-	-	174.25	54.99	-	-	-	-				
108	Pro	-	-	4.39	2.12,1.78	1.69,1.69	3.47,3.61	-	178.84	62.70	32.06	27.71	49.66	-				
109	Ser	8.38	114.60	4.26	3.74,3.83	-	-	-	174.93	58.18	64.51	-	-	-				
110	Gly	8.11	109.73	3.73,3.49	-	-	-	-	173.85	45.02	-	-	-	-				
111	Thr	8.00	112.54	4.26	4.16	1.09	-	-	174.73	61.72	69.67	21.64	-	-				
112	Val	8.02	121.06	4.11	2.04	0.84,0.84	-	-	175.83	62.29	32.79	21.22,20.25	-	-				
113	Ser	8.25	118.07	4.40	3.93,3.93	-	-	-	174.62	58.21	63.84	-	-	-				
114	His	-	-	4.54	3.19,3.14	-	-	-	175.37	57.46	30.15	-	-	-				
115	Asp	8.27	119.34	4.51	2.67,2.56	-	-	-	176.81	55.02	41.09	-	-	-				
116	Leu	8.17	121.49	4.24	1.50,1.62	-	0.81,0.76	-	177.99	56.18	42.07	27.03	23.67,24.78	-				
117	Glu	8.32	121.39	4.19	2.02,2.10	-	-	-	177.51	57.59	29.94	36.30	-	-				
118	Glu	8.40	121.40	4.15	2.07,2.07	-	-	-	178.41	58.40	30.08	36.42	-	-				
119	Lys	8.45	120.49	4.25	1.93,1.92	1.54,1.42	-	2.98,2.98	178.45	58.44	32.69	25.00	29.31	42.18				
120	Thr	8.24	113.52	4.19	4.18	1.15	-	-	176.55	64.10	69.05	22.04	-	-				
121	Gly	8.35	111.04	3.51,3.39	-	-	-	-	174.95	46.47	-	-	-	-				
122	Gly	8.20	108.93	4.00,3.91	-	-	-	-	176.22	47.10	-	-	-	-				
123	Glu	8.27	122.11	4.16	2.06,2.05	2.26,2.26	-	-	179.20	58.92	29.61	36.31	-	-				
124	Leu	8.34	123.69	3.98	1.82,1.43	-	0.74,0.65	-	177.87	58.86	41.00	27.12	23.45,25.53	-				
125	Ala	8.59	120.63	3.97	1.58	-	-	-	179.23	55.74	18.49	-	-	-				

126	Arg	8.18	116.29	4.07	1.95,1.88	1.57,1.78	3.24,3.24	-	179.93	59.80	30.39	27.36	43.29	-
127	Thr	8.35	118.32	3.88	4.20	1.10	-	-	175.93	67.61	68.66	20.92	-	-
128	Met	8.57	119.96	3.45	1.58,1.81	2.68,1.87	-	-	177.43	60.93	34.05	30.60	-	-
129	Arg	8.21	115.74	3.94	1.90,1.98	-	-	-	179.68	61.08	29.95	31.77	43.39	-
130	Thr	8.47	117.75	3.98	4.34	1.28	-	-	177.08	66.67	68.79	21.72	-	-
131	Leu	8.17	120.96	4.07	1.84,1.12	1.89	0.68,0.58	-	178.55	57.65	41.93	26.92	25.47,24.17	-
132	Met	7.21	112.80	4.34	1.69,1.32	2.77,2.77	-	-	176.65	54.42	31.63	-	-	-
133	Ala	7.35	121.68	4.32	1.46	-	-	-	176.54	52.65	19.20	-	-	-
134	Ala	7.51	127.78	4.12	1.38	-	-	-	-	54.08	20.10	-	-	-

Chemical Shifts – $CheY_6$-BeF_3^- pH 7.2

		H	N	HA	HB	HG	HD	HE	C	CA	CB	CG	CD	CE	
-8	Gly	8.24	108.75	-	-	-	-	-	-	45.59	-	-	-	-	
1	Ser	7.96	116.84	-	-	-	-	-	-	-	-	-	-	-	
2	Pro	-	-	3.86	1.35,1.80	1.88,1.88	3.70,3.55	-	176.00	62.38	32.03	27.28	50.39	-	
3	Tyr	8.19	121.04	4.43	2.74,2.65	-	-	-	175.40	58.12	38.83	-	-	-	
4	Asn	10.55	123.81	5.38	3.07,2.57	-	7.34,6.77	-	176.84	53.13	40.08	-	-	-	111.49:Nd2
5	Val	9.85	125.12	5.54	1.98	1.18,0.85	-	-	175.25	60.79	35.51	21.87,24.35	-	-	
6	Met	8.85	127.27	5.51	1.77,1.95	1.98,2.11	-	-	173.66	53.32	37.88	31.36	-	-	
7	Ile	8.12	126.58	4.38	1.70	0.97	0.92	-	173.99	61.09	41.64	17.96	15.87	-	
8	Val	8.74	127.93	4.81	2.15	0.24,0.47	-	-	173.68	60.20	32.60	21.22,21.25	-	-	
9	Asp	8.14	123.45	4.60	2.22,2.65	-	-	-	174.82	55.71	43.74	-	-	-	
10	Asp	9.20	124.10	4.90	2.83,2.84	-	-	-	175.51	55.84	41.02	-	-	-	
11	Ala	9.78	126.29	4.65	1.34	-	-	-	177.31	50.75	18.44	-	-	-	
12	Ala	9.21	131.84	3.71	1.47	-	-	-	180.79	56.03	18.42	-	-	-	
13	Met	9.20	114.76	4.17	1.81,2.01	2.54,2.54	-	-	178.04	57.25	31.78	32.32	-	-	
14	Met	6.77	116.02	4.57	-	-	-	-	178.46	56.60	31.98	32.69	-	-	
15	Arg	8.12	116.72	3.83	1.76,2.05	2.04,1.01	-	-	177.82	61.72	29.91	29.33	-	-	
16	Leu	7.59	118.39	4.13	1.63,1.70	1.57	0.86,0.78	-	180.19	58.43	41.41	27.23	24.43,24.43	-	
17	Tyr	8.09	120.34	4.51	3.20,3.16	-	-	-	180.04	60.60	37.71	-	-	-	
18	Ile	8.80	120.77	3.55	1.84	0.66,0.85,1.95	0.85	-	177.71	65.86	38.15	29.54,19.05	14.94	-	

19	Ala	9.00	122.69	3.86	1.48	-	-	-	180.82	56.23	17.66	-	-	-	
20	Ser	8.72	114.73	4.15	4.04,4.04	-	-	-	176.18	62.10	62.92	-	-	-	
21	Phe	7.88	122.42	4.52	3.23,3.14	-	-	-	178.51	60.29	38.73	-	-	-	
22	Ile	8.77	122.11	3.14	1.80	0.97,1.74,0.82	0.61	-	177.70	64.43	36.25	18.47,29.82	13.42	-	
23	Lys	7.73	119.48	4.14	2.01,2.01	1.68,1.56	1.73,1.73	3.00,3.00	177.49	58.90	32.44	25.54	29.56	42.23	
24	Thr	7.55	108.11	4.27	4.35	1.36	-	-	173.99	62.88	69.92	21.67	-	-	
25	Leu	7.97	124.43	4.85	2.33,1.66	1.32	0.43,0.58	-	174.78	51.31	41.38	25.55	26.09,21.72	-	
26	Pro	-	-	4.45	2.28,1.86	2.03,1.90	4.04,3.65	-	176.99	64.48	31.90	27.21	50.54	-	
27	Asp	10.72	111.88	4.08	2.46,2.46	-	-	-	174.04	52.48	37.01	-	-	-	
28	Phe	7.69	115.90	5.45	2.82,2.64	-	-	-	174.12	57.31	44.87	-	-	-	
29	Lys	9.13	120.03	4.58	1.75,1.62	1.32,1.16	1.62,1.62	2.91,2.91	174.88	55.37	36.48	24.34	29.51	42.22	
30	Val	9.19	126.44	4.39	2.12	0.96,1.00	-	-	176.97	63.47	31.77	23.94,21.77	-	-	
31	Val	9.21	119.85	4.71	2.36	0.90,0.75	-	-	175.19	60.37	33.19	18.69,21.70	-	-	
32	Ala	7.62	121.28	4.74	1.30	-	-	-	174.85	52.06	22.80	-	-	-	
33	Gln	8.69	118.62	5.40	1.94,1.83	2.31,2.10	-	6.57,7.27	173.46	54.40	33.12	34.42	-	-	109.82:Ne2
34	Ala	9.07	122.29	4.70	1.29	-	-	-	174.98	50.53	23.44	-	-	-	
35	Ala	8.76	120.78	4.72	1.42	-	-	-	176.11	51.00	21.25	-	-	-	
36	Asn	7.28	105.33	5.56	3.28,3.27	-	-	-	176.18	53.13	40.64	-	-	-	
37	Gly	8.59	103.13	3.58,3.43	-	-	-	-	173.50	47.65	-	-	-	-	
38	Gln	8.27	123.34	4.05	2.20,2.20	2.20,2.31	-	7.53,6.74	177.85	58.23	29.16	33.96	-	-	115.42:Ne2
39	Glu	8.38	120.37	4.13	1.97,1.97	2.54,2.23	-	-	178.80	58.86	30.57	36.59	-	-	
40	Ala	7.74	118.84	3.76	1.15	-	-	-	178.70	55.44	20.28	-	-	-	
41	Leu	8.09	119.66	4.06	2.09,1.51	2.19	0.58,0.68	-	180.02	58.51	41.47	26.77	26.51,22.93	-	
42	Asp	8.37	121.11	4.34	2.90,2.66	-	-	-	179.90	57.49	39.88	-	-	-	
43	Lys	8.47	121.00	4.12	1.70,1.94	1.57	-	-	178.97	59.48	32.57	26.67	29.36	42.64	
44	Leu	8.37	120.57	4.01	1.62,1.84	1.81	0.94,0.90	-	178.62	57.06	42.42	26.88	24.85,23.52	-	
45	Ala	7.59	118.86	4.12	1.50	-	-	-	178.95	54.24	18.34	-	-	-	
46	Ala	7.16	117.84	4.36	1.51	-	-	-	177.45	52.87	19.81	-	-	-	
47	Gln	7.92	118.44	4.74	2.09,1.88	2.20,2.26	-	6.71,7.72	178.74	52.87	29.76	34.35	-	-	110.57:Ne2
48	Pro	-	-	4.68	2.03,2.36	1.99,1.85	3.37,3.65	-	178.02	63.73	32.23	26.74	50.02	-	
49	Asn	8.41	118.66	4.71	2.80,2.72	-	7.59,6.87	-	173.92	52.90	36.77	-	-	-	111.76:Nd2
50	Val	7.61	121.44	3.59	1.79	0.85,0.78	-	-	174.03	63.55	34.25	22.35,23.25	-	-	
51	Asp	8.96	124.24	4.95	2.85,2.88	-	-	-	175.76	56.40	44.42	-	-	-	
52	Leu	8.09	122.16	5.25	1.58,1.64	1.35	0.77,0.76	-	173.06	53.81	45.10	27.86	24.43,27.86	-	
53	Ile	9.31	126.88	4.80	1.77	1.58,1.58,0.69	0.91	-	174.41	59.97	40.75	17.91,28.27	14.07	-	
54	Leu	8.69	129.42	5.15	1.68,1.56	1.43	0.78,0.79	-	175.05	53.69	42.92	27.49	26.32,23.92	-	
55	Leu	8.72	127.72	4.75	2.05,0.73	1.86	1.05,0.47	-	174.06	54.26	48.03	25.76	23.92,28.37	-	
56	Asp	8.19	127.45	5.14	3.59,3.05	-	-	-	174.66	52.99	43.99	-	-	-	

57	Ile	7.34	114.93	3.93	1.68	1.68,0.82,0.63	0.82	-	176.71	65.18	38.81	30.82,17.60	13.54	-					
58	Glu	8.77	118.00	4.36	2.03,2.23	2.05,2.23	-	-	173.47	57.74	28.04	36.35	-	-					
59	Met	7.40	128.48	4.63	2.09,2.09	2.98	-	-	171.89	53.87	38.11	32.84	-	-					
60	Pro	-	-	4.53	2.36,2.06	2.09,2.09	3.60,3.81	-	175.23	62.34	32.75	26.77	50.33	-					
61	Val	8.54	111.84	3.10	2.60	0.89,0.89	-	-	177.64	69.54	30.14	21.26,21.26	-	-					
62	Met	9.49	123.09	4.37	1.63,2.24	2.69,2.69	-	-	174.48	56.44	35.69	31.19	-	-					
63	Asp	8.96	128.74	4.62	2.87,3.93	-	-	-	176.10	53.80	40.90	-	-	-					
64	Gly	9.94	104.22	3.72,4.39	-	-	-	-	175.64	47.45	-	-	-	-					
65	Met	7.92	117.45	4.32	2.42,1.91	2.61,2.72	-	-	178.86	56.95	30.72	33.77	-	-					
66	Glu	8.49	121.02	4.08	2.16,2.02	2.53,2.46	-	-	179.07	58.85	29.29	36.19	-	-					
67	Phe	8.48	118.09	4.24	2.86,3.25	-	-	-	176.66	62.55	39.06	-	-	-					
68	Leu	7.94	119.40	3.61	1.58,2.13	1.98	0.85,1.02	-	178.30	58.77	42.66	27.42	26.15,24.96	-					
69	Arg	7.33	115.63	3.95	1.72,1.67	1.72,1.43	3.10,3.10	-	178.32	59.12	29.97	27.94	43.57	-					
70	His	7.31	115.59	4.37	2.89,2.75	-	-	-	178.50	58.13	33.10	-	-	-					
71	Ala	8.87	120.74	3.45	0.48	-	-	-	179.43	55.24	18.99	-	-	-					
72	Lys	7.72	114.18	4.14	1.90,1.88	-	-	-	177.62	57.73	30.76	24.40	27.62	-					
73	Leu	7.34	114.95	4.36	1.65,1.79	1.64	0.86,0.93	-	178.18	55.63	42.22	27.14	22.78,24.97	-					
74	Lys	7.75	116.68	4.47	1.58,1.91	1.40,1.40	1.63,1.53	2.97,2.97	175.60	55.92	35.28	24.60	28.75	42.06					
75	Thr	7.91	113.43	4.82	4.11	1.10	-	-	172.19	60.04	69.63	18.74	-	-					
76	Arg	8.59	125.12	4.58	2.07,1.78	1.68,1.68	3.21,3.21	-	176.43	55.23	29.95	26.87	43.21	-					
77	Ala	8.54	125.28	4.02	1.13	-	-	-	177.79	53.33	19.19	-	-	-					
78	Lys	7.57	118.37	4.52	1.77,1.42	1.58,1.58	-	-	176.48	54.41	33.83	24.95	-	-					
79	Ile	9.93	121.39	4.76	1.63	0.86	0.75	-	174.43	61.03	41.33	28.06,19.17	14.11	-					
80	Cys	9.34	129.00	4.83	2.99,1.75	-	-	-	173.60	56.11	28.93	-	-	-					
81	Met	8.90	126.48	5.44	2.02,2.01	2.35,2.71	-	-	176.14	53.91	30.43	33.33	-	-					
82	Leu	8.39	125.59	5.46	1.71,0.99	1.22	0.79,0.58	-	175.03	53.92	42.59	27.52	23.50,26.09	-					
83	Ser	7.86	115.00	5.37	3.37,4.09	-	-	-	175.76	56.13	65.83	-	-	-					
84	Ser	-	-	4.38	3.91,3.79	-	-	-	174.72	60.93	63.08	-	-	-					
85	Val	8.04	113.13	4.38	2.06	0.55,0.74	-	-	176.38	61.50	32.10	20.93,19.12	-	-					
86	Ala	6.92	124.47	4.50	1.03	-	-	-	174.82	50.72	17.22	-	-	-					
87	Val	7.22	114.66	4.09	2.17	0.90,0.94	-	-	177.11	60.93	33.30	21.47,20.04	-	-					
88	Ser	8.85	119.71	4.12	3.86,3.86	-	-	-	-	60.47	62.37	-	-	-					
89	Gly	-	-	3.78,4.18	-	-	-	-	174.36	45.42	-	-	-	-					
90	Ser	8.13	115.59	4.85	4.06,4.50	-	-	-	174.79	56.87	64.58	-	-	-					
91	Pro	-	-	4.47	1.74,2.30	1.90,2.03	4.00,4.00	-	179.10	64.64	31.88	27.77	50.97	-					
92	His	7.91	115.88	4.22	2.84,2.83	-	-	-	177.62	59.96	31.46	-	-	-					
93	Ala	7.87	120.66	3.83	1.38	-	-	-	178.56	55.58	18.46	-	-	-					
94	Ala	7.53	118.99	4.09	1.46	-	-	-	180.72	55.00	17.93	-	-	-					

95	Arg	8.36	119.78	4.08	1.88,1.91	-	3.28,3.11	-	177.94	58.25	30.06	26.77	43.31	-
96	Ala	8.22	119.53	3.94	1.38	-	-	-	179.68	55.22	16.84	-	-	-
97	Arg	7.70	115.90	4.23	1.94,1.89	1.47,1.86	3.13,3.13	-	180.44	59.51	29.44	28.03	42.76	-
98	Glu	8.22	122.46	4.01	2.25,2.16	2.25,2.39	-	-	178.79	59.39	29.62	36.19	-	-
99	Leu	7.84	117.43	4.21	1.91,1.60	1.76	0.91,0.81	-	176.55	55.24	43.50	27.72	26.56,22.76	-
100	Gly	7.57	103.86	3.69,4.43	-	-	-	-	174.63	45.17	-	-	-	-
101	Ala	8.59	122.98	3.98	1.24	-	-	-	176.86	53.78	18.57	-	-	-
102	Asp	8.79	120.71	4.63	2.40,2.74	-	-	-	175.60	56.05	44.10	-	-	-
103	Gly	7.94	103.48	4.43,3.59	-	-	-	-	171.30	44.98	-	-	-	-
104	Val	8.85	121.25	4.30	1.97	0.77,0.77	-	-	173.09	62.78	35.70	21.37,22.41	-	-
105	Val	8.72	128.46	4.11	1.81	0.76,0.68	-	-	173.59	61.02	34.90	21.44,22.16	-	-
106	Ala	8.68	129.12	4.85	1.25	-	-	-	178.69	50.76	19.41	-	-	-
107	Lys	7.17	121.01	-	-	-	-	-	175.96	54.75	33.19	-	-	-
108	Pro	-	-	4.39	1.79	-	3.33,3.75	-	-	63.72	32.24	-	49.74	-
109	Ser	8.23	115.61	4.58	3.86,3.86	-	-	-	174.08	57.20	62.99	-	-	-
110	Gly	8.23	108.89	3.70,4.31	-	-	-	-	174.71	44.11	-	-	-	-
111	Thr	8.42	113.09	3.98	4.27	1.30	-	-	175.46	64.37	69.03	21.89	-	-
112	Val	8.01	120.17	4.13	2.05	0.88,0.88	-	-	175.11	62.42	31.83	21.01,21.01	-	-
114	His	8.73	119.23	3.67	2.93,2.88	-	-	-	174.87	57.33	30.17	-	-	-
115	Asp	8.11	118.19	4.52	2.73,2.27	-	-	-	175.53	52.68	39.36	-	-	-
118	Glu	8.41	120.08	4.00	1.94,2.07	-	-	-	178.66	59.34	30.17	36.10	-	-
119	Lys	8.32	116.35	4.25	1.77,1.77	1.41,1.41	1.50,1.63	2.95,2.95	178.57	58.13	33.24	25.25	28.81	41.97
120	Thr	8.05	114.66	4.39	3.75	1.16	-	-	174.94	63.36	70.28	23.19	-	-
121	Gly	8.00	111.67	3.03,3.68	-	-	-	-	175.27	47.84	-	-	-	-
122	Gly	8.42	108.21	3.90,3.92	-	-	-	-	176.35	47.38	-	-	-	-
123	Glu	8.18	123.63	4.07	1.99,2.09	-	-	-	179.35	58.84	29.80	35.85	-	-
124	Leu	9.03	123.00	3.99	1.24,1.78	1.65	0.77,0.61	-	177.79	58.53	41.78	27.10	23.08,25.85	-
125	Ala	8.96	120.77	4.04	1.61	-	-	-	179.40	55.83	18.39	-	-	-
126	Arg	7.96	115.98	4.10	1.93,1.97	1.76,1.76	3.25,3.25	-	179.82	59.81	30.29	27.28	43.34	-
127	Thr	8.47	118.67	4.21	3.88	1.13	-	-	175.80	67.73	68.32	21.21	-	-
128	Met	8.77	120.10	3.44	1.63,1.80	1.93,2.67	-	-	177.48	60.87	34.24	30.81	-	-
129	Arg	8.25	115.70	3.92	1.98,1.98	-	3.04,3.24	-	179.71	61.01	29.67	-	-	-
130	Thr	8.50	118.15	3.99	4.36	1.29	-	-	177.07	66.78	68.77	21.64	-	-
131	Leu	8.17	120.98	4.07	1.86,1.14	1.97	0.60,0.68	-	178.49	57.70	41.53	27.18	23.89,24.70	-
132	Met	7.20	113.03	4.33	1.69,1.27	2.74,2.74	-	-	176.52	54.49	32.76	31.45	-	-
133	Ala	7.35	121.66	4.32	1.47	-	-	-	176.52	52.67	19.17	-	-	-
134	Ala	7.53	127.81	4.36	1.51	-	-	-	176.51	54.14	20.13	-	-	-

Chemical Shifts – CheY$_6$-Δloop pH 7.2

		H	N
1	Ser	7.94	116.98
2	Pro	-	-
3	Tyr	8.15	120.95
4	Asn	10.61	124.13
5	Val	9.89	125.44
6	Met	8.89	127.33
7	Ile	8.12	126.22
8	Val	9.03	128.61
9	Asp	8.08	123.98
10	Asp	9.01	124.56
11	Ala	10.06	127.20
12	Ala	9.14	131.80
13	Met	9.09	114.19
14	Met	6.92	118.49
15	Arg	7.96	118.12
16	Leu	7.85	117.20
17	Tyr	8.15	122.42
18	Ile	8.42	118.63
19	Ala	8.73	121.75
20	Ser	8.40	115.19
21	Phe	7.61	121.44
22	Ile	8.22	120.35
23	Lys	7.85	119.63
24	Thr	7.30	105.78
25	Leu	8.14	124.32
27	Asp	10.54	112.27
28	Phe	7.54	115.63
29	Lys	9.15	119.96
30	Val	9.31	126.62
31	Val	9.16	120.19
32	Ala	7.59	120.99
33	Gln	8.71	119.16
34	Ala	8.89	121.81
35	Ala	8.82	120.96
36	Asn	7.30	105.56
37	Gly	8.66	103.78
38	Gln	8.28	123.47
39	Glu	8.40	120.47
40	Ala	7.78	118.90
41	Leu	8.12	119.99
42	Asp	8.28	121.17
43	Lys	8.45	120.83
44	Leu	8.41	120.85
45	Ala	7.60	118.91
46	Ala	7.17	117.84
47	Gln	7.86	118.48
49	Asn	8.42	118.63
50	Val	7.62	121.44
51	Asp	9.05	124.01
52	Leu	8.02	122.14
53	Ile	9.36	126.62
54	Leu	8.67	128.17
55	Leu	8.77	127.68
56	Asp	8.62	128.62
57	Ile	7.65	120.66
58	Glu	8.07	118.37
59	Met	7.27	125.79
61	Val	8.55	112.30
62	Met	9.40	122.97
63	Asp	8.96	128.36
64	Gly	9.16	104.35
65	Met	7.92	118.93

66	Glu	8.56	121.28
67	Phe	8.41	118.58
68	Leu	8.07	119.31
69	Arg	7.39	116.08
70	His	7.31	115.74
71	Ala	8.83	120.75
72	Lys	7.78	115.17
73	Leu	7.42	114.87
74	Lys	7.81	116.83
75	Thr	7.87	113.44
76	Arg	8.63	125.43
77	Ala	8.51	125.00
78	Lys	7.58	118.55
79	Ile	9.93	121.81
80	Cys	9.16	128.96
81	Met	8.97	126.85
82	Leu	8.63	122.44
83	Ser	8.91	114.54
85	Val	7.56	113.84
86	Ala	8.56	125.55
87	Val	8.36	119.96
90	Ser	7.68	115.54
92	His	7.75	116.95
93	Ala	7.50	121.30
94	Ala	8.02	119.57
95	Arg	8.14	119.99
96	Ala	8.43	120.07
97	Arg	7.78	116.43
98	Glu	8.05	122.04
99	Leu	7.84	117.64
100	Gly	7.60	104.09
101	Ala	8.48	122.87
102	Asp	8.79	120.91
103	Gly	7.76	103.09
104	Val	8.42	121.28
105	Val	8.84	121.23
106	Ala	8.47	125.43
125	Ala	8.72	121.07
126	Arg	7.77	116.02
127	Thr	7.80	118.01
128	Met	8.49	118.85
129	Arg	8.51	116.63
130	Thr	8.10	116.37
131	Leu	7.88	121.26
132	Met	7.47	112.47
133	Ala	7.33	121.52
134	Ala	7.48	127.86

Exchange Rates and Protection Factors for $CheY_6$ and $CheY_6$-BeF_3^- (pH 7.2)

		$CheY_6$			$CheY_6$-BeF_3^-	
Number	Residue	Intrinsic Exchange Rate (s^{-1})	Experimental Exchange Rate (s^{-1})	Protection Factor	Experimental Exchange Rate (s^{-1})	Protection Factor
2	MP					
3	PY	2.05E+00	1.38E-03	1.49E+03	2.73E-03	7.51E+02
4	YN	2.30E+01	1.31E-03	1.76E+04	1.97E-03	1.17E+04
5	NV	2.77E+00				
6	VM	4.70E+00	8.00E-05	5.88E+04	2.00E-05	2.35E+05
7	MI	1.59E+00				
8	IV	7.80E-01				
9	VD	2.41E+00				
10	DD	2.20E+00			1.96E-03	1.12E+03
11	DA	4.39E+00	7.48E-03	5.87E+02	1.00E-05	4.39E+05
12	AA	6.64E+00				
13	AM	6.48E+00				
14	MM	8.35E+00				
15	MR	1.03E+01	1.49E-02	6.94E+02	4.88E-03	2.11E+03
16	RL	2.90E+00				
17	LY	2.20E+00			1.02E-02	2.15E+02
18	YI	1.39E+00	6.54E-03	2.13E+02		
19	IA	3.91E+00	3.40E-03	1.15E+03	4.10E-04	9.54E+03
20	AS	1.56E+01				
21	SF	7.62E+00	3.47E-03	2.20E+03	8.60E-04	8.86E+03
22	FI	1.42E+00	5.00E-05	2.84E+04		
23	IK	3.56E+00			9.07E-03	3.93E+02
24	KT	7.45E+00				
25	TL	2.77E+00	5.68E-03	4.88E+02	9.50E-04	2.92E+03
26	LP	-				
27	PD	1.92E+00				
28	DF	2.53E+00	1.10E-04	2.30E+04		
29	FK	6.95E+00	2.60E-04	2.67E+04	2.00E-05	3.48E+05
30	KV	1.75E+00				
31	VV	9.60E-01			1.95E-03	4.92E+02
32	VA	4.81E+00	1.84E-02	2.62E+02	9.32E-03	5.16E+02
33	AQ	7.62E+00	6.54E-03	1.17E+03		
34	QA	1.05E+01	3.61E-03	2.91E+03		
35	AA	6.64E+00				
36	AN	2.05E+01	7.31E-03	2.80E+03	9.40E-04	2.18E+04
37	NG	2.58E+01				
38	GQ	1.13E+01				
39	QE	3.25E+00			3.34E-03	9.73E+02

40	EA	4.70E+00	1.90E-04	2.47E+04		
41	AL	1.75E+00	3.10E-04	5.65E+03		
42	LD	2.05E+00				
43	DK	4.00E+00	1.39E-02	2.88E+02	9.17E-03	4.36E+02
44	KL	2.30E+00	4.61E-03	4.99E+02	4.47E-03	5.15E+02
45	LA	4.09E+00				
46	AA	6.64E+00				
47	AQ	7.62E+00				
48	QP	-				
49	PN	1.18E+01				
50	NV	2.77E+00	1.84E-02	1.51E+02	9.32E-03	2.97E+02
51	VD	2.41E+00	2.53E-03	9.53E+02	3.26E-03	7.39E+02
52	DL	1.16E+00				
53	LI	7.62E-01	1.80E-04	4.23E+03		
54	IL	1.03E+00				
55	LL	1.08E+00	2.00E-05	5.40E+04		
56	LD	2.05E+00	2.30E-04	8.91E+03		
57	DI	8.18E-01	8.80E-04	9.30E+02		
58	IE	1.21E+00				
59	EM	4.60E+00				
60	MP	-				
61	PV	7.62E-01				
62	VM	4.70E+00				
63	MD	4.29E+00				
64	DG	8.18E+00				
65	GM	9.59E+00				
66	ME	2.65E+00			9.17E-03	2.89E+02
67	EF	2.71E+00				
68	FL	2.00E+00	1.31E-02	1.53E+02	7.40E-04	2.70E+03
69	LR	4.92E+00				
70	RH	1.13E+01				
71	HA	1.11E+01				
72	AK	6.05E+00				
73	KL	2.30E+00				
74	LK	3.73E+00				
75	KT	7.45E+00				
76	TR	1.26E+01				
77	RA	1.10E+01				
78	AK	6.05E+00	6.50E-04	9.31E+03		
79	KI	1.63E+00	2.25E-03	7.24E+02	1.48E-03	1.10E+03
80	IC	1.39E+01	3.20E-04	4.34E+04	1.20E-04	1.16E+05
81	CM	1.87E+01			2.42E-03	7.73E+03
82	ML	2.25E+00	6.20E-04	3.63E+03		
83	LS	9.59E+00			8.41E-03	1.14E+03

84	SS	3.10E+01				
85	SV	2.64E+00				
86	VA	4.81E+00				
87	AV	1.32E+00				
88	VS	1.13E+01				
89	SG	2.47E+01				
90	GS	2.30E+01				
91	SP	-				
92	PH	3.92E+00				
93	HA	1.11E+01				
94	AA	6.64E+00	1.31E-02	5.08E+02		
95	AR	7.98E+00				
96	RA	1.10E+01				
97	AR	7.98E+00				
98	RE	3.41E+00				
99	EL	1.24E+00				
100	LG	7.62E+00				
101	GA	9.81E+00				
102	AD	3.33E+00				
103	DG	8.18E+00				
104	GV	1.96E+00	1.46E-02	1.34E+02		
105	VV	9.60E-01				
106	VA	4.81E+00				
107	AK	6.05E+00	1.39E-02	4.35E+02		
108	KP	-				
109	PS	8.95E+00			6.21E-03	1.44E+03
110	SG	2.47E+01				
111	GT	8.35E+00				
112	TV	2.10E+00				
113	VS	1.13E+01				
114	SH	1.36E+01				
115	HD	5.60E+00				
116	DL	1.16E+00	9.90E-04	1.17E+03		
117	LE	1.27E+00				
118	EE	1.46E+00				
119	EK	4.29E+00				
120	KT	7.45E+00				
121	TG	1.96E+01				
122	GG	1.83E+01				
123	GE	3.04E+00			9.30E-04	3.27E+03
124	EL	1.24E+00			2.46E-03	5.04E+02
125	LA	4.09E+00				
126	AR	7.98E+00				
127	RT	9.37E+00				

128	TM	1.03E+01	1.17E-02	8.81E+02	2.11E-03	4.88E+03
129	MR	1.03E+01			6.21E-03	1.66E+03
130	RT	9.37E+00				
131	TL	2.77E+00	1.38E-03	2.01E+03	2.73E-03	1.01E+03
132	LM	4.00E+00			2.64E-03	1.52E+03
133	MA	8.55E+00				
134	AA	1.06E-01				

Intrinsic exchange rates were calculated using SPHERE (Bai *et al*. 1993).

Bibliography

Adler, J. 1976. Chemotaxis in Bacteria. *Journal of Supramolecular Structure* 4(3):305–17.

Ahn, Dae Ro, HyoJin Song, Jowon Kim, Soyoung Lee, and SangYoun Park. 2013. The Crystal Structure of an Activated Thermotoga Maritima CheY with N-Terminal Region of FliM. *International Journal of Biological Macromolecules* 54(1):76–83.

Aigrain, Louise, Marko Sustarsic, Robert Crawford, Anne Plochowietz, and Achillefs N. Kapanidis. 2015. Internalization and Observation of Fluorescent Biomolecules in Living Microorganisms via Electroporation. *Journal of Visualized Experiments* (96):1–14.

Alexandre, Gladys. 2010. Coupling Metabolism and Chemotaxis-Dependent Behaviours by Energy Taxis Receptors. *Microbiology* 156(8):2283–93.

Anand, G. S., P. N. Goudreau, and a M. Stock. 1998. Activation of Methylesterase CheB: Evidence of a Dual Role for the Regulatory Domain. *Biochemistry* 37(40):14038–47.

Anderson, Jennifer K., Todd G. Smith, and Timothy R. Hoover. 2010. Sense and Sensibility: Agellum-Mediated Gene Regulation. *Trends in Microbiology* 18(1):30–37.

Armitage, J. P. 1992. Bacterial Motility and Chemotaxis. *Sci. Prog.* 76:451–77.

Bai, Fan *et al*. 2010. Conformational Spread as a Mechanism for Cooperativity in the Bacterial Flagellar Switch. *Science (New York, N.Y.)* 327(5966):685–89.

Bai, Y., J. S. Milne, L. Mayne and S. W. Englander. 1993. Primary Structure Effects on Peptide Group Hydrogen Exchange. Structure, Function and Genetics 17:75-86

Baker, Melinda D., Peter M. Wolanin, and Jeffry B. Stock. 2006. Signal Transduction in Bacterial Chemotaxis. *BioEssays* 28(1):9–22.

Bax, Ad, G. Mariu. Clore, and Angela M. Gronenborn. 1990. 1H-1H Correlation via Isotropic Mixing of 13C Magnetization, a New Three-Dimensional Approach for Assigning 1H and 13C Spectra of 13C-Enriched Proteins. *Journal of Magnetic Resonance (1969)* 88(2):425–31.

Bell, Christian H., Steven L. Porter, Annabel Strawson, David I. Stuart, and Judith P. Armitage. 2010. Using Structural Information to Change the Phosphotransfer Specificity of a Two-Component Chemotaxis Signalling Complex. *PLoS Biology* 8(2).

Bellsolell, L., J. Prieto, L. Serrano, and M. Coll. 1994. Magnesium Binding to the Bacterial Chemotaxis Protein CheY Results in Large Conformational Changes Involving Its Functional Surface. *Journal of Molecular Biology* 238(4):489–95.

Berg, H. C. and R. A. Anderson. 1973. Bacteria Swim by Rotating Their Flagellar Filaments. *Nature* 245(5425):380–82.

Berg, H. C. and D. A. Brown. 1972. Chemotaxis in *Escherichia Coli* Analysed by Three-Dimensional Tracking. *Nature* 239(5374):500–504.

Berg, Howard C. 2003. The Rotary Motor of Bacterial Flagella. *Annual Review of Biochemistry* 72:19–54.

Berjanskii, Mark V. and David S. Wishart. 2005. A Simple Method to Predict Protein Flexibility Using Secondary Chemical Shifts. *Journal of the American Chemical Society* 127(43):14970–71.

Berry, R. M. and J. P. Armitage. 1999. The Bacterial Flagella Motor. *Advances in Microbial Physiology* 41:291–337.

Bilwes, a M., L. a Alex, B. R. Crane, and M. I. Simon. 1999. Structure of CheA, a Signal Transducing Histidine Kinase. *Cell* 96:131–41.

Blair, David F. 2003. Flagellar Movement Driven by Proton Translocation. *FEBS Letters* 545(1):86–95.

Boldog, Thomas, Stephen Grimme, Mingshan Li, Stephen G. Sligar, and Gerald L. Hazelbauer. 2006. Nanodiscs Separate Chemoreceptor Oligomeric States and Reveal Their Signaling Properties. *Proceedings of the National Academy of Sciences of the United States of America* 103(31):11509–14.

Borkovich, Katherine. A. and Melvin. I. Simon. 1989. The Dynamics of Protein Phosphorylation in Bacterial Chemotaxis. *Cell* 63:1339–48.

Braun, Timothy F., Laith Q. Al-Mawsawi, Seiji Kojima, and David F. Blair. 2004. Arrangement of Core Membrane Segments in the MotA/MotB Proton-Channel Complex of *Escherichia Coli*. *Biochemistry* 43(1):35–45.

Bren, A. and M. Eisenbach. 1998. The N Terminus of the Flagellar Switch Protein, FliM, Is the Binding Domain for the Chemotactic Response Regulator, CheY. *Journal of Molecular Biology* 278(3):507–14.

Briegel, a. *et al*. 2012. Bacterial Chemoreceptor Arrays Are Hexagonally Packed Trimers of Receptor Dimers Networked by Rings of Kinase and Coupling Proteins. *Proceedings of the National Academy of Sciences* 109(10):3766–71.

Briegel, Ariane *et al*. 2014. Structure of Bacterial Cytoplasmic Chemoreceptor Arrays and Implications for Chemotactic Signaling. *eLife* 3:1–16.

Vande Broek, Ann, Mark Lambrecht, and Jos Vanderleyden. 1998. Bacterial Chemotactic Motility Is Important for the Initiation of Wheat Root Colonization by *Azospirillum Brasilense*. *Microbiology* 144(9):2599–2606.

Brown, Mostyn T. 2009. Control of the Unidirectional Motor in *Rhodobacter Sphaeroides*. University of Oxford.

Brown, Perry N., Michael a a Mathews, Lisa a Joss, Christopher P. Hill, and David F. Blair. 2005. Crystal Structure of the Flagellar Rotor Protein FliN from *Thermotoga Maritima* 187(8):2890–2902.

Bulyha, Iryna *et al.* 2009. Regulation of the Type IV Pili Molecular Machine by Dynamic Localization of Two Motor Proteins. *Molecular Microbiology* 74(3):691–706.

Del Campo, Ana Martínez *et al.* 2007. Chemotactic Control of the Two Flagellar Systems of *Rhodobacter Sphaeroides* Is Mediated by Different Sets of CheY and FliM Proteins. *Journal of Bacteriology* 189(22):8397–8401.

Cannistraro, V. J., G. D. Glekas, C. V. Rao, and G. W. Ordal. 2011. Cellular Stoichiometry of the Chemotaxis Proteins in Bacillus Subtilis. *Journal of Bacteriology* 193(13):3220–27. Retrieved (http://jb.asm.org/cgi/doi/10.1128/JB.01255-10).

Charon, N. W., E. P. Greenberg, M. B. Koopman, and R. J. Limberger. 1992. Spirochete Chemotaxis, Motility, and the Structure of the Spirochetal Periplasmic Flagella. *Research in microbiology* 143(6):597–603.

Chen, Songye *et al.* 2011. Structural Diversity of Bacterial Flagellar Motors. *The EMBO Journal* 30(14):2972–81.

Chen, X. and H. C. Berg. 2000. Torque-Speed Relationship of the Flagellar Rotary Motor of *Escherichia Coli*. *Biophysical journal* 78(2):1036–41.

Chervitz, S. A. and J. J. Falke. 1996. Molecular Mechanism of Transmembrane Signaling by the Aspartate Receptor: A Model. *Proceedings of the National Academy of Sciences of the United States of America* 93(6):2545–50.

Cho, H. *et al*. 2001. BeF(3)(-) Acts as a Phosphate Analog in Proteins Phosphorylated on Aspartate: Structure of a BeF(3)(-) Complex with Phosphoserine Phosphatase. *Proceedings of the National Academy of Sciences of the United States of America* 98(15):8525–30.

Clore, G. M., a M. Gronenborn, and a Bax. 1998. A Robust Method for Determining the Magnitude of the Fully Asymmetric Alignment Tensor of Oriented Macromolecules in the Absence of Structural Information. *Journal of magnetic resonance (San Diego, Calif. : 1997)* 133(1):216–21.

Clubb, Robert T., V. Thanabal, and Gerhard Wagner. 1992. A Constant-Time Three-Dimensional Triple-Resonance Pulse Scheme to Correlate Intraresidue 1HN, 15N, and 13C′ Chemical Shifts in 15N13C-Labelled Proteins. *Journal of Magnetic Resonance (1969)* 97(1):213–17.

Cluzel, P., M. Surette, and S. Leibler. 2000. An Ultrasensitive Bacterial Motor Revealed by Monitoring Signaling Proteins in Single Cells. *Science (New York, N.Y.)* 287(5458):1652–55.

Confer, D. L. and J. W. Eaton. 1982. Phagocyte Impotence Caused by an Invasive Bacterial Adenylate Cyclase. *Science (New York, N.Y.)* 217(4563):948–50.

Cornilescu, G., J. L. Marquardt, M. Ottiger, and a. Bax. 1998. Validation of Protein Structure from Anisotropic Carbonyl Chemical Shifts in a Dilute Liquid Crystalline Phase. *Journal of the American Chemical Society* 120(27):6836–37.

Crawford, Robert *et al*. 2013. Long-Lived Intracellular Single-Molecule Fluorescence Using Electroporated Molecules. *Biophysical Journal* 105(11):2439–50.

Day, Richard. N. and Michael. W. Davidson. 2009. The Fluorescent Protein Palette: Tools for Cellular Imaging. *Chemical Society reviews* 38(10):2887–2921.

Delaglio, Frank *et al.* 1995. NMRPipe: A Multidimensional Spectral Processing System Based on UNIX Pipes. *Journal of Biomolecular NMR* 6(3):277–93.

Delalez, Nicolas J. *et al.* 2010. Signal-Dependent Turnover of the Bacterial Flagellar Switch Protein FliM. *Proceedings of the National Academy of Sciences of the United States of America* 107(25):11347–51.

Delalez, Nicolas J., Richard M. Berry, and Judith P. Armitage. 2014. Stoichiometry and Turnover of the Bacterial Flagellar Switch Protein FliN. *mBio* 5(4)

Dempsey, Graham T., Joshua C. Vaughan, Kok Hao Chen, Mark Bates, and Xiaowei Zhuang. 2011. Evaluation of Fluorophores for Optimal Performance in Localization-Based Super-Resolution Imaging. *Nature Methods* 8(12):1027–36.

Diepold, Andreas and Judith P. Armitage. 2015. Type III Secretion Systems: The Bacterial Flagellum and the Injectisome. *Philosophical transactions of the Royal Society of London. Series B, Biological sciences* 370(1679)

Djordjevic, S., P. N. Goudreau, Q. Xu, a M. Stock, and a H. West. 1998. Structural Basis for Methylesterase CheB Regulation by a Phosphorylation-Activated Domain. *Proceedings of the National Academy of Sciences of the United States of America* 95(4):1381–86.

Duke, T. A., N. Le Novère, and D. Bray. 2001. Conformational Spread in a Ring of Proteins: A Stochastic Approach to Allostery. *Journal of Molecular Biology* 308(3):541–53.

Dyer, Collin M. *et al.* 2004. Structure of the Constitutively Active Double Mutant CheY D13K Y106W Alone and in Complex with a FliM Peptide. *Journal of Molecular Biology* 342(4):1325–35.

Dyer, Collin M. and Frederick W. Dahlquist. 2006. Switched or Not?: The Structure of Unphosphorylated CheY Bound to the N Terminus of FliM. *Journal of Bacteriology* 188(21):7354–63.

Dyer, Collin M., Armand S. Vartanian, Hongjun Zhou, and Frederick W. Dahlquist. 2009. A Molecular Mechanism of Bacterial Flagellar Motor Switching. *Journal of Molecular Biology* 388(1):71–84.

Egelman, Edward H. 2009. Divergence of the Flagellar Hook and Filament. *Structure* 17(11):1425–26.

Feher, V. a *et al.* 1997. High-Resolution NMR Structure and Backbone Dynamics of the *Bacillus Subtilis* Response Regulator, Spo0F: Implications for Phosphorylation and Molecular Recognition. *Biochemistry* 36(33):10015–25.

Feher, V. a and J. Cavanagh. 1999. Millisecond-Timescale Motions Contribute to the Function of the Bacterial Response Regulator Protein Spo0F. *Nature* 400(6741):289–93.

Ferré, Axelle, Javier De Mora, Teresa Ballado, Laura Camarena, and Georges Dreyfus. 2004. Biochemical Study of Multiple CheY Response Regulators of the Chemotactic Pathway of *Rhodobacter Sphaeroides*. *Journal of Bacteriology* 186(15):5172–77.

Fesik, Stephen W. *et al.* 1990. 2D and 3D NMR Spectroscopy Employing Carbon-13/carbon-13 Magnetization Transfer by Isotropic Mixing. Spin System Identification in Large Proteins. *Journal of the American Chemical Society* 112(2):886–88.

Fiedler, U. and V. Weiss. 1995. A Common Switch in Activation of the Response Regulators NtrC and PhoB: Phosphorylation Induces Dimerization of the Receiver Modules. *The EMBO journal* 14(15):3696–3705.

Foynes, S. *et al.* 2000. Helicobacter Pylori Possesses Two CheY Response Regulators and a Histidine Kinase Sensor, CheA, Which Are Essential for Chemotaxis and Colonization of the Gastric Mucosa. *Infection and immunity* 68(4):2016–23.

Francis, N. R., V. M. Irikura, S. Yamaguchi, D. J. DeRosier, and R. M. Macnab. 1992. Localization of the *Salmonella Typhimurium* Flagellar Switch Protein FliG to the Cytoplasmic M-Ring Face of the Basal Body. *Proceedings of the National Academy of Sciences of the United States of America* 89(14):6304–8.

Galkin, Vitold E. *et al.* 2008. Divergence of Quaternary Structures among Bacterial Flagellar Filaments. *Science (New York, N.Y.)* 320(5874):382–85.

Ganguli, S., H. Wang, P. Matsumura, and K. Volz. 1995. Uncoupled Phosphorylation and Activation in Bacterial Chemotaxis: The 2.1A Structure of a Threonine to Isoleucine Mutant at Position 87 of CheY*. *Journal of Biological Chemistry* 270(29):17386–93.

Glaser, P. *et al.* 1988. The Calmodulin-Sensitive Adenylate Cyclase of Bordetella Pertussis: Cloning and Expression in *Escherichia Coli*. *Molecular microbiology* 2(1):19–30.

Gluch, M. F. *et al.* 1995. Motility and Thermotactic Responses of Thermotoga Maritima . These Include : Motility and Thermotactic Responses of Thermotoga Maritima. *Journal of Bacteriology* 177(19):5473–79.

Gould, Marcus. 2006. Chemotaxis Gene Expression in *Rhodobacter Sphaeroides* WS8N. University of Oxford.

Graf, J., P. V. Dunlap, and E. G. Ruby. 1994. Effect of Transposon-Induced Motility Mutations on Colonization of the Host Light Organ by *Vibrio Fischeri*. *Journal of Bacteriology* 176(22):6986–91.

Grzesiek, Stephan and Ad Bax. 1992. Improved 3D Triple-Resonance NMR Techniques Applied to a 31 kDa Protein. *Journal of Magnetic Resonance (1969)* 96(2):432–40.

Grzesiek, Stephan, Mitsuhiko Ikura, G. Marius Clore, Angela M. Gronenborn, and Ad Bax. 1992. A 3D Triple-Resonance NMR Technique for Qualitative Measurement of Carbonyl-Hβ J Couplings in Isotopically Enriched Proteins. *Journal of Magnetic Resonance (1969)* 96(1):215–21.

Hall, Benjamin A., Judith P. Armitage, and Mark S. P. Sansom. 2012. Mechanism of Bacterial Signal Transduction Revealed by Molecular Dynamics of Tsr Dimers and Trimers of Dimers in Lipid Vesicles. *PLoS Computational Biology* 8(9):e1002685.

Hamblin, P. a, B. a Maguire, R. N. Grishanin, and J. P. Armitage. 1997. Evidence for Two Chemosensory Pathways in *Rhodobacter Sphaeroides*. *Molecular microbiology* 26(5):1083–96.

Hamer, Rebecca, Pao-Yang Chen, Judith P. Armitage, Gesine Reinert, and Charlotte M. Deane. 2010. Deciphering Chemotaxis Pathways Using Cross Species Comparisons. *BMC Systems Biology* 4:3.

Hazelbauer, G. L. and P. Engstrom. 1981. Multiple Forms of Methyl-Accepting Chemotaxis Proteins Distinguished by a Factor in Addition to Multiple Methylation. *Journal of Bacteriology* 145(1):35–42.

Hazelbauer, Gerald L., Joseph J. Falke, and John S. Parkinson. 2008. Bacterial Chemoreceptors: High-Performance Signaling in Networked Arrays. *Trends in Microbiology* 33(1):9–19.

Hazelbauer, Gerald L. and Wing-cheung Lai. 2010. Bacterial Chemoreceptors: Providing Enhanced Features To Two-Component Signaling. *Curr Opin Micriobiol.* 13(2):124–32.

Hirano, T., S. Yamaguchi, K. Oosawa, and S. I. Aizawa. 1994. Roles of FliK and FlhB in Determination of Flagellar Hook Length in *Salmonella Typhimurium*. *Journal of Bacteriology* 176(17):5439–49.

Ind, Alice C. *et al.* 2009. Inducible-Expression Plasmid for *Rhodobacter Sphaeroides* and *Paracoccus Denitrificans. Applied and Environmental Microbiology* 75(20):6613–15.

Jarrell, Ken F. and Mark J. McBride. 2008. The Surprisingly Diverse Ways That Prokaryotes Move. *Nature Reviews. Microbiology* 6(6):466–76.

Jiang, Meiying., Robert. B. Bourret, Metlvin. I. Simon, and K. Volz. 1997. Uncoupled Phosphorylation and Activation in Bacterial Chemotaxis: The 2.3A Structure of An Aspartate to Lysine Mutant at Position 13 of CheY*. *Journal of Biological Chemistry* 272(18):11850–55.

Kaiser, Dale. 2007. Bacterial Swarming: A Re-Examination of Cell-Movement Patterns. *Current Biology* 17(14):561–70.

Karimova, G., J. Pidoux, a Ullmann, and D. Ladant. 1998. A Bacterial Two-Hybrid System Based on a Reconstituted Signal Transduction Pathway. *Proceedings of the National Academy of Sciences of the United States of America* 95(10):5752–56.

Karimova, G., a Ullmann, and D. Ladant. 2001. Protein-Protein Interaction between Bacillus Stearothermophilus Tyrosyl-tRNA Synthetase Subdomains Revealed by a Bacterial Two-Hybrid System. *Journal of molecular microbiology and biotechnology* 3(1):73–82.

Karimova, Gouzel, Nathalie Dautin, and Daniel Ladant. 2005. Interaction Network among *Escherichia Coli* Membrane Proteins Involved in Cell Division as Revealed by Bacterial Two-Hybrid Analysis Interaction Network among *Escherichia Coli* Membrane Proteins Involved in Cell Division as Revealed by Bacterial Two-Hybrid. *Journal of bacteriology* 187(7):2233–43.

Kay, L. E., D. A. Torchia, and A. Bax. 1989. Backbone Dynamics of Proteins as Studied by 15N Inverse Detected Heteronuclear NMR Spectroscopy: Application to Staphylococcal Nuclease. *Biochemistry* 28(23):8972–79.

Kay, Lewis E., Mitsuhiko Ikura, Rolf Tschudin, and Ad Bax. 1990. Three-Dimensional Triple-Resonance NMR Spectroscopy of Isotopically Enriched Proteins. *Journal of Magnetic Resonance* 213(2):423–41.

Kearns, Daniel B. 2010. A Field Guide to Bacterial Swarming Motility. *Nature Reviews. Microbiology* 8(9):634–44

Kim, E. A., M. Price-Carter, W. C. Carlquist, and D. F. Blair. 2008. Membrane Segment Organization in the Stator Complex of the Flagellar Motor: Implications for Proton Flow and Proton-Induced Conformational Change. *Biochemistry* 47(43):11332–39.

Kim, Yun Kyeong and Linda L. McCarter. 2000. Analysis of the Polar Flagellar Gene System of *Vibrio Parahaemolyticus*. *Journal of Bacteriology* 182(13):3693–3704.

Kojadinovic, Mila, Antoine Sirinelli, George H. Wadhams, and Judith P. Armitage. 2011. New Motion Analysis System for Characterization of the Chemosensory Response Kinetics of *Rhodobacter*

Sphaeroides under Different Growth Conditions. *Applied and Environmental Microbiology* 77:4082–88.

Kojetin, Douglas J. *et al.* 2005. Structural Analysis of Divalent Metals Binding to the Bacillus Subtilis Response Regulator Spo0F: The Possibility for in Vitro Metalloregulation in the Initiation of Sporulation. *Biometals : an international journal on the role of metal ions in biology, biochemistry, and medicine* 18(5):449–66.

Kojima, Seiji and David F. Blair. 2004. Solubilization and Purification of the MotA/MotB Complex of *Escherichia Coli. Biochemistry* 43(1):26–34.

Krissinel, Evgeny and Kim Henrick. 2007. Inference of Macromolecular Assemblies from Crystalline State. *Journal of Molecular Biology* 372(3):774–97.

Kudo, S., Y. Magariyama, and S. Aizawa. 1990. Abrupt Changes in Flagellar Rotation Observed by Laser Dark-Field Microscopy. *Nature* 346(6285):677–80.

Ladant, D. 1988. Interaction of Bordetella Pertussis Adenylate Cyclase with Calmodulin. Identification of Two Separated Calmodulin-Binding Domains. *Journal of Biological Chemistry* 263(6):2612–18.

Ladant, D. *et al.* 1989. Characterization of the Calmodulin-Binding and of the Catalytic Domains of Bordetella Pertussis Adenylate Cyclase. *Journal of Biological Chemistry* 264(7):4015–20.

Laub, Michael T. and Mark Goulian. 2007. Specificity in Two-Component Signal Transduction Pathways. *Annual Review of Genetics* 41:121–45.

Lee, A. G. and J. T. Fitzsimons. 1976. Motility in Normal and Filamentous Forms of *Rhodospirillum Rubrum*. *Journal of General Microbiology* 93(2):346–54.

Lee, Lawrence K., Michael a Ginsburg, Claudia Crovace, Mhairi Donohoe, and Daniela Stock. 2010. Structure of the Torque Ring of the Flagellar Motor and the Molecular Basis for Rotational Switching. *Nature* 466(7309):996–1000.

Lefèvre, Christopher T. and Dennis a Bazylinski. 2013. Ecology, Diversity, and Evolution of Magnetotactic Bacteria. *Microbiology and Molecular Biology Reviews : MMBR* 77(3):497–526.

Lele, Pushkar P., Richard W. Branch, Vedhavalli S. J. Nathan, and Howard C. Berg. 2012. Mechanism for Adaptive Remodeling of the Bacterial Flagellar Switch. *Proceedings of the National Academy of Sciences of the United States of America* 109(49):20018–22.

Li, J., R. V Swanson, M. I. Simon, and R. M. Weis. 1995. The Response Regulators CheB and CheY Exhibit Competitive Binding to the Kinase CheA. *Biochemistry* 34(45):14626–36.

Li, X., P. Romero, M. Rani, Ak Dunker, and Z. Obradovic. 1999. Predicting Protein Disorder for N-, C-, and Internal Regions. *Genome informatics. Workshop on Genome Informatics* 10(I):30–40.

Lowry, David F. *et al*. 1994. Signal Transduction in Chemotaxis. *The Journal of Biological Chemistry* 269:26358–62.

Lukat, G. S., A. M. Stock, and J. B. Stock. 1990. Divalent Metal Ion Binding to the CheY Protein and Its Significance to Phosphotransfer in Bacterial Chemotaxis. *Biochemistry* 29(23):5436–42.

Lukat, G. S. and J. B. Stock. 1993. Response Regulation in Bacterial Chemotaxis. Pp. 41–46 in *Journal of Cellular Biochemistry*, vol. 51.

Macfarlane, Stuart A. and Mike Merrick. 1985. The Nucleotide Sequence of the Nitrogen Regulation Gene ntrB and the glnA-ntrBC Intergenic Region of *Klebsiella Pneumoniae. Nucleic Acids Research* 13(21):7591–7606.

Macnab, Robert M. 1992. Genetics and Chemistry of Bacterial Flagella. *Annual review of genetics* 26:131–58.

Macnab, Robert M. 2003. How Bacteria Assemble Flagella. *Annual Review of Microbiology* 57:77–100.

Maddock, Janine R. and Lucille Shapiro. 1993. Polar Location of the Chemoreceptor Complex in the *Escherichia Coli* Cell. *A. A. A. Of Science* 259(5102):1717–23.

Martin, a. C. *et al.* 2001. CheR- and CheB-Dependent Chemosensory Adaptation System of *Rhodobacter Sphaeroides*. *Journal of Bacteriology* 183(24):7135–44.

McEvoy, M. M., a Bren, M. Eisenbach, and F. W. Dahlquist. 1999. Identification of the Binding Interfaces on CheY for Two of Its Targets, the Phosphatase CheZ and the Flagellar Switch Protein fliM. *Journal of molecular biology* 289(5):1423–33.

Merritt, Peter M., Thomas Danhorn, and Clay Fuqua. 2007. Motility and Chemotaxis in *Agrobacterium Tumefaciens* Surface Attachment and Biofilm Formation. *Journal of Bacteriology* 189(22):8005–14.

Messerle, Barbara A., Gerhard Wider, Gottfried Otting, Christoph Weber, and Kurt Wuethrich. 1989. Solvent Suppression Using a Spin Lock in 2D and 3D NMR Spectroscopy with Aqueous Solutions. *J. Magn. Reson.* 85:608–13.

Mignot, Tâm, Joshua W. Shaevitz, Patricia L. Hartzell, and David R. Zusman. 2007. Evidence That Focal Adhesion Complexes Power Bacterial Gliding Motility. *Science (New York, N.Y.)* 315(5813):853–56.

Mimori-Kiyosue, Y., F. Vonderviszt, and K. Namba. 1997. Locations of Terminal Segments of Flagellin in the Filament Structure and Their Roles in Polymerization and Polymorphism. *Journal of Molecular Biology* 270:222–37.

Minamino, Tohru *et al.* 2004. Domain Organization and Function of *Salmonella* FliK, a Flagellar Hook-Length Control Protein. *Journal of Molecular Biology* 341(2):491–502.

Minamino, Tohru, Katsumi Imada, and Keiichi Namba. 2008. Molecular Motors of the Bacterial Flagella. *Current Opinion in Structural Biology* 18(6):693–701.

Mitchell, J. G., M. Martinez-Alonso, J. Lalucat, I. Esteve, and S. Brown. 1991. Velocity Changes, Long Runs, and Reversals in the Chromatium Minus Swimming Response. *Journal of Bacteriology* 173(3):997–1003.

Mizuno, T. 1997. Compilation of All Genes Encoding Two-Component Phosphotransfer Signal Transducers in the Genome of *Escherichia Coli*. *DNA Research* 4(2):161–68.

Mizuno, T. 1998. His-Asp Phosphotransfer Signal Transduction. *Journal of Biochemistry* 123(4):555–63.

Mo, Guoya, Hongjun Zhou, Tetsuya Kawamura, and Frederick W. Dahlquist. 2012. Solution Structure of a Complex of the Histidine Auto Kinase CheA with Its Substrate CheY. *Biochemistry* 51(18):3786–98.

Moorthy, Sudha and Paula I. Watnick. 2005. Identification of Novel Stage-Specific Genetic Requirements through Whole Genome Transcription Profiling of *Vibrio Cholerae* Biofilm Development. *Molecular Microbiology* 57(6):1623–35.

Morimoto, Yusuke and Tohru Minamino. 2014. Structure and Function of the Bi-Directional Bacterial Flagellar Motor. *Biomolecules* 4(1):217–34.

Mowbray, S. L. and D. E. Koshland. 1987. Additive and Independent Responses in a Single Receptor: Aspartate and Maltose Stimuli on the Tar Protein. *Cell* 50(2):171–80.

Nakane, Daisuke, Keiko Sato, Hirofumi Wada, Mark J. McBride, and Koji Nakayama. 2013. Helical Flow of Surface Protein Required for Bacterial Gliding Motility. *Proceedings of the National Academy of Sciences* 110(27):11145–50.

Nguyen, Annalee W. and Patrick S. Daugherty. 2005. Evolutionary Optimization of Fluorescent Proteins for Intracellular FRET. *Nature Biotechnology* 23(3):355–60.

Nixon, B. T., C. W. Ronson, and F. M. Ausubel. 1986. Two-Component Regulatory Systems Responsive to Environmental Stimuli Share Strongly Conserved Domains with the Nitrogen Assimilation Regulatory Genes ntrB and ntrC. *Proceedings of the National Academy of Sciences of the United States of America* 83(20):7850–54.

Park, Sang-Youn, Bryan Lowder, Alexandrine M. Bilwes, David F. Blair, and Brian R. Crane. 2006. Structure of FliM Provides Insight into Assembly of the Switch Complex in the Bacterial Flagella Motor. *Proceedings of the National Academy of Sciences of the United States of America* 103(32):11886–91.

Paul, Koushik and David F. Blair. 2006. Organization of FliN Subunits in the Flagellar Motor of *Escherichia Coli.* 188(7):2502–11.

Pearson, Melanie M., David a. Rasko, Sara N. Smith, and Harry L. T. Mobley. 2010. Transcriptome of Swarming *Proteus Mirabilis. Infection and Immunity* 78(6):2834–45.

Penfold, R. J. and J. M. Pemberton. 1992. An Improved Suicide Vector for Construction of Chromosomal Insertion Mutations in Bacteria. *Gene* 118(1):145–46.

Pilizota, Teuta *et al.* 2009. A Molecular Brake, Not a Clutch, Stops the *Rhodobacter Sphaeroides* Flagellar Motor. *Proceedings of the National Academy of Sciences of the United States of America* 106(28):11582–87.

Poggio, Sebastian *et al.* 2007. A Complete Set of Flagellar Genes Acquired by Horizontal Transfer Coexists with the Endogenous Flagellar System in *Rhodobacter Sphaeroides*. *Journal of Bacteriology* 189(8):3208–16.

Porter, J. P. Armitage, and G. H. Wadhams. 2008. *Rhodobacter Sphaeroides*: Complexity in Chemotactic Signalling. *Trends in Microbiology* 16(6):251–60.

Porter, Steven L. *et al.* 2006. The CheYs of *Rhodobacter Sphaeroides*. *Journal of Biological Chemistry* 281(43):32694–704.

Porter, Steven L. and Judith P. Armitage. 2002. Phosphotransfer in *Rhodobacter Sphaeroides* Chemotaxis. *Journal of Molecular Biology* 324(1):35–45.

Porter, Steven L. and Judith P. Armitage. 2004. Chemotaxis in *Rhodobacter Sphaeroides* Requires an Atypical Histidine Protein Kinase. *Journal of Biological Chemistry* 279(52):54573–80.

Porter, Steven L., George H. Wadhams, and Judith P. Armitage. 2007. In Vivo and In Vitro Analysis of the *Rhodobacter Sphaeroides* Chemotaxis Signaling Complexes. *Methods in Enzymology* 423(07):392–413.

Porter, Steven L., George H. Wadhams, and Judith P. Armitage. 2011. Signal Processing in Complex Chemotaxis Pathways. *Nature Reviews. Microbiology* 9(3):153–65.

Purcell, E. M. 1976. Life at Low Reynolds Number. *AIP Conference Proceedings Physics and Our World: A Symposium in Honor of Victor F. Weisskopf, 17-18 Oct. 1974* (28):49–64.

Riepl, Hubert, Birgit Scharf, Rüdiger Schmitt, Hans Robert Kalbitzer, and Till Maurer. 2004. Solution Structures of the Inactive and BeF3-Activated Response Regulator CheY2. *Journal of Molecular Biology* 338(2):287–97.

Rolig, Annah S., James Shanks, J. Elliot Carter, and Karen M. Ottemann. 2012. *Helicobacter Pylori* Requires TlpD-Driven Chemotaxis to Proliferate in the Antrum. *Infection and Immunity* 80(10):3713–20.

Romagnoli, Simona, Helen L. Packer, and Judith P. Armitage. 2002. Tactic Responses to Oxygen in the Phototrophic Bacterium *Rhodobacter Sphaeroides* WS8N. *Journal of Bacteriology* 184(20):5590–98.

Römling, U. and C. Balsalobre. 2012. Biofilm Infections, Their Resilience to Therapy and Innovative Treatment Strategies. *Journal of Internal Medicine* 272(6):541–61.

Rückert, Markus and Gottfried Otting. 2000. Alignment of Biological Macromolecules in Novel Nonionic Liquid Crystalline Media for NMR Experiments. *Journal of the American Chemical Society* 122(32):7793–97.

Sackett, Marcella J., Judith P. Armitage, Elizabeth E. Sherwood, and Thomas P. Pitta. 1997. Photoresponses of the Purple Nonsulfur Bacteria *Rhodospirillum Centenum* and *Rhodobacter Sphaeroides. Journal of Bacteriology* 179(21):6764–68.

Samatey, Fadel a *et al.* 2004. Structure of the Bacterial Flagellar Hook and Implication for the Molecular Universal Joint Mechanism. *Nature* 431(7012):1062–68.

Sanders, D. A., B. L. Gillece-Castro, A. M. Stock, A. L. Burlingame, and D. E. Koshland. 1989. Identification of the Site of Phosphorylation of the Chemotaxis Response Regulator Protein, CheY. *Journal of Biological Chemistry* 264(36):21770–78.

Sanders, D. A., B. Mendez, and D. E. Koshland. 1989. Role of the CheW Protein in Bacterial Chemotaxis: Overexpression Is Equivalent to Absence. *Journal of Bacteriology* 171(11):6271–78.

Sarkar, Mayukh K., Koushik Paul, and David Blair. 2010. Chemotaxis Signaling Protein CheY Binds to the Rotor Protein FliN to Control the Direction of Flagellar Rotation in *Escherichia Coli. Proceedings of the National Academy of Sciences of the United States of America* 107(20):9370–75.

Sato, K. and Michio Homma. 2000. Functional Reconstitution of the Na^+-Driven Polar Flagellar Motor Component of. *Biochemistry* 275(8):5718–22.

Scharf, B. E., K. a Fahrner, L. Turner, and H. C. Berg. 1998. Control of Direction of Flagellar Rotation in Bacterial Chemotaxis. *Proceedings of the National Academy of Sciences of the United States of America* 95(1):201–6.

Schmitt, Rüdiger. 2003. Helix Rotation Model of the Flagellar Rotary Motor. *Biophysical journal* 85(2):843–52.

Schubert, Mario, Dirk Labudde, Hartmut Oschkinat, and Peter Schmieder. 2002. A Software Tool for the Prediction of Xaa-Pro Peptide Bond Conformations in Proteins Based on 13C Chemical Shift Statistics. *Journal of Biomolecular NMR* 24(2):149–54.

Schwieters, Charles D., John J. Kuszewski, Nico Tjandra, and G. Marius Clore. 2003. The Xplor-NIH NMR Molecular Structure Determination Package. *Journal of magnetic resonance (San Diego, Calif. : 1997)* 160(1):65–73.

Scott, Kathryn a. *et al.* 2010. Specificity of Localization and Phosphotransfer in the CheA Proteins of *Rhodobacter Sphaeroides*. *Molecular Microbiology* 76(2):318–30.

Shaner, Nathan C., Paul a Steinbach, and Roger Y. Tsien. 2005. A Guide to Choosing Fluorescent Proteins. *Nature methods* 2(12):905–9.

Shen, Y. and A. Bax. 2015. Protein Structural Information Derived from Nmr Chemical Shift with the Neural Network Program Talos-N. *Methods in Molecular Biology* (April):1–15.

Shi, Xingqi *et al.* 2008. Bioinformatics and Experimental Analysis of Proteins of Two-Component Systems in *Myxococcus Xanthus*. *Journal of Bacteriology* 190(2):613–24.

Simms, S. a., M. G. Keane, and J. Stock. 1985. Multiple Forms of the CheB Methylesterase in Bacterial Chemosensing. *Journal of Biological Chemistry* 260(18):10161–68.

Sockett, R. E. and J. P. Armitage. 1991. Isolation, Characterization, and Complementation of a Paralyzed Flagellar Mutant of *Rhodobacter Sphaeroides* WS8. *Journal of Bacteriology* 173(9):2786–90.

Sourjik, Victor and Howard C. Berg. 2002. Binding of the *Escherichia Coli* Response Regulator CheY to Its Target Measured in Vivo by Fluorescence Resonance Energy Transfer. *Proceedings of the National Academy of Sciences of the United States of America* 99(20):12669–74.

Stock, a, T. Chen, D. Welsh, and J. Stock. 1988. CheA Protein, a Central Regulator of Bacterial Chemotaxis, Belongs to a Family of Proteins That Control Gene Expression in Response to Changing Environmental Conditions. *Proceedings of the National Academy of Sciences of the United States of America* 85(5):1403–7.

Stock, a M., J. M. Mottonen, J. B. Stock, and C. E. Schutt. 1989. Three-Dimensional Structure of CheY, the Response Regulator of Bacterial Chemotaxis. *Nature* 337(6209):745–49.

Stock, A. M. *et al*. 1993. Structure of the Mg(2+)-Bound Form of CheY and Mechanism of Phosphoryl Transfer in Bacterial Chemotaxis. *Biochemistry* 32(49):13375–80.

Stock, Ann M., Victoria L. Robinson, and Paul N. Goudreau. 2000. Two-Component Signal Transduction. *Annual Review of Biochemistry* 69:183–215.

Stock, J. 1999. Signal Transduction: Gyrating Protein Kinases. *Current Biology : CB* 9(10):R364–67.

Suzuki, Hirofumi, Koji Yonekura, and Keiichi Namba. 2004. Structure of the Rotor of the Bacterial Flagellar Motor Revealed by Electron Cryomicroscopy and Single-Particle Image Analysis. *Journal of Molecular Biology* 337(1):105–13.

Tanaka, T. *et al.* 1998. NMR Structure of the Histidine Kinase Domain of the *E. Coli* Osmosensor EnvZ. *Nature* 396(6706):88–92.

Taylor, Barry. L. 2007. Aer on the Inside Looking Out: Paradigm for a PAS-HAMP Role in Sensing Oxygen, Redox and Energy. *Molecular Microbiology* 65(6):1415–24.

Terashima, Hiroyuki, Hajime Fukuoka, Toshiharu Yakushi, Seiji Kojima, and Michio Homma. 2006. The Vibrio Motor Proteins, MotX and MotY, Are Associated with the Basal Body of Na+-Driven Flagella and Required for Stator Formation. *Molecular Microbiology* 62(4):1170–80.

Thomason, Peter a., David Traynor, Jeffry B. Stock, and Robert R. Kay. 1999. The RdeA-RegA System, a Eukaryotic Phospho-Relay Controlling cAMP Breakdown. *Journal of Biological Chemistry* 274(39):27379–84.

Toker, a S. and R. M. Macnab. 1997. Distinct Regions of Bacterial Flagellar Switch Protein FliM Interact with FliG, FliN and CheY. *Journal of Molecular Biology* 273(3):623–34.

Tomomori, C. *et al*. 1999. Solution Structure of the Homodimeric Core Domain of *Escherichia Coli* Histidine Kinase EnvZ. *Nature Structural Biology* 6(8):729–34.

Vladimirov, Nikita and Victor Sourjik. 2009. Chemotaxis: How Bacteria Use Memory. *Biological Chemistry* 390(11):1097–1104.

Volkman, B. F., D. Lipson, D. E. Wemmer, and D. Kern. 2001. Two-State Allosteric Behavior in a Single-Domain Signaling Protein. *Science (New York, N.Y.)* 291(5512):2429–33.

Volz, K. and P. Matsumura. 1991. Crystal Structure of *Escherichia Coli* CheY Refined at 1.7-A Resolution. *The Journal of Biological Chemistry* 266(23):15511–19.

Vranken, Wim F. *et al.* 2005. The CCPN Data Model for NMR Spectroscopy: Development of a Software Pipeline. *Proteins: Structure, Function and Genetics* 59(4):687–96.

Wadhams, G. H. *et al*. 2002. TlpC, a Novel Chemotaxis Protein in *Rhodobacter Sphaeroides*, Localizes to a Discrete Region in the Cytoplasm. *Molecular Microbiology* 46(5):1211–21.

Wadhams, G. H., a. V. Warren, a. C. Martin, and J. P. Armitage. 2003. Targeting of Two Signal Transduction Pathways to Different Regions of the Bacterial Cell. *Molecular Microbiology* 50(3):763–70.

Wadhams, George H. and Judith P. Armitage. 2004. Making Sense of It All: Bacterial Chemotaxis. *Nature reviews. Molecular Cell Biology* 5(12):1024–37.

Wadhams, George H., Angela C. Martin, and Judith P. Armitage. 2000. Identification and Localization of a Methyl-Accepting Chemotaxis Protein in *Rhodobacter Sphaeroides*. *Molecular Microbiology* 36(6):1222–33.

Welch, M., K. Oosawa, S. Aizawa, and M. Eisenbach. 1993. Phosphorylation-Dependent Binding of a Signal Molecule to the Flagellar Switch of Bacteria. *Proceedings of the National Academy of Sciences of the United States of America* 90(19):8787–91.

West, M. a and G. Dreyfus. 1997. Isolation and Ultrastructural Study of the Flagellar Basal Body Complex from *Rhodobacter Sphaeroides* WS8 (wild Type) and a Polyhook Mutant PG. *Biochemical and Biophysical Research Communications* 238(3):733–37.

Wilkinson, David a., Sarah J. Chacko, Catherine Vénien-Bryan, George H. Wadhams, and Judith P. Armitage. 2011. Regulation of Flagellum Number by FliA and FlgM and Role in Biofilm Formation by *Rhodobacter Sphaeroides. Journal of Bacteriology* 193(15):4010–14.

Wishart, David S., Colin G. Bigam, Arne Holm, Robert S. Hodges, and Brian D. Sykes. 1995. 1H, 13C and 15N Random Coil NMR Chemical Shifts of the Common Amino Acids. I. Investigations of Nearest-Neighbor Effects. *Journal of Biomolecular NMR* 5(1):67–81.

Wolfe, Alan J., Deborah S. Millikan, Joy M. Campbell, and Karen L. Visick. 2004. *Vibrio Fischeri* σ54 Controls Motility, Biofilm Formation, Luminescence, and Colonization. *Applied and Environmental Microbiology* 70(4):2520–24.

Yan, D. *et al*. 1999. Beryllofluoride Mimics Phosphorylation of NtrC and Other Bacterial Response Regulators. *Proceedings of the National Academy of Sciences of the United States of America* 96(26):14789–94.

Yang, F., L. G. Moss, and G. N. Phillips. 1996. The Molecular Structure of Green Fluorescent Protein. *Nature biotechnology* 14(10):1246–51.

Yao, Lishan, Jinfa Ying, and Ad Bax. 2009. Improved Accuracy of 15N-1H Scalar and Residual Dipolar Couplings from Gradient-Enhanced IPAP-HSQC Experiments on Protonated Proteins. *Journal of Biomolecular NMR* 43(3):161–70.

Zhang, Haiyan, Stephen Neal, and David S. Wishart. 2003. RefDB: A Database of Uniformly Referenced Protein Chemical Shifts. *Journal of Biomolecular NMR* 25(3):173–95.

Zhao, Rui, Edward J. Collins, Robert B. Bourret, and Ruth E. Silversmith. 2002. Structure and Catalytic Mechanism of the *E. Coli* Chemotaxis Phosphatase CheZ. *Nature Structural Biology* 9(8):570–75.

Zhu, Xiangyang, Charles D. Amsler, Karl Volz, and Philip Matsumura. 1996. Tyrosine 106 of CheY Plays an Important Role in Chemotaxis Signal Transduction in *Escherichia Coli*. *Journal of Bacteriology* 178(14):4208–15.

Zhu, Xiangyang, Joseph Rebello, Philip Matsumura, and Karl Volz. 1997. Crystal Structures of CheY Mutants Y106W and T87I / Y106W. *The Journal of Biological Chemistry* 272(8):5000–5006.

Zweckstetter, Markus and Ad Bax. 2000. Prediction of Sterically Induced Alignment in a Dilute Liquid Crystalline Phase: Aid to Protein Structure Determination by NMR. *Journal of the American Chemical Society* 122(15):3791–92.